AD NUMBER
AD378688
CLASSIFICATION CHANGES
TO: **UNCLASSIFIED**
FROM: **CONFIDENTIAL**
LIMITATION CHANGES
TO: **Approved for public release; distribution is unlimited.**
FROM: **Distribution authorized to U.S. Gov't. agencies and their contractors; Administrative/Operational Use; JAN 1967. Other requests shall be referred to Air Force Rocket Propulsion Lab., Edwards AFB, CA.**
AUTHORITY
AFRPL ltr 7 May 1973 ; AFRPL ltr 7 May 1973

SECURITY MARKING

The classified or limited status of this report applies to each page, unless otherwise marked.
Separate page printouts MUST be marked accordingly.

THIS DOCUMENT CONTAINS INFORMATION AFFECTING THE NATIONAL DEFENSE OF THE UNITED STATES WITHIN THE MEANING OF THE ESPIONAGE LAWS, TITLE 18, U.S.C., SECTIONS 793 AND 794. THE TRANSMISSION OR THE REVELATION OF ITS CONTENTS IN ANY MANNER TO AN UNAUTHORIZED PERSON IS PROHIBITED BY LAW.

NOTICE: When government or other drawings, specifications or other data are used for any purpose other than in connection with a definitely related government procurement operation, the U. S. Government thereby incurs no responsibility, nor any obligation whatsoever; and the fact that the Government may have formulated, furnished, or in any way supplied the said drawings, specifications, or other data is not to be regarded by implication or otherwise as in any manner licensing the holder or any other person or corporation, or conveying any rights or permission to manufacture, use or sell any patented invention that may in any way be related thereto.

AFRPL-TR-66-331
VOLUME IV

TA5-5-1-7
COPY NO. 163

FINAL REPORT

156 INCH FIBERGLASS CASE LITVC MOTOR PROGRAM (U)

THIOKOL CHEMICAL CORPORATION
WASATCH DIVISION

TECHNICAL REPORT NO. AFRPL-TR-66-331

VOLUME IV
APPENDICES

JANUARY 1967

PREPARED FOR

HEADQUARTERS, SPACE SYSTEMS DIVISION
AIR FORCE SYSTEMS COMMAND
UNITED STATES AIR FORCE
LOS ANGELES, CALIFORNIA 90045

NOTICES

When U. S. Government drawings, specifications, or other data are used for any purpose other than a definitely related Government procurement operation, the Government thereby incurs no responsibility nor any obligation whatsoever, and the fact that the Government may have formulated, furnished, or in any way supplied the said drawings, specifications, or other data, is not to be regarded by implication or otherwise, or in any manner licensing the holder or any other person or corporation, or conveying any rights or permission to manufacture, use, or sell any patented invention that may in any way be related thereto.

In addition to security requirements which must be met, this document is subject to special export controls and each transmittal to foreign governments or foreign nationals may be made only with prior approval of AFRPL (RPPR/STINFO) Edwards, California 93523.

AFRPL-TR-66-331
Volume IV

TA5-5-1-7
Copy No.

FINAL REPORT

156 INCH FIBERGLASS CASE LITVC MOTOR PROGRAM (U)

THIOKOL CHEMICAL CORPORATION
WASATCH DIVISION

TECHNICAL REPORT NO. AFRPL-TR-66-331

VOLUME IV

APPENDICES

January 1967

Approved by

W. G. Ramroth

W. G. Ramroth, Manager
Large Space Booster
Project Engineering

Approved by

C. G. Kennedy

C. G. Kennedy, Manager
Space Booster Development

Publications No. 167-11000

FOREWORD

This Final Technical Engineering Report covers the work performed under Contract AF 04(695)-773, "156-7 Fiberglass Case Liquid Injection Thrust Vector Control Motor Program". The program motor, designated by the Air Force as the 156-7 rocket motor, is identified for inhouse processing as the TU-393 rocket motor.

This program was conducted under the overall direction of Col H. W. Robbins of SSD, with technical direction by the Air Force Rocket Propulsion Laboratory (AFRPL). Mr. Carver G. Kennedy, Manager Space Booster Development, was the Wasatch Division Program Manager and Mr. W. G. Ramroth, Manager Large Space Booster Project Engineering was the Project Engineer.

This technical report has been reviewed and is approved.

Mr. R. Felix
Senior Project Engineer (RPMMS)
AFRPL, Edwards, California

ABSTRACT

The 156 in. diameter case LITVC motor program was conducted by the Wasatch Division, Thiokol Chemical Corporation for the Air Force Space Systems Division with technical direction by the Air Force Rocket Propulsion Laboratory. The two major objectives were (1) the design and fabrication of a flightweight 156 in. diameter monolithic solid propellant motor utilizing a fiberglass reinforced plastic monolithic case, a 34 to 1 expansion ratio submerged fixed nozzle, and a N_2O_4 LITVC system; and (2) the demonstration static test of the motor in a simulated altitude environment to provide meaningful LITVC data in a high expansion ratio nozzle. Both objectives were successfully attained. The program was culminated on 13 May 1966 with a static test of the motor utilizing a 10 ft diameter by 82 ft long diffuser for altitude simulation. The motor had a mass fraction in excess of 0.90 and operated for 110 sec at an average thrust level of approximately 325,000 lb. The static test was successful and all motor components were intact and in good condition at the completion of the firing. Two abnormalities occurred during the firing. At approximately 70 sec, a burnthrough occurred in the diffuser tube approximately four feet aft of the nozzle exit plane, apparently due to high localized erosion of the ablative insulation on the inside diameter. The diffuser continued to operate throughout the test although at a lower simulated altitude. A malfunction of the pressure regulating subsystem portion of the LITVC system caused a degradation of injectant pressure during the firing and subsequent degradation of the LITVC performance. Post-test inspection of the motor and components revealed that internal insulation, nozzle design, and case design were satisfactory and the motor had functioned as expected. The static test demonstrated attainment of all program objectives. After post-test analysis of the fired motor and components, the fired case was hydroburst tested to obtain additional data on fiberglass case design. The case burst at 963 psig, very near the design ultimate pressure of 970 psig. This hydroburst, performed under a supplemental agreement to the contract, demonstrated the validity of the design and fabrication techniques used for this case.

REPORT OUTLINE

VOLUME I MOTOR DESIGN AND FABRICATION

Book 1

I Program Summary and Design Criteria
II Insulation and Liner
III Case Design and Fabrication
IV Grain Design and Fabrication
V Igniter Design, Fabrication and Support Testing
VI Nozzle Design and Fabrication

Book 2

VII LITVC System Design, Fabrication, and Support Testing
VIII Diffuser Design and Fabrication
IX Motor Assembly
X Tooling Design and Fabrication
XI System Support

VOLUME II NOZZLE DESIGN ANALYSIS

I Introduction
II Nozzle Design and Fabrication
III Loads and Analysis Summary
IV Design Analysis
V Weight Analysis
VI List of References

VOLUME III STATIC TEST REPORT

Book 1

I Introduction
II Test Objectives
III Test Results and Summary
IV Conclusions
V Motor Case
VI Insulation and Liner
VII Ballistics

Book 2

VIII Nozzle
IX LITVC System
X Ignition System
XI Diffuser
XII Quench System
XIII Instrumentation
XIV Chronological Assembly in Test Area
XV Conclusions and Recommendations

VOLUME IV APPENDICES

Appendix I Test Plan for Verification of Liner and Insulation Bonds for TU-393 Motor
Appendix II Test Plan for TU-393 Rocket Motor Case Hydrotest
Appendix III Test Plan for TU-393 Rocket Motor Case No. 2 Hydrotest
Appendix IV Stress Analysis of Thiokol TU-393 Motor
Appendix V Stress Analysis of the 156-7 (TU-393.01) Propellant Grain
Appendix VI LITVC Integrated Systems Test Report
Appendix VII Hydroburst Test Report
Appendix VIII Documentation

TABLE OF CONTENTS

APPENDIX I

TEST PLAN
FOR
VERIFICATION OF LINER AND INSULATION BONDS
FOR
TU-393 MOTOR

DLB-079-TP
Revision "A"

TEST PLAN

FOR

VERIFICATION OF LINER AND INSULATION BONDS

FOR

TU-393 MOTOR

THIOKOL CHEMICAL CORPORATION

WASATCH DIVISION

BRIGHAM CITY, UTAH

20 September 1965

DLB-079-TP
Revision "A"

THIOKOL CHEMICAL CORPORATION

WASATCH DIVISION

BRIGHAM CITY, UTAH

TEST PLAN

FOR

VERIFICATION OF LINER AND INSULATION BONDS

FOR

TU-393 MOTOR

C. R. Bratton
R. F. Zeigler
Large Space Booster
Project Engineering

C. R Bratton
C. R. Bratton
Large Space Booster
Project Engineering

TABLE OF CONTENTS

LIST OF ILLUSTRATIONS

LIST OF TABLES

TEST PLAN
FOR
VERIFICATION OF LINER AND INSULATION BONDS
FOR
TU-393 MOTOR

1.0 INTRODUCTION

To insure successful bond of the propellant to the case wall in the TU-393 motor, a series of tests will be conducted prior to propellant casting. These tests will verify the design, processes, actual motor materials, and the product, and will utilize standard testing procedures and equipment.

2.0 SCOPE

This plan outlines all of the testing planned by Thiokol to verify insulation-liner-propellant bond. Three types of quantitative load tests are planned (1) 180° rubber peel, (2) tenshear, and (3) constant load 180° rubber peel. These are outlined in detail in this plan. A 9" X 9" bulk sample will also be used to further verify processability. The tests will be conducted in five distinct phases. Scheduling is compatible with the over-all program.

3.0 TEST OBJECTIVES

The primary objective of this program is to verify that the insulation-liner-propellant system will meet or exceed the minimum design requirements of 70 psi tensile adhesion and 5 pli for the 180° rubber peel test for propellant to insulation bond to insure a F.S. fo 5. Other objectives are to (1) optimize liner formulation using the procedures described in Phase I, (2) verify bondability described in Phase 2 and 3, (3) characterize

the processability of the insulation-liner-propellant system using the methods described in Phases 4 and 5, (4) insure that the scheduled processes and materials contain elements compatible with planned motor construction.

Tests will be conducted to verify bond strengths of the interfaces at:

(a) Case to bladder

(b) Bladder to insulation

(c) Liner to bladder

(d) Liner to insulation

(e) Propellant to liner.

Interface bond strengths will be evaluated by 180° peel, and tensile adhesion tests. In addition, tensile adhesion tests will be conducted on composite insulation-liner-propellant specimens. Type of failure as well as strengths will be evaluated.

Tests will be conducted to verify process techniques simulating actual conditions expected during manufacture of the motor. These tests will determine effects of moisture, elevated temperatures, raw material variations, liner slump, and mold release use.

4.0 TEST SCHEDULE

Tests will be conducted in accordance with the schedule given in Figure 1. (See Appendix A for description of phases.)

5.0 DESCRIPTION OF TESTS AND APPARATUS

Three types of tests are to be used in insulation-liner-

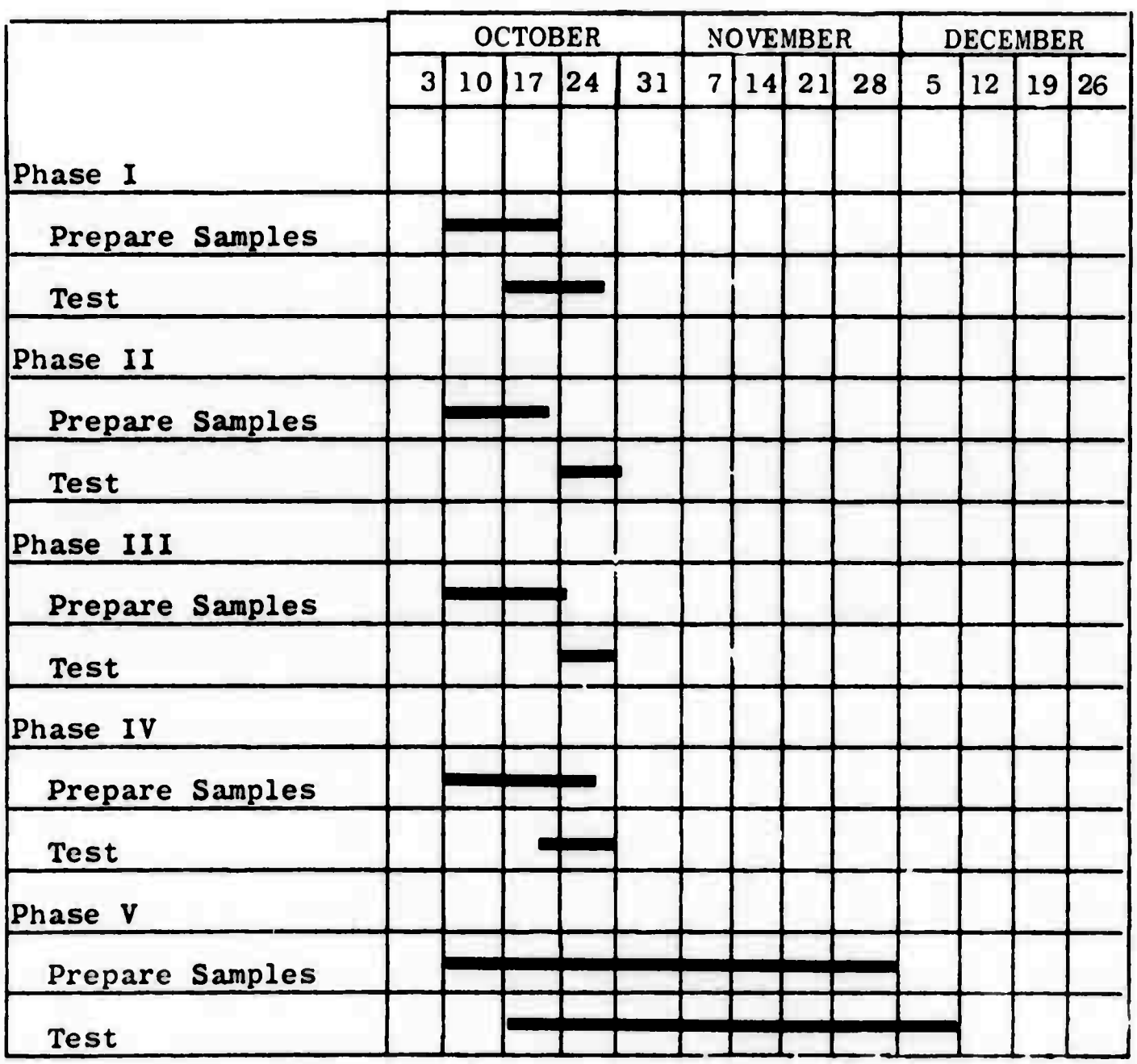

Figure 1 Test Schedule

propellant compatibility verification. They are:

(a) Peel, 180°

(b) Tenshear

(3) Constant load 180° peel.

5.1 180-DEGREE PEEL TEST

This test is used to determine the comparative peel or stripping characteristics of adhesives. Results are expressed in average load per unit width of liner bond required to separate one member from the adhered surface at a separation angle of approximately 180°. Units are pounds per linear inch. The test specimen consists of a piece of flexible material which is bonded to a steel plate or to a slab of insulation or propellant by the formulation under test. Testing is done in a power-driven machine which can apply tension at a uniform rate and record the applied load. The apparatus and test is detailed in Federal Test Standard No. 175 (See Figure 2).

5.2 TENSHEAR

The apparatus for this test provides for measuring bond strength in tension and shear at various angles. For the purposes of this test program, the tenshear samples will be used to determine only straight tensile adhesion.

The sample consists of two (2) flat plates with the various composites built up between (See Figure 3). The specimen is pulled to failure in an instron tensile tester where force is recorded in pounds. The force in psi is then calculated by dividing by area of the bond surface.

5.3 CONSTANT LOAD 180-DEGREE PEEL

The constant load 180° peel specimen is prepared exactly the same as the standard 180° peel specimen. When testing the sample, a weight is attached to the free end of the specimen. The load is applied for a predetermined time or until failure occurs.

6.0 INSTRUMENTATION AND DATA ACQUISITION REQUIREMENTS

(Not Applicable)

7.0 TEST PROCEDURES

The specimens for this test program are specified in Table 1. Requirement for detailed processing and formulation variables are included therein.

General specimen process requirements shall simulate predicted processing of the TU-393 motor except where specified otherwise in Table 1. Scheduled motor raw materials lots shall be utilized for all tests herein. Predicted motor processing is as follows:

(a) Insulation Materials

(1) Dome insulation is Asbestos Filled NBR (V-44) .10 in sheet stock, vacuum bagged and autoclave cured at 300° F for 4 hours in CO_2 atmosphere. Then cured with case 20 hours @ 300°F.

(2) Bladder material is Silica Filled NBR (V-45) .060 in sheet stock, pres-

sure cured at 60 psi nominal according to the planned case cure cycle.

(b) Hydrotest

(1) 7-10 hours soak (case filled with water-no pressure).

(2) 1-2 hours @ 800 psi.

(c) Dry case hours @ 135° F

(d) Insulation surface buffed and cleaned with MEK

(e) Insulation surface is spray coated with Koropon and cured 24 hours @ ambient.

(f) Koropon surface cleaned with MEK.

(g) Liner application with sweep-extruder.

(h) 16-24 hours ambient liner cure.

(i) 24 hour liner cure at 135° F.

(j) 50 hours maximum casting at 135°F with TPH 8163 propellant.

(k) 7 days propellant and liner cure at 135°F.

(l) Liner thickness to be .090" nominal with .070 minimum.

The actual raw materials assigned to the motor as follows shall be used for all tests where applicable:

Material	Lot
Koropon Part A	9505-0002
Koropon Part B	9506-0001
HC Polymer	9407-0099
MAPO	9606-0014

Material	Lot
ERLA 0500	9267-0038
Thixcin E	9851-0032
Iron Octoate	9455-0019
Asbestos Floats	9016-0014

8.0 PREDICTED RESULTS

Since the insulation, liner, and propellant are materials that have been used in previous motors, it is predicted that test results will verify the design and processes with little or no modification. Variables to be considered are limited to changes in propellant formultation to obtain burn rate, wetting of insulation during hydrotest and modification of liner to insure compatibility.

9.0 EFFECT OF SUCCESS OR FAILURE ON OVER-ALL PROGRAM OBJECTIVES

These tests are necessary to verify product design and must be successfully accomplished to insure final bond of propellant to case.

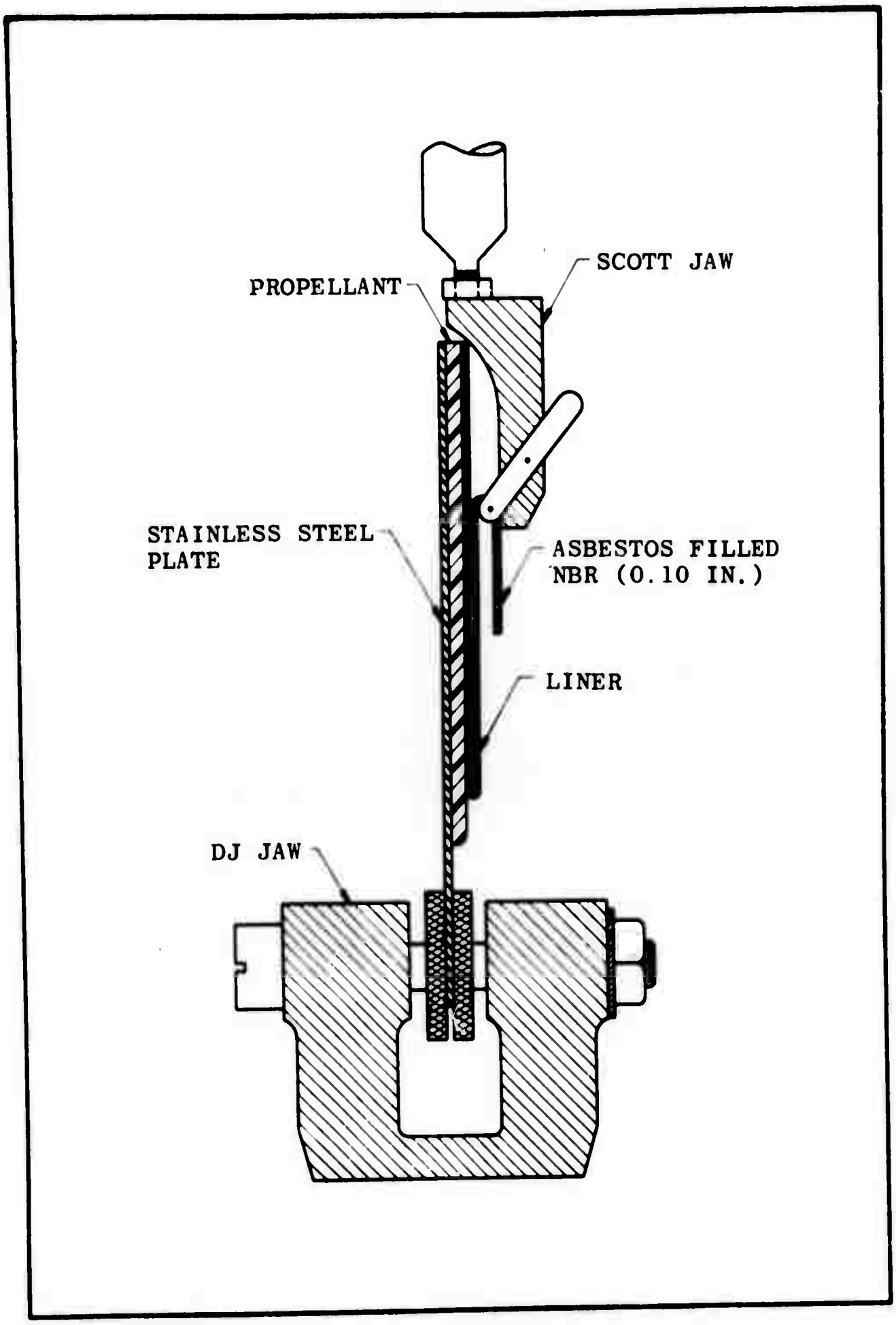

Figure 2. 180 Deg Peel Test Specimen and Arrangement

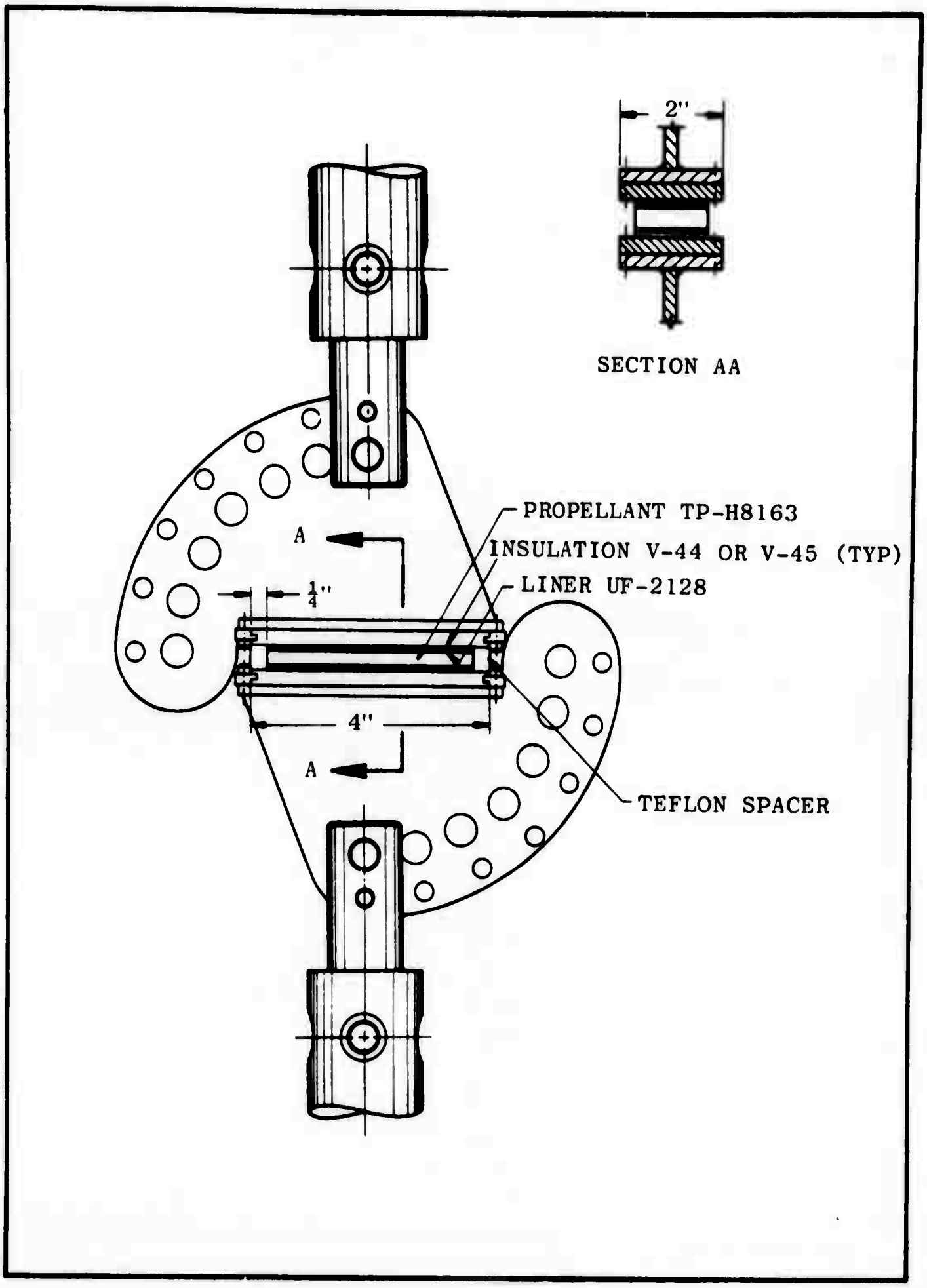

Figure 3. Tenshear Test Apparatus

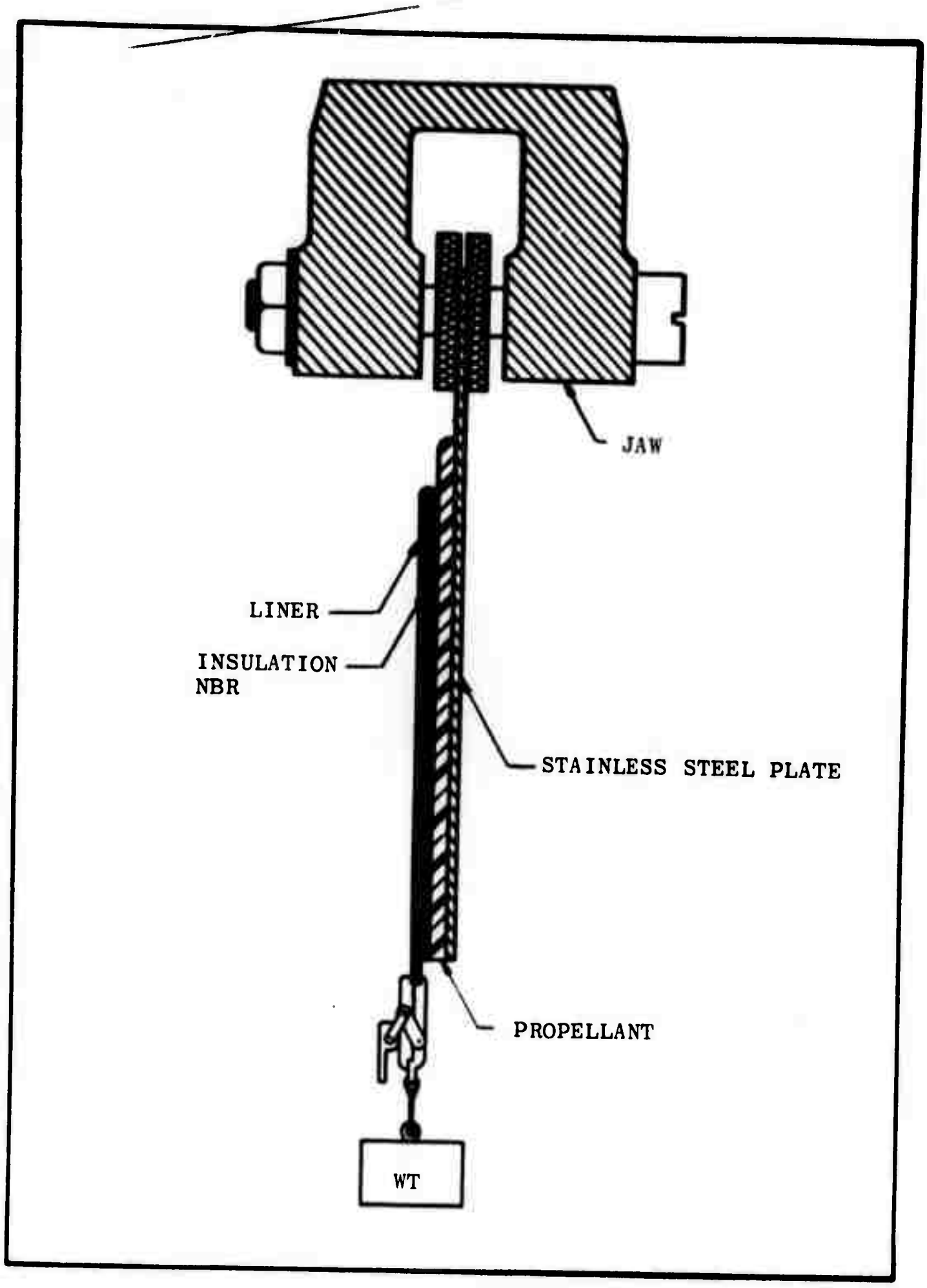

Figure 4. Constant Load 180° Peel Test
Specimen & Apparatus

TABLE 1

TEST MATRIX

Phase I

Purpose: To optimize liner formulation using motor raw material to minimize liner slumpage.

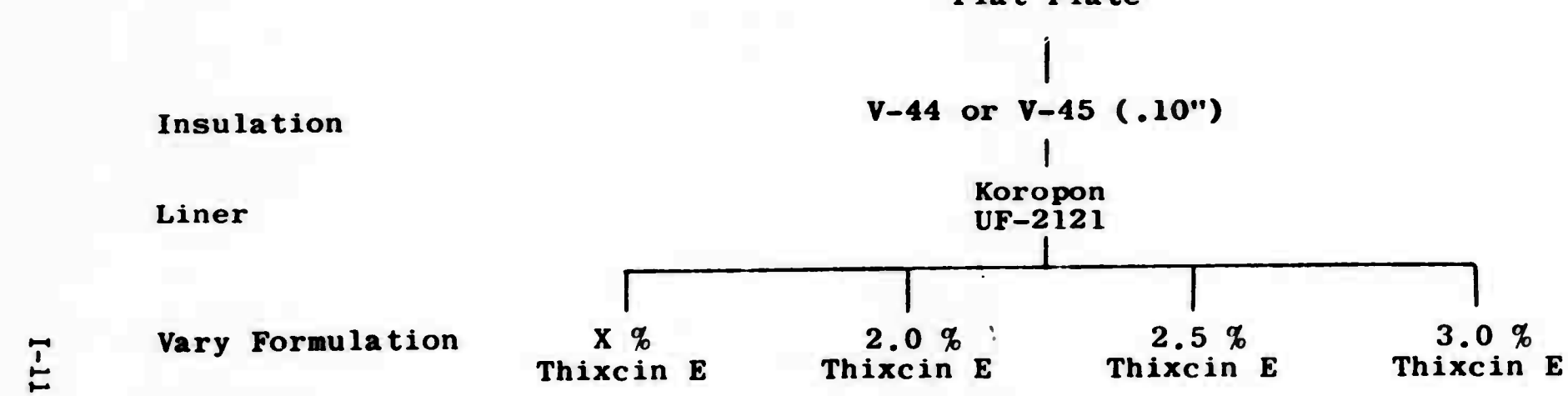

Test: 9" X 9" plate placed in vertical position for 16 hours at ambient temperature; then in 135° F atmosphere for 48 hours. Record Slumpage.

1 Specimen each condition

4 Total

TABLE 1 (Cont)

TEST MATRIX

Phase II

Purpose: To determine bond strength of V-45 at fiberglass and V-44 interfaces under motor conditions.

Interface Material	Fiberglass	V-44
Insulation	V-45 (.10")	V-45 (.10")
Conditions	Lay up uncured V-45 on aluminum plate, wrap with fiberglass using wrapping machine, bag and cure	Place 2 layer cured V-44 on aluminum plate layup .060 uncured V-45 wrap with fiberglass, bag and cure
Hydrotest Simulation	Not Wetted / Wetted & Dried	Not Wetted / Wetted & Dried
Tests	3 - 180° Peels, 3 - Tenshears / 5 - 180° Peels, 5 - Tenshears	3 - 180° Peels, 3 - Tenshears / 5 - 180° Peels, 5 - Tenshears

Total Tests 32

Peel and tenshear tests will be conducted in the peel and tensile apparatus shown in Figures 2 and 3.

TABLE 1 (Cont)

TEST MATRIX

Phase III

Purpose: To determine bond strength of liner at V-44, V-45 and TP-H-8163 interfaces under motor conditions.

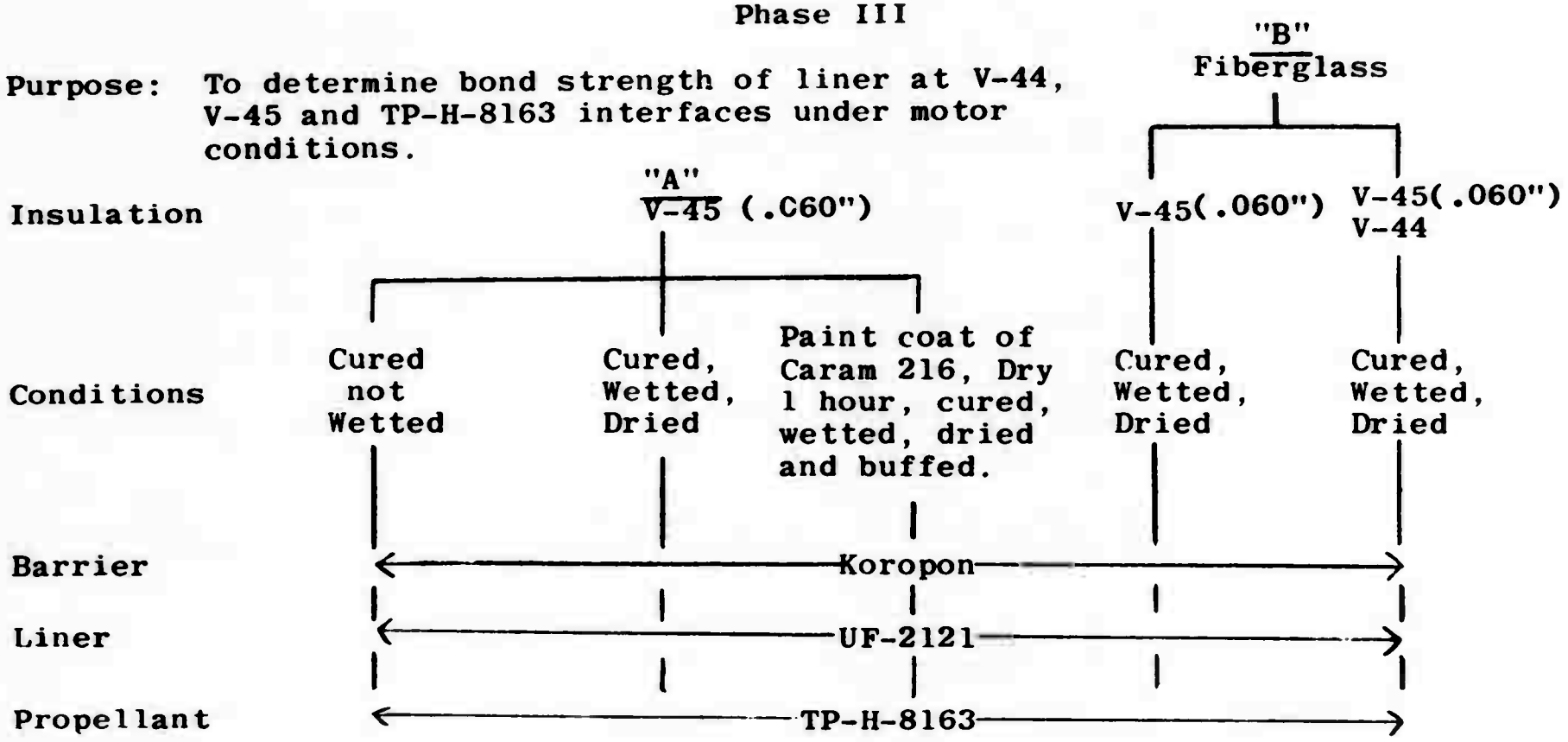

Tests	Tests Each Condition
5 180° Peels	5 Tenshear
5 Tenshears	2 Composite 9X9X9 Samples
Total 30	Total 12

TABLE 1 (Cont)

TEST MATRIX

Phase III (Continued)

"C"

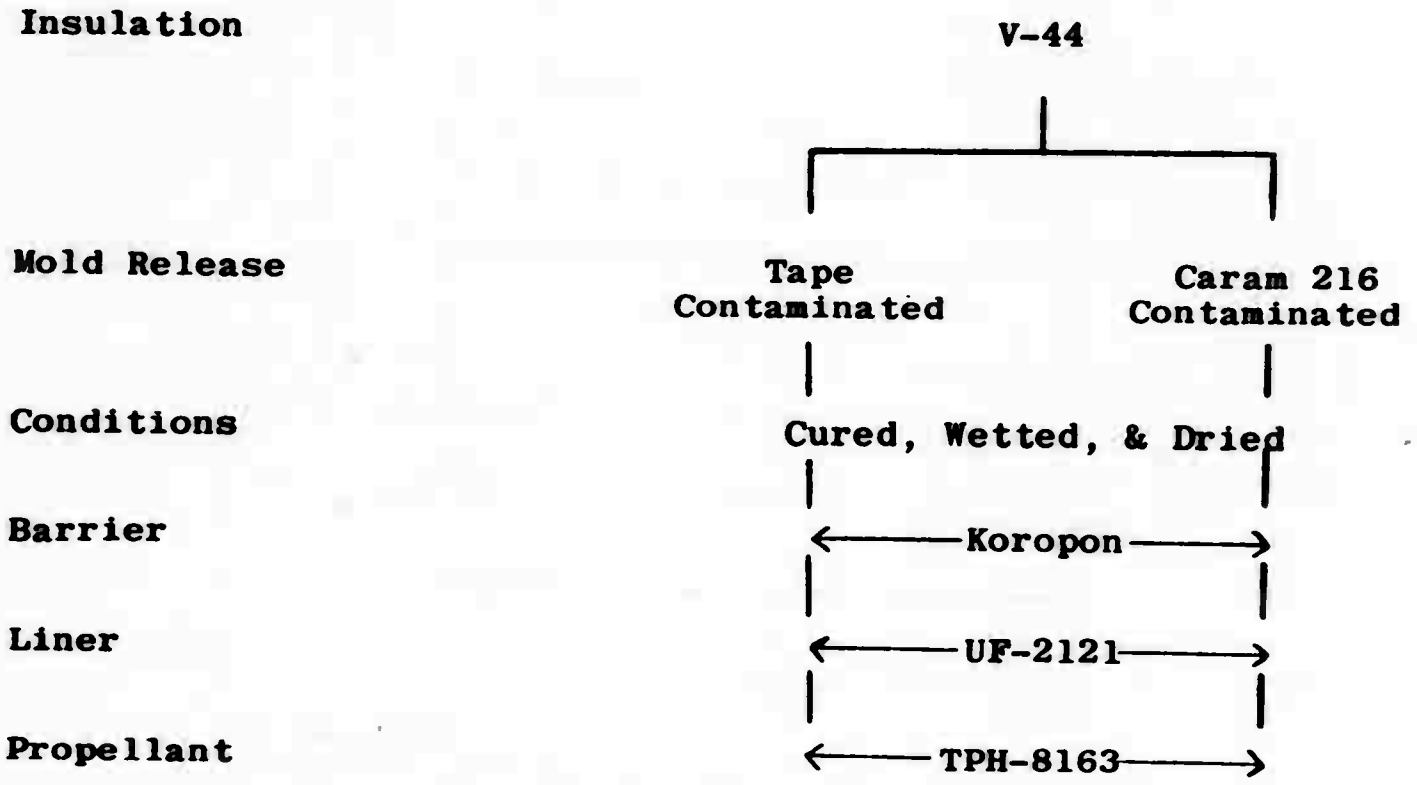

Tests: 5 100° peel

5 Tenshear

Total 20

TABLE 1 (Cont)

TEST MATRIX

Phase IV

Purpose: To determine effect of liner cure upon liner bond strength.

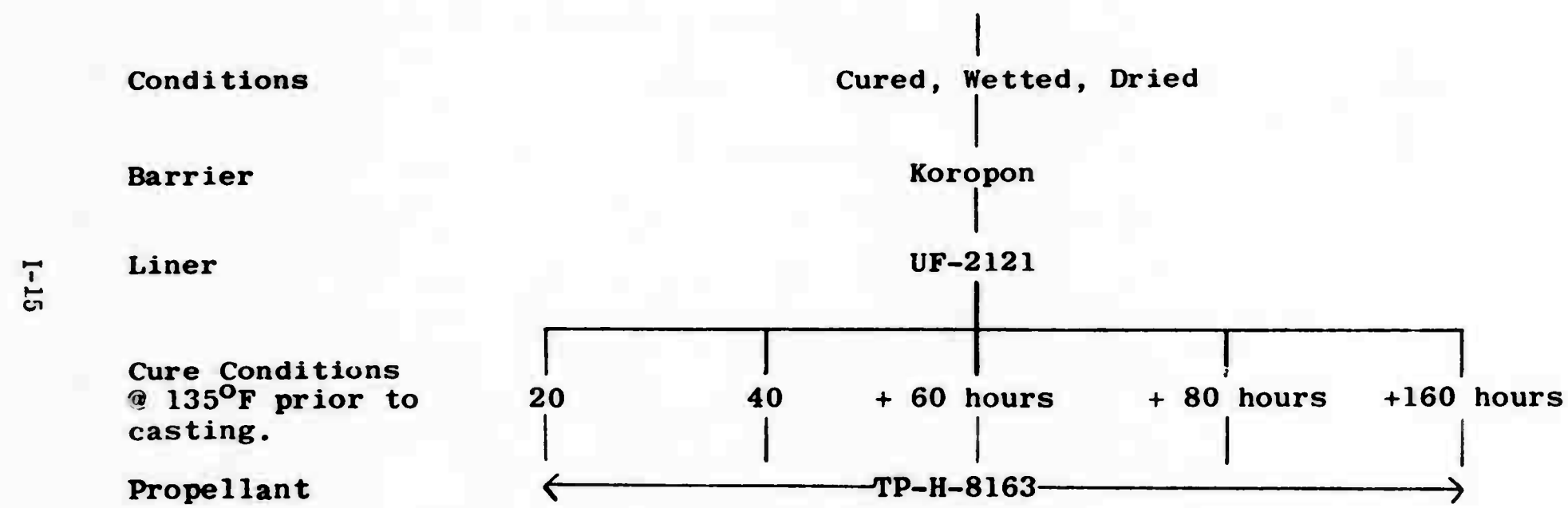

Tests: 5 180° Peel
5 Tenshear

Total 50

TABLE 1 (Cont)

TEST MATRIX

Phase V

Purpose: To determine compatibility of insulation-liner-propellant under constant load and aging effects.

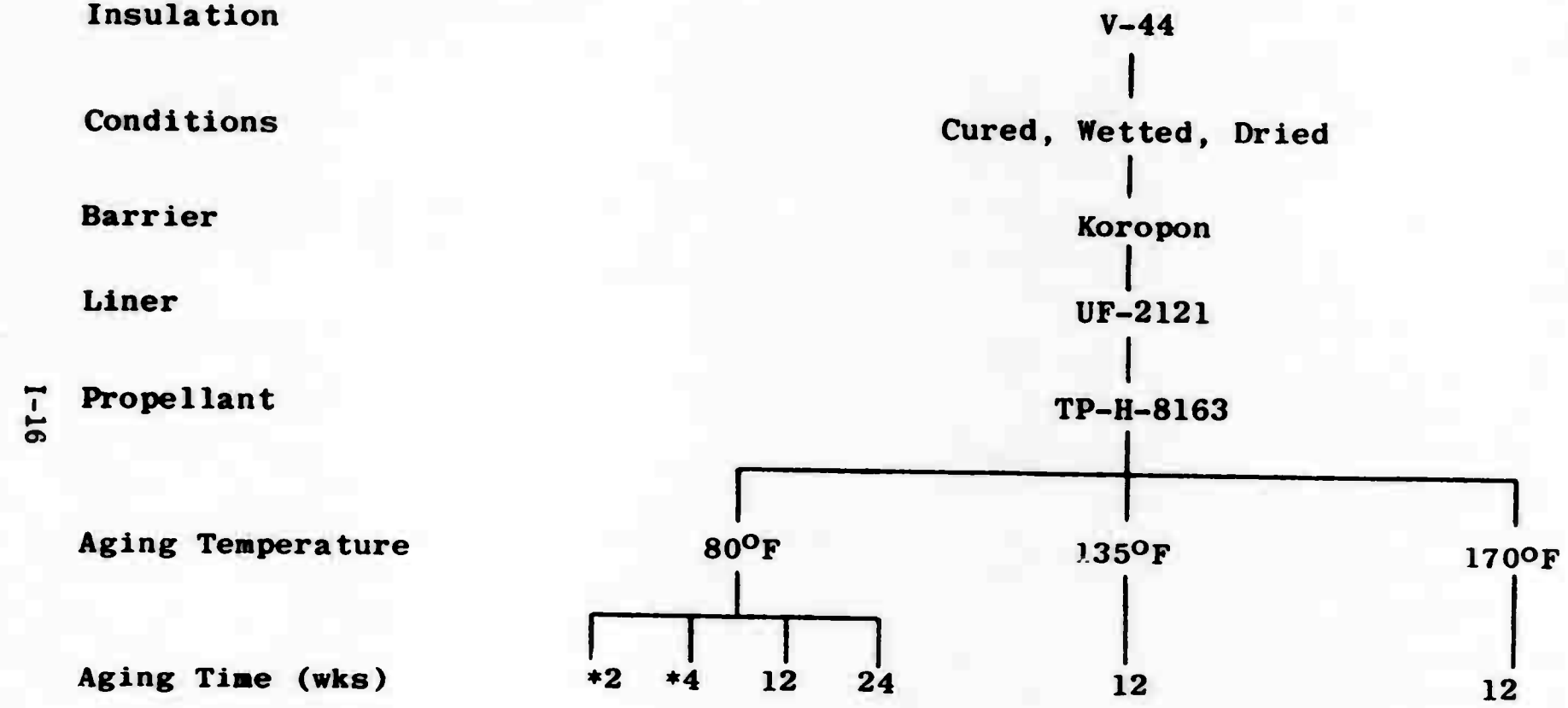

Tests: 5 180° Peels

5 Tenshears

Total 80

* Constant load 180° peels @ 80% of average strength from Phase III A. (These specimens are in addition to short time load specimens.)

APPENDIX II

TEST PLAN
FOR
TU-393 ROCKET MOTOR CASES
HYDROTEST

DLB-086-TP
Revision "C"

TEST PLAN

FOR

TU-393 ROCKET MOTOR CASES

HYDROTEST

THIOKOL CHEMICAL CORPORATION
WASATCH DIVISION
BRIGHAM CITY, UTAH

15 November 1965

DLB-086-TP
Revision "C"

THIOKOL CHEMICAL CORPORATION

WASATCH DIVISION

BRIGHAM CITY, UTAH

TEST PLAN

FOR

TU-393 ROCKET MOTOR CASES

HYDROTEST

Prepared by:

C. R. Bratton

J. A. Melehes
Large Space Booster
Project Engineering

Approved by:

C. R. Bratton

C. R. Bratton
Large Space Booster
Project Engineering

L. M. Murphy BY RCE

D. A. Sherar
Manager
Test Division

FOREWORD

This test plan covers the hydrotesting and hydrobursting of TU-393 fiberglass reinforced plastic rocket motor cases. It has been prepared by Thiokol Chemical Corporation for use on Contract AF 04(695)-773.

TABLE OF CONTENTS

LIST OF FIGURES

LIST OF TABLES

I. INTRODUCTION

Two identical TU-393 cases will be fabricated. The first one will be proof tested to 790 $^{+10}_{-0}$ psig and then hydroburst. The second will be proof tested to 790 $^{+10}_{-0}$ psig only, then loaded and fired. Test setup, equipment, instrumentation procedures, etc., will be the same for both cases. The only difference will be the addition of a waterproof bag to protect the bladder of the second case. Therefore, this plan outlines the criteria and detailed procedures for both tests.

Assembly, instrumentation and hydrotesting will be conducted at the Wasatch Division Test Area. The test fixture will provide a floating piston device which will apply a simulated thrust load to the forward skirt.

II. OBJECTIVES

Although test methods are the same for both cases, the primary test objectives differ.

A. The primary objective of hydrotest/hydroburst of case No. 1 is to determine the actual strength levels obtainable before failure and thus appraise the accuracy of analytical calculations.

B. The primary objective in hydrotesting case No. 2 is to prove the case satisfactory for subsequent loading and firing.

C. Secondary objectives of both tests are:

1. To verify the manufacturing methods, process controls, quality assurance provisions, etc., used to fabricate the case.

2. To demonstrate the feasibility of using large filament wound plastic cases for solid propellant rocket motors.

3. To determine behavior characteristics of large plastic cases including:

   Percent elongation of glass laminate

   Deflections

   Stress/strain relationships

III. HARDWARE INSPECTION

A. Pretest

The following pretest inspection of the case and related test hardware shall be performed prior to pressurization. Departures and deviations, to this plan, or established drawings shall be coordinated with the cognizant Project Engineer.

1. Visually inspect the outside case wall and note any apparent flaws by description and location.

2. Measure and record the length at each longitudinal extensometer location.

3. Measure and record the case circumference at each circumferential extensometer location.

4. Measure and record the actual location of each strain gage.

B. Post-test

Post-test evaluations will be directed by the Project Engineer.

IV. INSTRUMENTATION

Instrumentation will be installed on the case assembly in accordance with Instrumentation Installation Drawing 7U37716. All instrumentation readings will be recorded continuously throughout the test on magnetic tape. (See Table I for Instrumentation Coding System.)

A. Strain Gages

Sixty (60) strain gages will be located on the case as shown on the instrumentation drawing. Overall accuracy of the strain measurements will be $\pm$ 5 percent, at 3 percent strain.

B. Extensometers

Fifteen (15) extensometers will be located on the case per the instrumentation drawing (7U37716-03). Overall accuracy of extensometer measurements will be $\pm$ 5 percent at maximum deflection.

C. Pressure Transducers

Two (2) pressures will be recorded continuously at the aft dome. The transducers will be located as close to the case as possible. Overall accuracy of the pressure measurements will be ± 2 percent.

The test will be conducted in Test Bay T-17 of the Wasatch Division Test Area. The test stand shall be assembled per drawing 2U25060-02. Pumping facilities shall be capable of delivering 300 gpm at a pressure of 1,500 psig. There will be a minimum of 1,000 gallons makeup water required to reach failure pressure.

The case will be hydrotested in the vertical position with the forward skirt resting on the base structure of the test stand (per Test Stand Drawing 2U25060-02).

Nozzle thrust is simulated by a floating piston in a flanged cylinder attached to the aft polar boss. This thrust load is applied to the overhead test stand structure by the piston and is reacted against the forward skirt by the base structure.

The piston cylinder device allows free axial expansion of the case while lateral and gimbal bearing units compensate for any twisting or lateral movements.

In order to guarantee a flat surface and uniform bearing loads, an Epocast 31-D filler will be provided between the piston and overhead structures. The filler will be installed per 2U25060-02, with the piston raised to its maximum height (Note: hydrant pressure only required for this operation).

Pressurization fluid shall be water at ambient temperature.

VI. TEST PROCEDURE

A. To minimize time in the test bay, all possible strain gages and all possible extensometer brackets and guides shall be mounted before the case is placed in the test stand.

B. Following strain gage and extensometer mounting, the case will be installed in the test fixture and aligned. The floating piston will be installed in the aft section and the assembly of the test stand completed.

C. The case shall be inspected as specified in Section III A.3 and A.4 Pretest Inspection.

D. The portable pumping facility will be connected and the air in the case purged.

E. The case will then be leak tested at 100 psig for ten (10) minutes before returning to 0 psig pressure. Criteria for successful leak test is zero leakage. A cognizant Project Engineer must be present for observation and evaluation in this cycle.

F. Instrumentation will be zeroed and balanced--cameras will be loaded.

G. The case will then be pressurized to 790 $^{+10}_{-0}$ psig at the prescribed rate of 4 psig per second (min) to 8 psig per second (max). The pressure will be held for 120 $^{+5}_{-0}$ seconds and then reduced to a zero at a maximum rate of 15 psig per second.

H. <u>The following paragraph applies to case No. 1 only</u>:

After proof testing the performance of instrumentation and data acquisition equipment will be assessed. Remove all extensometers. Cameras will be reloaded, if needed. The case will then be pressurized at a rate of 4 to 8 psig per second to 705 $^{+10}_{-0}$ psig and held at this pressure for 110 $\pm$ 5 seconds. The pressure will then be increased at a rate of 4 to 8 psig per second until failure occurs.

VII. PHOTOGRAPHIC COVERAGE

Photographic coverage for the two proof tests at 790 psig will consist of the following:

1. Two (2) high speed cameras (64 frames per second). One located to provide an unobstructed view of the entire motor case and the other to provide an unobstructed view of the aft case area. This will include the piston assembly and aft portion of the test stand.

2. Appropriate still photographs in color and black and white will be taken to document the entire test effort. This will include installing the case in the test stand, instrumentation, test setup, test stand, etc., in all phases of buildup.

3. Documentary still photographs will be taken of the completed setup before and after test.

4. Photographic coverage for the hydroburst test will include all of the above, plus the following:

   a) Four (4) additional high speed cameras (64 frames per second), giving a total of six (6). These will provide unobstructed views of the entire case from three (3) radial directions at the top and at the bottom.

   b) Three (3) very high speed cameras (400 frames per second). These will be placed 120 deg apart at the case center, thus giving complete coverage of all of the cylindrical portions. Figure 1 shows the photographic layout.

VIII. DATA REDUCTION AND REPORT SCHEDULE

A. All films will be processed within three (3) working days.

B. Selective gages (selected by Development Engineering with the aid of the film) shall be run through the quick look recorder.

C. Following the quick look run, the tapes will be processed through the IBM and the IBM output will be made available to Development Engineering within five (5) days.

D. Final data from the hydrotest will be made available to Development Engineering within six (6) working days following receipt of the IBM runs.

E. Development Engineering will analyze the data and prepare a test report four (4) weeks after the hydrotest.

IX. REFERENCED DRAWINGS

7U37701	Case Assembly--TU-393
7U37716-03	Instrumentation Installation--TU-393
2U25060-02	Hydrostatic Test Stand

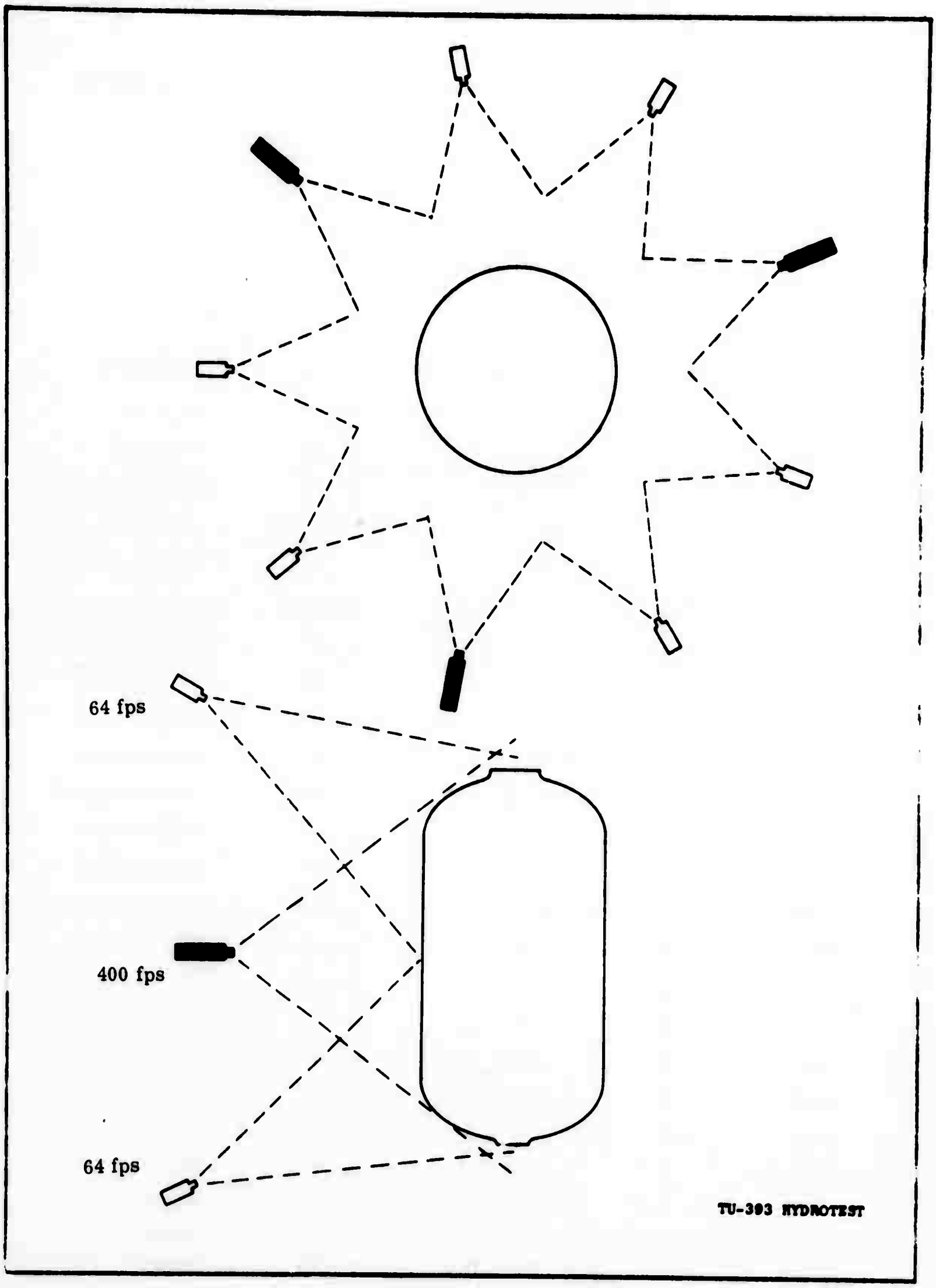

Figure 1. Camera Locations

TABLE I

INSTRUMENTATION CODING SYSTEM

Pickup Code	Priority	Expected Range	Required Accuracy	Remarks
P001	M	0-1,000 psig	± 2.0%	Pressure
P002	M	0-1,000 psig	± 2.0%	Pressure
D001	R	0-15 in.	± 5.0%	Displacement
D002	R	0-15 in.	± 5.0%	Displacement
D003	R	0-15 in.	± 5.0%	Displacement
D004	R	0-15 in.	± 5.0%	Displacement
D005	R	0-15 in.	± 5.0%	Displacement
D006	R	0-15 in.	± 5.0%	Displacement
D007	R	0-15 in.	± 5.0%	Displacement
D008	R	0-15 in.	± 5.0%	Displacement
D009	R	0-15 in.	± 5.0%	Displacement
D010	R	0-15 in.	± 5.0%	Displacement
D011	R	0-15 in.	± 5.0%	Displacement
D012	R	0-15 in.	± 5.0%	Displacement
D013	R	0-5 in.	± 5.0%	Displacement
D014	R	0-5 in.	± 5.0%	Displacement
D015	R	0-5 in.	± 5.0%	Displacement
S001	R	0.030 in./in.	± 5.0%	Strain
S002	R	0.030 in./in.	± 5.0%	Strain
S003	R	0.030 in./in.	± 5.0%	Strain
S004	R	0.030 in./in.	± 5.0%	Strain
S005	R	0.030 in./in.	± 5.0%	Strain
S006	R	0.030 in./in.	± 5.0%	Strain
S007	R	0.030 in./in.	± 5.0%	Strain

TABLE I (Cont)

Pickup Code	Priority	Expected Range	Required Accuracy	Remarks
S008	R	0.030 in./in.	± 5.0%	Strain
S009	R	0.030 in./in.	± 5.0%	Strain
S010	R	0.030 in./in.	± 5.0%	Strain
S011	R	0.030 in./in.	± 5.0%	Strain
S012	R	0.030 in./in.	± 5.0%	Strain
S013	R	0.020 in./in.	± 5.0%	Strain
S014	R	0.020 in./in.	± 5.0%	Strain
S015	R	0.020 in./in.	± 5.0%	Strain
S016	R	0.020 in./in.	± 5.0%	Strain
S017	R	0.020 in./in.	± 5.0%	Strain
S018	R	0.020 in./in.	± 5.0%	Strain
S019	R	0.020 in./in.	± 5.0%	Strain
S020	R	0.020 in./in.	± 5.0%	Strain
S021	R	0.020 in./in.	± 5.0%	Strain
S022	R	0.020 in./in.	± 5.0%	Strain
S023	R	0.020 in./in.	± 5.0%	Strain
S024	R	0.020 in./in.	± 5.0%	Strain
S025	R	0.020 in./in.	± 5.0%	Strain
S026	R	0.020 in./in.	± 5.0%	Strain
S027	R	0.020 in./in.	± 5.0%	Strain
S028	R	0.020 in./in.	± 5.0%	Strain
S029	R	0.020 in./in.	± 5.0%	Strain
S030	R	0.020 in./in.	± 5.0%	Strain
S031	R	0.020 in./in.	± 5.0%	Strain
S032	R	0.020 in./in.	± 5.0%	Strain
S033	R	0.020 in./in.	± 5.0%	Strain
S034	R	0.030 in./in.	± 5.0%	Strain
S035	R	0.030 in./in.	± 5.0%	Strain

TABLE I (Cont)

Pickup Code	Priority	Expected Range	Required Accuracy	Remarks
S036	R	0.030 in./in.	± 5.0%	Strain
S037	R	0.030 in./in.	± 5.0%	Strain
S038	R	0.030 in./in.	± 5.0%	Strain
S039	R	0.030 in./in.	± 5.0%	Strain
S040	R	0.030 in./in.	± 5.0%	Strain
S041	R	0.030 in./in.	± 5.0%	Strain
S042	R	0.030 in./in.	± 5.0%	Strain
S043	R	0.030 in./in.	± 5.0%	Strain
S044	R	0.030 in./in.	± 5.0%	Strain
S045	R	0.020 in./in.	± 5.0%	Strain
S046	R	0.020 in./in.	± 5.0%	Strain
S047	R	0.020 in./in.	± 5.0%	Strain
S048	R	0.020 in./in.	± 5.0%	Strain
S049	R	0.020 in./in.	± 5.0%	Strain
S050	R	0.020 in./in.	± 5.0%	Strain
S051	R	0.020 in./in.	± 5.0%	Strain
S052	R	0.020 in./in.	± 5.0%	Strain
S053	R	0.030 in./in.	± 5.0%	Strain
S054	R	0.030 in./in.	± 5.0%	Strain
S055	R	0.030 in./in.	± 5.0%	Strain
S056	R	0.030 in./in.	± 5.0%	Strain
S057	R	0.030 in./in.	± 5.0%	Strain
S058	R	0.030 in./in.	± 5.0%	Strain
S059	R	0.030 in./in.	± 5.0%	Strain
S060	R	0.030 in./in.	± 5.0%	Strain

APPENDIX III

TEST PLAN FOR
TU-393 ROCKET MOTOR CASE
7U37721-04 S/N 2
HYDROTEST
REV. A

TWR-1410
Rev. A

TEST PLAN

FOR

TU-393 ROCKET MOTOR CASE

7U37721-04 S/N 2

HYDROTEST

Rev. A

17 January 1966

THIOKOL CHEMICAL CORPORATION

WASATCH DIVISION

BRIGHAM CITY, UTAH

TWR-1410
Rev. A

THIOKOL CHEMICAL CORPORATION

WASATCH DIVISION

BRIGHAM CITY, UTAH

TEST PLAN

FOR

TU-393 ROCKET MOTOR CASE

7U37721-04 S/N 2

HYDROTEST

PREPARED BY:

R. F. Zeigler
Large Space Booster
Project Engineering

APPROVED BY:

C. R. Bratton
Large Space Booster
Project Engineering

D. A. Sherar
Manager
Test Division

FOREWORD

This test plan covers the hydrotesting of a TU-393 fiberglass reinforced plastic rocket motor case. It has been prepared by Thiokol Chemical Corporation for use on Contract AF 04(695)-773.

TABLE OF CONTENTS

I. INTRODUCTION

The TU-393 case S/N 2 per drawing 7U37721-04 will be hydroproof tested, then loaded and static tested. This case is different from case S/N 1 only in that the insulation has been installed and other minor design improvements incorporated. Test setup, equipment and instrumentation procedures will be the same. The amount and location of instrumentation is different to obtain maximum data. The insulation surface will be protected by a waterproof bag during hydrotesting.

II. OBJECTIVES

A. The primary objective in hydrotesting case No. 2 is to prove the case satisfactory for subsequent loading and firing.

B. Secondary objectives of the test are:

1. To verify the manufacturing methods, process controls, quality assurance provisions, etc., used to fabricate the case.

2. To demonstrate the feasibility of using large filament wound plastic cases for solid propellant rocket motors.

3. To determine behavior characteristics of large plastic cases including:

Percent elongation of glass laminate

Deflections

Stress/strain relationships

III. HARDWARE INSPECTION

A. Pretest

The following pretest inspection of the case and related test hardware shall be performed prior to pressurization. Departures and deviations, to this plan, or established drawings shall be coordinated with the cognizant Project Engineer.

1. Visually inspect the outside case wall and note any apparent flaws by description and location.

2. Measure and record the length at each longitudinal extensometer location.

3. Measure and record the case circumference at each circumferential extensometer location.

4. Measure and record the actual location of each strain gage.

B. Post-test

Post-test evaluations will be directed by the Project Engineer.

IV. INSTRUMENTATION

Instrumentation will be installed on the case assembly in accordance with Instrumentation Installation Drawing 7U37716-01. All instrumentation readings will be recorded continuously throughout the test (see Table I for Instrumentation Coding System).

A. Strain Gages

Thirty (30) strain gages will be located on the case as shown on the instrumentation drawing. Overall accuracy of the strain measurements will be $\pm$ 5 percent, at 3 percent strain.

B. Extensometers

Ten (10) extensometers will be located on the case per the instrumentation drawing (7U37716-01). Overall accuracy of extensometer measurements will be $\pm$ 5 percent at maximum deflection.

C. Pressure Transducers

Two (2) pressures will be recorded continuously at the aft dome. The tranducers will be loacted as close to the case as possible. Overall accuracy of the pressure measurements will be $\pm$ 2 percent.

The test will be conducted in Test Bay T-17 of the Wasatch Division Test Area. The test stand shall be assembled per drawing 2U25060-02. Pumping facilities shall be capable of delivering 300 gpm at a pressure of 1, 500 psig. There will be a minimum of 1, 000 gallons makeup water required to reach failure pressure.

The case will be hydrotested in the vertical position with the forward skirt resting on the base structure of the test stand (per Test Stand Drawing 2U25060-02).

Nozzle thrust is simulated by a floating piston in a flanged cylinder attached to the aft polar boss. This thrust load is applied to the overhead test stand structure by the piston and is reacted against the forward skirt by the base structure.

The piston cylinder device allows free axial expansion of the case while lateral and gimbal bearing units compensate for any twisting or lateral movements.

Pressurization fluid shall be water at ambient temperature.

V. TEST PROCEDURE

A. The case will be installed in the test stand and aligned. The floating piston will be installed in the aft section and the assembly of the test stand completed.

B. Instrumentation will be installed.

C. The case shall be inspected as specified in Section III A.3 and A.4 Pretest Inspection.

D. The portable pumping facility will be connected and the air and the case purged.

E. The case will then be leak tested at 100 psig for ten (10) minutes before returning to 0 psig pressure. Criteria for successful leak test is zero leakage. A cognizant Project Engineer must be present for observation and evaluation in this cycle.

F. Instrumentation will be zeroed and balanced--cameras will be loaded.

G. The case will then be pressurized to 775 $^{+10}_{-0}$ psig at the prescribed rate of 4 psig per second (min) to 8 psig per second (max). The pressure will be held for held for 120 $^{+5}_{-0}$ seconds and then reduced to a zero at a maximum rate of 15 psig per second.

VI. PHOTOGRAPHIC COVERAGE:

Photographic coverage for the proof test at 790 psig will consist of the following:

1. Two (2) high speed cameras (64 frames per second). One located to provide an unobstructed view of the entire motor case and the other to provide an unobstructed view of the aft case area. This will include the piston assembly and aft portion of the test stand.

2. Appropriate still photographs in color and black and white will be taken to document the entire test effort. This will include installing the case in the test stand, instrumentation, test setup, test stand, etc., in all phases of buildup.

3. Documentary still photographs will be taken of the completed setup before and after test.

4. Two (2) high speed cameras (400 frames per second) will be placed to give an unobstructed view of the case.

VII. DATA REDUCTION AND REPORT SCHEDULE

A. All films will be processed within three (3) working days.

B. Selective gages (selected by Development Engineering with the aid of the film) shall be run through the quick look recorder.

C. Following the quick look run, the tapes will be processed through the IBM and the IBM output will be made available to Development Engineering within five (5) days.

D. Final data from the hydrotest will be made available to Development Engineering within six (6) working days following receipt of the IBM runs.

E. Development Engineering will analyze the data and prepare a test report four (4) weeks after the hydrotest.

VIII. REFERENCED DRAWINGS

7U37721	Case Assembly - TU-393
7U37722	Adapter Assembly Rocket Motor FWD
7U37716	Instrumentation Installation - TU-393
2U25060	Hydrostatic Test Stand

TABLE I

INSTRUMENTATION CODING SYSTEM

Pickup Code	Priority	Expected Range	Required Accuracy	Remarks
P001	M	0-1,000 psig	± 2.0%	Pressure
P002	M	0-1,000 psig	± 2.0%	Pressure
D001	R	0-5 inches	± 5.0%	Displacement
D002	R	0-5 inches	± 5.0%	Displacement
D003	R	0-5 inches	± 5.0%	acement
D005	R	0-15 inches	± 5.0%	placement
D006	R	0-15 inches	± 5.0%	Displacement
D007	R	0-15 inches	± 5.0%	Displacement
D008	R	0-5 inches	± 5.0%	Displacement
D009	R	0-5 inches	± 5.0%	Displacement
D010	R	0-3 inches	± 5.0%	Displacement
D011	R	0-3 inches	± 5.0%	Displacement
S001	R	0-0.030 in./in.	± 5.0%	Strain
S002	R	0-0.030 in./in.	± 5.0%	Strain
S003	R	0-0.030 in./in.	± 5.0%	Strain
S004	R	0-0.030 in./in.	± 5.0%	Strain
S005	R	0-0.030 in./in.	± 5.0%	Strain
S006	R	0-0.030 in./in.	± 5.0%	Strain
S007	R	0-0.030 in./in.	± 5.0%	Strain

TABLE I (Cont)

INSTRUMENTATION CODING SYSTEM

Pickup Code	Priority	Expected Range	Required Accuracy	Remarks
S008	R	0-0.030 in./in.	± 5.0%	Strain
S009	R	0-0.030 in./in.	± 5.0%	Strain
S010	R	0-0.030 in./in.	± 5.0%	Strain
S011	R	0-0.030 in./in.	± 5.0%	Strain
S012	R	0-0.030 in./in.	± 5.0%	Strain
S013	R	0-0.030 in./in.	± 5.0%	Strain
S014	R	0-0.030 in./in.	± 5.0%	Strain
S015	R	0-0.030 in./in.	± 5.0%	Strain
S016	R	0-0.030 in./in.	± 5.0%	Strain
S017	R	0-0.030 in./in.	± 5.0%	Strain
S018	R	0-0.030 in./in.	± 5.0%	Strain
S019	R	0-0.030 in./in.	± 5.0%	Strain
S020	R	0-0.030 in./in.	± 5.0%	Strain
S021	R	0-0.030 in./in.	± 5.0%	Strain
S022	R	0-0.030 in./in.	± 5.0%	Strain
S023	R	0-0.030 in./in.	± 5.0%	Strain
S024	R	0-0.030 in./in.	± 5.0%	Strain
S025	R	0-0.030 in./in.	± 5.0%	Strain
S026	R	0-0.030 in./in.	± 5.0%	Strain
S027	R	0-0.030 in./in.	± 5.0%	Strain

TABLE I (Cont)

INSTRUMENTATION CODING SYSTEM

Pickup Code	Priority	Expected Range	Required Accuracy	Remarks
S028	R	0-0.030 in./in.	± 5.0%	Strain
S029	R	0-0.030 in./in.	± 5.0%	Strain
S030	R	0-0.030 in./in.	± 5.0%	Strain

APPENDIX IV

STRESS ANALYSIS
OF
THIOKOL TU-393 MOTOR

MSC Report No. 65-33-1

STRESS ANALYSIS OF THIOKOL TU-393 MOTOR

Final Report
Contract No. 65-04527
October, 1965

to

THIOKOL CHEMICAL CORPORATION
WASATCH DIVISION

Approved by

M. E. Fourney
Director of Engineering

MATHEMATICAL SCIENCES CORPORATION
Seattle Office
1107 Northeast 45th Street
Seattle, Washington

TABLE OF CONTENTS

1. INTRODUCTION

A stress analysis of the Thiokol solid propellant motor TU-393 has been conducted. The analysis used was based on linear elastic theory and utilized a finite element stiffness method approach. Two loading conditions were considered, internal pressurization and a uniform temperature variation. This motor is encased in a Fiberglas case. The analysis performed accounts for the orthotropic characteristics of the case. The results of this analysis are presented in the form of plots of stresses, strains, and displacements at various locations in the motor. Also the entire computer data output is present in the Appendix to this report.

The analysis is complicated by the presence of an irregular star-shaped perforation of the forward portion of the grain. This portion is analyzed using the results of photoelastic studies. The results of this analysis are also presented in this report.

2. PROCEDURE

In this analysis the stresses and deformations are determined under the restriction of linear elasticity. The solution is complicated by the presence of a star shape in the forward 30 percent of the inner bore, the aft portion of the bore being circular. The star perforation was evaluated using photoelastic results. An equivalent axisymmetric grain was analyzed by MSC's stiffness method programs. The results are combined

in Section 5 to obtain an estimation of the actual three-dimensional stress and strain states. In the propellant the star-perforated section of the inner bore was replaced by a circular port, the radius of the circular port being an equal area radius. This results in a geometry which is a circular port in the head end of one radius expanding at station 44.8 (i.e., z the axial location is 44.8 inches from the head end) to a larger circular port. This provides a circular port to circular port transition geometry to represent the star-perforated port to circular port transition. Since the case liner and filler materials have material properties similar to the propellant, they were considered part of the propellant grain. This results in the equivalent axisymmetric grain shown in Figure 1. Two separate numerical analyses were conducted, one using the geometry defined by ABCFED and the other using the geometry defined by ABC'FED of Figure 1. Geometry C was used in one analysis for numerical reasons.

For the Fiberglas case two idealizations were employed. The aluminum bosses for retaining the head-end closure and the nozzle were viewed as rigid boundaries in rotation and radial deflection. In addition the aft end was held in the axial direction to prevent rigid body motion in the analysis, the head end being free to expand in the axial direction. These case boundary conditions are shown in Figure 2. In order to account for the "Y" joints in the case the thickness was increased to one inch at both locations. The resulting variation in case thickness is shown in Table 1. The case thickness varies linearly between the points given.

Two values of the elastic modulus were used to approximate the viscoelastic behavior of the propellant. For the internal pressurization a short-time modulus of 1,000 lbs/in^2 was used. For the uniform thermal contraction (equivalently cure shrinkage and cooldown) a long-time modulus of 200 lbs/in^2 was used. In all problems the value of Poisson's ratio was held constant at 0.49. For the coefficient of thermal expansion a typical value of 5.75×10^{-5} in/in$^{\circ}$F was used.

For the Fiberglas case the orthotropic material properties supplied by the Thiokol Chemical Corporation were used. They are as follows:

$$E_{Cir.} = 6.17 \times 10^6 \text{ lbs/in}$$
$$E_{Long.} = 4.78 \times 10^6 \text{ lbs/in} .$$

An average value of 0.25 for Poisson's ratio was provided by TCC. Since symmetry requires

$$\nu_{CL} E_L = \nu_{LC} E_C ,$$

the Poisson's ratios were taken as

$$\nu_{CL} = 0.282$$
$$\nu_{LC} = 0.218 .$$

Typically in Fiberglas cases the product $\alpha_L E_L$ equals $\alpha_C E_C$. Thus, the values for the coefficients of thermal expansion were taken as

$$\alpha_C = 5 \times 10^{-6} \text{ in/in}^{\circ}\text{F}$$
$$\alpha_L = 6.4 \times 10^{-6} \text{ in/in}^{\circ}\text{F} .$$

3. INTERNAL PRESSURE

Since the flaps at either end of the motor are filled and sealed after manufacture, they were assumed to be nonexistent for the pressure loading condition. The pressure acts on the inner bore between the points A and C or C' shown in Figure 1. The pressure loading occurs during ignition, thus the short-time modulus of 1,000 lbs/in^2 was used to represent the response of the propellant.

The propellant was bonded to the case from the point A to point F as shown in Figure 1. The propellant was held rigidly from F to C or C'; this is the location of the aft-end boss. The shear load experienced by the case due to the reaction of the head-end closure under pressurization is shown in Figure 2 as V_z.

The major results of this analysis are shown in Figures 3 through 13 for an internal pressure of 100 lbs/in^2. Figures 3 and 4 show the case displacements, while Figures 5 and 6 show the bond stresses generated by the internal pressure. The overall bore behavior is shown in Figures 7 to 11. It should be noted that the peak shown in the hoop strain curve of Figure 9 does not exist in the actual motor. For the strains existing in the forward region, Section 5 dealing with the application of the concentration factors should be consulted. Figures 10 and 11 show the stress behavior in the circular port to circular port transition region. These may be used as bounding values in determining the three-dimensional stress state existing in this region of the actual motor.

These results have been obtained from two independent computer analyses. Sections I and II of the Appendix contain a complete tabulation of the computer results for internal pressure.

4. THERMAL LOADS

For use in the cure shrinkage and cooldown studies, the motor was subjected to a uniform temperature drop of 100°F. The relief flaps at either end were assumed to be unfilled and hence the grain unbonded in that region. The flap in the head end extends to a radius of 60 inches and to a radius of 47 inches in the aft end. These points are approximately located in Figure 1 by D and F, respectively.

Stresses are developed due to the difference in coefficient of thermal expansion of the case and propellant material. The propellant coefficient of expansion is approximately ten times greater than that of the case. The resulting case displacements and bond stresses are shown in Figures 14 through 17. The behavior of the bore is shown in Figures 18 through 22.

A complete tabulation of the results is contained in Section III of the Appendix.

5. APPLICATION OF CONCENTRATION FACTORS

The analysis thus far has not accounted for the star-perforated forward section of the motor. This is done by use of concentration factors determined from photoelastic studies. The photoelastic tests of Reference 1 have two assumptions which are pertinent to this analysis. The factors obtained are exact for the case of an infinitely long cylindrical grain with a uniform internal and external pressure. Hence the reaction of the case must be approximated by a uniform external pressure, and the actual stress state must be approximated by a plane strain stress state.

Obviously the stress state existing at the head end of the motor where the external boundary is a curved boundary is not one of plane strain. In the region where the web fraction is large the assumption of uniform pressure being exerted by the case is fairly good. However, in spite of these difficulties some estimation of the stress and strain fields must be made.

The geometry of the star perforation is shown in Figure 23. The outer radius b varies with the axial station. This type of configuration has been tested photoelastically by Fourney and Parmerter. A plot of the concentration factor H versus the port fraction a/b is shown in Figure 24. The variation of H with z the axial station is shown in Figure 25.

Pressure Problem

Two approaches will be used to calculate the strains that exist in the forward section of the motor. The first approach will be a straightforward plane strain analysis with a judicious selection of the equivalent circular inner port. The second approach will consider that there are two separate effects which are being approximated, the first is that of the irregular star shape, the second is the finite length of the circular cylindrical grain.

In the first approach it is necessary to calculate an interface pressure that would exist between an infinitely long flexible case and a circular port propellant grain. The difficulty here occurs in the selection of the proper equivalent grain to simulate the behavior of the star-perforated grain. This has been discussed in detail in Reference 1. Figure 26 shows the variation of the interface pressure p' with axial station. Shown in this figure are curves of p'/p_i for both the equal web fraction and equal area equivalence. Also shown is the result of the computer solution for the radial pressure at the case-grain interface. It is seen that the variation in these various "equivalents" becomes significant as z increases. Based on experience and recent results of Reference 2, a value of $p'/p_i = 0.80$ is chosen. Using this with the formulas provided in Reference 1, for an internal pressure of 550 psi a maximum strain of

$$\epsilon_{max} = 39.4\%$$

is obtained. The calculations were made for axial station z = 30" as it is felt that this is more realistic than larger values of z.

Using the second approach one assumes that the computer analysis has taken into account the effect of the finite length of the grain and the effects of the flexible case. The strain thus obtained must then be multiplied by a factor to account only for the star perforation. Hence the strains in an infinitely long grain encased in a rigid case are calculated on an equal area equivalence. The ratio of the maximum strain in a star-perforated grain to the maximum strain in a circular port grain is calculated to be: $F = 2.4$.

When one multiplies this by the strain obtained by the computer analysis of station 30 for an internal pressure of 550 psi, a maximum strain of

$$\epsilon_{max} = 42.7\%$$

is obtained.

The close agreement of the maximum strains calculated by these two approaches lends credibility to these results.

Thermal Loading

As in the pressure problem the two separate approaches will be used in calculating the stresses due to a uniform temperature change. Using the first approach the following values of interface pressure are obtained for a 100°F temperature drop at station 30:

Equal Web Fraction:	$p' = -4.9$ psi
Equal Area:	$p' = -10.7$ psi
Results from Computer Analysis:	$p' = -5.0$ psi

Hence as in the pressure problem the equal web fraction and computer solution appear to be in agreement and the value of p' for the equal web fraction is used. This results in a maximum strain of

$$(\epsilon_{max})_T = 7.7\%$$

using again the formulas presented in Reference 1.

Using the second approach a factor of $F = 2.25$ is obtained. This results in a maximum strain at station 30 of

$$(\epsilon_{max})_T = 5.4\% \quad .$$

Hence, again the close agreement leads one to the conclusion that values used should be between the values calculated.

It is important to note that the strain due to the temperature drop is of the same sign as that due to the pressurization.

6. CONCLUSIONS

A stress analysis of the Thiokol motor TU-393, under the assumptions previously stated, indicated that the maximum strains occur in the star-perforated forward portion of the grain. Due to an internal pressurization of 550 psi a maximum strain of approximately 40 percent is obtained. For a uniform temperature decrease of $100^{\circ}F$ the maximum strain occurs in the same general location and has a value of approximately six percent.

Note that these maximum strains due to temperature decrease and pressurization are additive.

The linear analysis used is not adequate to predict strains of this magnitude. A nonlinear analysis would probably show some reduction in these values. Unfortunately, the present state of the art does not permit such an analysis to be conducted.

Calculations of the strains in an infinitely long grain bonded to a flexible case with a geometry equivalent to that of the center section of the motor indicate that the strain is a strong function of Poisson's ratio. For example:

$$\nu = 0.490, \quad \epsilon_{max} = 18.6\%$$

$$\nu = 0.50, \quad \epsilon_{max} = 10.5\% \quad .$$

Therefore if the actual value of Poisson's ratio is greater than 0.49, a reduction in strain could be expected. However the actual amount of this reduction must be obtained by additional analysis and cannot be directly inferred by the results presented above.

It is the recommendation of MSC that additional analysis of and/or modification to this motor be made.

REFERENCES

1. R. R. Parmerter and M. E. Fourney, "Parametric Study of Rocket Grain Configurations by Photoelastic Analysis," MSC Report No. 65-29-6, 1 August 1965.

2. E. B. Becker and J. J. Brisbane, "The Effect of Propellant-Case Interaction on Stress/Strain Concentration Factors in Solid Propellant Rocket Grains," Bulletin of the 4th Meeting, ICRPG Working Group on Mechanical Behavior, October, 1965.

FIGURE 1

EFFECTIVE SOLID AXISYMETRIC CROSS SECTION
TCC Wasatch Div. Motor TU-393
Ref: Drawings 7U37721 and 7U37701

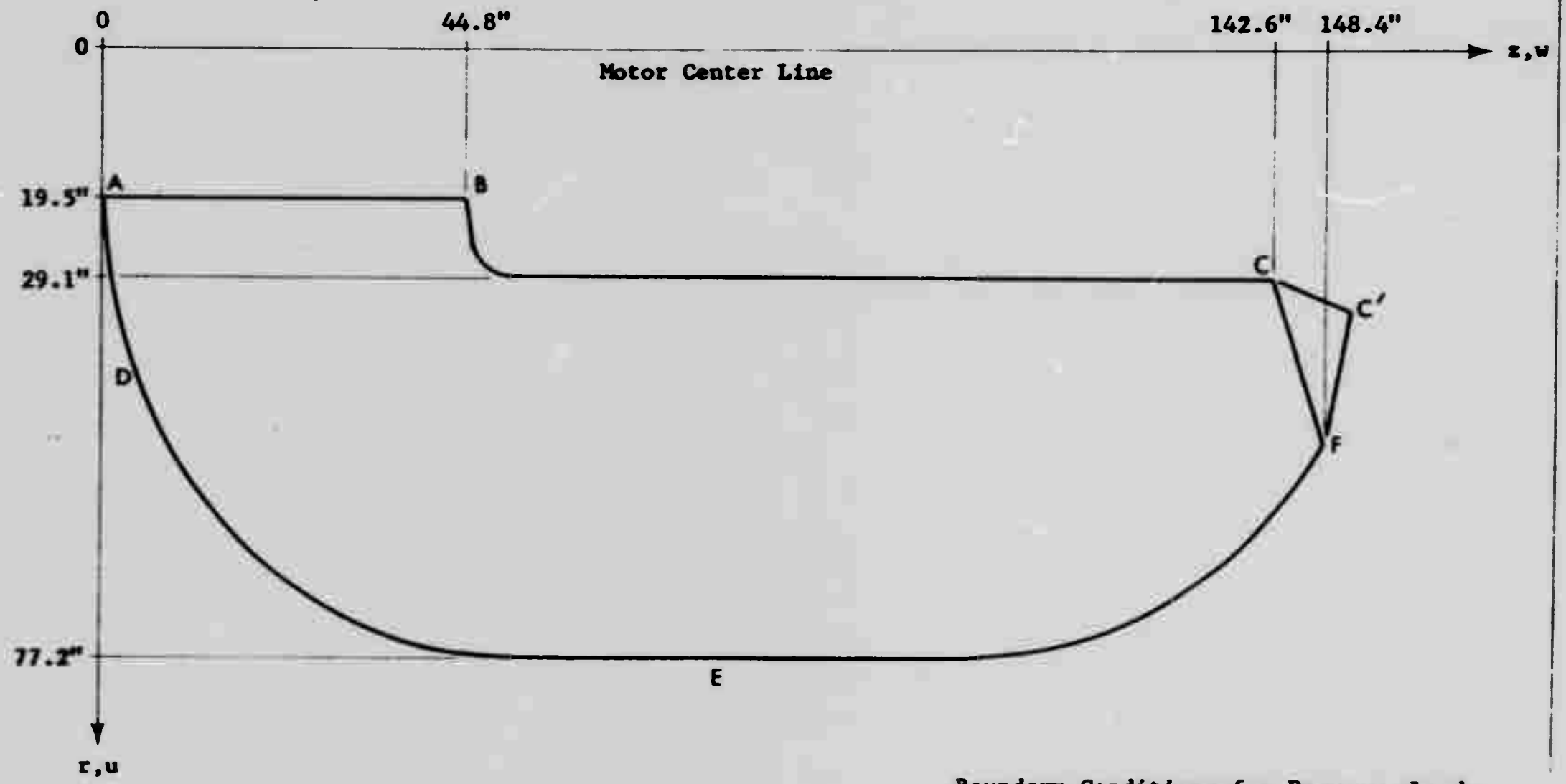

Boundary Conditions for Thermal Loads

Case Bonded D-E-F

Boundary Conditions for Pressure Loads

Internal Pressure A-B-C/C'
Case Bonded A-D-E-F-C/C'
(Rigid Boundary C/C'-F)

EFFECTIVE CASE AXISYMMETRIC CROSS SECTION
TCC Wasatch Div. Motor TU-393
Ref: Drawings 7U37721 and 7U37701

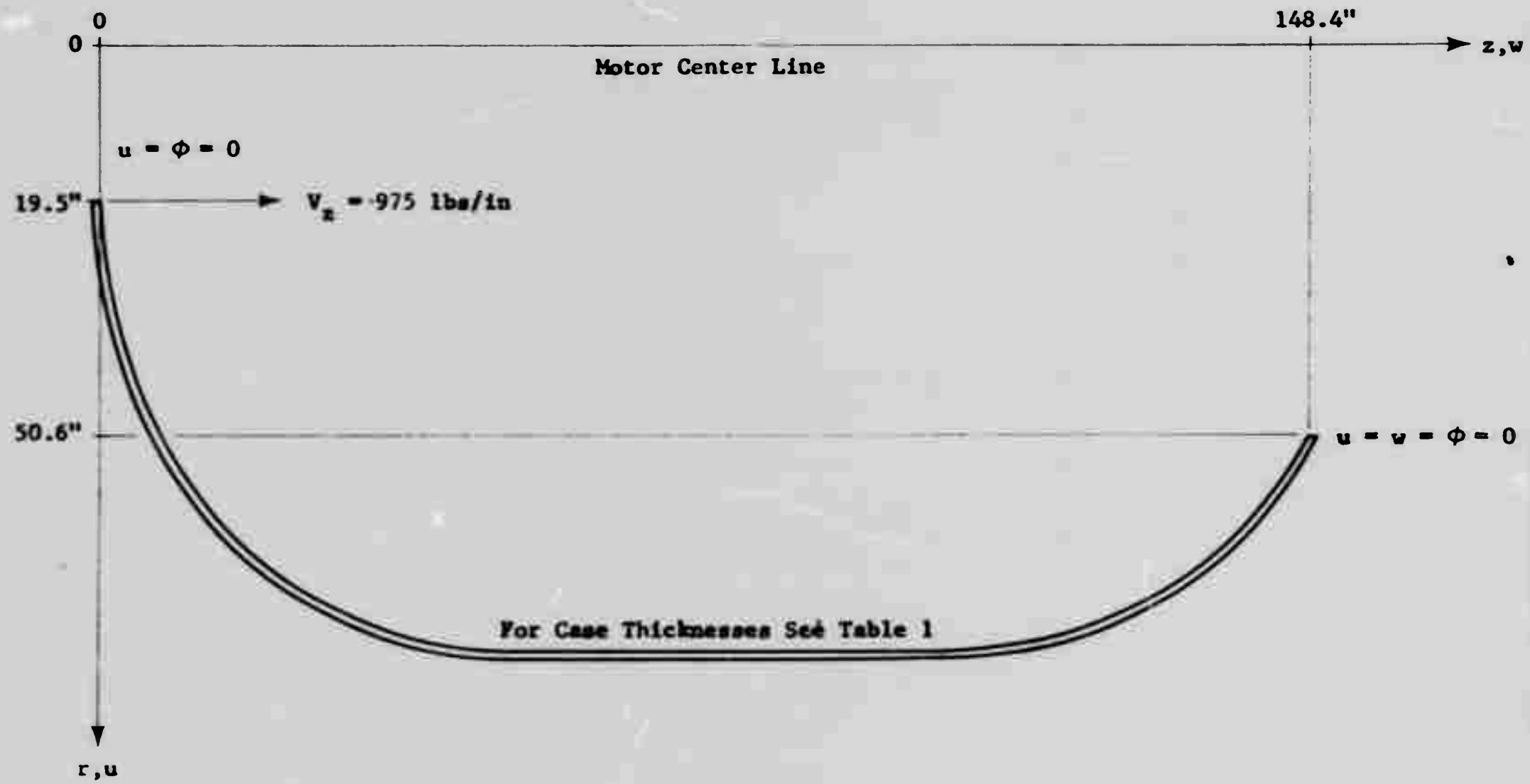

FIGURE 2

TABLE 1

CASE THICKNESSES

Case Coordinates		Case Thickness
r	z	t
19.5	0.0	1.400
32.0	1.4	0.500
44.7	4.9	0.450
56.5	11.0	0.400
66.0	19.6	0.350
73.2	30.8	0.350
76.5	43.4	1.000*
77.2	56.4	0.600
77.2	69.5	0.600
77.2	78.5	0.600
77.2	87.5	0.600
77.2	96.4	0.600
76.3	104.1	1.000*
76.1	111.9	0.350
74.5	119.5	0.350
71.5	126.6	0.350
67.2	133.0	0.400
62.0	139.0	0.450
56.2	144.0	0.550
50.6	148.4	0.650

(All Numbers in Inches)

*Added thickness to represent the behavior of the "Y" joints.

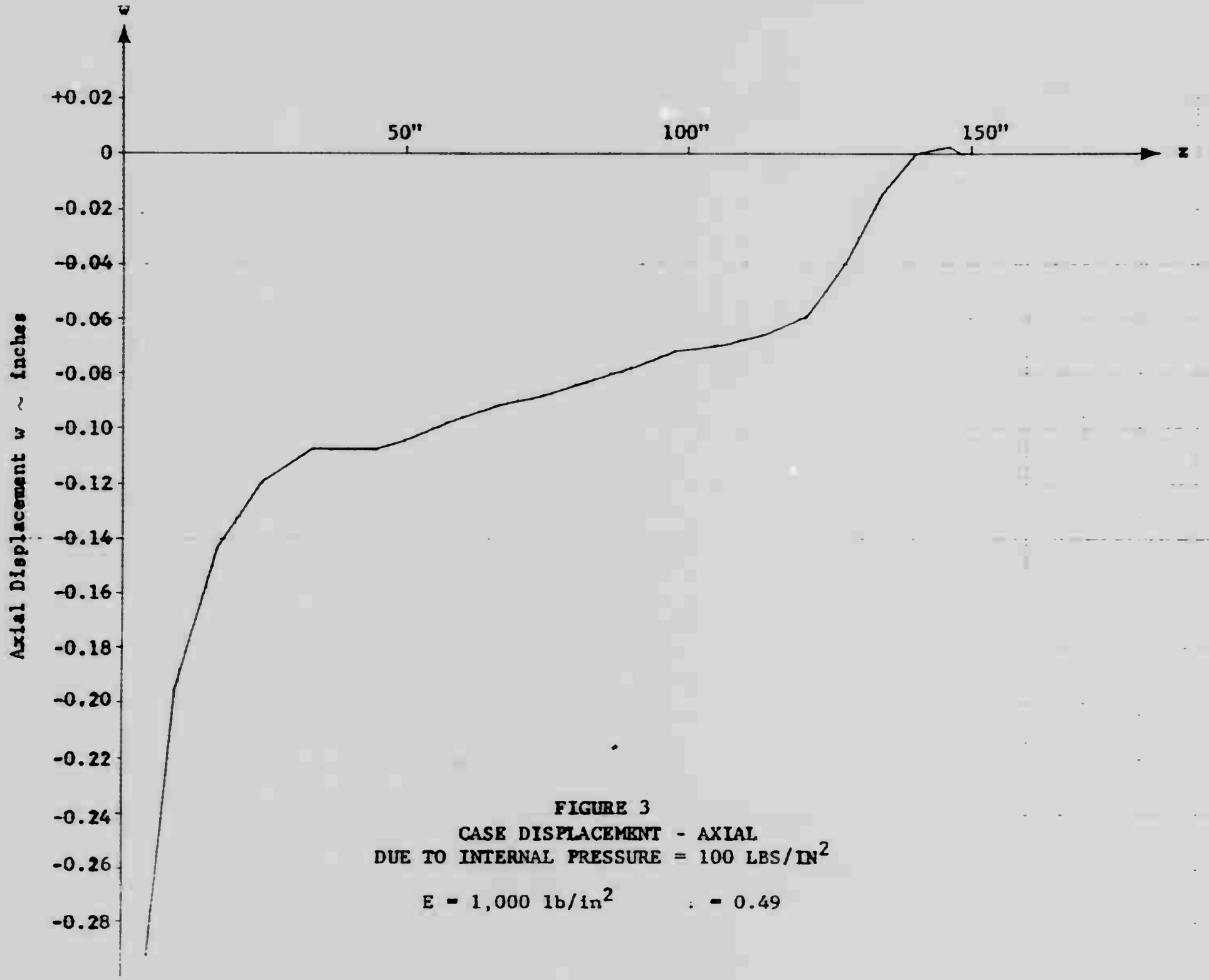

FIGURE 3
CASE DISPLACEMENT - AXIAL
DUE TO INTERNAL PRESSURE = 100 LBS/IN^2

E = 1,000 lb/in^2 : = 0.49

CASE DISPLACEMENT - RADIAL
DUE TO INTERNAL PRESSURE = 100 LBS/IN^2

E = 1,000 lbs/in^2 ν = 0.49

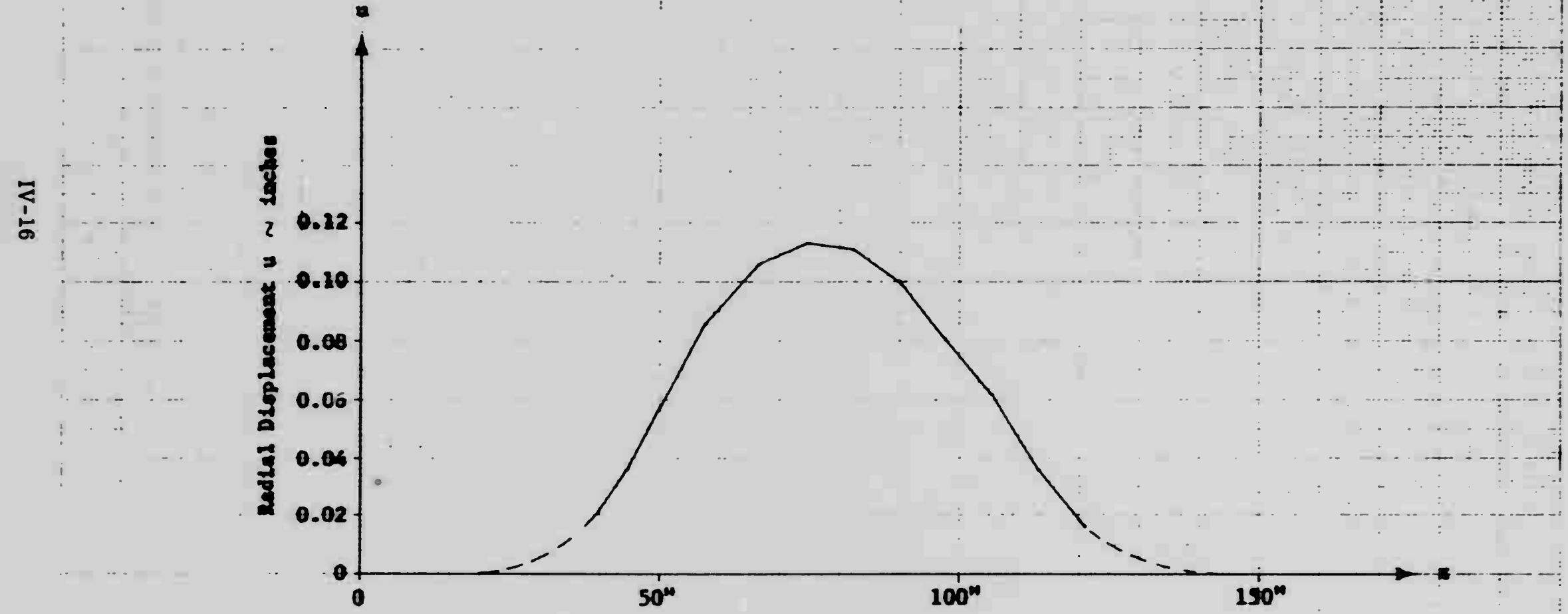

FIGURE 4

CASE BOND STRESS

Normal Stress
Due to Internal Pressure = 100 lbs/in^2

E = 1,000 lbs/in^2 ν = 0.49

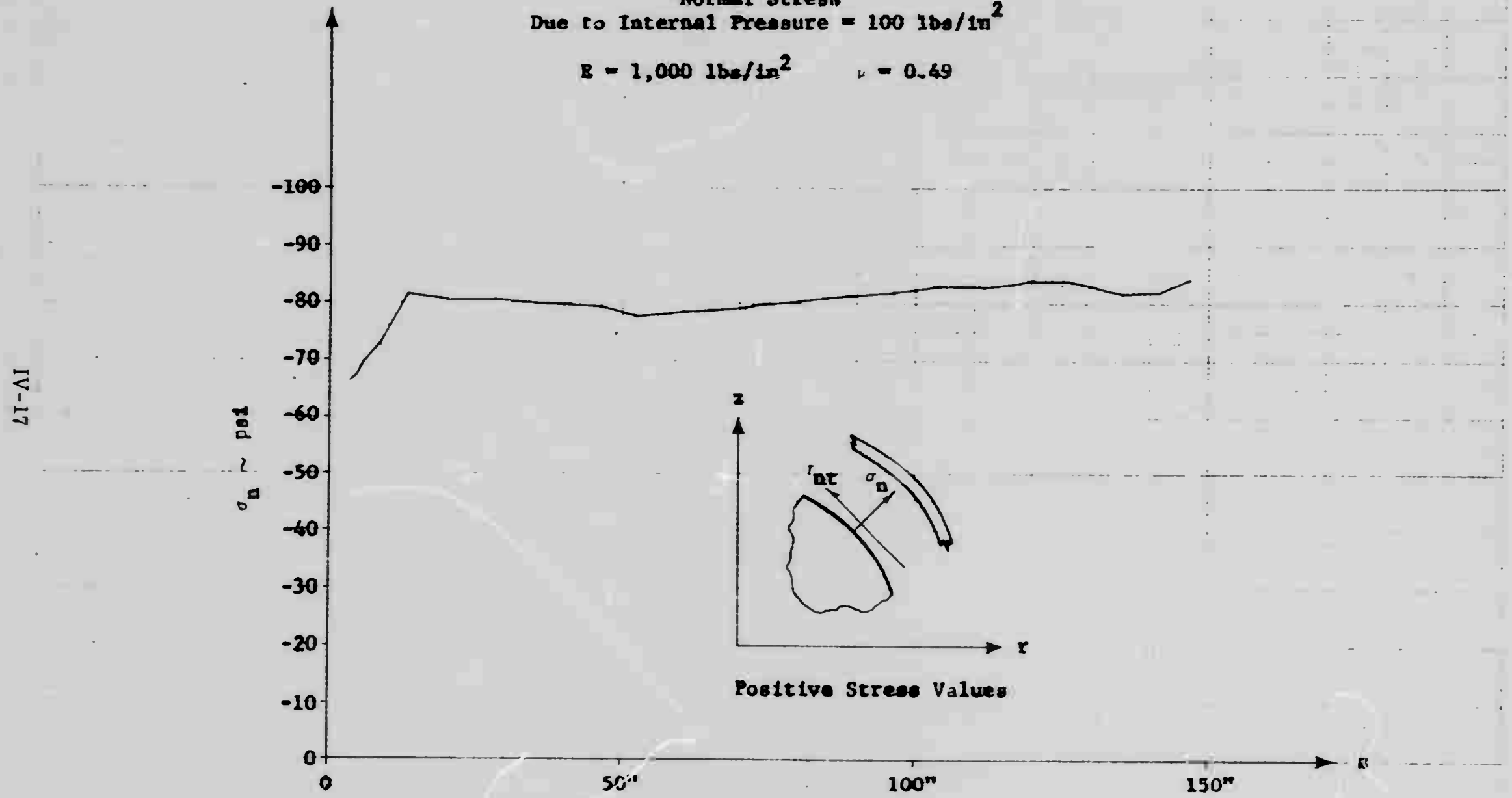

FIGURE 5

CASE BOND STRESS

Tangential Shear Stress
Due to Internal Pressure = 100 lbs/in^2

E = 1,000 lbs/in^2 ν = 0.49

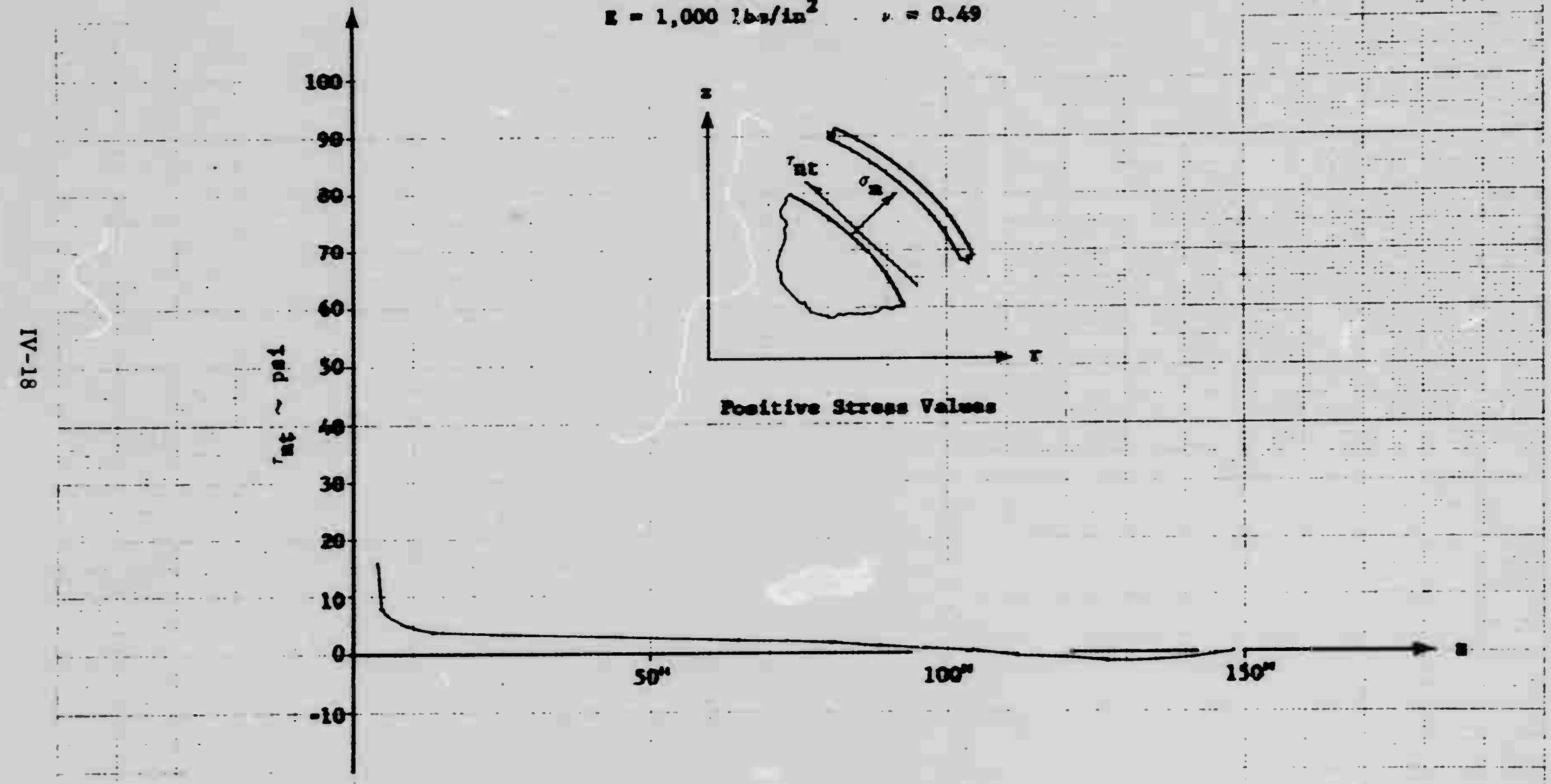

FIGURE 6

BORE DISPLACEMENT - AXIAL
DUE TO INTERNAL PRESSURE = 100 LBS/IN^2

E = 1,000 lbs/in^2 ν = 0.49

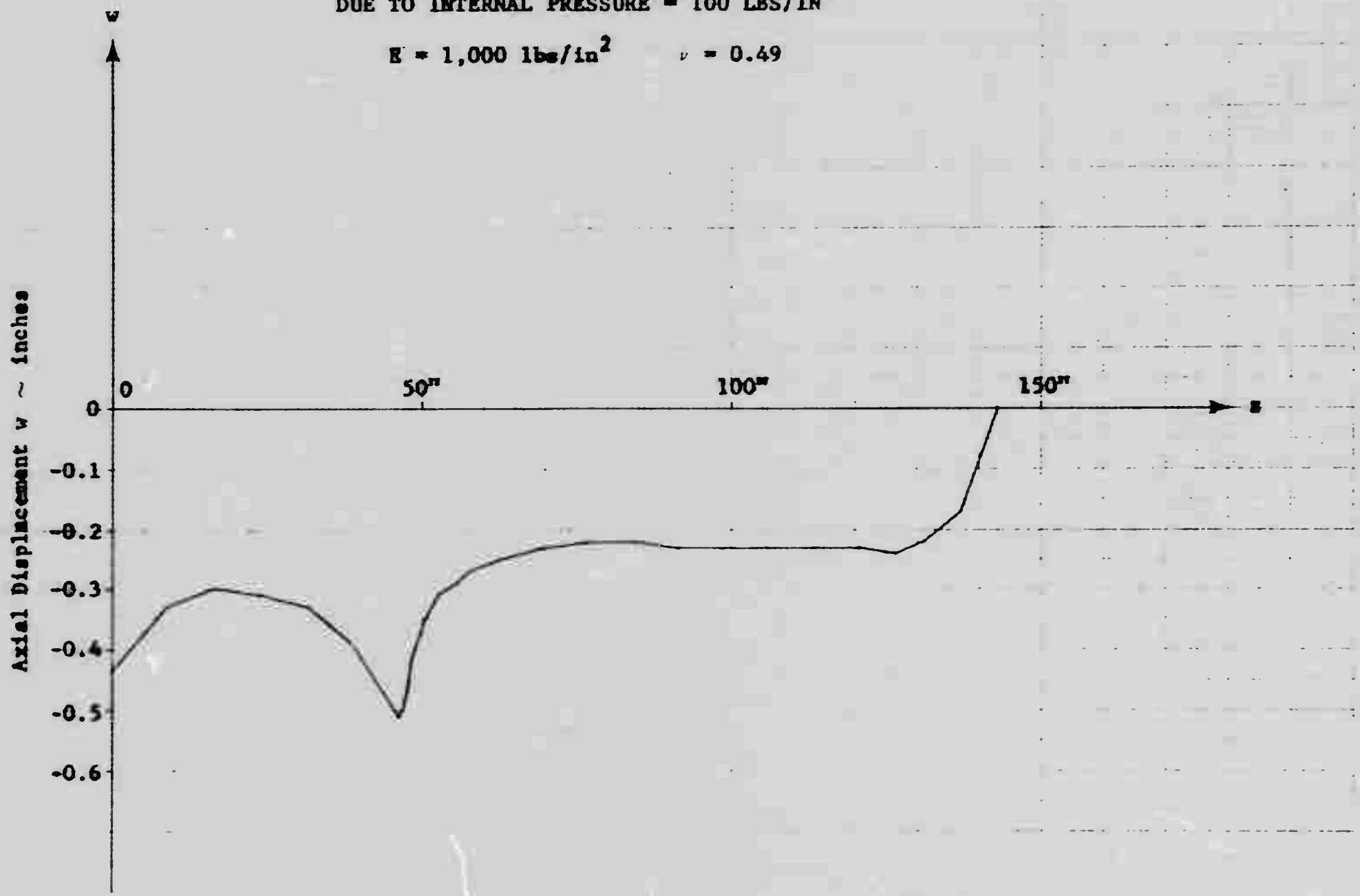

FIGURE 7

BORE DISPLACEMENT - RADIAL
DUE TO INTERNAL PRESSURE = 100 LBS/IN^2

E = 1,000 lbs/in^2 ν = 0.49

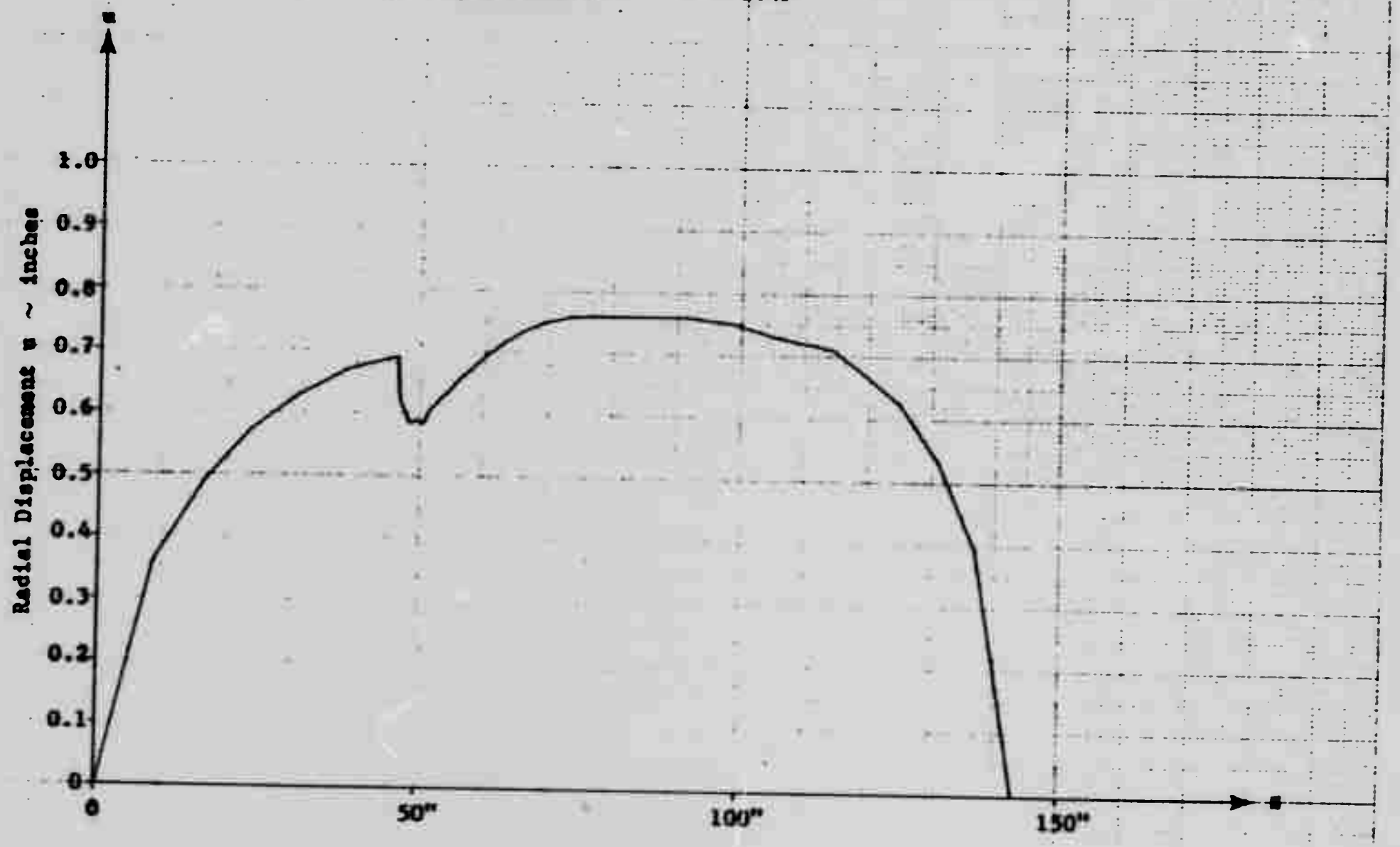

FIGURE 8

BORE STRAIN - HOOP
DUE TO INTERNAL PRESSURE = 100 LBS/IN^2

E = 1,000 lbs/in^2 ν = 0.49

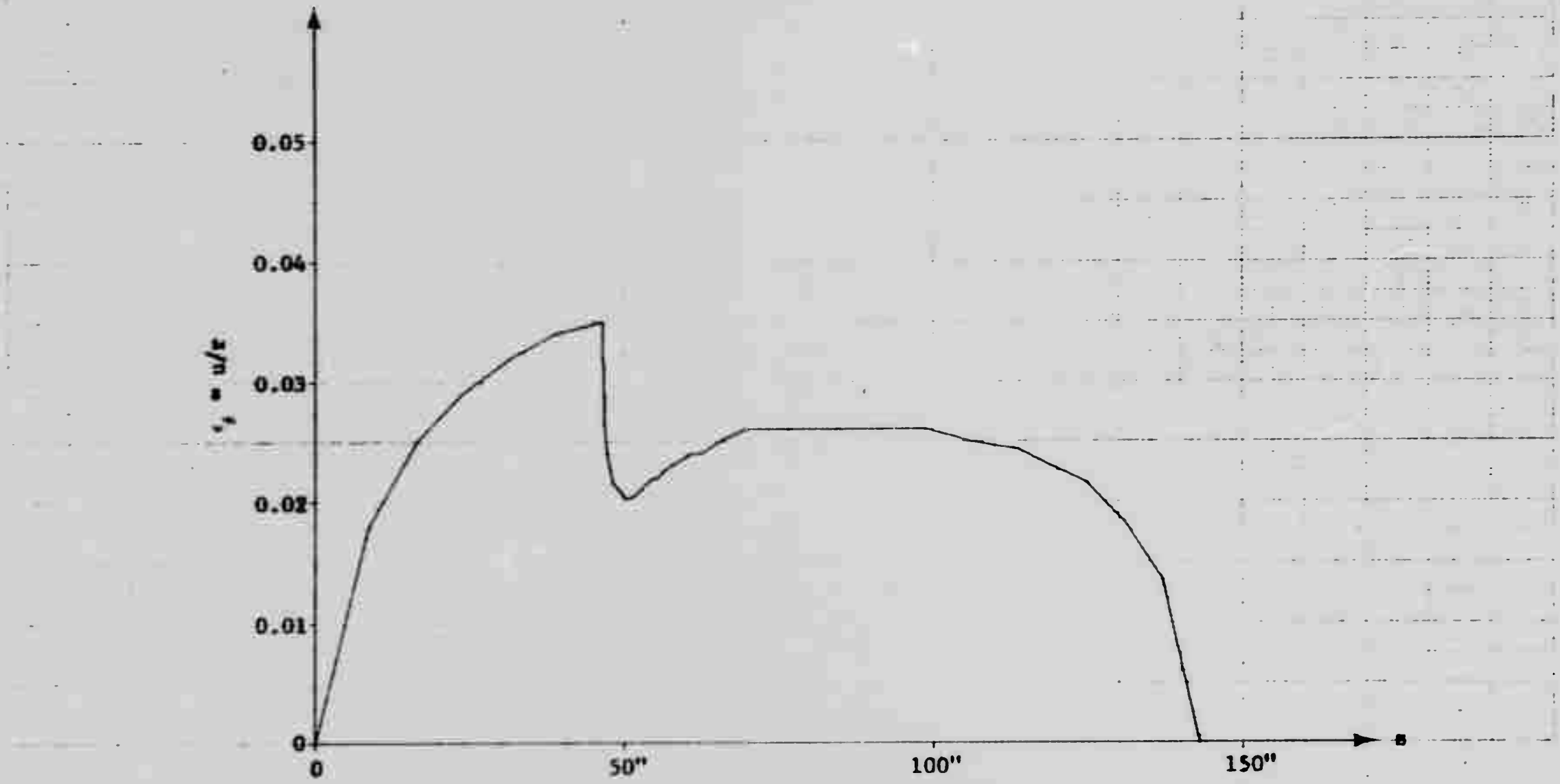

FIGURE 9

BORE STRESS - HOOP
DUE TO INTERNAL PRESSURE = 100 LBS/IN^2

E = 1,000 lbs/in^2 ν = 0.49

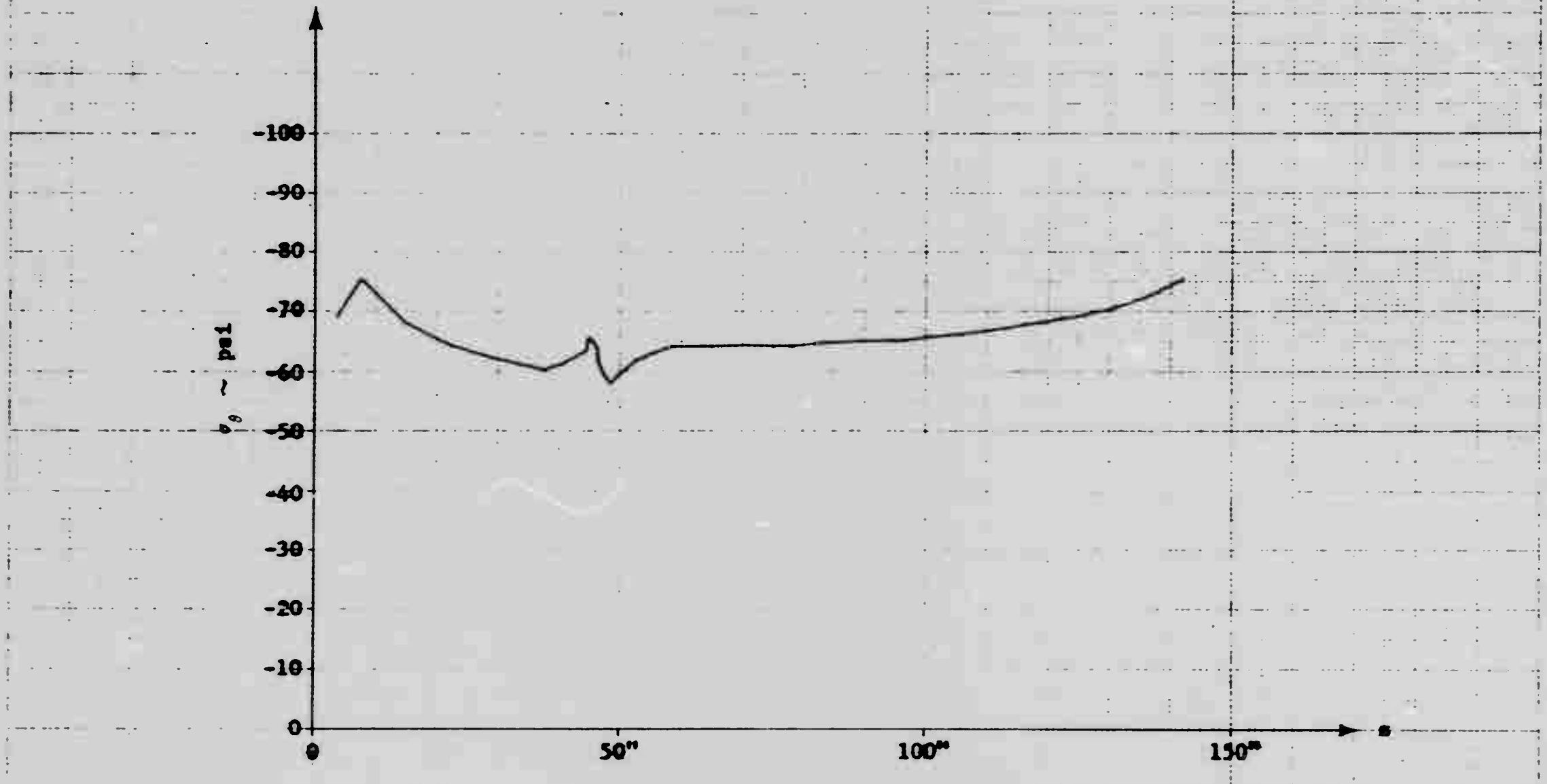

FIGURE 10

BORE STRESS - AXIAL
DUE TO INTERNAL PRESSURE = 100 LBS/IN^2

E = 1,000 lbs/in^2 ν = 0.49

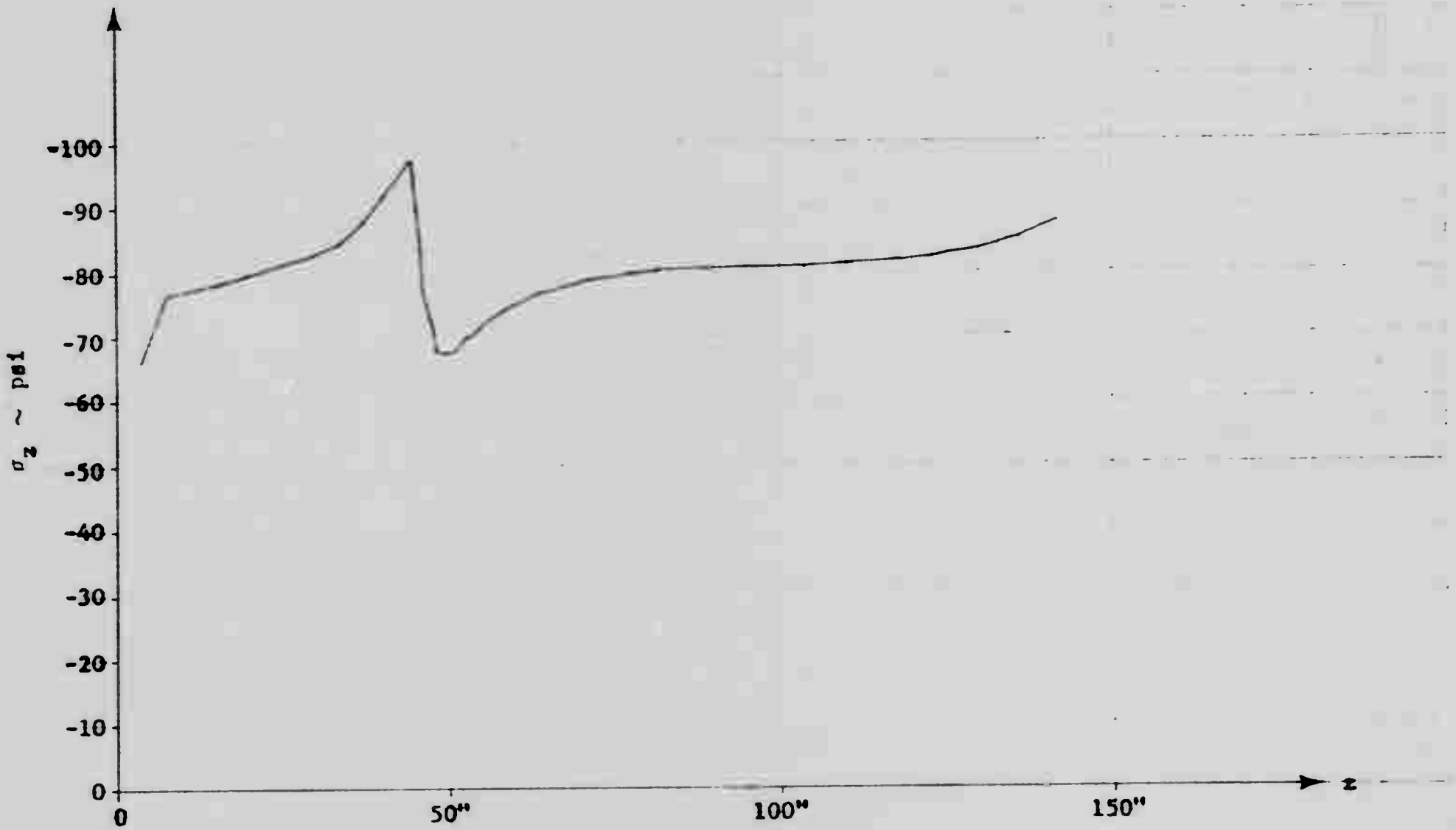

FIGURE 11

CIRCULAR PORT TO CIRCULAR PORT TRANSITION

Normal, Tangential, and Hoop Stresses
Due to Internal Pressure = 100 lbs/in^2

E = 1,000 lbs/in^2 ν = 0.49

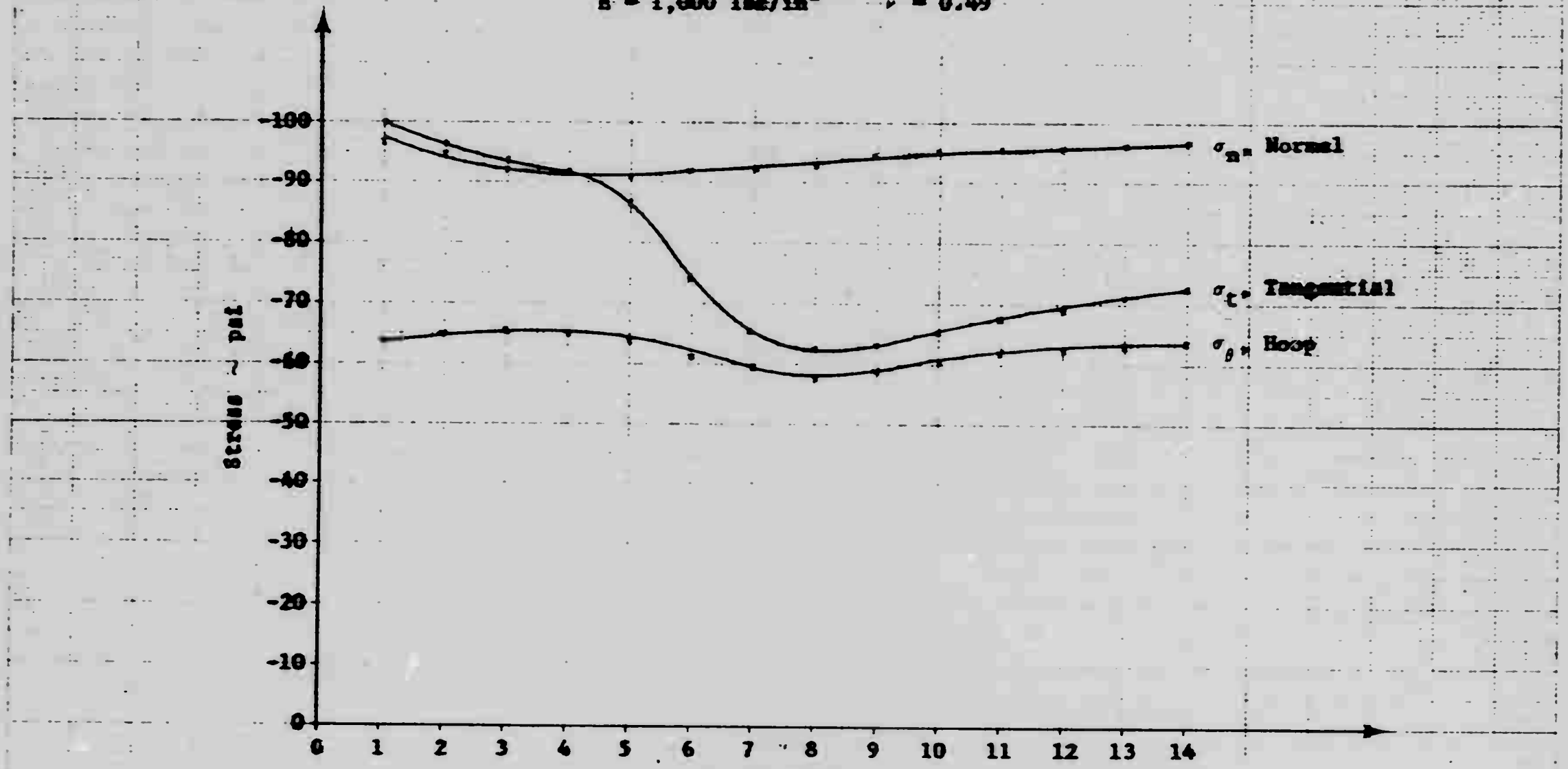

FIGURE 12

CIRCULAR PORT TO CIRCULAR PORT TRANSITION

Stress Point Locations

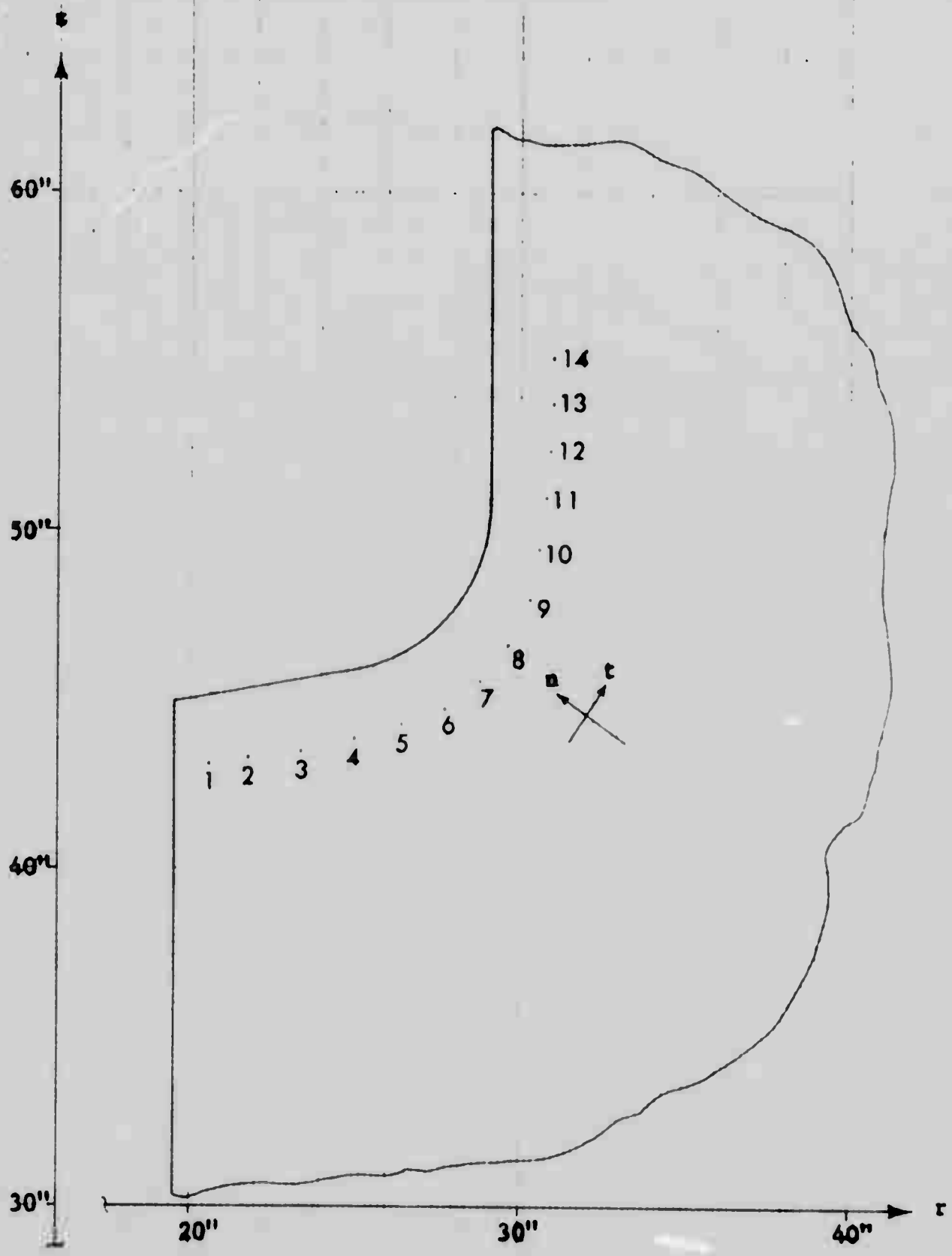

FIGURE 13

CASE DISPLACEMENT - AXIAL
DUE TO A TEMPERATURE CHANGE = -100°F

E = 200 lbs/in^2 ν = 0.49 α = 5.75 x 10^{-5} in/in°F

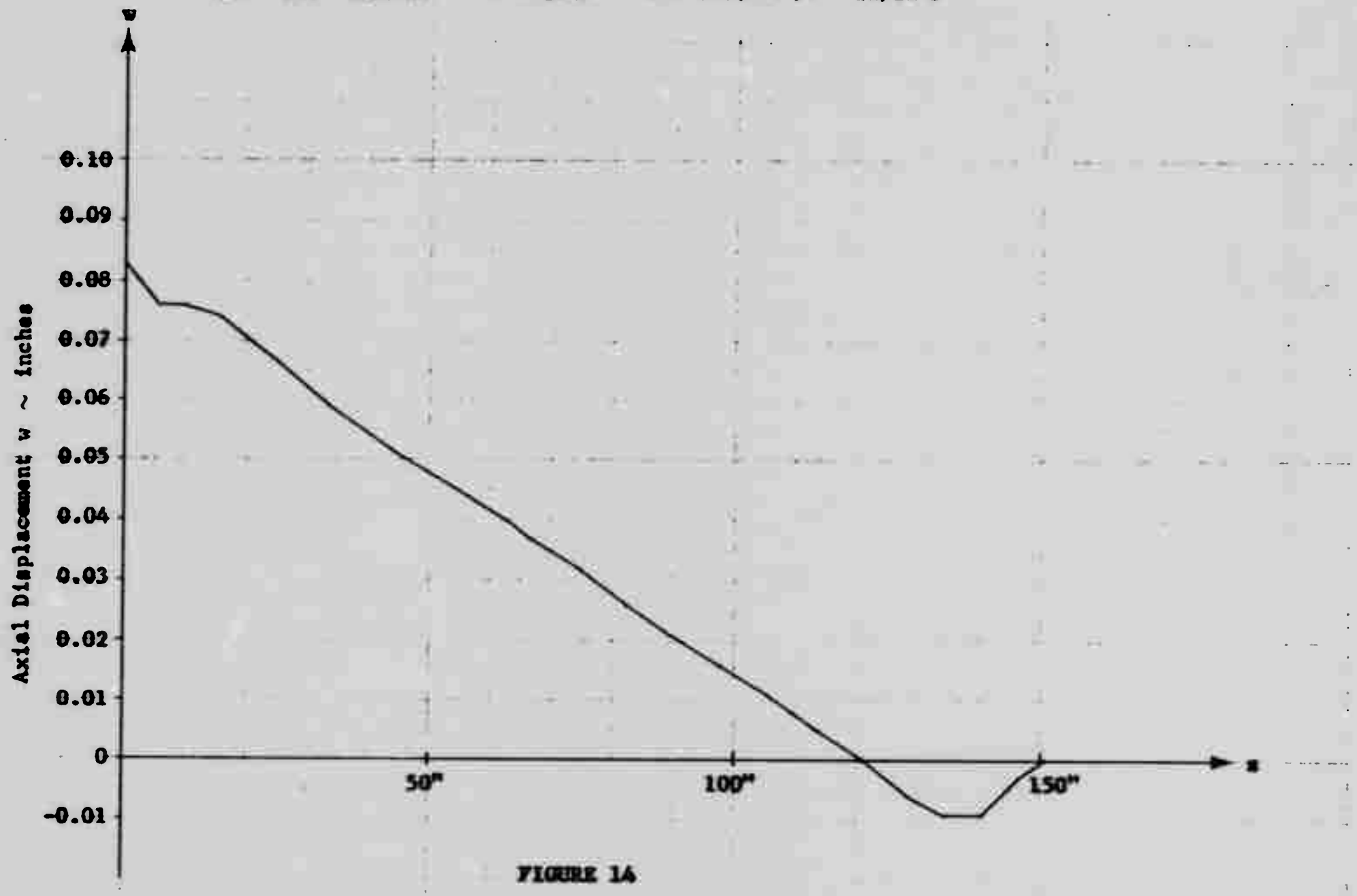

FIGURE 14

CASE DISPLACEMENT - RADIAL
DUE TO A TEMPERATURE CHANGE = -100°F

E = 200 lbs/in^2 ν = 0.49 α = 5.75 x 10^{-5} in/in°F

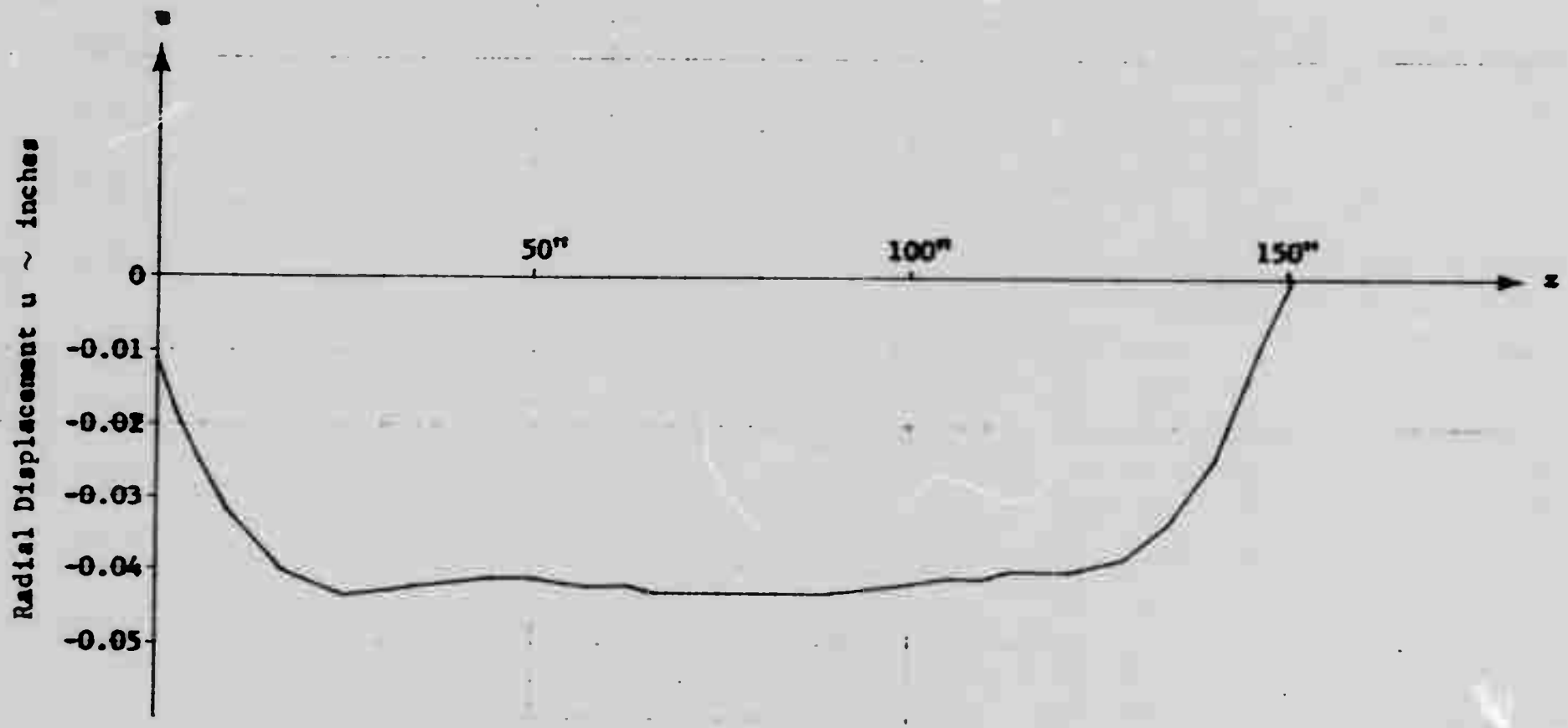

FIGURE 15

CASE STRESS

Normal Stress
Due to a Temperature Change = -100°F

E = 200 lbs/in^2 ν = 0.49

α = 5.75 x 10^{-5} in/in°F

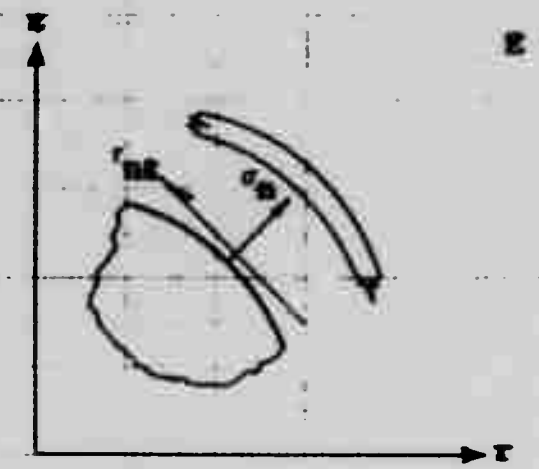

Positive Stress Values

FIGURE 16

CASE STRESS

Tangential Shear Stress
Due to a Temperature Change = -100°F

E = 200 lbs/in^2 ν = 0.49 α = 5.75 x 10^{-5} in/in°F

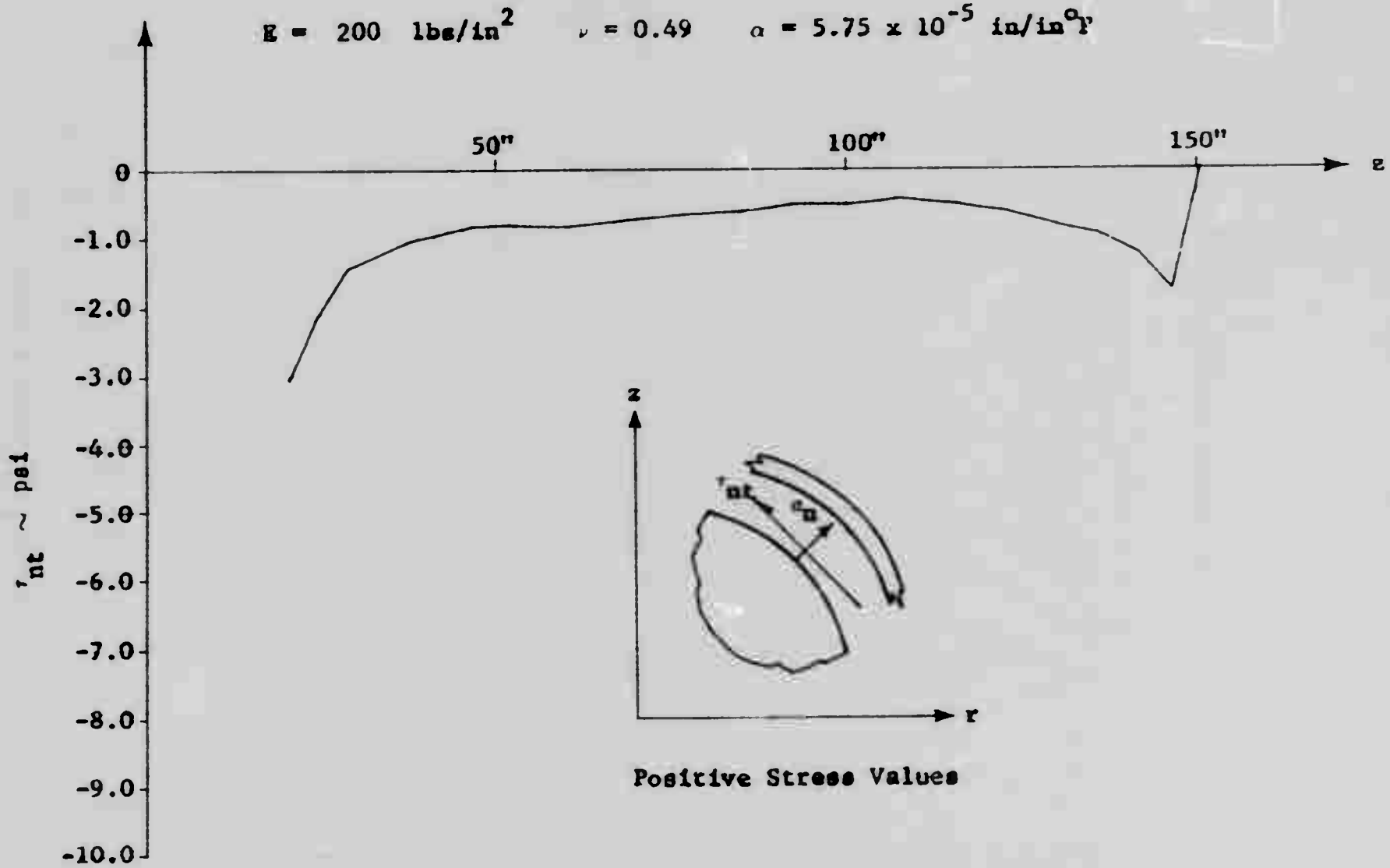

Positive Stress Values

FIGURE 17

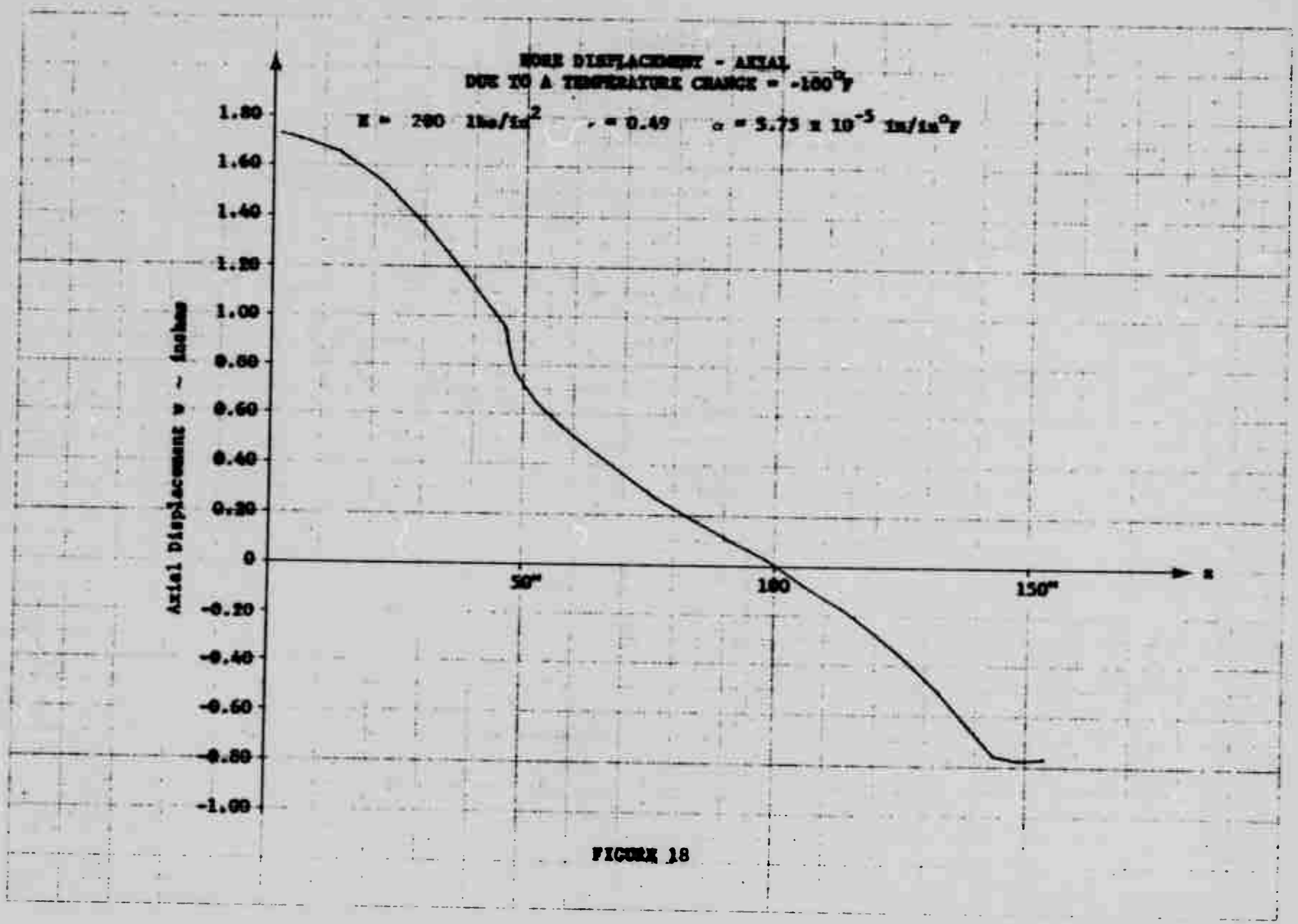
BORE DISPLACEMENT - AXIAL
DUE TO A TEMPERATURE CHANGE = -100°F
E = 280 lbs/in²
ν = 0.49
α = 5.75 x 10⁻⁵ in/in°F
Axial Displacement w - inches
1.80
1.60
1.40
1.20
1.00
0.80
0.60
0.40
0.20
0
-0.20
-0.40
-0.60
-0.80
-1.00
50"
100
150"
z

FIGURE 18

BORE DISPLACEMENT - RADIAL
DUE TO A TEMPERATURE CHANGE = -100°F

E = 200 lbs/in^2 , = 0.49 α = 5.75 x 10^{-5} in/in°F

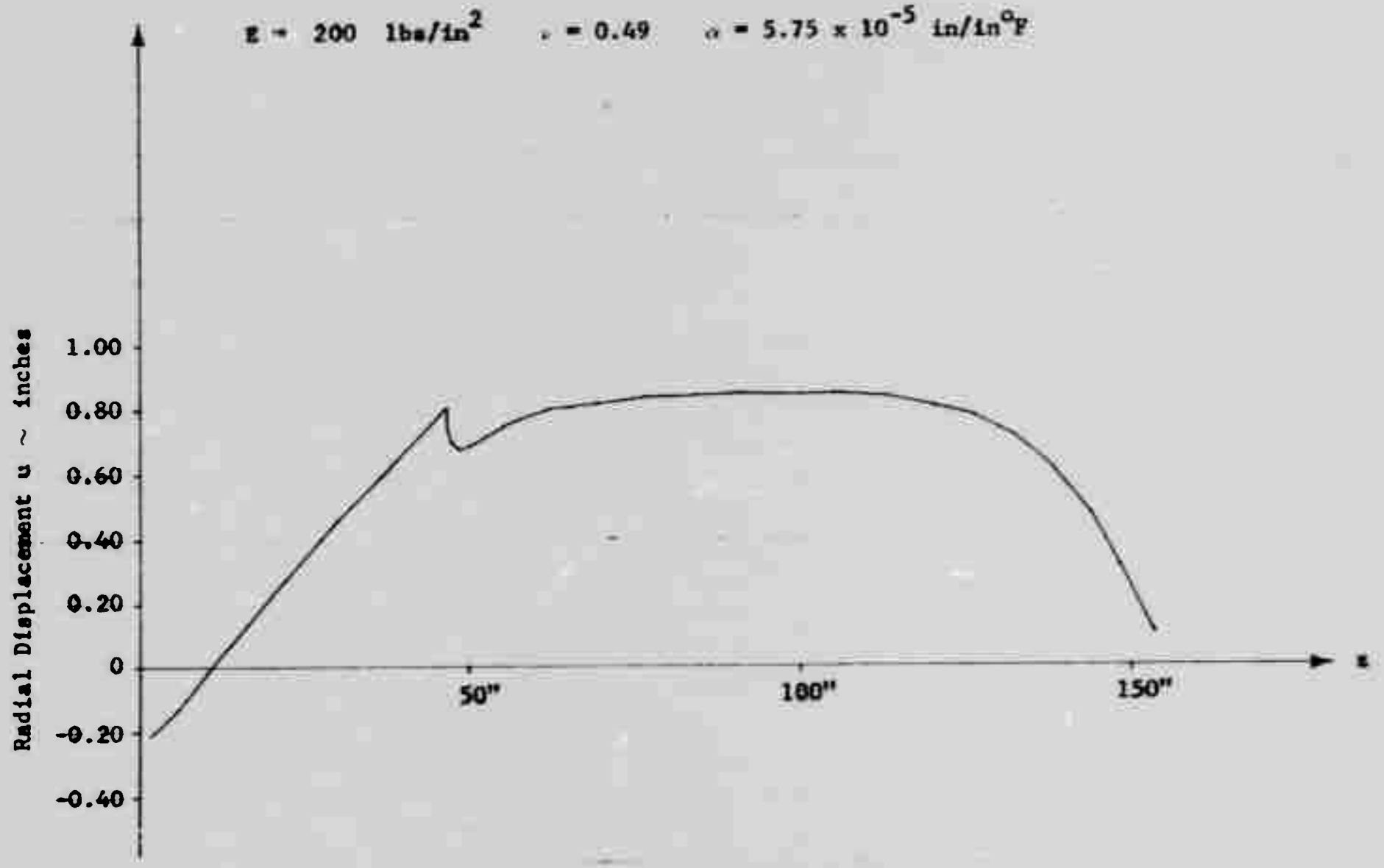

FIGURE 19

BORE STRAIN - HOOP
DUE TO A TEMPERATURE CHANGE = -100°F

E = 200 lbs/in^2 ν = 0.49 α = 5.75 x 10^{-5} in/in°F

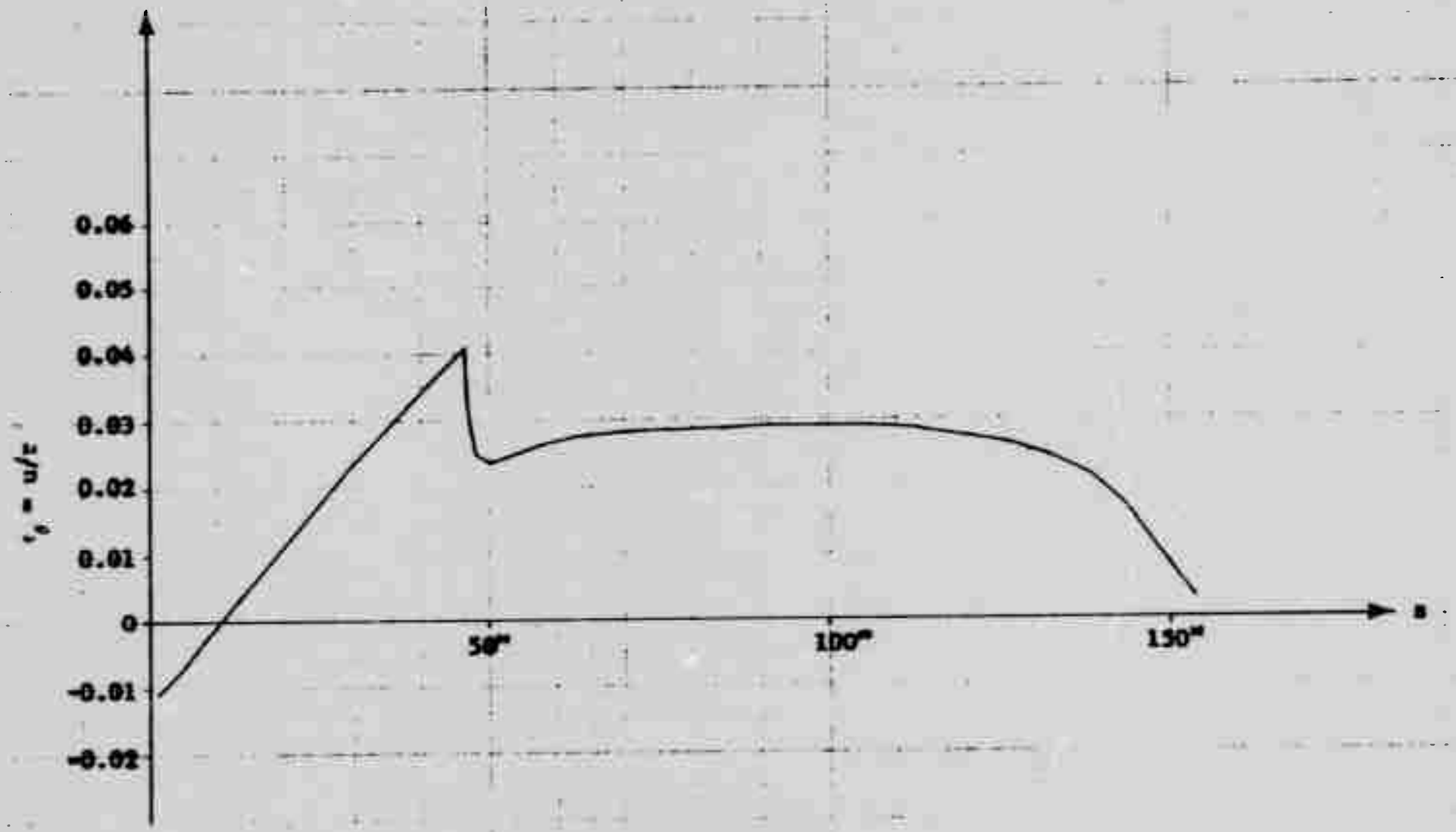

FIGURE 20

BORE STRESSES - AXIAL
DUE TO A TEMPERATURE CHANGE = -100°F

E = 200 lbs/in^2 ν = 0.49 α = 5.75 x 10^{-5} in/in°F

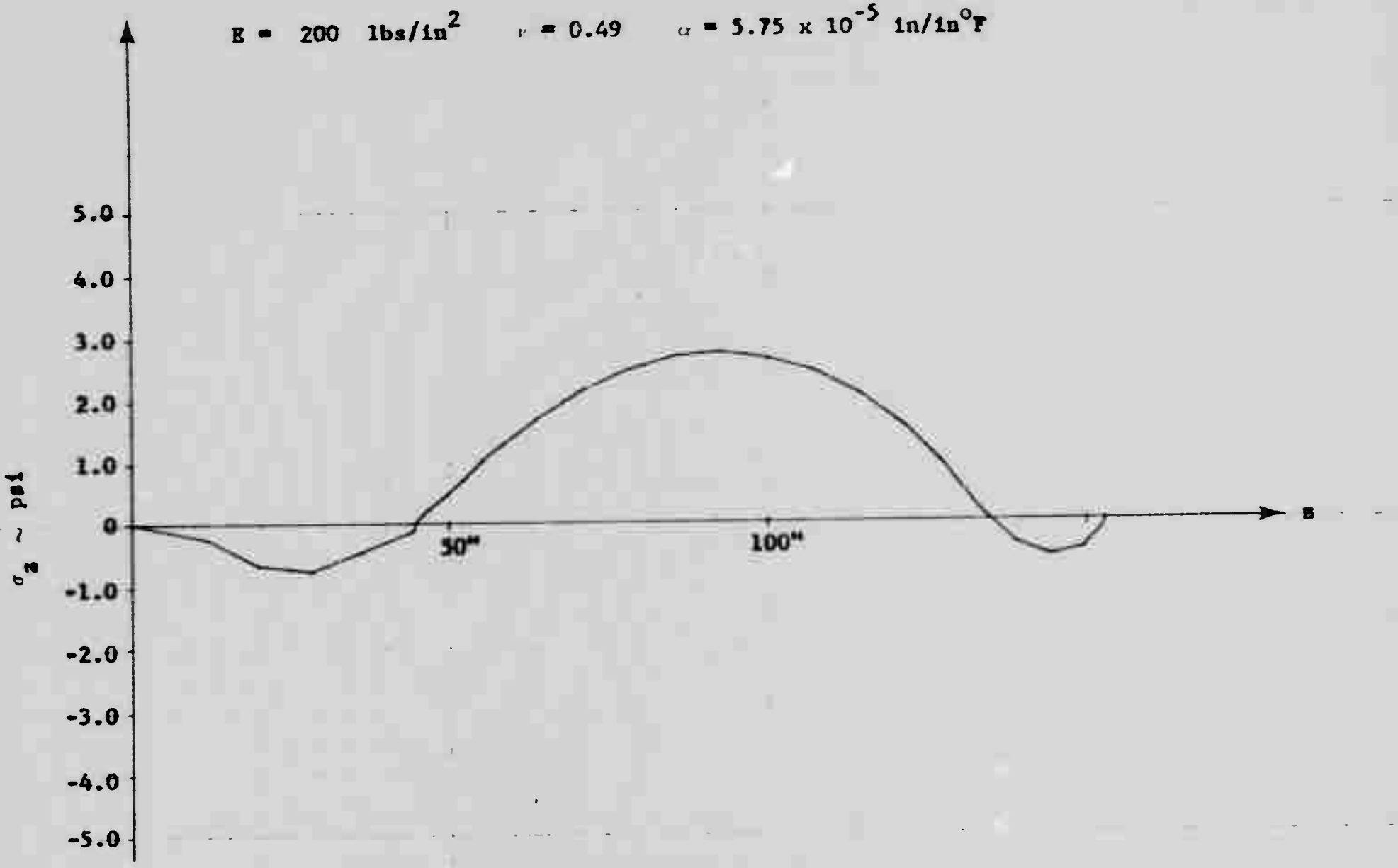

FIGURE 21

BORE STRESSES - HOOP

DUE TO A TEMPERATURE CHANGE = -100°F

E = 200 lbs/in^2 ν = 0.49 α = 5.75 x 10^{-5} in/in°F

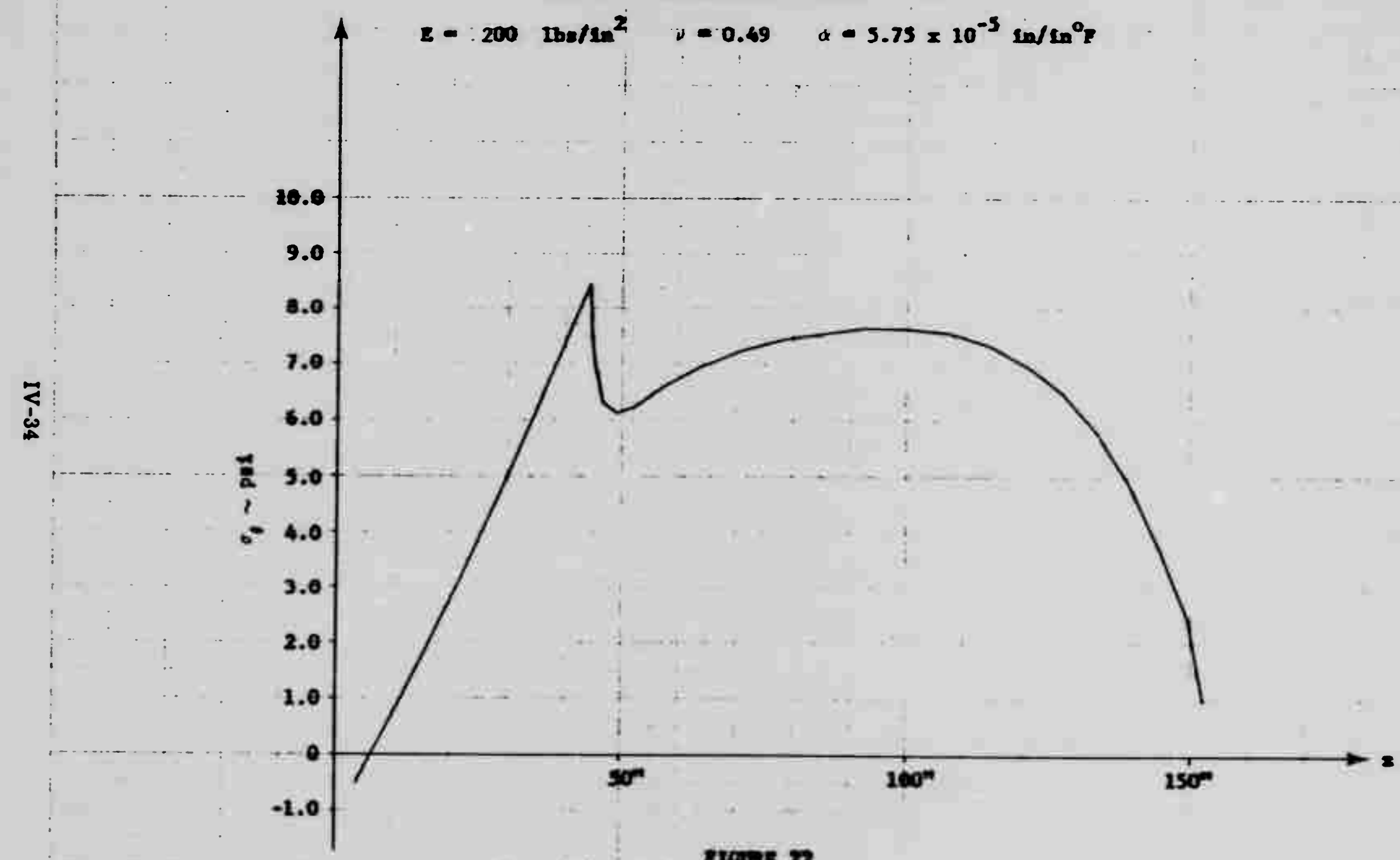

FIGURE 22

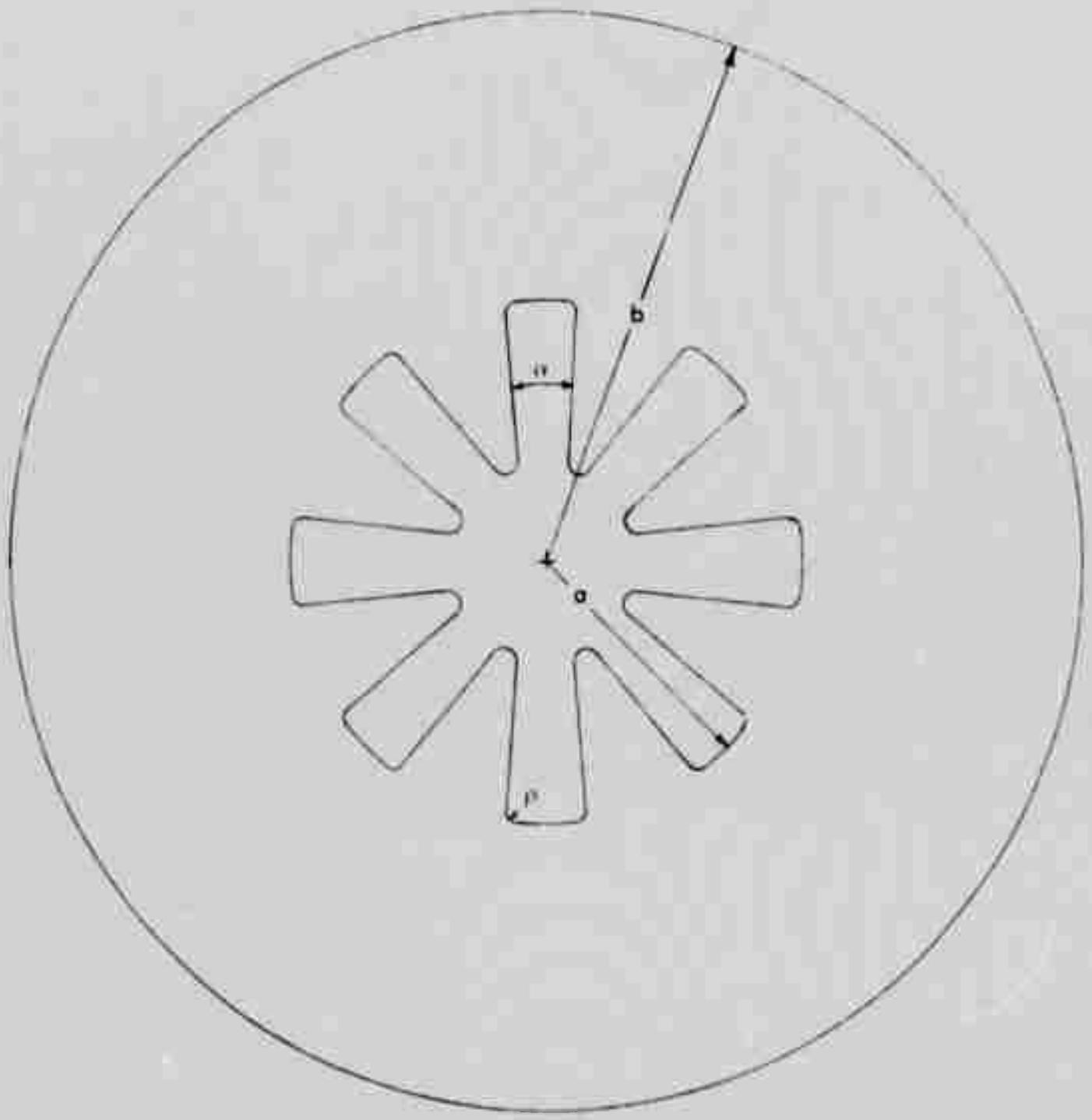

FIGURE 23

GEOMETRY OF STAR GRAIN

$\alpha = 10^{o}$ a = 29.5" $\rho = 2$

FIGURE 24

CONCENTRATION FACTOR

$\alpha = 10^{\circ}$ N = 8 $a/\rho = 14.5$

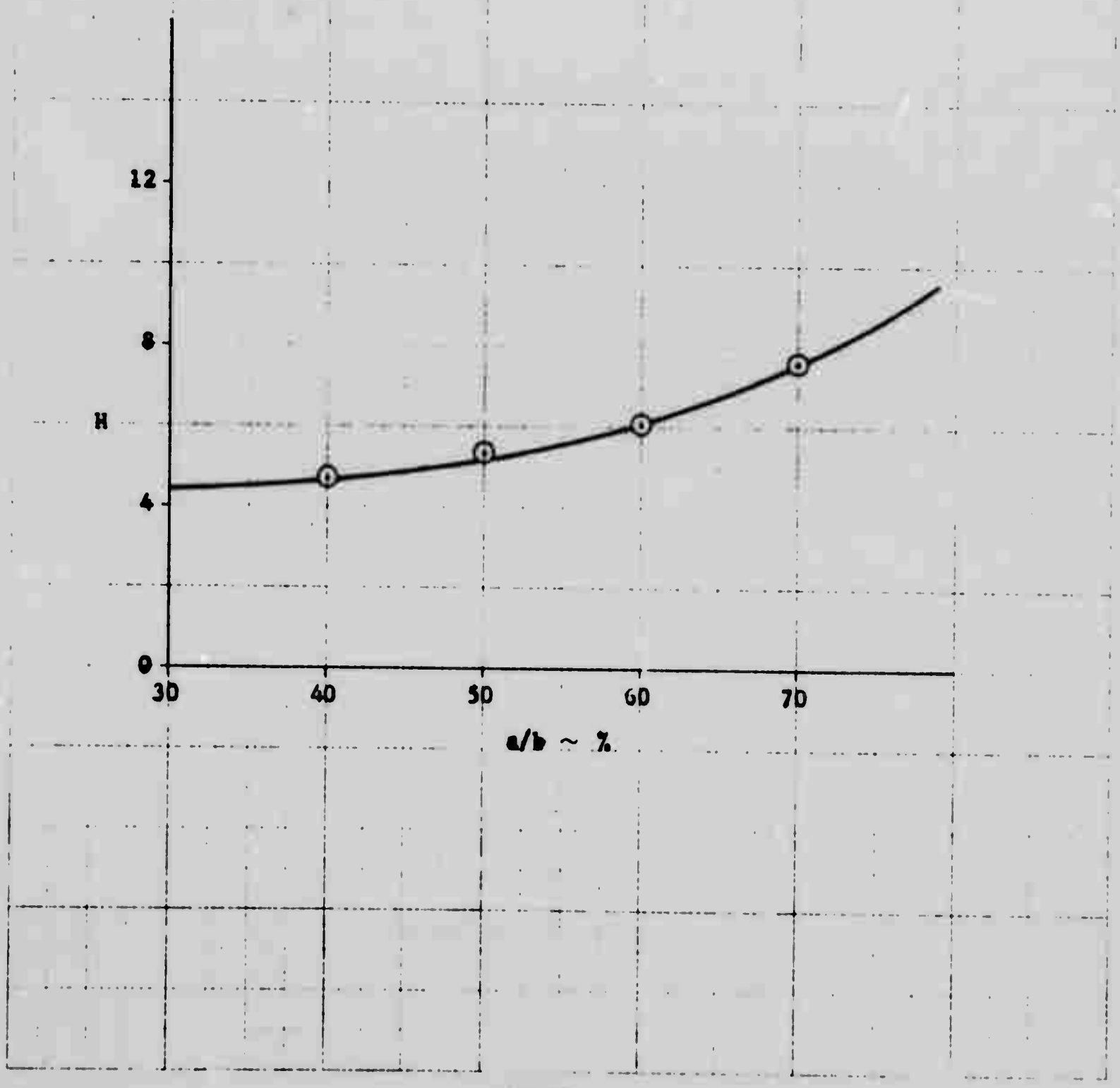

FIGURE 25

STAR GRAIN CONCENTRATION FACTOR

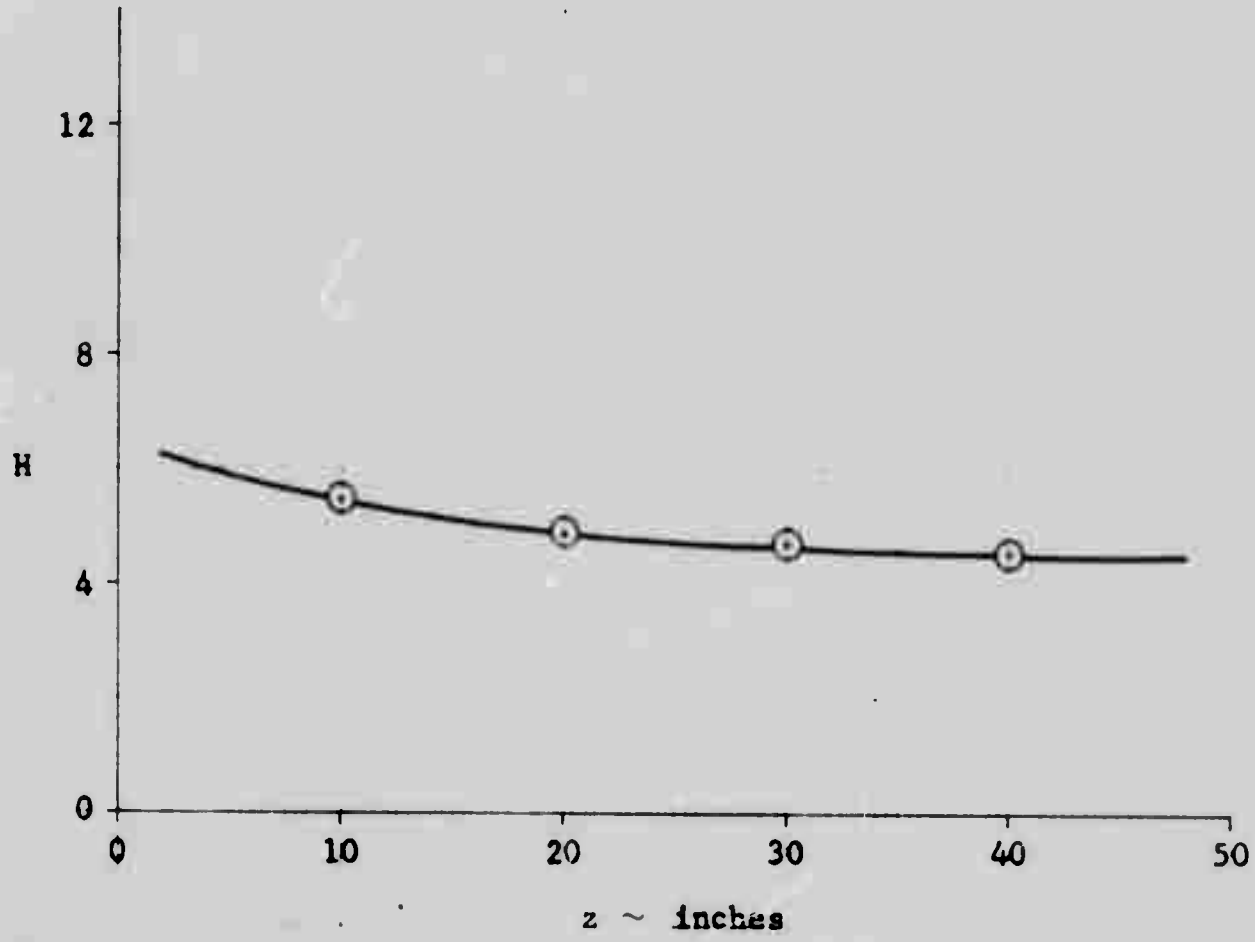

FIGURE 26

CASE-GRAIN INTERFACE PRESSURE

$\mu = 0.49$

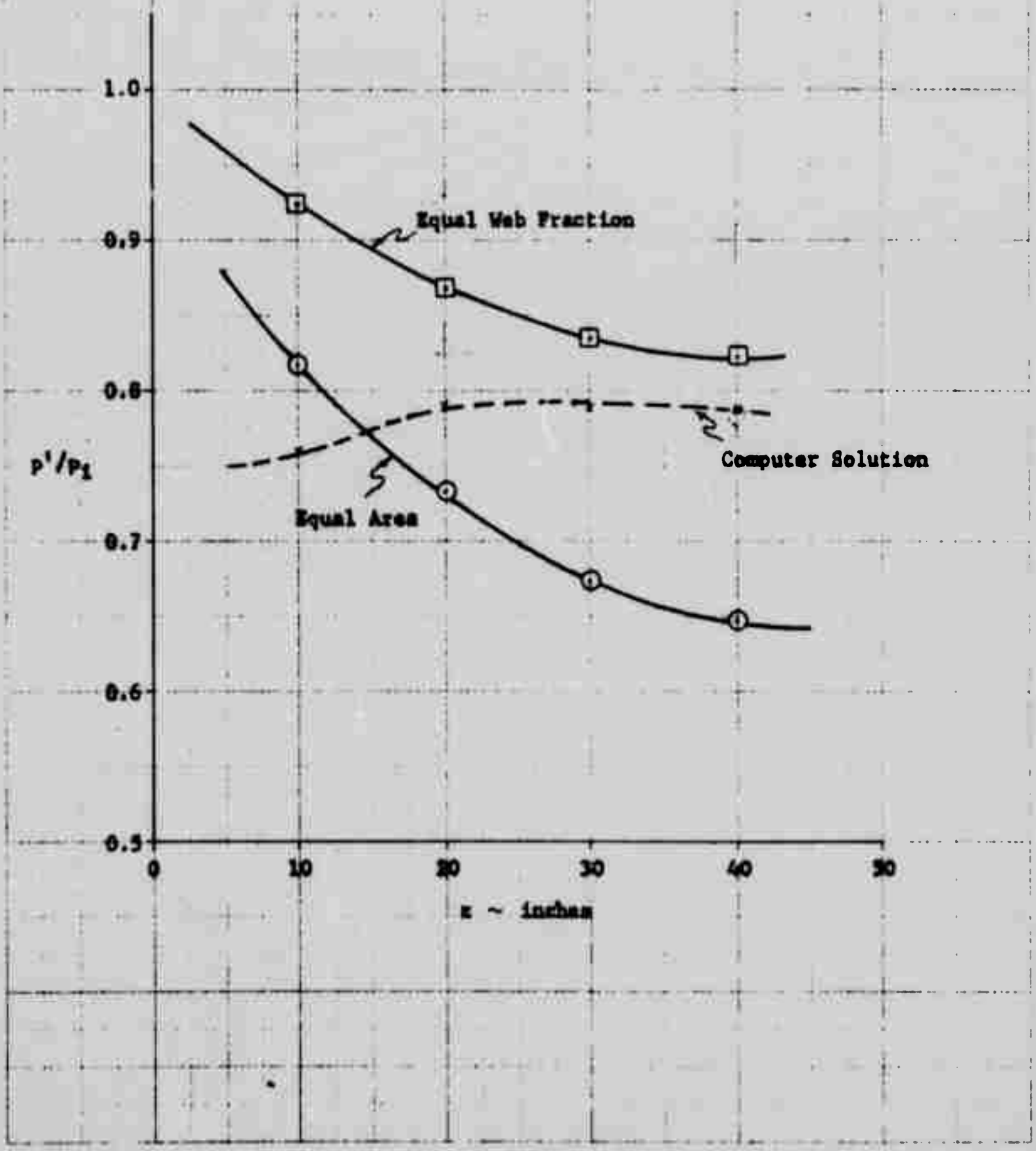

APPENDIX V

STRESS ANALYSIS OF THE
156-7 (TU-393.01) PROPELLANT GRAIN

APPENDIX V

TWR-1421

STRESS ANALYSIS
OF THE
156-7 (TU-393.01) PROPELLANT GRAIN

THIOKOL CHEMICAL CORPORATION
Wasatch Division
Brigham City, Utah

15 April 1966

TWR-1421

STRESS ANALYSIS
OF THE
TU-393 PROPELLANT GRAIN

15 April 1966

Prepared By

A. W. Macbeth
Applied Studies Department

Approved By

J. A. Peterson, Manager
Applied Studies Department

W. G. Ramroth, Manager
Large Space Booster
Project Engineering

THIOKOL CHEMICAL CORPORATION
Wasatch Division
Brigham City, Utah

TABLE OF CONTENTS

LIST OF FIGURES

Attachments

STRESS ANALYSIS OF THE FINAL TU-393 GRAIN DESIGN

I. Introduction.

The TU-393 rocket motor features a large 156-inch diameter fiberglass case. The grain design in this motor has a 62.4 percent web. It consists of a cylindrically perforated primary grain, reference Figure 1 for a sketch. As can be seen in Figure 1 there is a secondary grain bonded to the forward dome. Although this grain is essentially stress strain free, it could possibley slump. Attachment A of this report considers this aspect of the secondary grain. Both the forward and the aft dome of the motor have large stress relief flaps on the primary grain. The L/D of this motor is less than 1. The propellant used in this motor is TP-H8163, an HB formulation developed by the Space Booster Division of Thiokol. The motor is developmental and, as such, not intended for wide deployment temperatures. It will not be deliberately conditioned below 80°F.

Although the motor has a fiberglass case, it is relatively rigid (more so than most high performance fiberglass cases) during the ignition pressurization loading period. For conservatism during the cure and thermal shrinkage and gravity loading, the case is assumed rigid. The reason for the effective rigidity of the pressurization is that the peak pressure will be less than one-half the design pressure of the case. Therefore, the elongation of the case, even if full bore pressure were experienced at the case, would be only one-half that of a motor of optimum design.

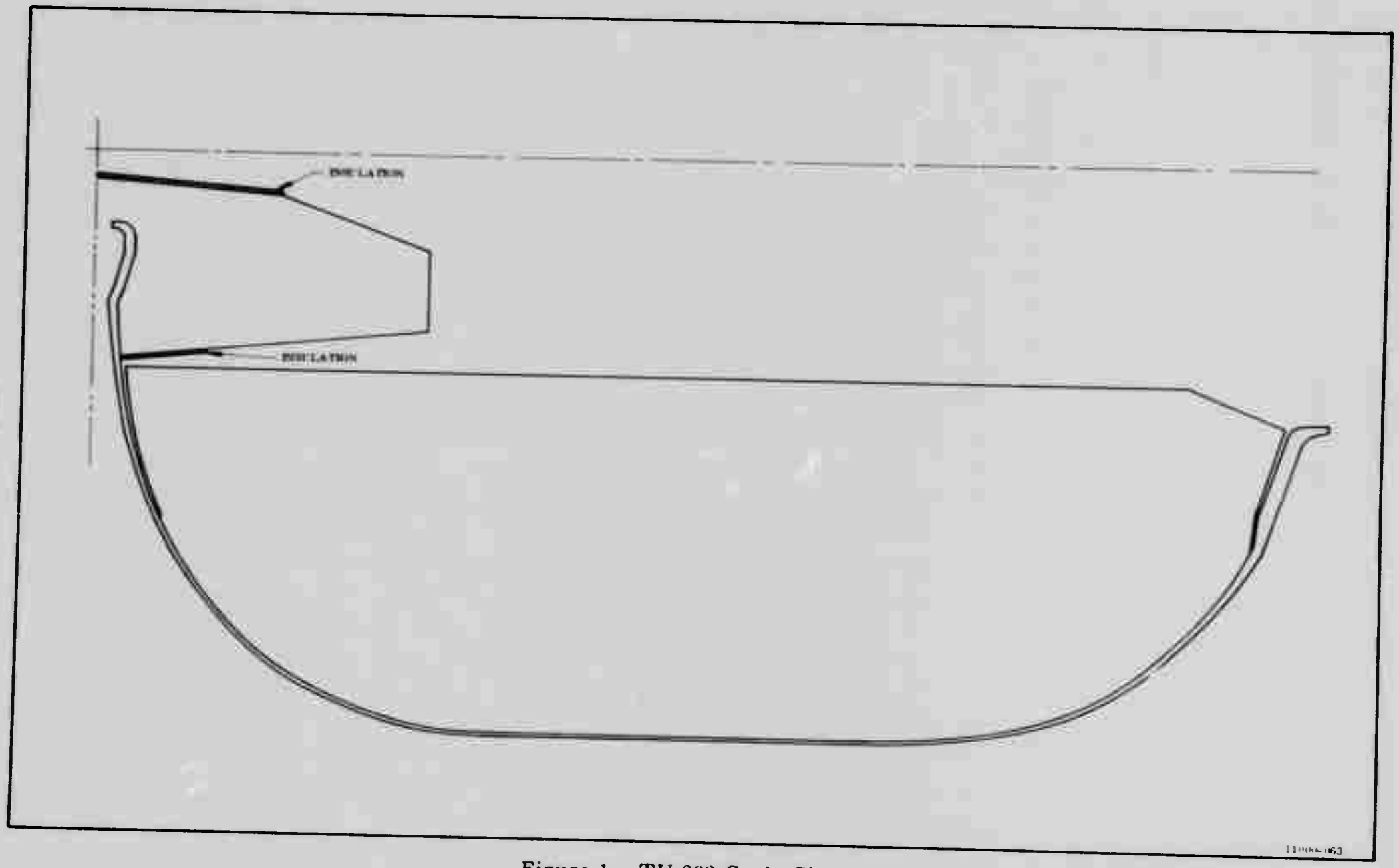

Figure 1. TU-393 Grain Sketch

II. Analytical Procedures and Assumptions.

The analytical stress program currently operational at the Wasatch Division is one obtained from the Mathematical Sciences Corporation in Seattle, Washington. Since completion of the analytical studies discussed here, a new program has become operational and it has neither of the limitations of the above program. Attachment B presents a brief description of the new program. Also, limited TU-393 runs were made and then results are shown. Although a copy of theprogram write-up has been supplied to the customer, a brief synopsis of the program's capabilities and limitations will be presented below. The program permits the stress analysis of axisymmetrical problems pertinent to solid rocket motor geometry. The geometry may be any arbitrary hollow body of revolution. The materials may be cylindrically orthotropic or isotropic. Arbitrary distributions can be specified as long as the resulting displacement increments are small compared to unity. The solution is obtained by the stiffness method using a finite element technique in which the body is divided into a large number of finite elements by a grid work of lines intersecting at node points. The present program determines the values of the stress and displacement fields at each node point. By reapplication of the basic program in an interactive manner, arbitrary stress-strain relations can be treated; hence, problems of non-linear elasticity with small displacements can be solved.

The equations of the stiffness methods can be derived from the theorem of minimum potential energy. An approximate solution for displacements is obtained in the usual way. The displacement field is expressed as a linear combination of functions through undetermined coefficients. The coefficients are then determined so that the potential energy is a minimum.

Although the program is an excellent program, it has two shortcomings regarding propellant grain analysis. The first is the inability to consider Poisson's Ratio input of 0.5. Further, even though Poisson's Ratio near 0.5 can be accepted, the resulting stresses are unrealistic. The program can consider layered materials. Therefore, one would assume that the case is just another layer of material. The second shortcoming is that this procedure consumes so many of the elements and nodes that poor resolution of the strains result. When a plastic or any very flexible case is under consideration, it is necessary to resort to artifices to circumvent the second drawback. For ultra-conservatism, the usual procedure is to assign no strength to the propellant; i.e. the propellant is an incompressible viscous fluid which means that bore and case-propellant interface pressure are synonomous. The bore chamber pressure is then used to determine the mid cylinderical length case growth from hydrotest and/or design data. These growth data are then applied to the entire case. Thus, two points of conservatism are incorporated; (1) the propellant does have strength even at a total relaxed condition therefore the case will not experience the full effects of bore pressure, and (2) the maximum case growth occurs at the mid length, thus the growth will be too large on the domes. With regard to the first drawback which can be a serious one, several brief studies have been made, not on the TU-393 motor, but on similar motors applicable to the conditions involved. For cure,

thermal, and gravity loads as Poisson's Ratio approaches 0.5, the strains of the bore and the case-propellant bond stresses increase. Prior studies of the stiffness program have shown that even though the stresses are unrealistic the strains are valid. Thus, one can make an analysis with a Poisson's Ratio very near to 0.5 for the strains and deformations. To obtain useful stress resolution one must calculate at a Poisson's Ratio near 0.49. The same type of logic can also be applied to the pressure loading; however, it must be noted that now the strains rapidly decrease as Poisson's Ratio of 0.5 is approached, but as with cure and thermal, the stresses increase. (This latter increase in stress for pressure loadings is a hydrostatic compression field, and as far as is known the propellant to be used in this motor is traditionally undamageable under hydrostatic compression.) To illustrate the trends under discussion, two figures have been prepared. Figure 2 is a plot of induced bond stress versus Poisson's Ratio, and Figure 3, a plot of induced bore strain versus Poisson's Ratio. Figure 2 indicates that the bond stress at Poisson's Ratio of 0.5 is 1.3 times that of 0.49 for the cure and thermal loading.

The TPH-8163 propellant to be used in the TU-393 has not been characterized at Wasatch, however, TPH-1096 has and is equivalent to 8163. For the cure, thermal, and gravity loadings the primary parameter of importance is the thermal coefficient of linear expansions and the coefficient of cure shrinkage. The stress relaxation modulus at equilibrium or rubbery conditions is also of importance. For the cure and thermal shrinkage calculation, however, this value may be perturbated over a wide range with a negligible effect on the

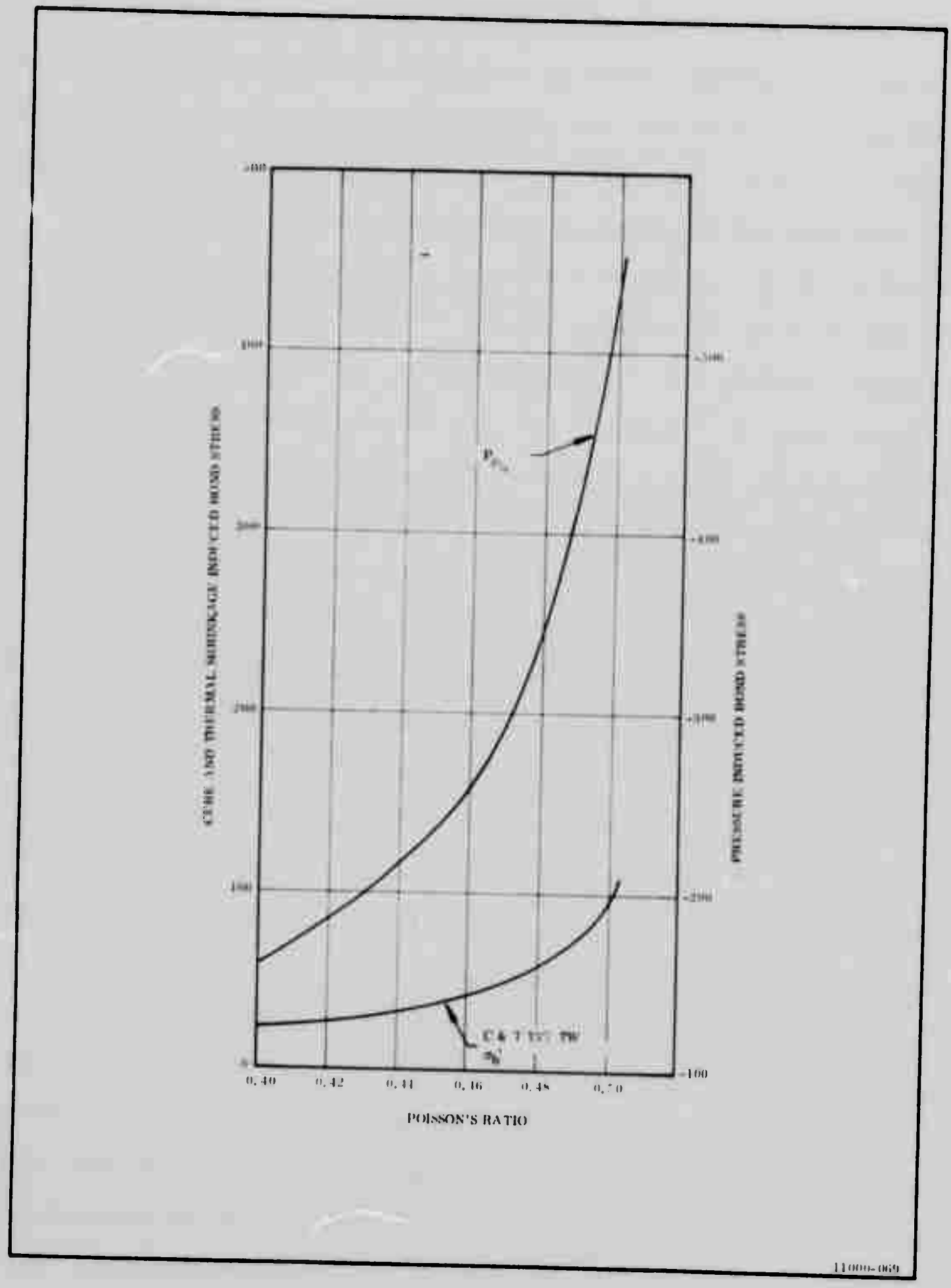

Figure 2. Effect of Poisson's Ratio on Bond Stress

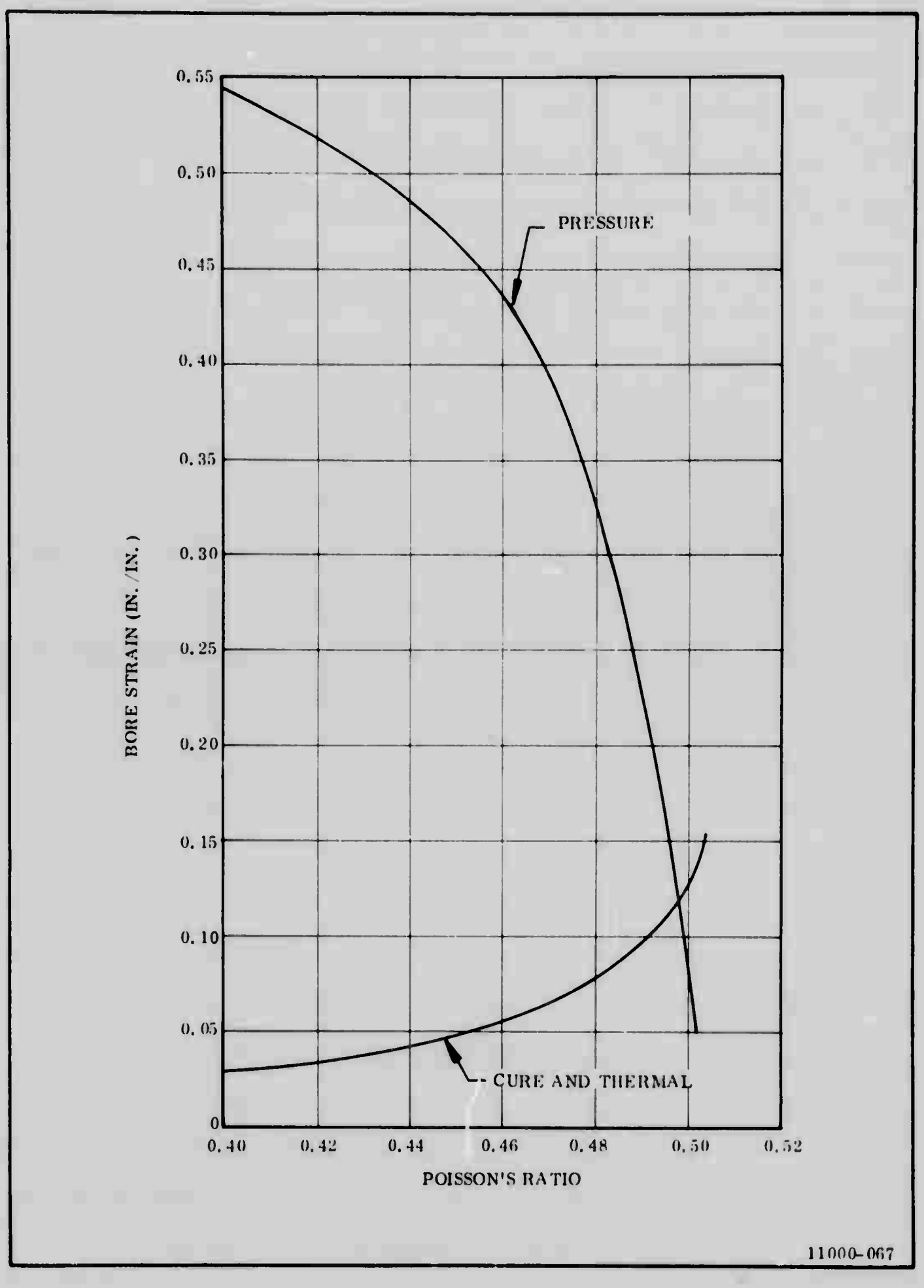

Figure 3. Effect of Poisson's Ratio on Bore Tangential Strain

stress-strain results. It is of importance in the gravity load. The coefficient of thermal expansion has been shown to be between 3.5 and 6.3 x 10^{-5} in/in/^{o}F. The value selected for this study was 6 x 10^{-5} in/in/^{o}F which should nearly represent the upper limit. The stress relaxation modulus selection for these runs was 200 psi, which appears to be fairly typical of this type propellant. The coefficient of cure shrinkage is not handled directly by the computer program, but it is necessary to convert this number to some equivalent increment of temperature to include the effect. To illustrate the procedures used in deriving an equivalent increment of temperature for the cure shrinkage factor, Figure 4 has been prepared. It is a plot of thermal coefficient of linear expansion versus increments of temperature for lines of constant shrinkage factors.

Unfortunately, the value of the cure shrinkage factor that should be used in this stress analysis is difficult to determine. In general, if a value of 0.002 in^3/in^3 is selected for the Thiokol H series propellant, it will be found that the bore strains calculated at cure temperature will be very close to those measured(1). Although the values determined per laboratory specimen may range as high as 0.008 in^3/in^3 after gelation occurs, these are unrealistic with respect to motor values. Therefore a value double the normal calculated one will be used; i.e. 0.004 in^3/in^3. It will be seen in Figure 4 that this results in an incremental temperature of 22^{o}F.

---

(1) Nelson, J.M., Special Report Improvement of the Elastic Analysis Method of Predicting Low Temperature Operational Capability of Solid Propellant Motors (u) Thiokol Chemical Corporation - Alpha Division - Huntsville Plant, 27 November 1963.

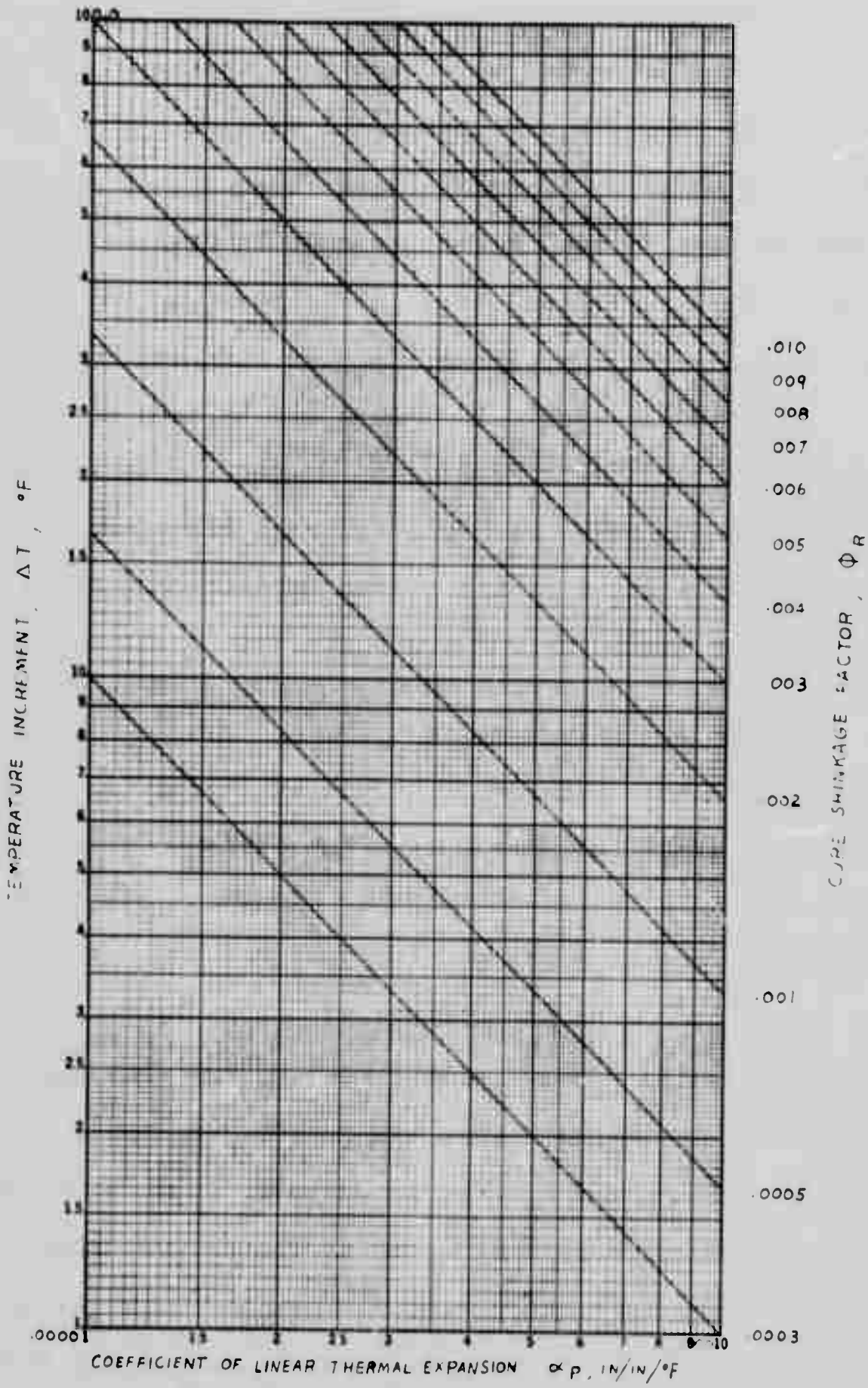

Figure 4. Design Curves for Selecting Temperature Increment Equivalent to the Cure Shrinkage Factor

To perform the pressure stress analysis requires determination of propellant properties analogous to the above discussion. However, the parameter of prime interest in pressure studies is the short term relaxation modulus. By combining experimental stress relaxation data and the calculated ignition transient time trace, it is possible to develop a viscoelastic stress analysis [1]. It has been found, however, that a relatively simple procedure can be used which will result in calculated bore strains slightly greater than those of the viscoelastic ones. The ignition transient time is used to determine a value of the stress relaxation modulus. The value used in this study is 1000 psi.

III. Stress Analysis Results

The primary purpose of stress analyzing the TU-393 propellant grain is to ascertain the difference between induced grain stresses and strains and the propellant capability (i.e. failure criteria).

A multitude of propellant failure criteria currently exist within the solid propellant rocket industry, however, Thiokol has found that the Smith failure boundary is the most universally useful for all grain loading conditions. Extensive experimentation has been conducted for the cure and thermal shrinkage loads, and it has been unequivocally demonstrated that the failure boundary

(1) Schapery, R.A. Irreversible Thermodynamics and Variational Principles with Applications to Viscoelasticity, PHD Thesis California Institute of Technology, 1962

established by uniaxial tensile tests relistically establishes the failure limits of the multiaxial motor configuration. The failure boundary is composed of the following data points obtained from uniaxial tensile specimens: corrected maximum stress versus true strain at corrected maximum stress. These data are obtained at various test strain rates and temperatures. The resulting stress-strain curve is then modified so that the stress ordinate becomes the deviatoric stress from the uniaxial test (uniaxial deviation stress equals two-thirds the maximum principle stress). Numerous Thiokol propellants have been subjected to such testing, and in no instance has superposition of multiaxial motor or specimen data resulted in decreased propellant capability. Indeed, for the pressure induced motor grain strains it has been found that the hydrostatic conditions improve propellant capability if the propellant exhibits such improvement under pressurized uniaxial tests. Thus, the only adjustment to the failure boundary necessary for pressure loading is also obtainable from uniaxial tests.

It would appear that the propellant capability is directly related to the stress imposed, but at high strain and low stress (resulting from time at load), the strain is nearly independent of stress. Figure 5 illustrates this point, wherein it is a failure boundary for a high solids HC propellant. Prior to the efforts described above, many analog motor experiments were performed and it was found that motor failure strain exceeded the strain at corrected maximum stress of routine (2 in/min. crosshead rate) JANAF data. Although this seems contrary to the Smith failure boundary work, it is not. The analog motor data will lie on that portion of the boundary that is basically independent of stress.

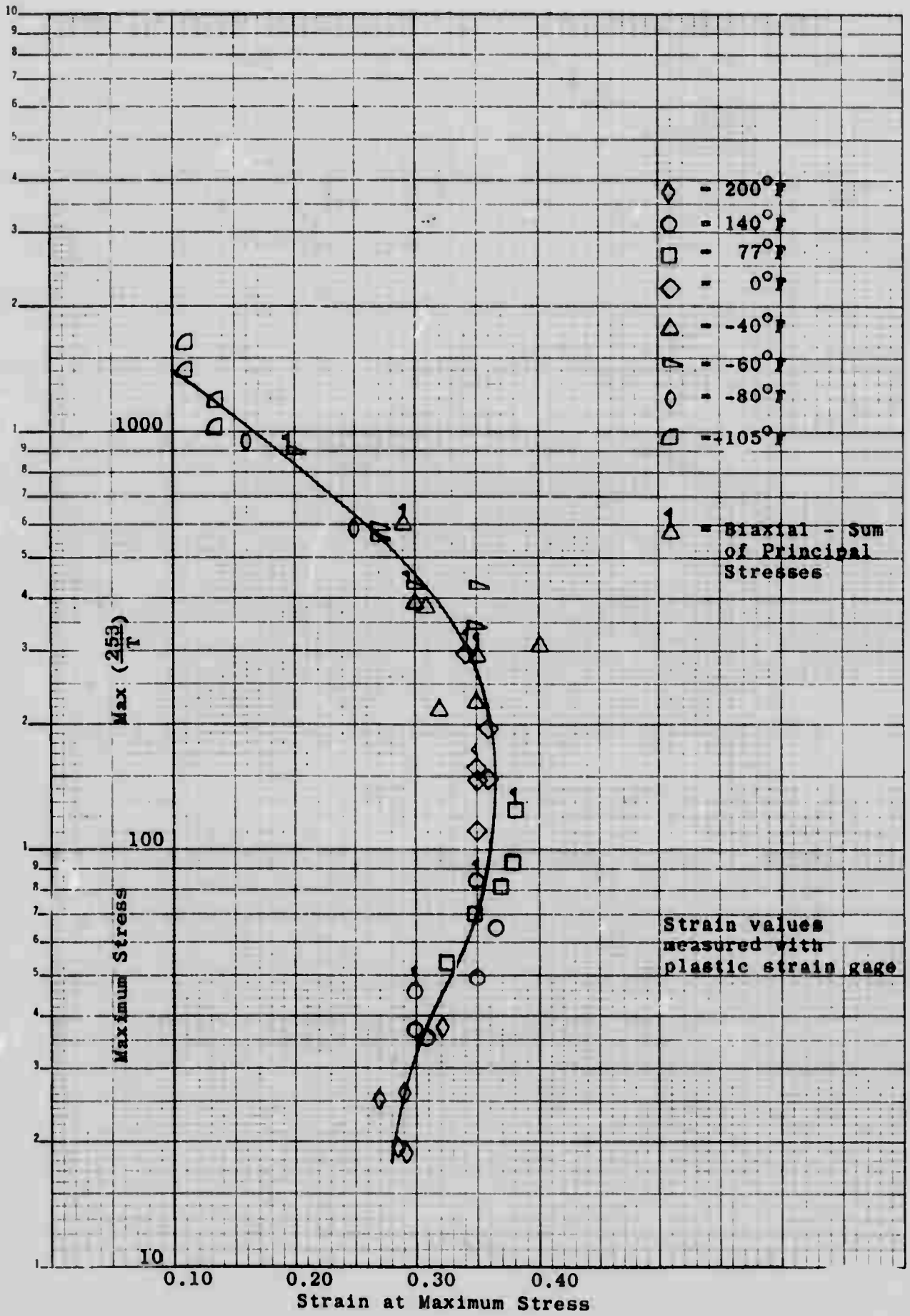

Figure 5. Typical Failure Boundary for High Solids HC Propellant

The cure and thermal shrinkage and 1 g slump failure criteria selected for this effort will be strain at uncorrected maximum stress from JANAF data. Note that conservatism has been interjected in that strain at uncorrected maximum stress is always less than that at corrected maximum stress. Note that if the correct effective gauge length is used on the JANAF data, there will be no change between measured and calculated data.

Extensive propellant-liner bond testing has indicated that the failure is a propellant cohesive failure. Consequently, the "bond" strength is that of the propellant. Traditionally, bond capability has been oriented towards stress considerations rather than strain. Thiokol, however, is currently investigating bond capabilities more generally. Since these efforts are inconclusive to date, it is necessary to assume that stress failure criteria applies. The specimen used to measure bond properties is rectangular where the propellant size is 2 x 3 x $\frac{1}{4}$ inches. The testing device is such that pure tension or pure shear can be applied as well as combinations of each. Obviously, a specimen of this size will reflect biaxial or triaxial properties, but these have not been evaluated as yet. The normal test cross-head rate for the tenshear specimen is 0.5 in/min, however, it has been tested at other rates. In all cases the tensile bond stress slightly exceeds the maximum tensile stress capability as determined by JANAF uniaxial tests. Therefore, the bond stress failure criteria will be based on the maximum stress capability of the propellant as obtained from low rate JANAF tests.

The pressure induced strains of this motor appear large due to the conservatives applied in the analysis. Although it has not been completely explored as yet, it would appear that two or three methods of applying pressurized grain stress-strain values to the Smith Failure Boundary could be used. First, the mean deviatoric stress; second, maximum principal stress magnitude; and third, the maximum difference of principal stresses all versus maximum induced strain. Since any one of these (ignoring sign convention) will occur in the same general region as the cure and thermal shrinkage strains for this motor, the pressure strains will merely be added to the cure and thermal strains.

Finally, one further conservatism will be included in the results. Arbitrarily, all propellant capability limits will be divided by 1.5. The primary justification for this is to account for batch to batch variation, variation in post cure, and effective gauge length variation. It has been inferred by some individuals in the solid propellant industry that a biaxial degradation must be included in the stress analysis. Since Thiokol has not been able to substantiate a biaxail decay with their propellants, it is ignored.

The results of this stress analysis with regard to the two loading conditions studied can best be presented graphically. Figure 6 is a sketch of the original grain shape with the deformation due to cure and thermal shrinkage and 1 g slump at 80°F. The deformations are emphasized to more clearly delineate their true shape, and it will be found that their scale factor is larger than the motor sketch, as noted in the Figure.

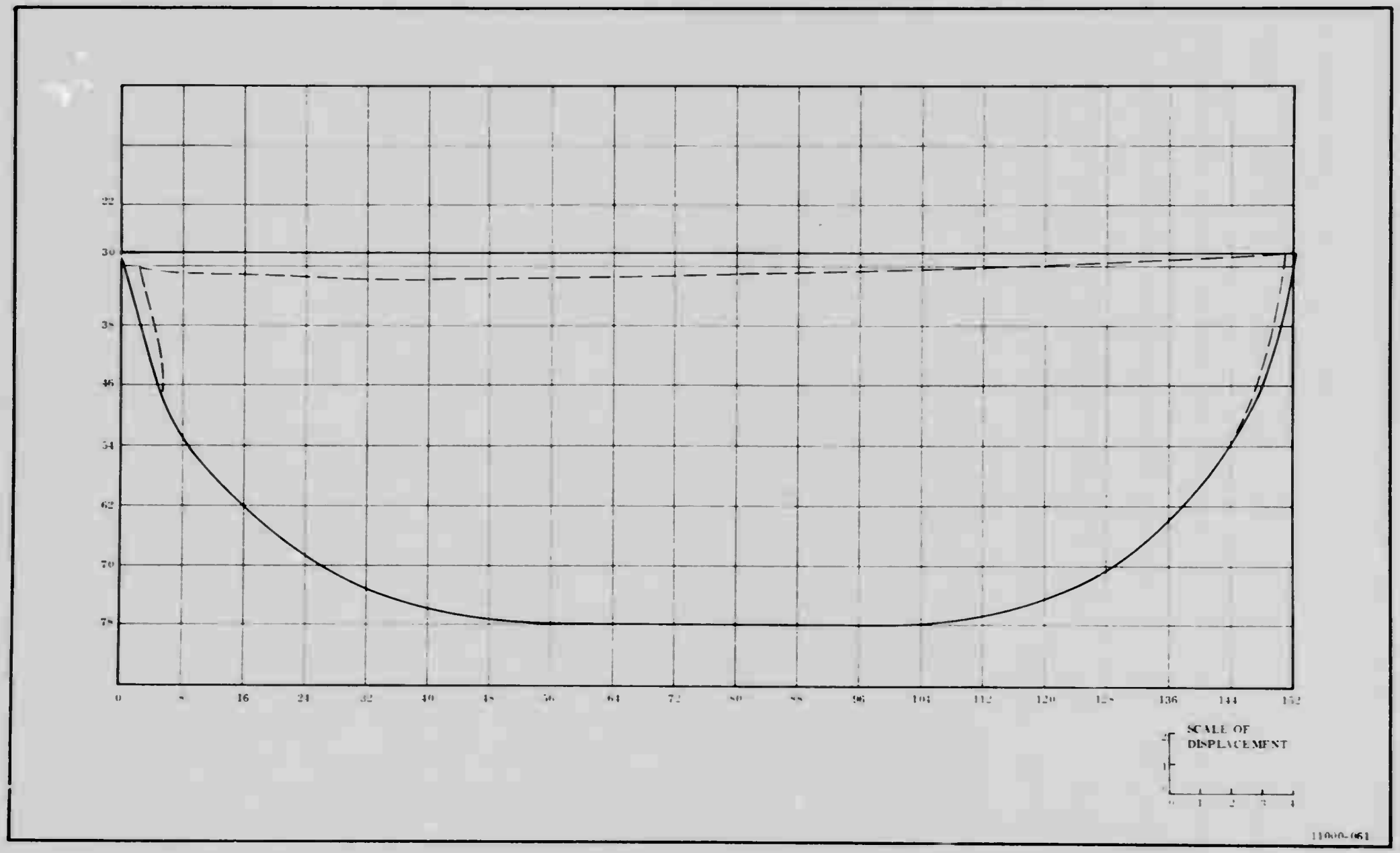

Figure 6. TU-393 Cure and Thermal Shrinkage with 1g Slump (Stress Analysis Sketch)

The maximum bore deformation occurs slightly aft of the center of the grain and at this point the maximum strain is 4.0 percent. Since the propellant capability far exceeds this level of strain, there is obviously no significant strain problem in this motor design. Therefore, it becomes necessary to investigate the bond stresses of the motor due to cure, thermal, and gravity loads to ascertain any deleterious conditions that may arise. Figures 7, 8, 9, and 10, respectively, present the radial, axial, shear, and tangential stress distributions as a function of the axial location in the motor. As can be seen, the only large stresses occur at the grain end, and these are still less than propellant capability, even when one considers the increase,as shown in Figure 2. The maximum tensile stress will be found in Figure 10 and it is 13.8 psi, which will increase to 17.8 psi when modified according to Figure 2. The maximum shear stress is found in Figure 9 and it is 1.25 psi.

The pressure induced deformations are presented in Figure 11, noting again the deformation scale-up in the sketch. The maximum bore strain is 14.96 percent, which when combined with the above strains results in a total of approximately 19 percent.

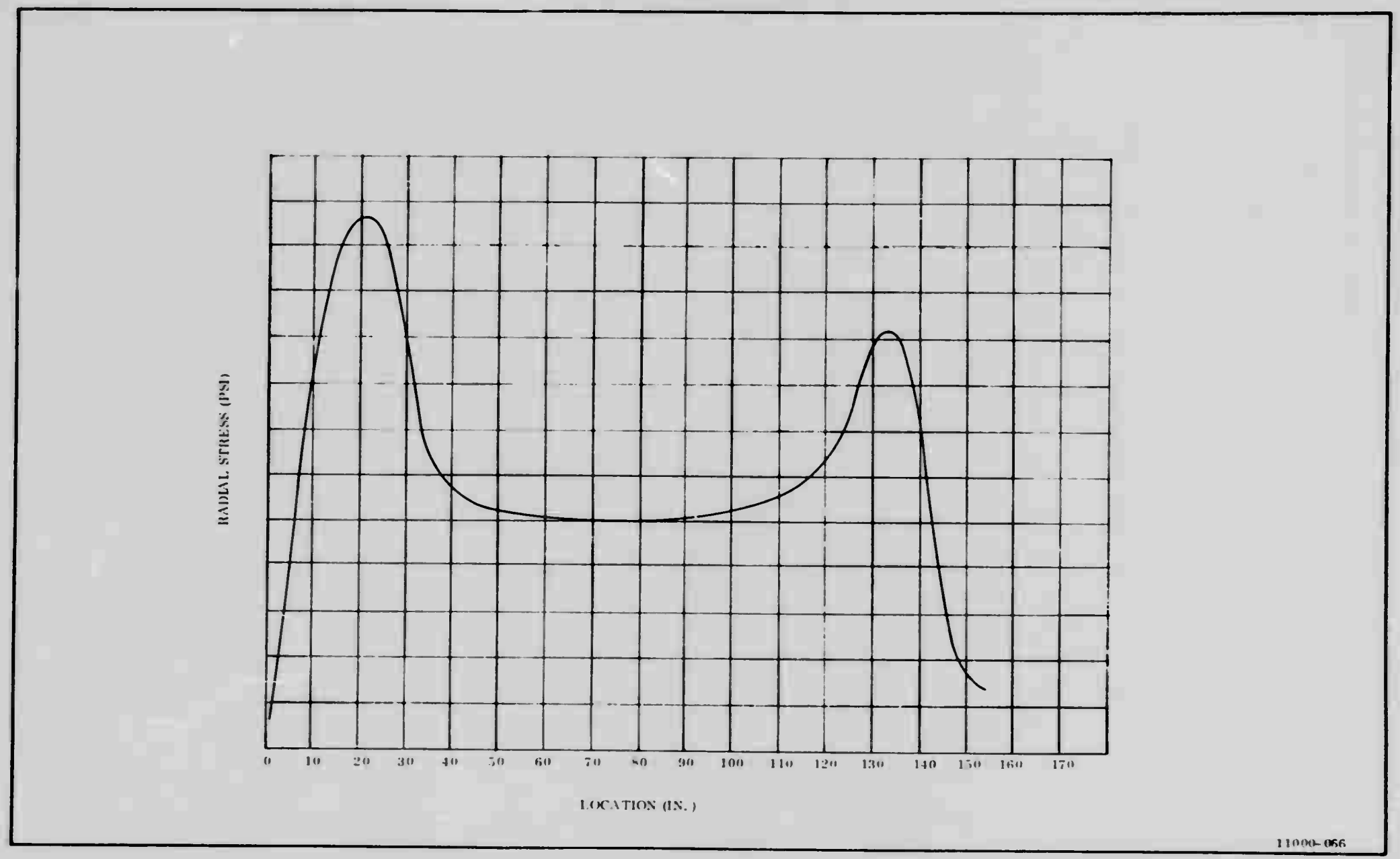

Figure 7. Radial Stress vs Axial Location, TU-393 With Flaps

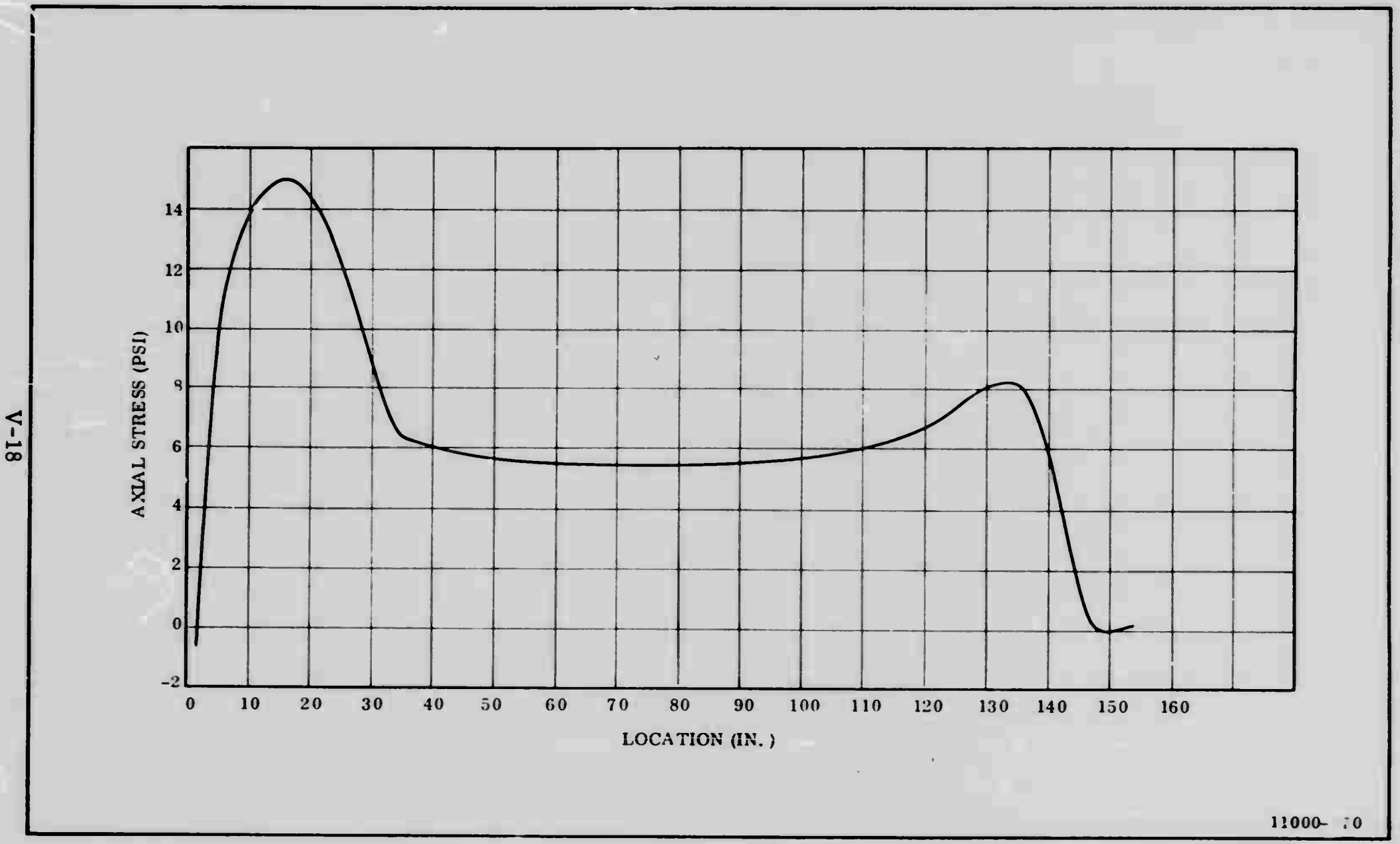

Figure 8. Axial Stress vs Axial Location, TU-393 With Flaps

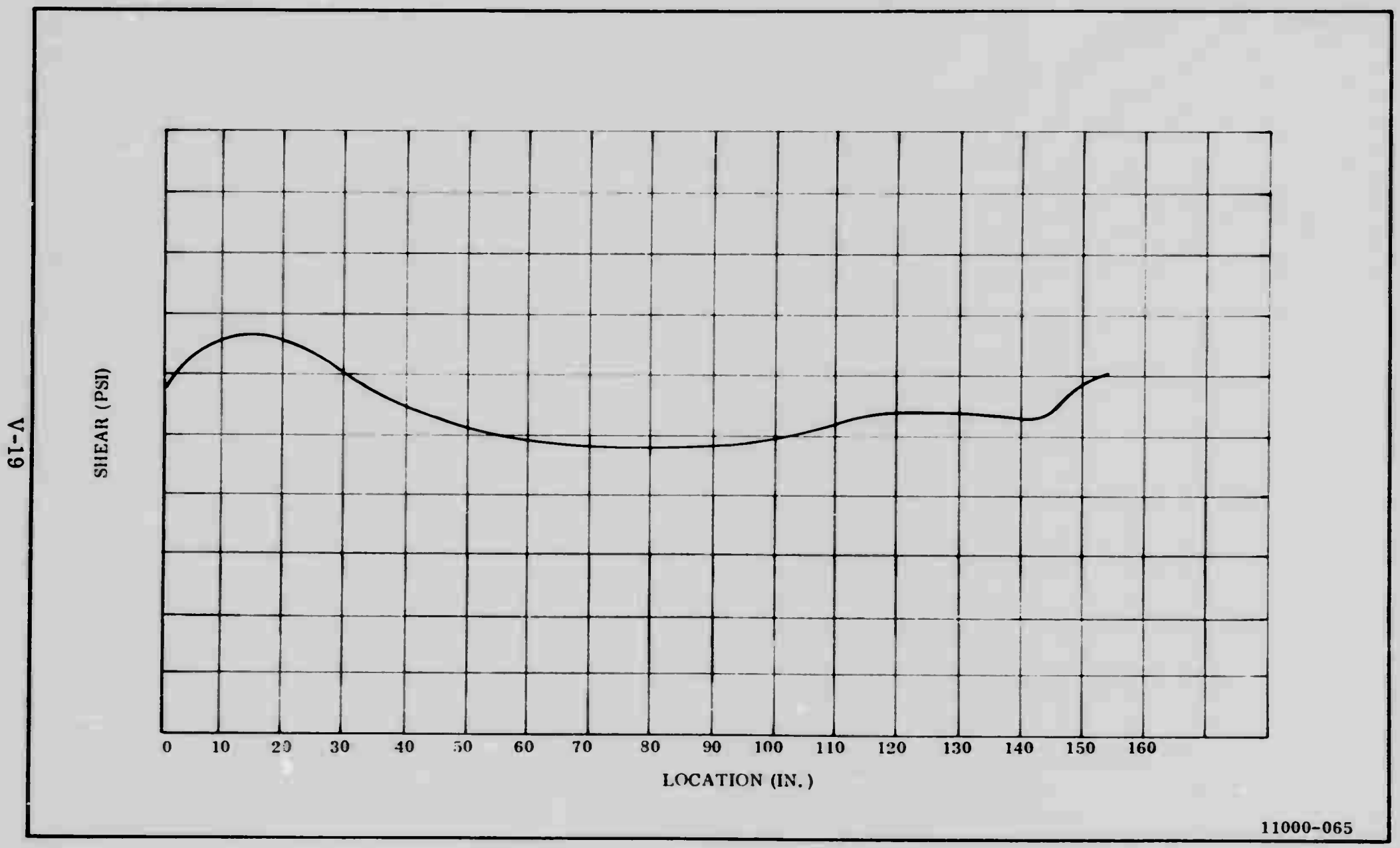

Figure 9. Shear vs Axial Location, TU-393 with Flaps

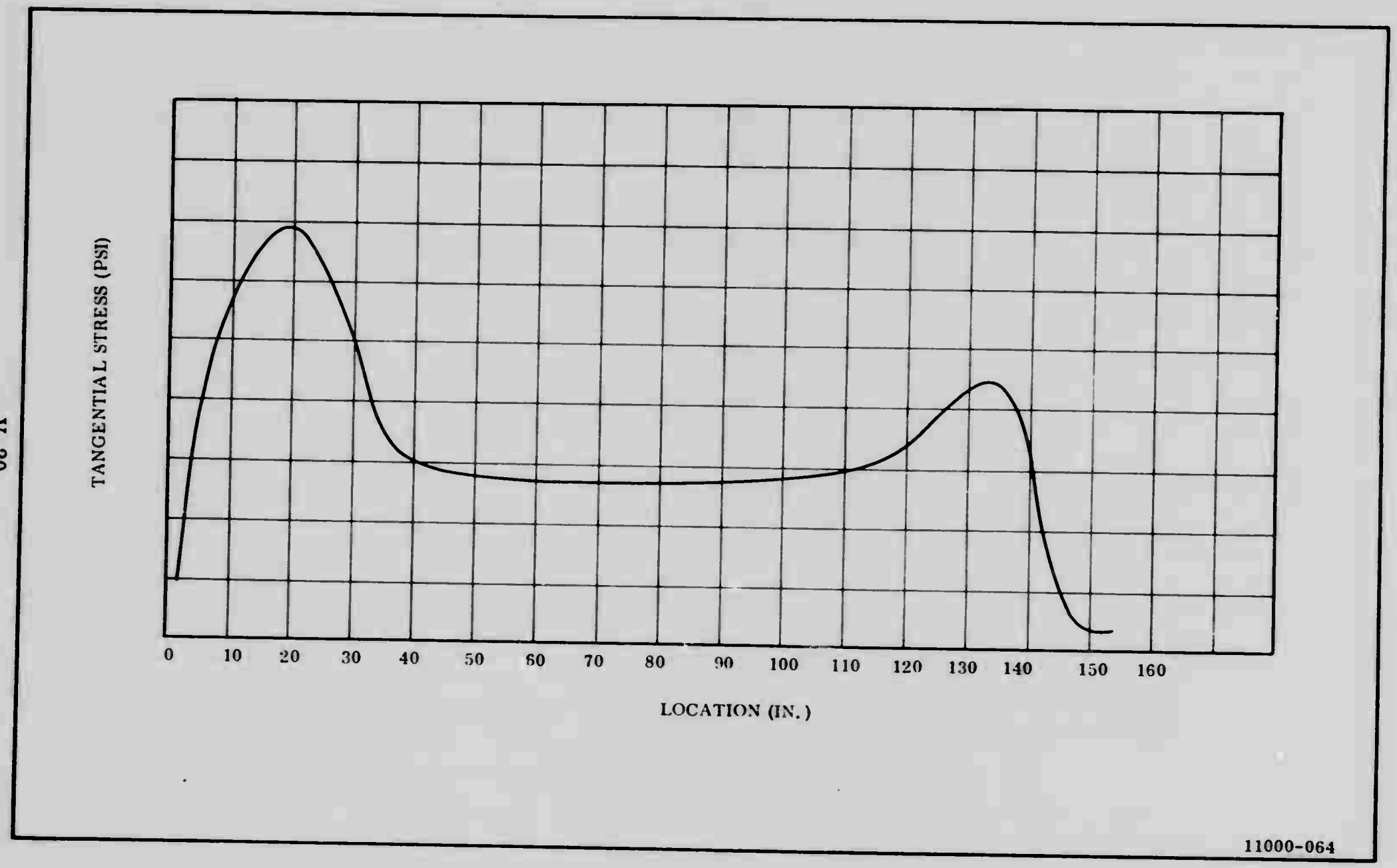

Figure 10. Tangential Stress vs Axial Location

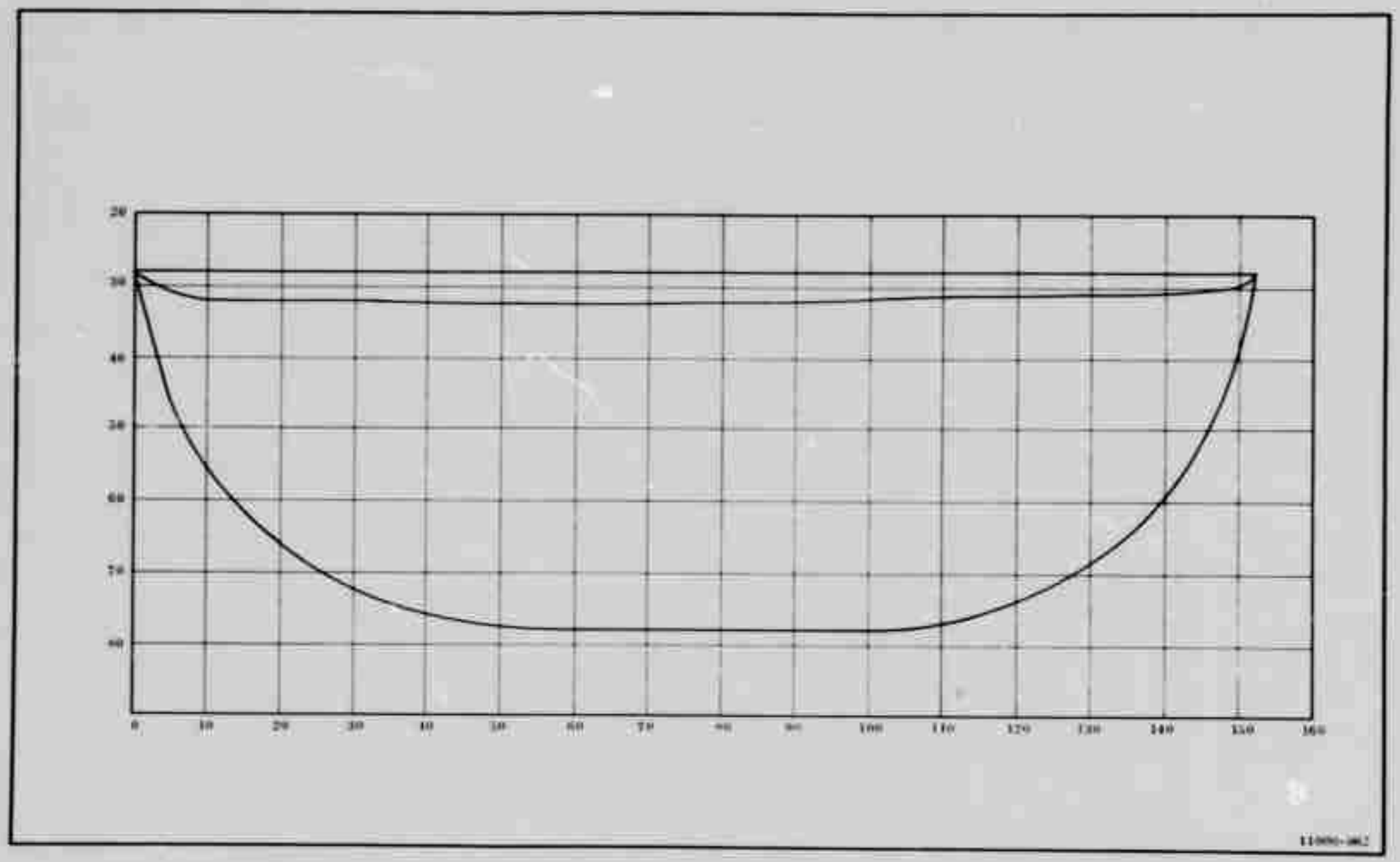

Figure 11. TU-393 Pressure Deformed CP Grain Stress Analysis Sketch (550 psi)

IV. Conclusions.

As was shown in the preceeding section, there are no deleterious stresses or strains in the TU-393 motor. To further portray the intrinsic reliability of this grain design, Table I has been prepared, relating the effective margins of safety; a comparison between the induced conditions and a very conservative estimate of the propellant capability. Based upon these results, one must conclude that there will be no structural integrity problems with this motor.

TABLE I

MARGIN OF SAFETY
FOR TU-395 LOADING CONDITIONS

Conditions	Maximum Induced Tensile Stress or Strain	Capability*	Margin of Safety
80°F plus 1g Slump	17.8 psi	90 psi	3.3
	0.04 in/in	0.22 in/in	5.35
80°F 1g Slump and 450 psi pressure	0.190 in/in	0.22 in/in	1.13

*Note that propellant capability has been reduced by a factor of 1.5

ATTACHMENT A

ATTACHMENT A

Stress Analysis of TU-393 Secondary Grain

The secondary grain of the TU-393 motor consists of a long cantilevered hollow cylinder of propellant, reference Figure 1A. The cure and thermal shrinkage and subsequent pressurization loads are insignificant. The body is essentially only effected at the bond interface by the former load and the latter load will be pure hydrostatic compression. However, the stresses and deformations due to the cantilever effect when the motor is horizontal must be carefully examined.

The exact grain geometry as shown in the figure is not rigorously tractable, therefore certain simplifying assumptions must be made. The approach was as follows:

The triangular areas in the figure were distributed over the full body length as concentric layers of material. Thus, the problem analyzed was a right circular cylinder 43.5" long with O.D. and I.D. of 31.55" and 14.7" respectively.

The applicable equations are as follows:

1) Tip deflection at free end,

$$w = \frac{-\rho L^2}{E} \left[\frac{L^2}{2 (R_0^2 + R_1^2)} + 3 \right]$$

2) Shear stress, $\sigma_{\theta_z} = 2\rho L$

3) Tensile stress, $$\sigma_z = \frac{2\rho \, L^2 \, R_o}{(R_o^2 + R_1^2)}$$

where:

ρ = Propellant density, lb/in^3, 0.064

L = Grain Length inches, 43.5

R_o = Grain O.R. inches, 25.75"

R_i = Grain I.R. inches, 7.35

E = Relaxation modulus at equilibrium conditions, estimated range from 75 to 225 psi.

Based on the equations 2 and 3 the maximum stresses are 5.6 and 8.7 psi respectively, either of which is well within the limits of propellant capability. The tip deflection range is 6.96 to 2.33 for the range of equilibrium modulus. Obviously, the former an undesirable condition. One method of preventing this slumpage would be to pot the forward 10 inches of the primary-secondary gap with liner or flap-gap filler. This effectivity shortens the cantilever length resulting in a maximum slump of only 3.32 inches. Another method would be to determine the bottom of the motor with respect to horizontal storage, and then insert a small saddle of foam between the grains.

Although the analysis used is quite conservative, it would appear advantageous to assure that contact between the grains is positively prevented. Therefore, it is recommended that one of the procedures described above be used. Note also that in preventing the slump the shear and tensile stresses are reduced.

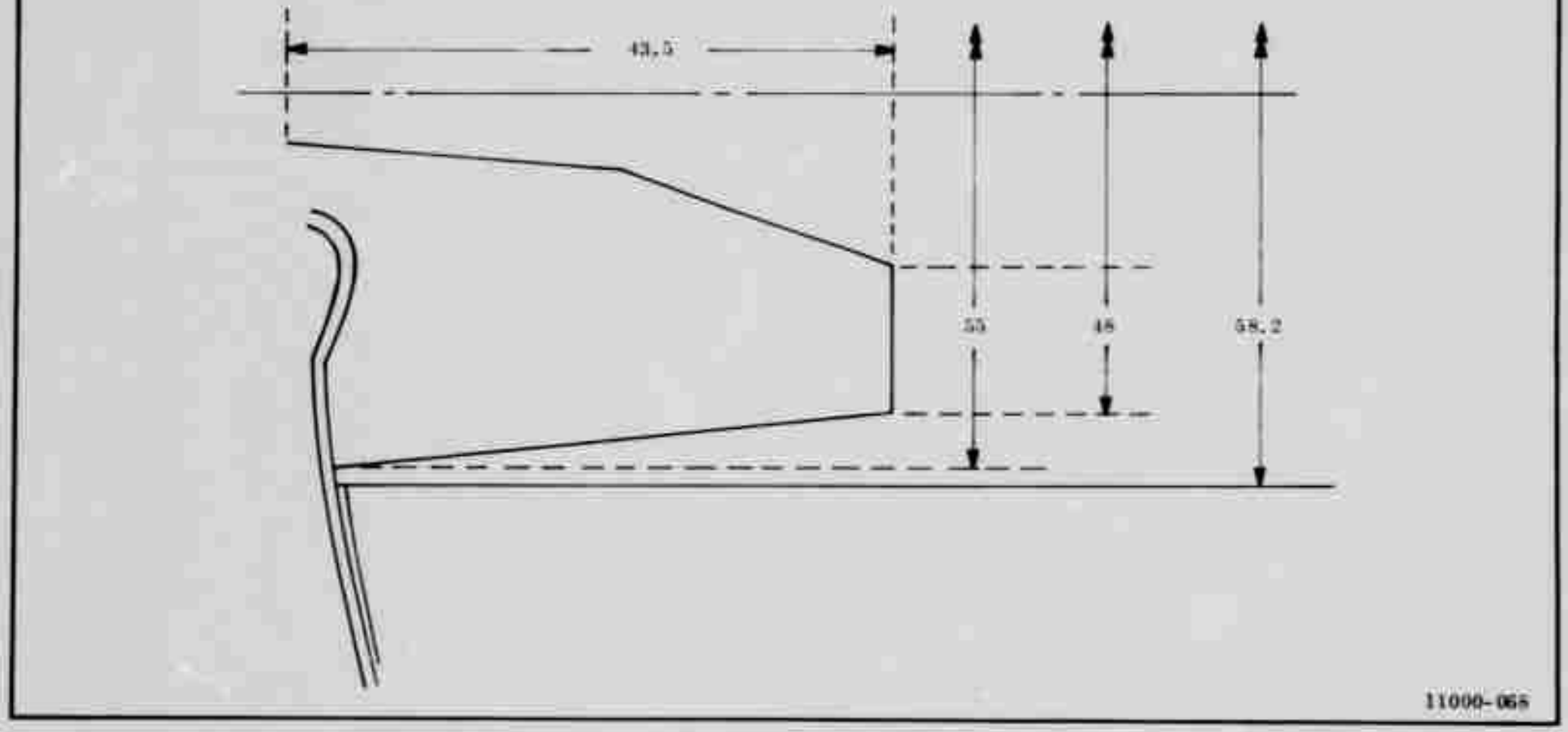

Figure 1A. Sketch of TU-393 Secondary Propellant Grain

ATTACHMENT B

ATTACHMENT B

ADDITIONAL TU-393 STRESS ANALYSIS EFFORTS

Since the TU-393 stress analysis studies were completed, an advanced version of the computer program described above has been put into operation. A change in the formulation of the equations governing the thermal and mechanical response of the isotropic and linearly elastic continuum has removed the singularity associated with an incompressible material, i.e., $\nu = 0.5$. This change in the finite element analysis permits more realistic values of Poisson's ratio to be used and results in the ability to obtain excellent resolution of the stress fields. Also included in the new program is the ability of considering the effect of an elastic case bonded to the propellant grain. This eliminates much of the manual input in the form of displacement boundary conditions to the computer program and provides a solution to the existent situation.

Using the new program, the TU-393 grain was analyzed for stresses and strains induced by cure, thermal, slump, and pressurization loads. It should be noted that an alteration has been made in the split flaps at both ends of the grain since the original grain analysis was performed. This modification entails much longer split flaps than were previously considered. Also, the longer split flaps will remain unfilled after cure and motor cooldown.

It is obvious that the increase in flap length will decrease the bore hoop strains induced by cure and thermal shrinkage. By keeping the split flaps unfilled during motor firing or internal pressurization, the bore hoop strains will be reduced; equally important, the stresses induced by the pressurization load will approach isotropic compression, thereby decreasing the deviatoric stress components.

Since a considerable amount of the main body of this report concerns failure criteria and propellant stress-strain capability, these items will not be repeated here and the data will be presented in a rather matter-of-fact manner. A sketch of the deformed grain resulting from cure and thermal shrinkage is shown in Figure 1-B. Note the exaggeration in the deformation scale with reference to the grain size. Figure 2-B is a similar presentation of grain deformation under internal pressurization with the unfilled split flaps. The printed results from the computer were carefully examined and the maximum stresses and strains induced in the TU-393 grain during the two specific loading situations are compared to a conservative value of propellant stress/strain capability in Table 1-B.

As is shown in Table 1-B, the smallest margin of safety is 3.22 and is related to the bore hoop strain which occurs upon internal pressurization of the motor. Sufficient margins of safety are indicated to assure total grain structural integrity under the loading conditions of cure and thermal shrinkage, slump, and internal pressurization.

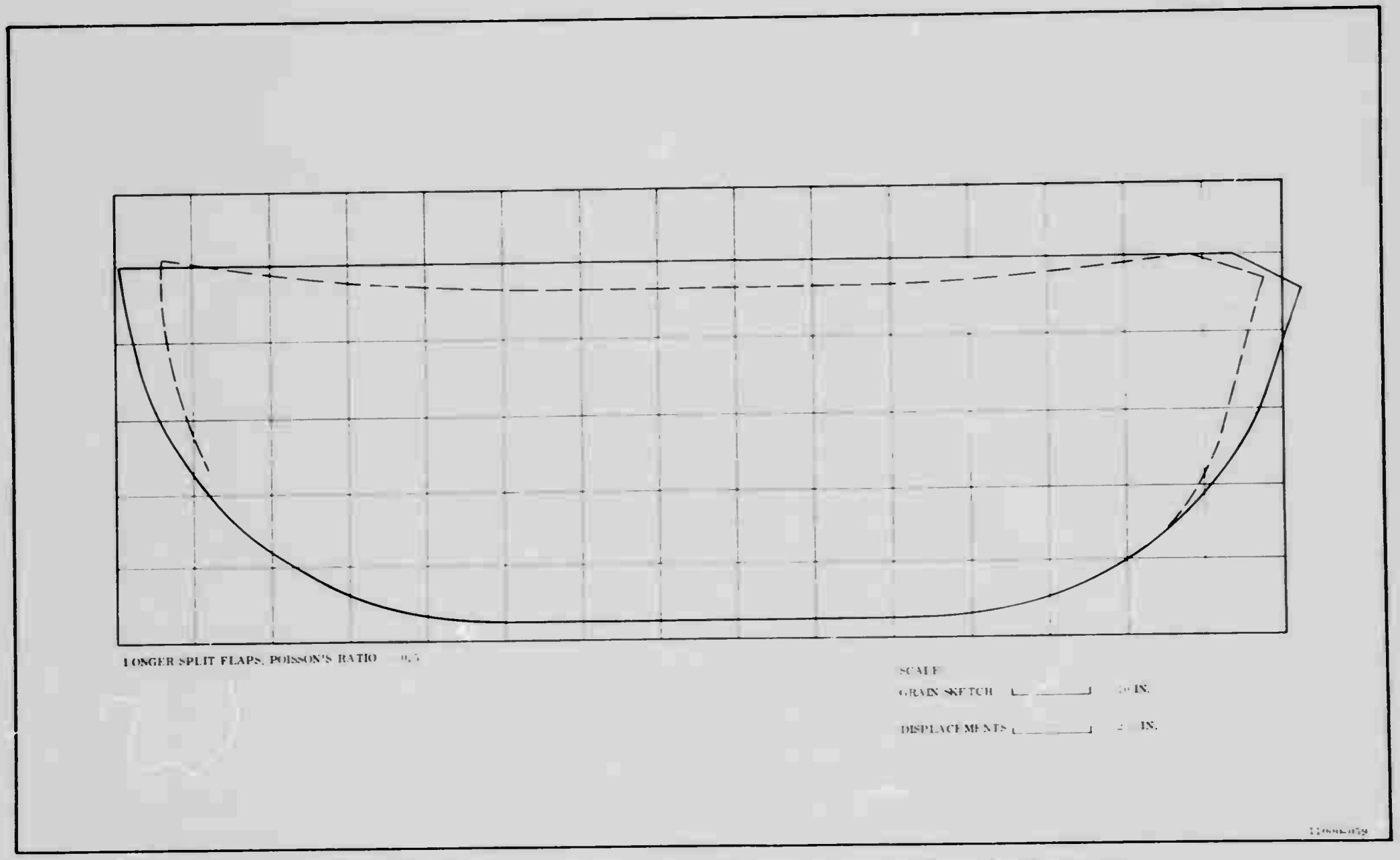

Figure 1B. TU-393 Deformed Grain Curve, Thermal and 1-G Axial Acceleration

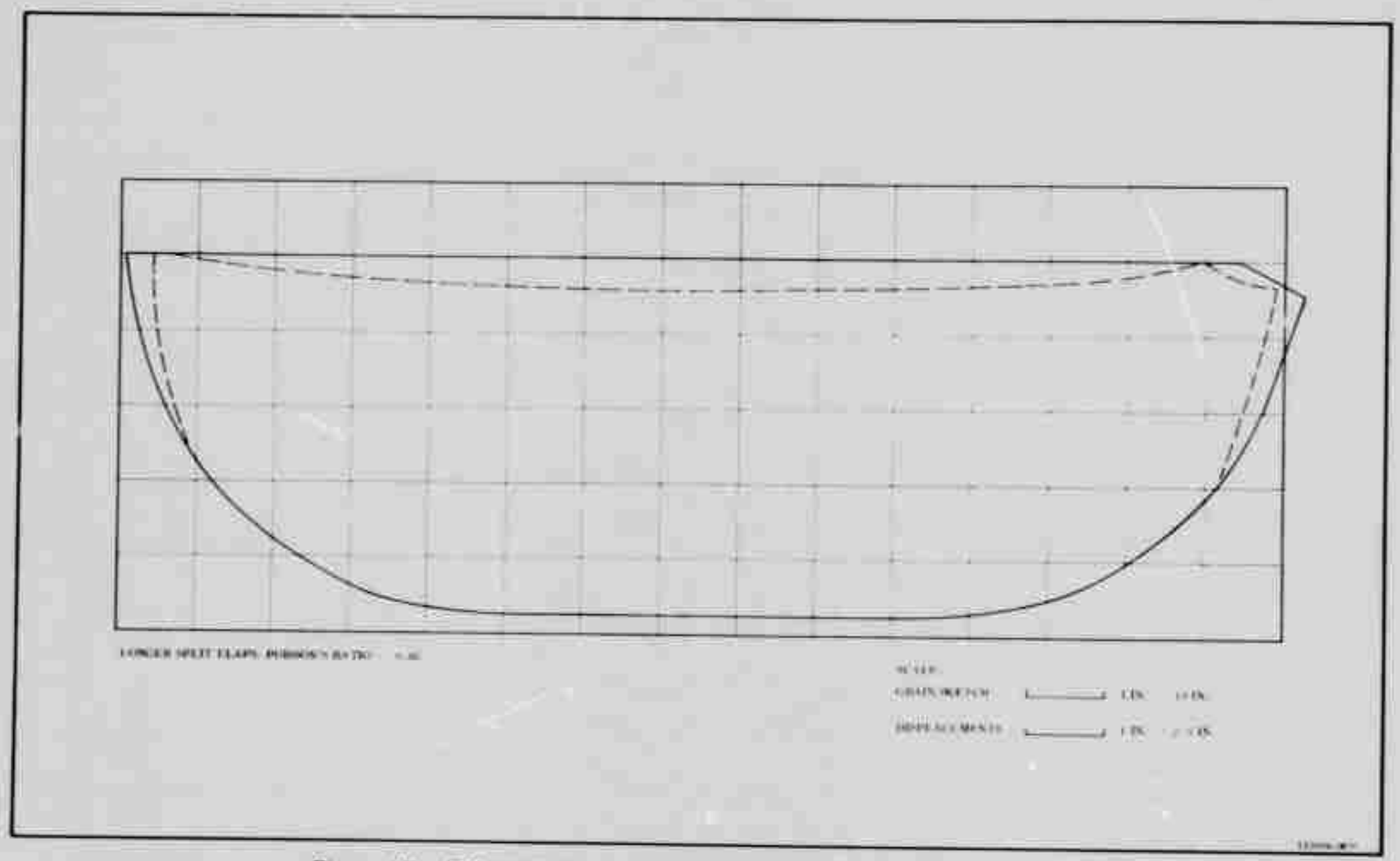

Figure 2B. TU-393 Deformed Grain Internal Pressurization (450 psi)

TABLE 1-B

MARGIN OF SAFETY FOR TU-393 LOADING CONDITIONS

(Longer Split Flats; Poisson's Ratio = 0.5)

Conditions	Maximum Induced Tensile Stress or Strain	Capability*	Margin of Safety
80°F plus 1g Slump	15.37 psi	90 psi	5.86
	0.0307 in/in	0.22 in/in	7.17
80°F 1g Slump and 450 psi Pressure	0.0683 in/in	0.22 in/in	3.22

*Note that propellant capability has been reduced by a factor of 1.5 .

APPENDIX VI

TEST REPORT
FOR
TU-393 LITVC INTEGRATED SYSTEM TESTS (U)

APPENDIX VI

TEST REPORT

FOR

TU-393 LITVC INTEGRATED SYSTEM TESTS (U)

Prepared by

THIOKOL CHEMICAL CORPORATION

WASATCH DIVISION

BRIGHAM CITY, UTAH

12 MAY 1966

TEST REPORT
FOR
TU-393 LITVC INTEGRATED SYSTEM TESTS (U)

12 May 1966

THIOKOL CHEMICAL CORPORATION
WASATCH DIVISION
Brigham City, Utah

Prepared by

H. Money

H. Money
Nozzles and Controls Design Department

Approved by

A. H. Von Der Esch
Manager
Rocket Design Division

L. E. Dufka
Project Engineer
Large Space Booster

TABLE OF CONTENTS

LIST OF ILLUSTRATIONS

LIST OF ILLUSTRATIONS
(continued)

LIST OF ILLUSTRATIONS
(continued)

LIST OF TABLES

SECTION I

PURPOSE

The LITVC integrated system tests were conducted to verify the design of the system and to insure satisfactory system performance prior to installation on the 156-7 motor. The primary test objectives were to evaluate the system slew rate, phase lag, response to sinusoidal inputs, water hammer effects, and overall performance. A secondary objective was to determine the effects of an induced pressurization subsystem failure and hydraulic power supply failure.

SECTION II

INTRODUCTION

The integrated system tests were conducted from 15 thru 28 March 1966, in the Wasatch Division Test Bay T-24. A total of eight test runs were conducted, using the motor duty cycle for three runs and special duty cycles for five runs to evaluate response to step input commands, sinusoidal input commands, simulated failures, and to evaluate overall performance. Tests were performed in accordance with test requirements document TWR-1611, Rev. B. Freon 11 the density of which is approximately the same as N_2O_4, was employed as an injectant in lieu of N_2O_4 for safety. The system was fully instrumented with pressure, flow, temperature, strain, voltage, and accelerometer sensors located to determine performance. Refer to Figure 1 dash 01 configuration for details on instrumentation.

SECTION III

SYSTEM DESCRIPTION

The test configuration for the integrated system tests was identical to the one that will be used for the 156-7 motor static test. See Figures 2 and 3. The plumbing, components and mounting bracketry were the same as will be installed in the motor. The system was installed on a simulated nozzle fixture that had been designed and fabricated to the same dimensions and tolerances as the motor nozzle. This same fixture also served as a catch tank to contain the fluid from the injectors. The fluid was then routed to a storage tank where it was transferred through a filter back into the injectant tank under approximately 10 psig pressure in preparation for the next test run. The test fixture was positioned in the test bay in a centerline horizontal attitude to simulate the motor static firing attitude.

The TVC system for the 156-7 motor is a flight type liquid injection system utilizing nitrogen tetroxide as the injectant. See Figure 4. The system consists of four subsystems; injectant, pressurization, hydraulic and electrical.

Side thrust is produced by expelling the injectant into the nozzle exhaust stream at approximately a 13.1 to 1 expansion ratio through four equally spaced servoinjector valves. Each injector valve is a three pintle individually electrohydraulically operated valve that modulates to the commands from a predetermined duty cycle. Maximum flow rate is 50.5 lb/sec per injector.

Deflection angles up to two degrees can be obtained in any plane by controlling any two adjacent injector valves at the same time. A toroidal manifold feeds N_2O_4 to each injector valve from a pressurized spherical N_2O_4 storage tank mounted on the side of the nozzle.

The N_2O_4 tank, made of 18 percent maraging steel, contains a butyl rubber expulsion bladder and a standpipe to prevent the bladder from collapsing and trapping fluid. Efficiency of the expulsion system exceeds 98 percent as proven by prior expulsion tests. Fluid is contained in the bladder interior and expelled by a nominal 850 psig nitrogen pressure from the pressurization system. A 0.25 inch vent line running through the standpipe to the top of the tank facilitates tank filling. The tank is filled by first expanding the bladder (by drawing a vacuum between the tank and bladder) and introducing fluid through the fill quick disconnect under approximately 10 psig pressure. A flowmeter is installed between the tank and manifold to monitor the total flow rate used during the duty cycle. Burst discs are installed immediately upstream of each injector valve to provide positive sealing

and prevent N_2O_4 leakage into the nozzle prior to pressurization of the system.

The pressurization system consists of a 3,000 psig gaseous nitrogen spherical storage tank mounted on the nozzle opposite the N_2O_4 tank, and a dual pressure regulating system. An initiator solenoid valve is installed in the line between the nitrogen tank and the dual regulation system. This is a normally closed valve which is opened at T minus 40 sec in the countdown. Opening of the initiator valve is delayed as long as practical to prevent the system from being pressurized, rupturing the burst disc and exposing the nozzle to N_2O_4 leakage from the injectors. From the initiator valve, the one inch OD pressurization line separates and each line is routed to a normally open solenoid valve thru a set of pressure regulators and a pressure switch, and then the two lines are tied together and routed to the N_2O_4 tank. Redundant regulation is provided in the event that either regulator fails open or closed. The pressure switch will sense an overpressure condition (1,000 psi) and close the upstream normally open solenoid valve, stopping flow to the malfunctioning regulator. A motorized switch for each pressure switch is incorporated to keep the solenoid valve closed once it has received a signal to close. The regulators are set to deliver an 850 psig nitrogen pressure to the N_2O_4 tank.

The nitrogen tank is made of titanium and is filled remotely through a test facility regulation and plumbing system from 6,000 psi nitrogen bottles. A 3,450 psig relief valve is mounted on the tank to protect the tank from overpressurization.

Hydraulic pressure to operate the injector valves is supplied from an electric motor driven hydraulic pump through a supply and return line manifold going to each injector. Supply pressure is 750 psig utilizing MIL-H-5606 hydraulic oil with a return pressure of approximately 100 psig. Electrical power to the pump motor is supplied from a ground power source. On a flight motor, power would be supplied from a motor mounted battery. A battery bracket is installed on the nozzle but is not used for the static test. A hydraulic relief valve is provided between the supply and return lines in case the pump compensator fails, causing an overpressure condition. A 10 micron filter is provided in the supply line to prevent hydraulic system contamination.

The electrical system provides control of the overall LITVC system including control of the solenoid valves, the hydraulic power supply unit, the servocontrol unit, and the injector valves. The main component in the electrical system is the servocontrol unit. This unit takes the input signals from the guidance system, in this case the ground test signal programmer located in central control, and converts them to the appropriate signals for controlling the injector valves. Power to operate the servocontrol unit is provided by the test facility power source.

SECTION IV

GENERAL RESULTS

The integrated system test results showed that the system will perform satisfactorily. In general, actual system performance during all runs closely approximated the predicted performance. All test objectives were satisfactorily met despite minor difficulties with the expulsion bladder rupturing and leaky fittings in the injectant system. The bladder failures did not appear to affect system performance. The hydraulic and pressurization systems performed exceptionally well; no difficulties whatsoever were experienced.

The system exhibited underdamping tendencies which caused a slight peaking of pintle travel during the 2.5 cps duty cycle events. Underdamping also caused approximately four oscillations before steady state was reached during the hold events. However, steady state was achieved in less than 1/3 second, and the underdamped system did not have any apparent affect on system performance. Slew rates were slightly faster than predicted for the 2.5 cps cycles. The slew rate was 26 deg/sec versus a design rate of 20 deg/sec. Slew rates were up to 49 deg/sec for hold events. Phase lag was 18 degrees. Steady state error for the two degree hold event beginning at 7.5 sec was less than 0.01 deg in terms of pintle travel. Hold and 2.5 cps cycling event outputs were within two percent of inputs based on full travel of the pintle. Pintle travel in response to sinusoidal wave outputs were 2.5 percent greater than the inputs for the 2.5 cps events.

Results of the overpressurization simulated failure tests indicated that either of the dual regulation systems will operate properly and provide adequate pressure if the other system were to fail. The pressure sensing and shutoff safety feature operated as predicted.

SECTION V

DISCUSSION OF RESULTS

Each test run was designed to evaluate specific equipment performance of the system and to evaluate the overall integrated system performance. All runs were conducted using predetermined duty cycles as shown in Figures 5, 22, 26, 31 and 36. Command signals for the duty cycle events were fed through the test facility programmer and then to the servo control unit where they were resolved and sent to the appropriate pitch or yaw injector valves.

Test runs were performed in the following sequence:

Run No.	Date	Ambient Temperature (°F)
1	15 March 1966	57
2	17 March 1966	44
4	18 March 1966	52
5	21 March 1966	50
6	23 March 1966	54
7	24 March 1966	62
3	25 March 1966	57
8	28 March 1966	77

A. BLADDER

In preparation for each run, a prescribed quantity of Freon 11 was drained from the injectant tank by applying 20 psig pressure at the nitrogen vent disconnect and opening the fill line disconnect for Run No. 1. The draining operation for subsequent runs was 10 psig. After the draining operation was completed and pressure reduced to zero, fluid was observed coming from the N_2 vent line indicating a bladder failure. Subsequent to Run No. 1, the tank was opened and the bladder found to be ripped on the nipple end. The split apparently originated at the tip end of the nipple where the standpipe fits in the socket of the deflector plate, and apparently occurred during the draining operation. A new bladder was installed and the tank reconnected for the next run. Bladder failure did not appear to affect the performance of the system.

During the countdown for Run No. 2, the automatic countdown system aborted at T minus 3 seconds. Since pressurization of the system was made at T minus 15 seconds, the system had to be depressurized and recharged. After depressurization, fluid again

ran out of the nitrogen vent line, indicating bladder rupture. Examination of the bladder after the test run showed that the bladder had failed at the same place as the one used for run No. 1. Performance apparently was not affected by the bladder rupture.

The remaining four new bladders in stock were returned to the vendor for rework. A five inch diameter reinforcement made of Dacron mesh was added in the nipple area. The reinforcement was sandwiched between the original bladder and a six inch diameter butyl rubber patch. A reworked bladder was installed for run No. 6, with no leakage indicated after the run. Run No. 6 bladder was reused for run No. 7. After run No.7, the bladder had a 0.25 inch long tear at the neck. This type of failure is not considered significant since all or majority of the injectant is expelled before the folds enter the neck area and put stress on the bladder neck.

During next run, No. 3, no bladder failure was noted except that 1/8 inch diameter holes were punched in the bladder after all fluid had been expelled. Holes in the standpipe are 1/8 inch diameter. This type of failure was as predicted because when all fluid is expelled, the bladder receives the full 850 psig differential. Prior bench tests simulating the standpipe indicated that the bladder can withstand approximately 650 psig before rupture.

During the last run, No. 8, the bladder failed in the nipple area and around the neck. However, the split did not propagate outside the reinforcement area. After rework of this bladder, the reinforcement had several large air bubbles between the layers of rubber which apparently contributed to the failure.

Below is a summary of bladder performance during the integrated system tests.

Run No.	Configuration	Performance
1	New bladder	Failed in nipple area
2	New bladder	Failed in nipple area
4	No bladder	
5	No bladder (a deviation from test plan)	
6	New reworked bladder	No failure
7	Run No. 6 bladder reused	Failed at neck
3	New reworked bladder	Punched 1/8 inch diameter holes as predicted
8	New reworked bladder	Failed in nipple area and neck

Bladder failure apparently does not affect performance of the system since all injectant apparently was expelled when the duty cycle requires complete expulsion, and no indication of flow interruption was seen on any of the data traces. Two new bladders are being fabricated for the motor test with a fiberglass mesh reinforcement which will provide greater strength in the nipple area than the Dacron reinforcement used for the integrated system tests. In addition, the rubber reinforcement will be cured as an integral part of the main body of the bladder, giving a superior bond to hold the reinforcement in place. Ruptures in the neck area are not considered to be significant for the motor static test. These failures obviously occur at the end of the expulsion because, upon examination of the fully collapsed bladder after the standpipe is removed, several folds were seen terminating at the neck in the area where the tears were located. Bladder failure is not anticipated during the motor static test.

B. LEAKAGE

Some leakage was encountered in the injectant subsystem lines during the first five test runs. Major points of leakage were in the 2.5-inch line connections and two 2-inch hose connections. Leakage rates varied from drops to spurting of the fluid. These leaks were essentially stopped by using Teflon tape on the flared fittings and increasing the torque on the connections. Conical aluminum seals were tried with no success. During the last two runs (No. 3 and No. 8), no leaks were encountered. All 2.5-inch lines were fabricated from welded 304 stainless steel tubing per Specification MIL-T-6845. Both seamless and welded tubing meet this specification. The welded tubing appeared to be the main cause of the leaks. Seamless tubing will be used for the motor static test.

C. SERVO CONTROL UNIT ADJUSTMENT

Prior to the initial test run, the servo control unit gain, null bias, and range of travel settings were adjusted by removing the servo injector valves from the test fixture and measuring pintle travel with a dial indicator while feeding null and full travel commands to the SCU.

The servo amplifier gain setting had to be reduced from 9.0 max/volt to approximately 4.5 max/volt when referred to the followup to achieve stability. A closed loop frequency response test indicated performance requirements would be met with these gain settings during the integrated system testing. The bias and range settings appeared to remain stable throughout the testing period.

D. DISCUSSION OF COMMON DATA

In general, the system performance during all runs appeared to be approximately as predicted. The hydraulic system and the pressurization system performed exceptionally well without difficulty. Temperature rise of the nitrogen tank during filling varied from 54° to 81°F for all runs with approximately 15 minutes required to charge the tank. Table I shows the temperature rise for all runs. All test objectives were met satisfactorily although difficulties were encountered with the bladders and leaky fittings in the injectant system. Typical pressurization system traces are shown in Figures 8 and 41. Regulation pressures were within acceptable limits for all runs. Hydraulic system pressures are presented in Figures 9 thru 11 and Figures 42 thru 44. No abnormalties are seen on these traces which are representative of all runs. Hydraulic pump maximum run current was 119 amperes. Starting currents were not measured since the pump was switched on approximately one minute prior to starting the data recording system.

Strain data show the maximum stress on the nitrogen tank to have been 43,832 psi. This stress occurred at zero seconds on run No. 6, which corresponds to a tank pressure of 2,740 psig. The N_2O_4 tank has a maximum stress of 80,386 psi which occurred at zero seconds during run No. 2. Run No. 2 injectant tank pressure was 970 psig when the simulated pressurization was initiated. This gives a 2.5 factor of safety based on yield. Table II shows the maximum stresses measured on the nitrogen tank, injectant tank, and system tubing. These stresses are relatively low, with ample margins of safety. The minimum factor of safety for the tubing was 2.8 based on yield.

TABLE I

NITROGEN TANK TEMPERATURES

Run No.	Test Bay Temperature (°F)	N_2 Tank Temperature (°F) Before Filling	N_2 Tank Temperature (°F) After Filling
1	57	65	122
2	44	54	116
4	52	56	112
5	50	55	109
6	54	54	117
7	62	62	120
3	57	53	124
8	77	60	141

TABLE II

MAXIMUM STRAIN AND ACCELERATION FOR ALL RUNS

Maximum Strain Data

Item	Location	Time (sec)	Strain (micro in./in.	Run No.	Stress (psi)
Nitrogen Tank	S604	0	1765	6	43,832
Injectant Tank	S601	0	2022	2	80,389
2.5 in. OD Tubing	S607	8.8	562	1	17,9[illegible]
1.5 in. OD Tubing	S609	8.8	620	2	29,760
1 in. OD Tubing	S612	0	557	5	17,752

Vibration Maximum G's

Item	Location	Time (sec)	Max. G	Run No.
Nitrogen Tank	A601	8.1	8.8	4
Injectant Tank	A602	7.7	29.7	4

E. DISCUSSION OF EACH TEST RUN

The following paragraphs discuss the results of each run. Only the complete set of data traces for runs No. 1 and No. 8 are included in this report. Plots are included for each of the other runs to present the data showing that the objective of the run was demonstrated. The same corresponding curves as shown for runs No. 1 and No. 8 are available at Thiokol for runs No. 2 thru No. 7. Most of these data are repetitious of runs No. 1 and No. 8, and are omitted to prevent redundancy.

1. RUN NO. 1 - This run was conducted to determine the overall LITVC system performance during the initial 96 sec of the motor static firing duty cycle. In accordance with the test plan, 453 cu. in of injectant were removed from the tank after filling to maximum capacity. This left more than adequate injectant for the duty cycle to insure that injectant flowed through the flowmeter throughout the run. Damage to the flowmeter could be sustained if gas came through the injectant system. The duty cycle is illustrated in Figure 5. Results of this run are presented in Figures 6 through 20.

On the first event, in response to a step signal of 1.0 deg, the output was low by 0.055 degrees. Actual output was approximately 0.945 degrees. The input was signal for 0.0409 in. of pintle travel. Since the accuracy of the data acquisition system is five percent, travel can only be relied on to an accuracy of 0.0135 in., which corresponds to 0.17 degrees. This means that the 0.055 degree error lies well within the accuracy of the recording system.

Since the system is slightly underdamped, approximately four oscillations occur before steady state is reached at initiation of the first event. The time of first crossover occurs at 0.041 seconds after input, and steady state is reached at 0.310 seconds. Oscillations are approximately 15 cps. The slew rate as obtained from the digital data indicated a velocity of 49.5 deg/sec at one point in the first event. Response time for step holds is faster than expected. Maximum slew rate for the two degrees, 2.5 cps event at 78 to 79 seconds was 26 deg/sec.

The steady state error in the two degrees hold event at 7.5 to 9 seconds was less than 0.01 degrees when computed from the tabulated data. Actually the error is so small it cannot be determined accurately.

Steady state injectant flow was slightly higher than predicted. Below is a table of actual flow rates vs predicted flow rates.

TIME (sec)	RECORDED FLOW (gpm)	PREDICTED FLOW (gpm)
5.0	86 to 86	84
7.5-9.0	220 to 225	217
42.0	167 to 170	165

Some electrical noise was present in the input and was transferred to the output. It can be seen on the position feedback plots. The noise only appears on the plots when a command is given. The reason for this is that during a hold the data are plotted at one point per second while during an event data are plotted every six milliseconds. The noise probably is present but is filtered by the low plotting rate. This input noise does not appear to affect performance of the system appreciably.

2. RUN NO. 2 - This run was conducted to determine performance of the system with an artificially induced malfunction of one side of the dual pressurization system. Malfunction was simulated by overpressurizing the dome of the main regulator from a solenoid valve controlled pressure source. The duty cycle was the same as used for Run No. 1 (Figure 5).

Figure 21 shows that the pressurization system will operate on one regulator within acceptable limits. This test also demonstrated that the overpressurization detection system senses the overpressure condition and shuts off the N. O. solenoid valve upstream of the regulator as planned. The solenoid valve remained closed throughout the run as anticipated.

The overpressure condition should have been initiated at T plus 7 seconds. However, the operator inadvertently actuated the overpressurization control switch at T minus 7 seconds, causing the system to be overpressurized already at T equals 0. This explains why the trace shows 970 psig at the beginning of the run.

3. RUN NO. 3 - This run was conducted to determine system performance with an artificially induced malfunction by overpressurization of the opposite side of the dual pressurization system. Malfunction was simulated by the same method as for Run No. 2. Duty cycle for this run was the full duration motor duty cycle as shown in Figure 22.

This run was made out of sequence and after Run No. 4; therefore, a total of 1,843 cu. in. of Freon 11 were drained from the tank after filling. Run No. 4 used the same duty cycle except with 1,728 cu. in. of injectant were removed and approximately 21.5 lb. were left in the system after the run. Run No. 3 was conducted using less injectant in the tank in an attempt to determine the exact amount of fluid required for the motor duty cycle. The data, Figure 23, show that all fluid was expelled at 97.5 seconds at that point, pressure dropped abruptly.

Figure 24 shows the trace of the reduced nitrogen pressure. A spike can be seen beginning at T plus 7 seconds, indicating that the overpressure malfunction occurred as planned and that the system performed satisfactorily on one side of the dual pressurization system. Valve position indicator lights on the control panel verified that the N. O. solenoid valve remained closed for the remainder of the run.

4. RUN NO. 4 - This run was conducted to determine whether the system would function without the injectant tank bladder. The bladder was removed and the motor duty cycle (Figure 22) was used.

Figure 25 does not show any excessive changes in pressure over those of the other runs, probably indicating that no gas was flowing through the injectant system. Therefore, the system apparently functions properly without a bladder.

5. RUN NO. 5 - This run was conducted to determine the system response to sinusoidal commands. The duty cycle for this run is shown in Figure 26.

The response to full scale sine wave inputs at 2.5 cps shows an amplification of approximately +0.36 db for injectors No. 1 and 3, and +0.24 db and +0.13 db for injectors No. 2 and 4, respectively. The peaking at this frequency is characteristic of this underdamped system. For a critically damped system, a slight attenuation would be expected. Position feedback voltages in terms of pintle travel are shown in Figures 27 thru 30.

Phase lag cannot be calculated accurately because of the length of the time intervals of the recording devices (1/156 sec), is equivalent to six degrees at 2.5 cps. From the printout of the digital data, the phase lag appears to be less than 18 degrees for all injectors.

6. RUN NO. 6 - The objective of this run was to determine response to step input commands and to determine static position error. The duty cycle is illustrated in Figure 31.

Steady state errors resulting from a maximum input command do not exceed 0.006 in. of pintle position. The indicated error was always in the direction to increase the pintle position. For example, input for the two degree event beginning at T plus 44 seconds was for a pintle travel of 0.140 in. and the output was 0.146 in. steady state for injector No. 3. The time for the output to reach 90 percent of its final value for a two degree command was approximately 0.060 sec for all injectors. Figures 32 thru 35 show the response to step input commands.

7. RUN NO. 7 - This run was conducted to determine the ability of the injector valves to return to the closed position in the event of hydraulic power failure during valve operation. Hydraulic power failure was simulated by venting the supply line and venting the low pressure side of the No. 4 plus yaw injector valve piston simultaneously. See Figure 36 for the duty cycle.

Figure 37 shows the hydraulic pressure in injector No. 4 dropped to almost zero as scheduled. Figure 38, shows that the valve was at a position equivalent to a two degree hold event when

simulated failure occurred and the feedback position plot shows that the valve closed immediately upon loss of pressure. As soon as pressure was restored, the valve functioned as scheduled for remainder of the run.

The position feedback plot (Figure 38) shows the valve closing to a negative value. This is caused by an input signal commanding the valve to a maximum opening and, since the hydraulic pressure is zero, the valve is closed and the error signal is maximum, resulting in an overloaded or saturated amplifier.

8. **RUN NO. 8** - The objective of this run was to determine the system performance under simulated motor conditions. The full duration motor firing duty cycle was employed (Figure 22). The countdown was the same as will be used on the motor, i.e. hydraulic pressure was initiated at T minus 1 minute and the pressurization system was activated at T minus 50 seconds.

Complete data traces for Run No. 8 appear in Figures 39 thru 52. All pressures, temperatures, response times, and position feedback traces were approximately the same as describe' for Run No. 1.

Based on the results of this last run, no problems are anticipated in meeting the predicted performance of the system during the motor static test.

F. WEIGHTS

The following tabulation shows the system weight as determined during the integrated system testing. System weight does not include weight of the injectant, pressurant, hydraulic fluid, or instrumentation. The weight shown reflects the weight of the complete dry system that will be used during the motor static test.

LITVC System	668.4 lb
Injectant (Freon-11)	503.1 lb

SECTION VI

CONCLUSION

The LITVC integrated system tests proved that the system will perform satisfactorily. All test objectives were met with satisfactory results. No problems are anticipated during the motor static test; the system is expected to perform as predicted. Minor problems encountered on the integrated tests, such as leaky connections and bladder rupture have been resolved by minor design changes. The system is slightly underdamped, allowing some oscillations of the injector valve pintle before steady state is reached in the hold events. However, steady state is delayed approximately 1/3 second and these oscillations do not have any significant effect on performance.

The pressurization subsystem regulates the pressure to the injectant tank within acceptable limits. All components in the system functioned exceptionally well during all runs. Simulated overpressurization failure tests indicated that the system will close the malfunctioning side of the dual system and the opposite side will continue to regulate pressure to the injectant tank. Injectant tank initial full pressurization occurs approximately 1/4 second after opening the initiator valve.

System response is faster than expected. Maximum slew rate is approximately thirty percent greater than what was predicted for the 2.5 cps cycling rate. The maximum slew rate for the duty cycles used in these tests occurs when a two degree hold is initiated. A maximum pintle travel is commanded in an infinitesmal amount of time. This causes the system to respond to its maximum capability, which is 49 deg/sec.

No evidence of water hammer effect was indicated in any of pressure traces. The pressure fluctuations shown on the pressure traces are not of sufficient magnitude to be caused by water hammer.

INSTRUMENTATION (REF)				
[illegible]	PARAMETER	LOCATION	[illegible]	[illegible]
[illegible]	[illegible]	[illegible]	[illegible]	[illegible]

DETAIL [illegible]
SCALE 1/1
(TYPICAL BOTH TANKS)

TU37709

Figure 1. Inst

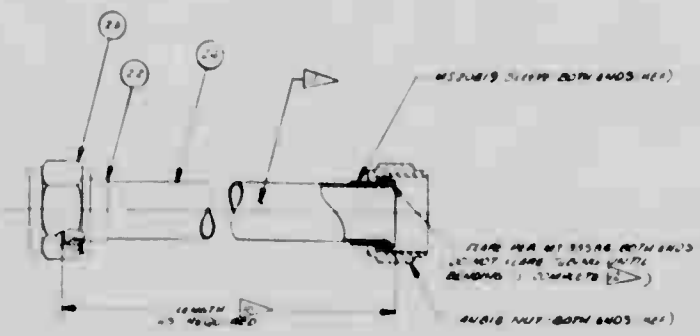

3 TUBE ASSY

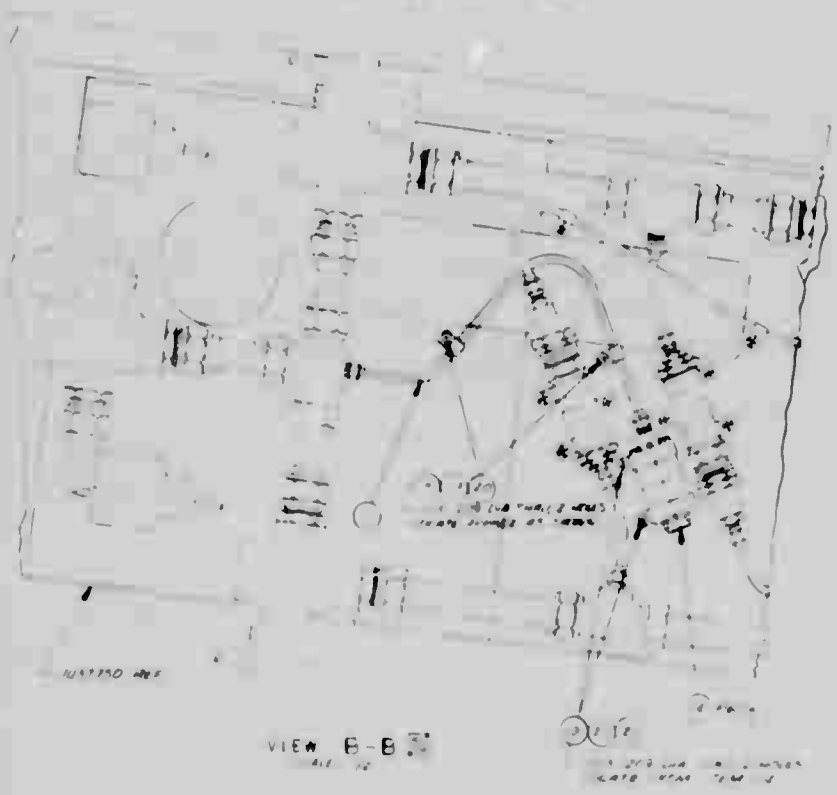

VIEW B-B

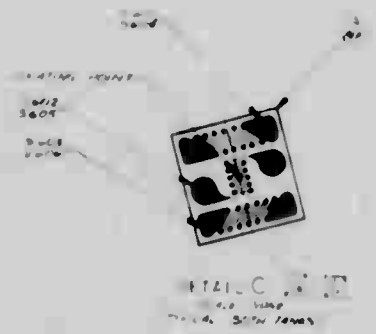

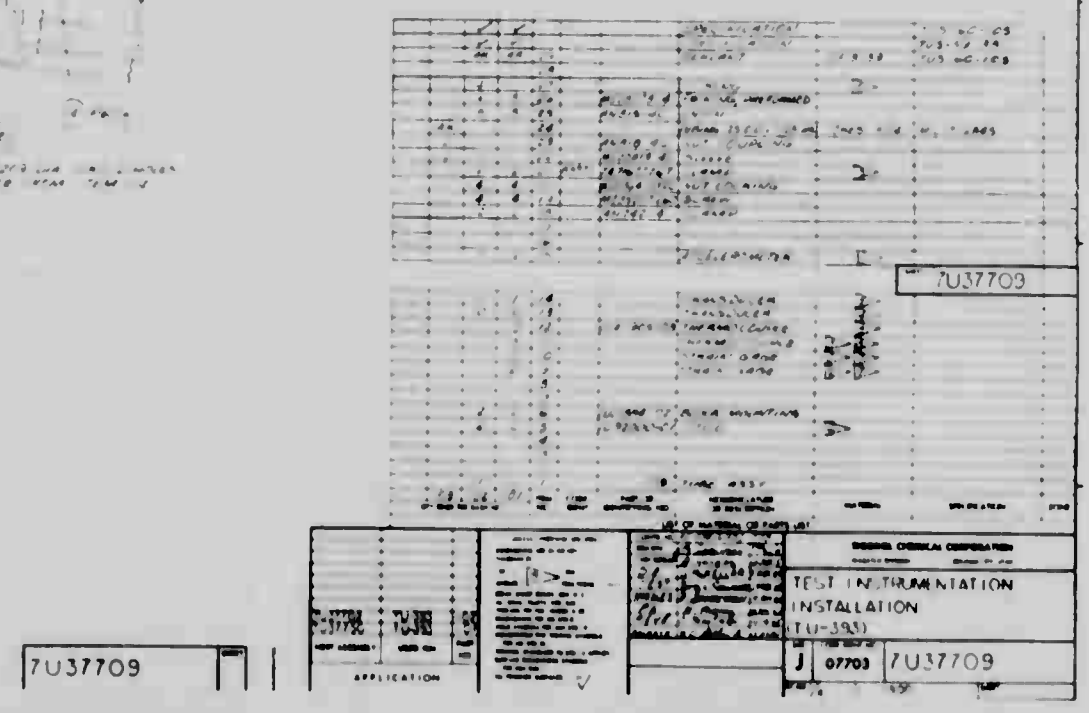

Figure 1. Instrumentation for Integrated System Tests

3

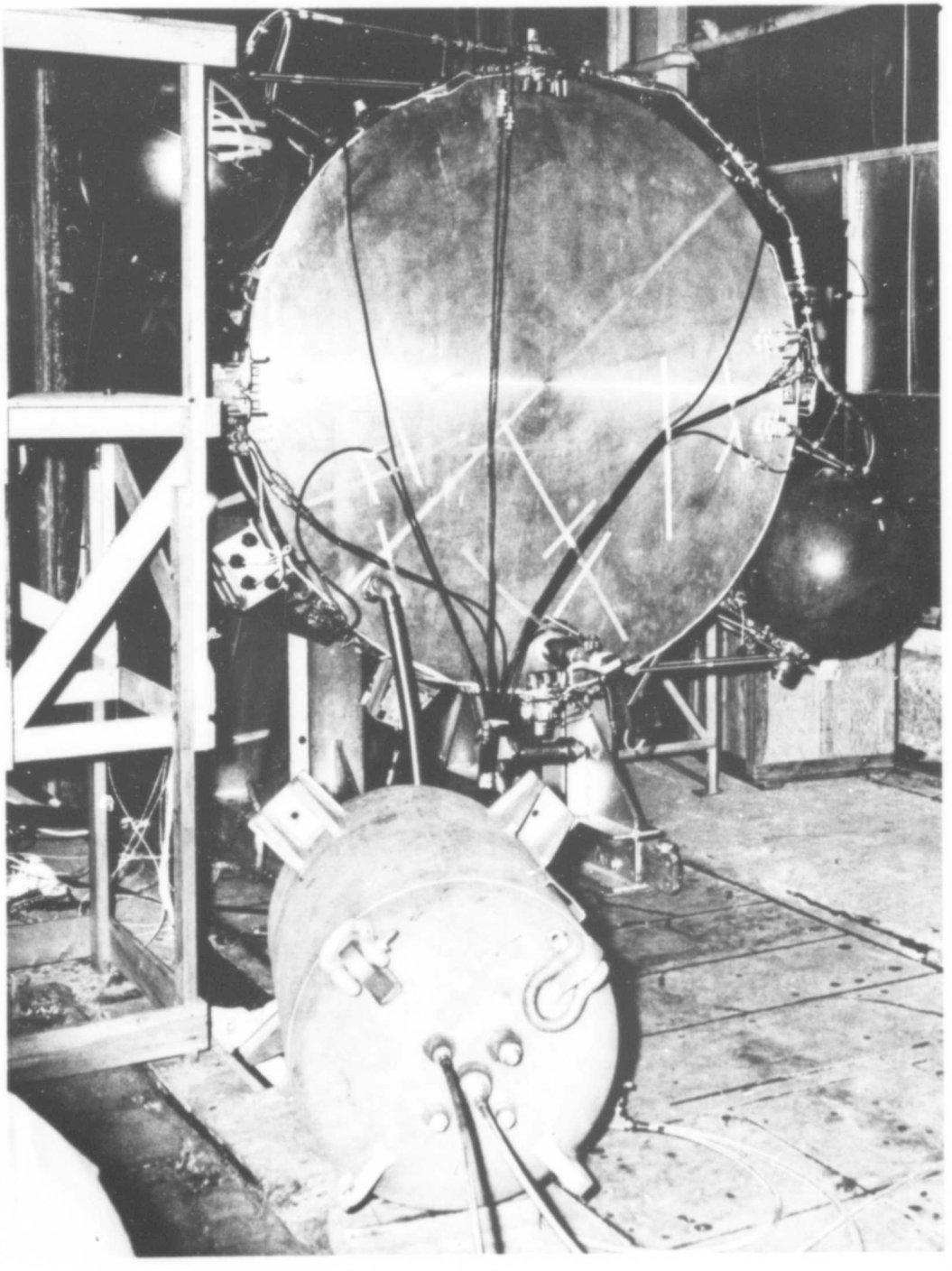

Figure 2. Integrated System Test Set-Up

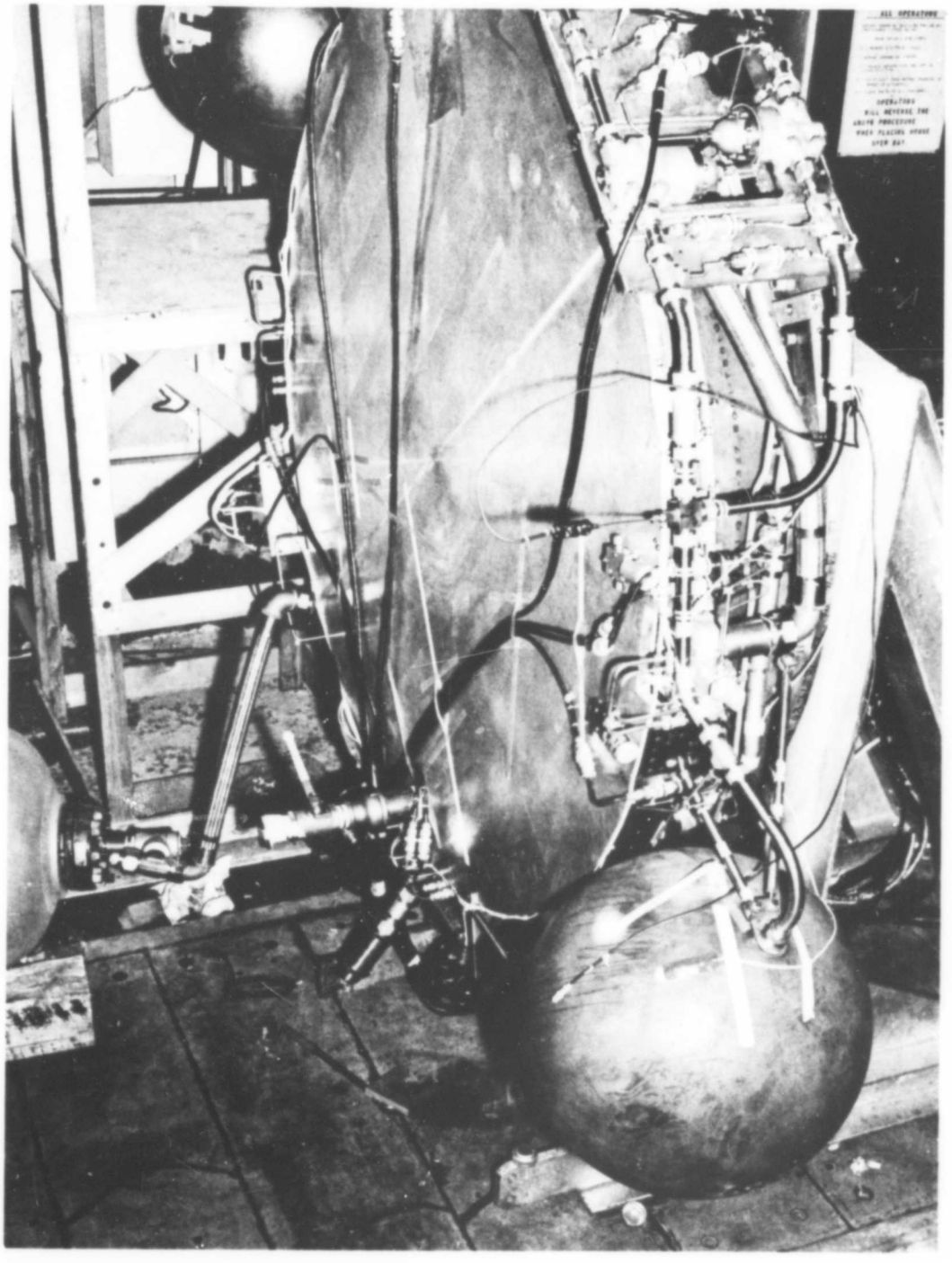

Figure 3. Integrated System Test Set-Up

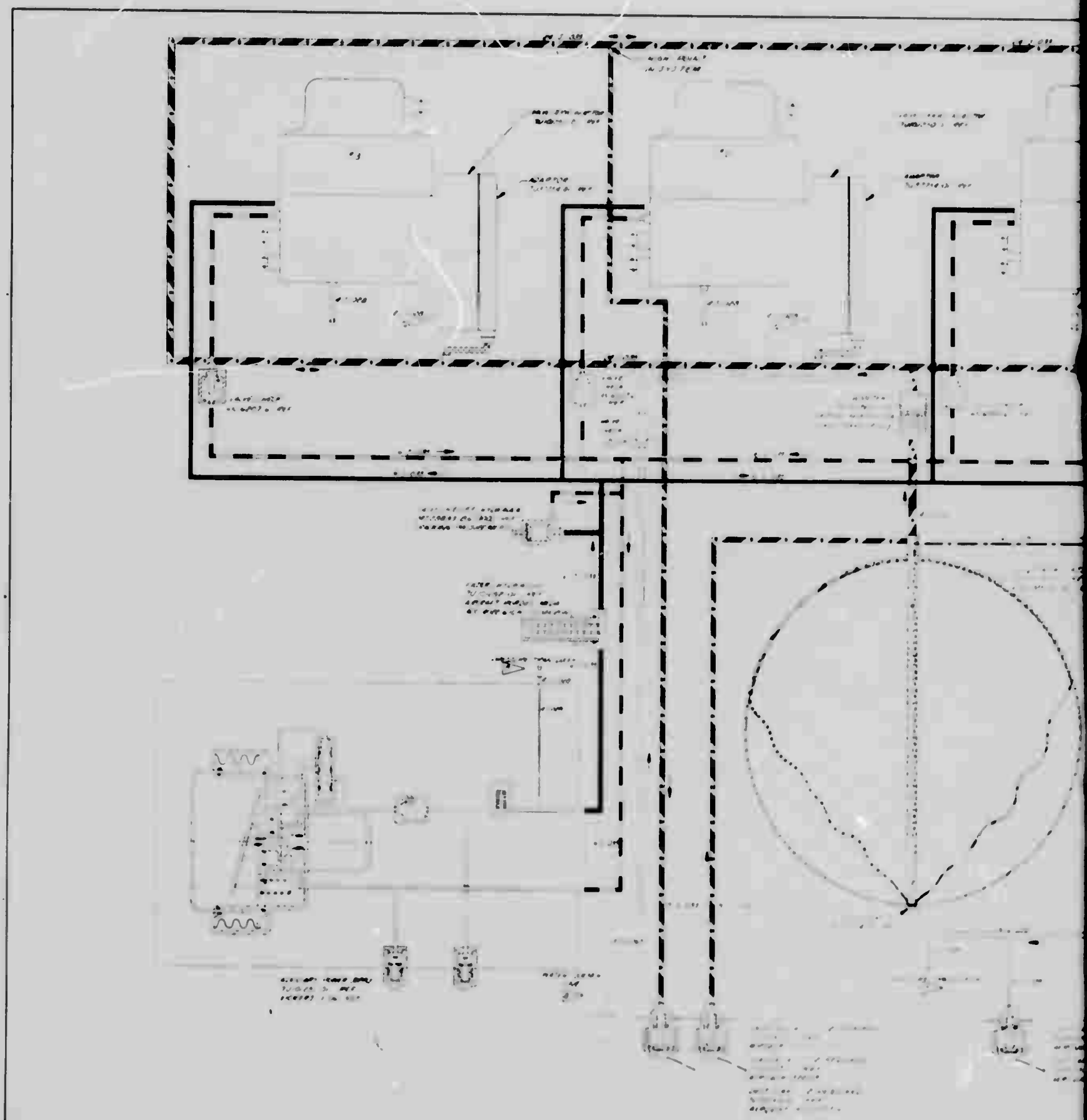

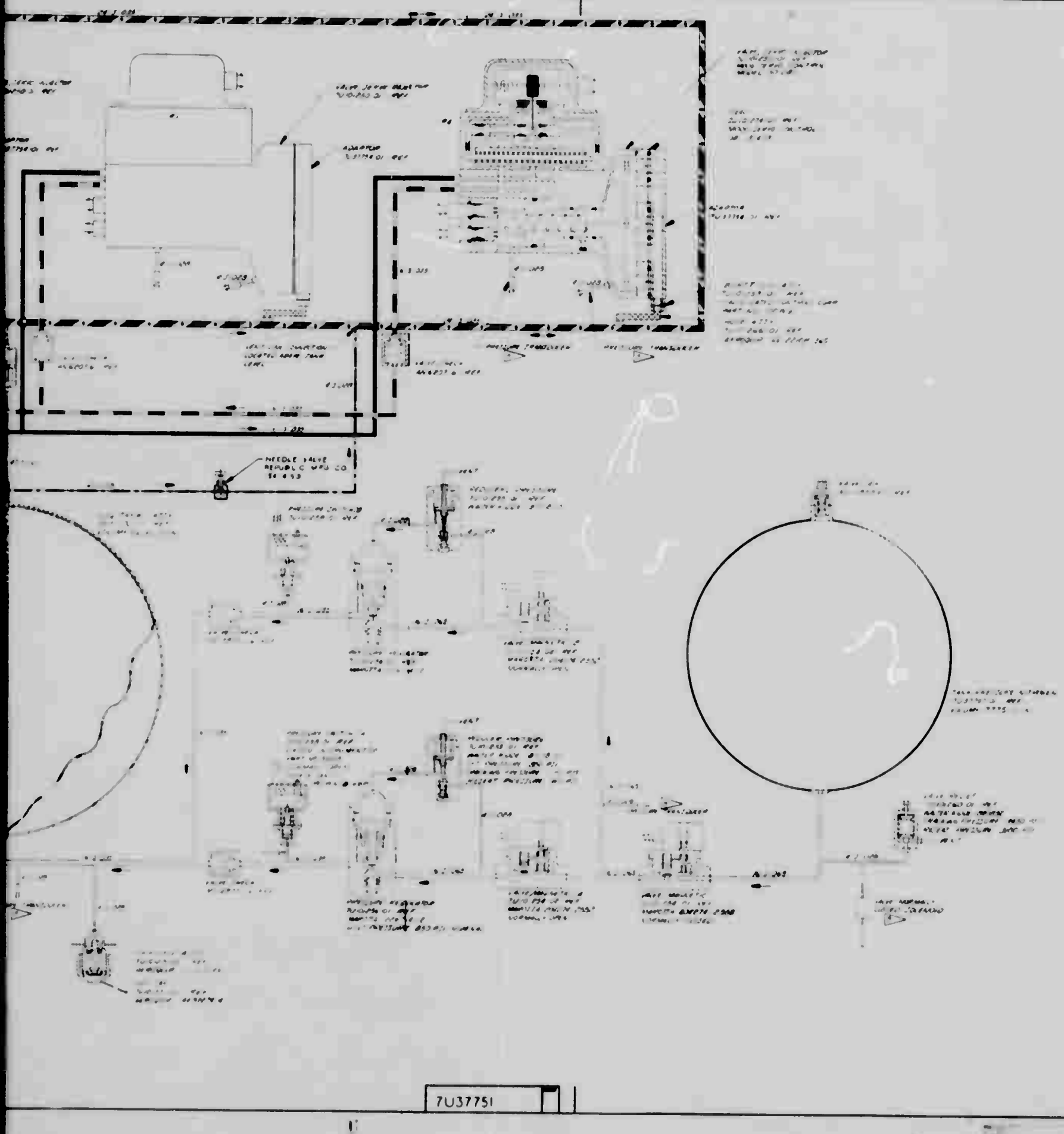

Figure 4. LITVC

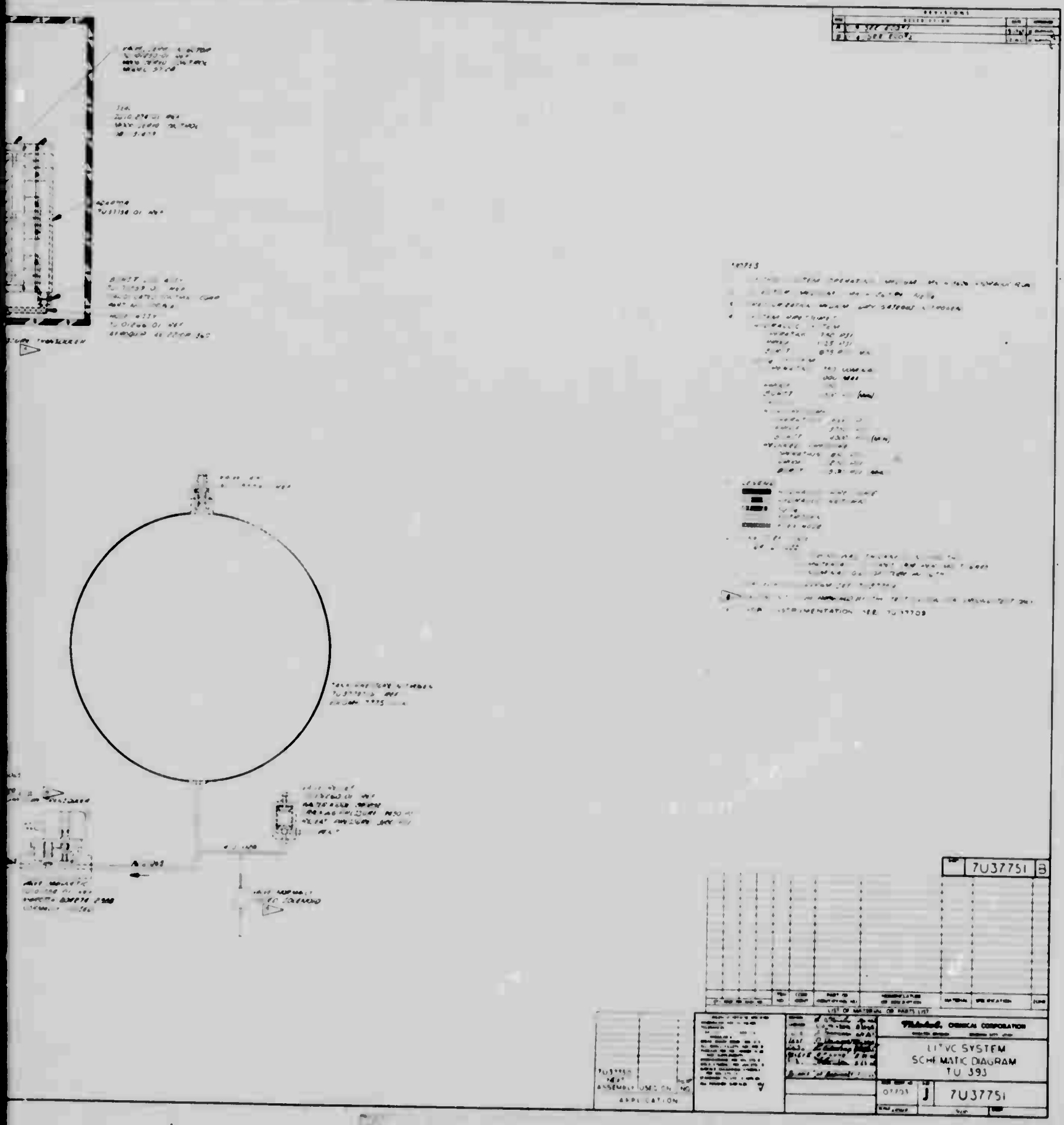

Figure 4. LITVC System Schematic for [illegible]-7 Motor

PREVIOUS PAGE WAS BLANK, THEREFORE WAS NOT FILMED.

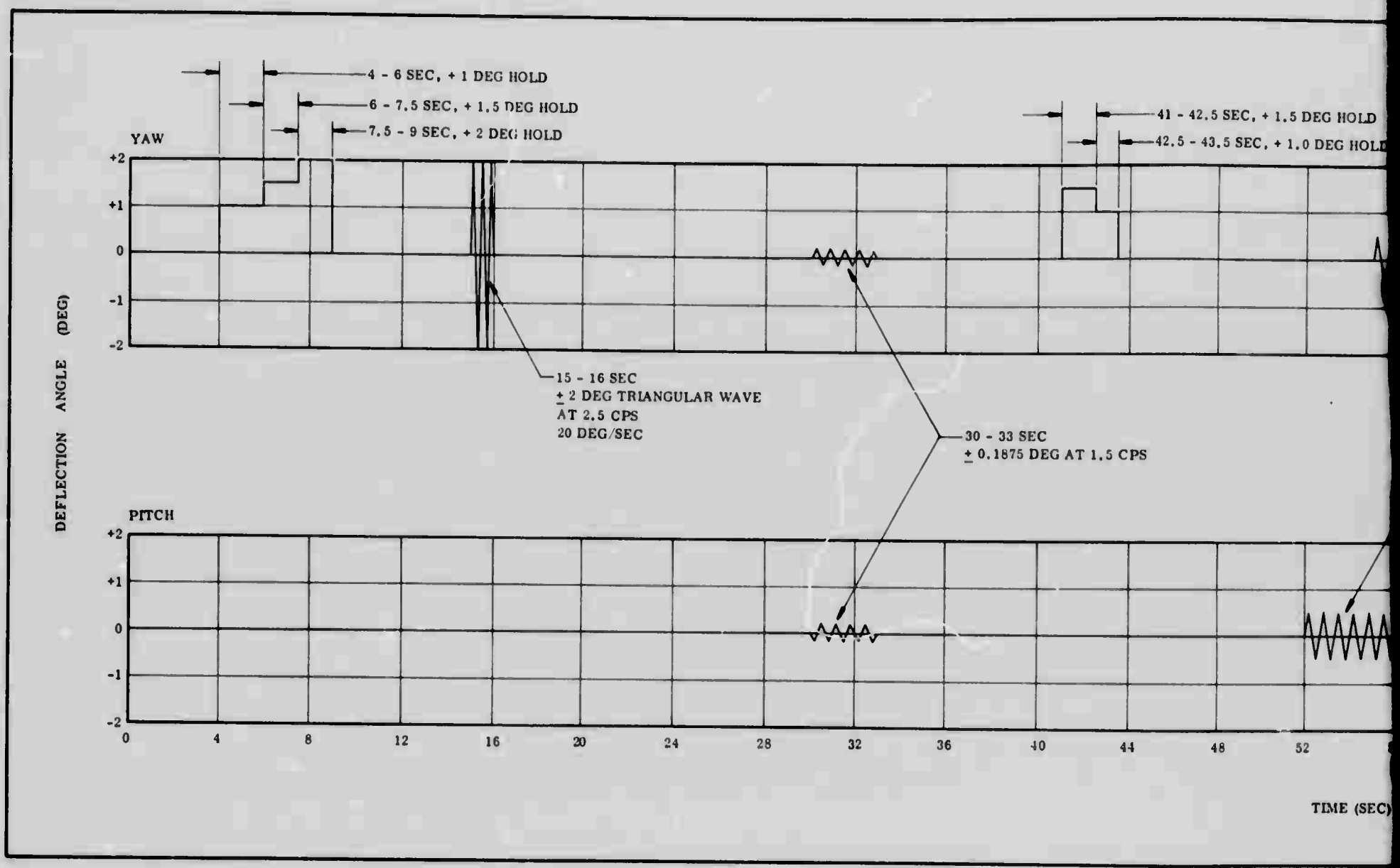

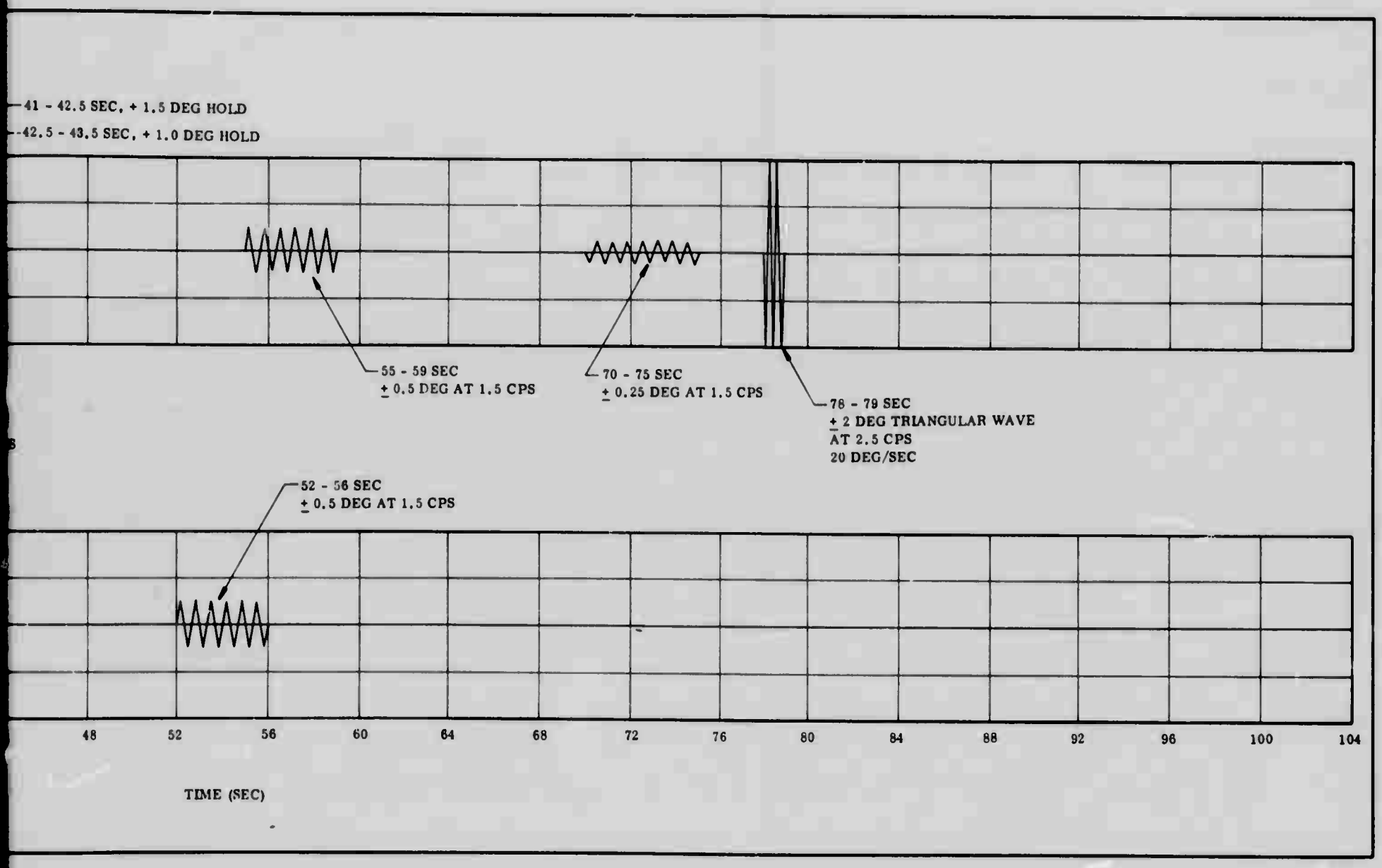

Figure 5. Duty Cycle for Run No.'s 1 & 2

PREVIOUS PAGE WAS BLANK, THEREFORE WAS NOT FILMED.

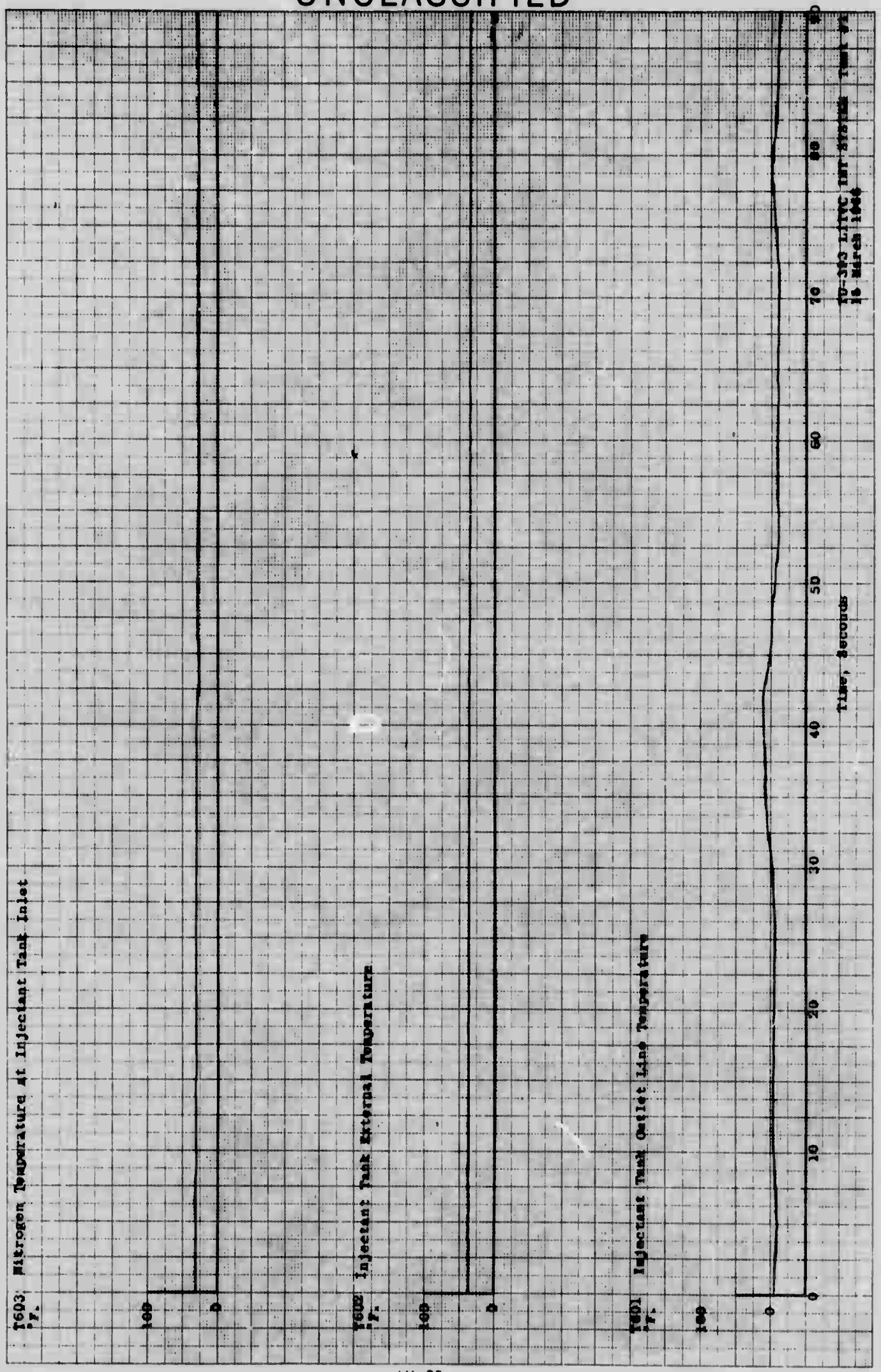

Figure 6. Temperatures - Run No. 1

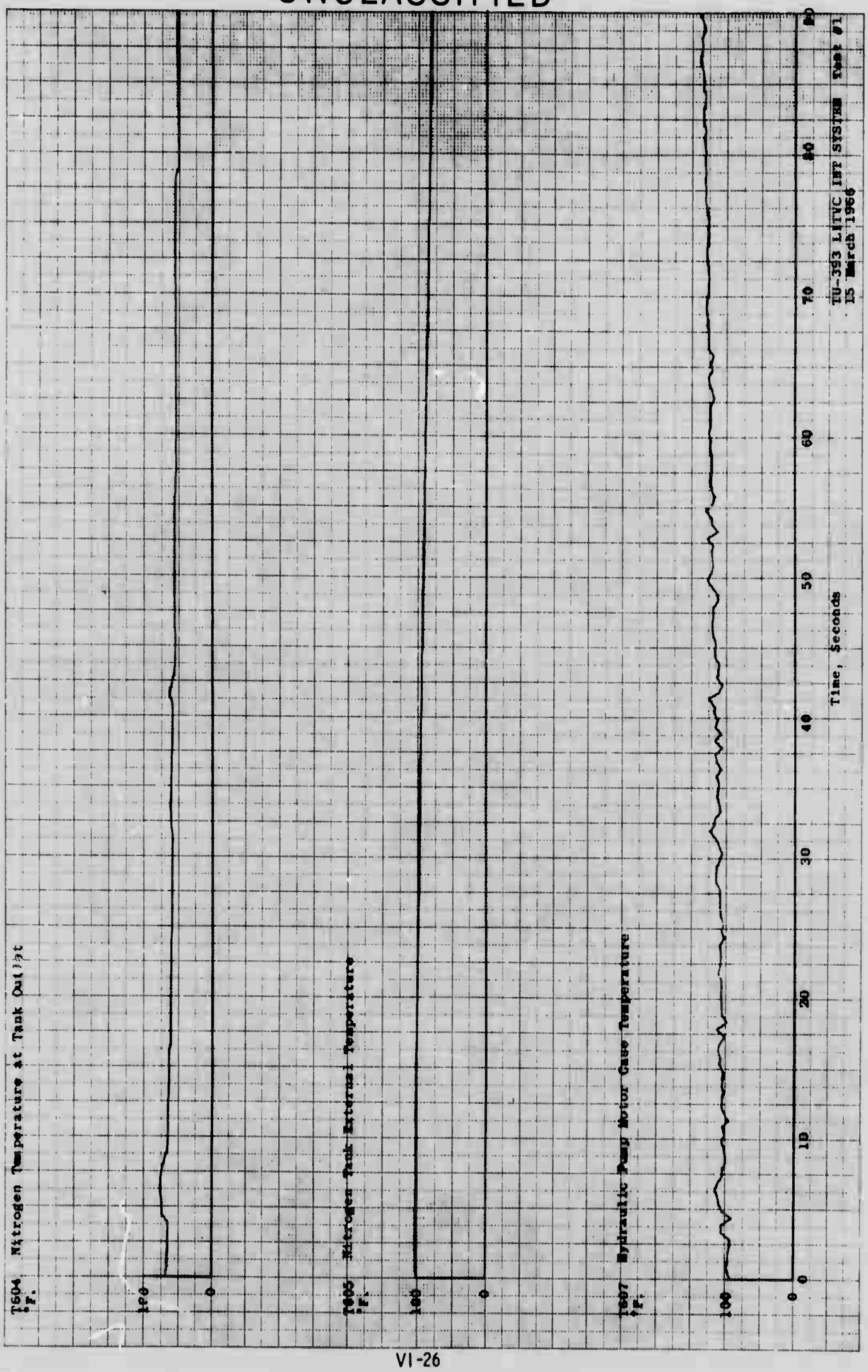

Figure 7. Temperatures - Run No. 1

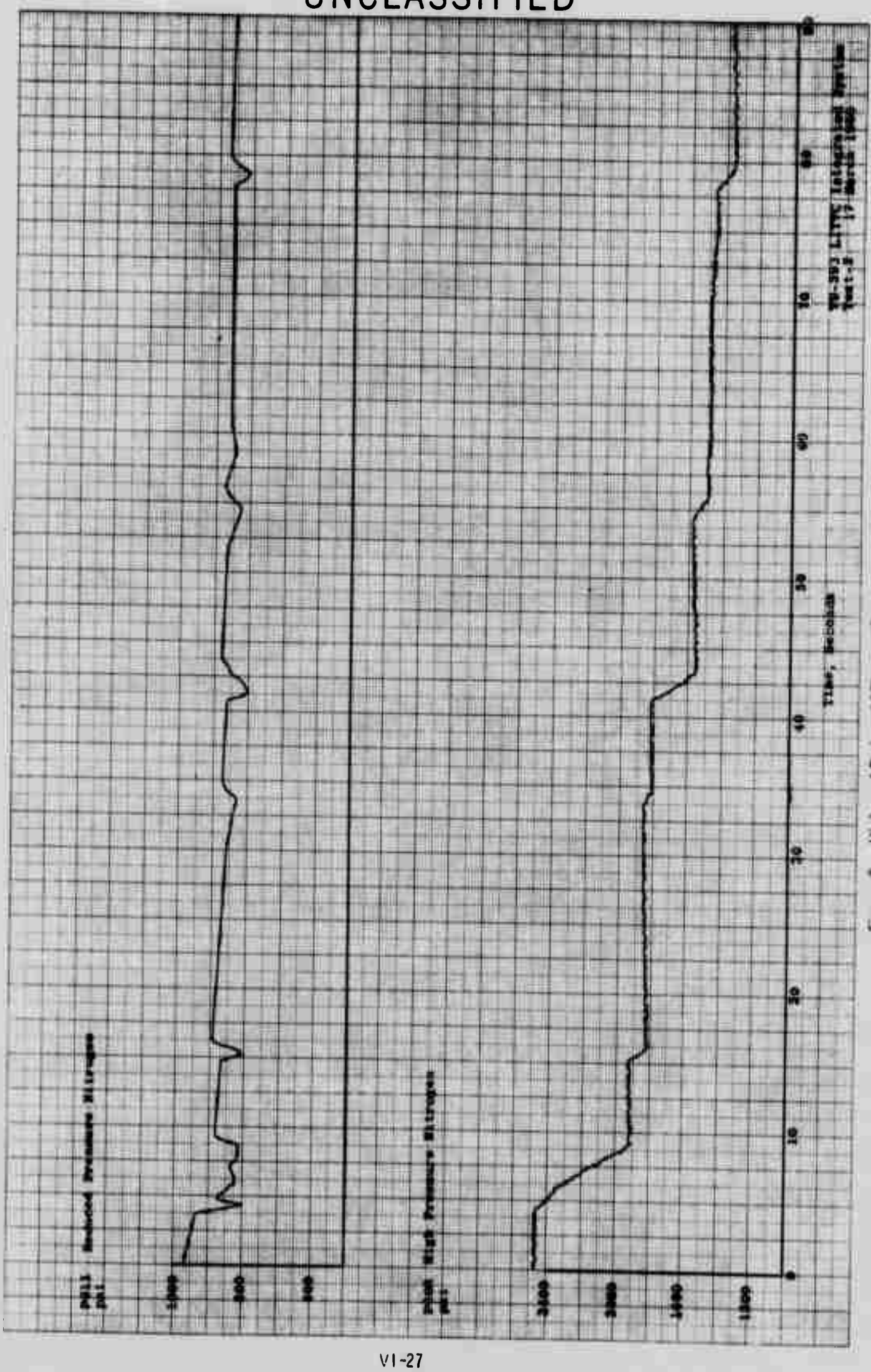

Figure 8. High and Reduced Nitrogen Pressures - Run No. 1

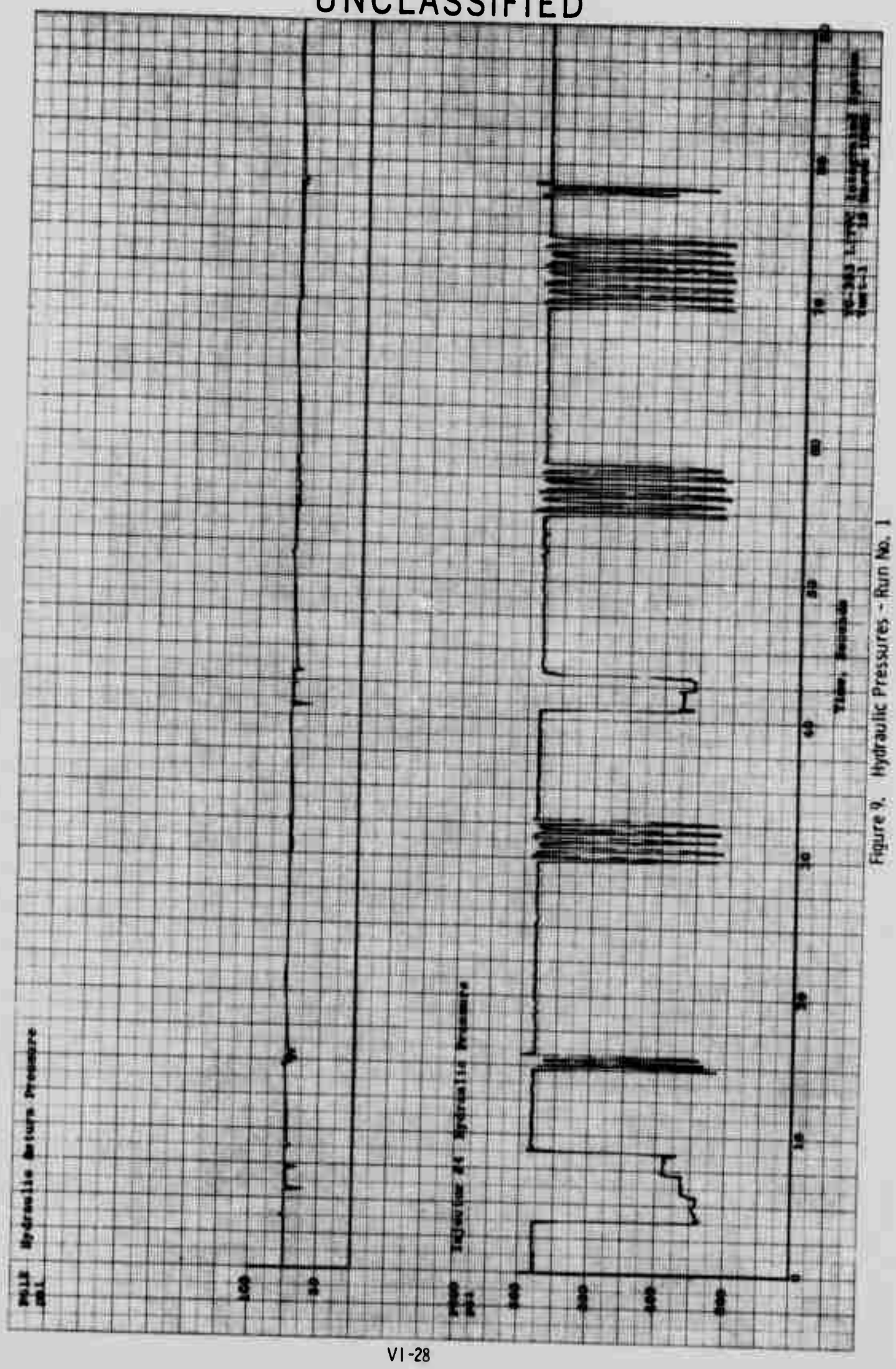

Figure 9. Hydraulic Pressures - Run No. 1

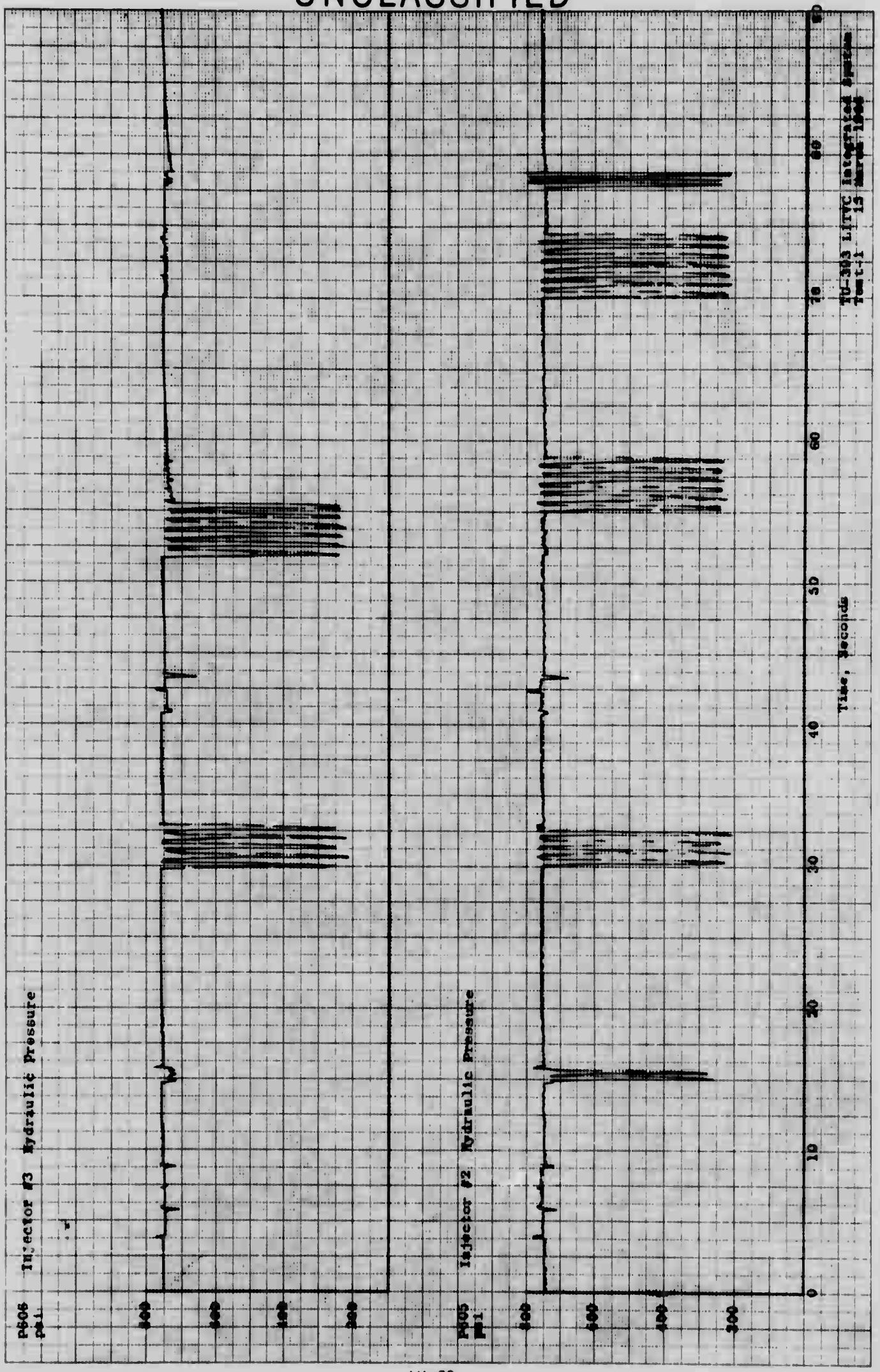

Figure 10. Injector Hydraulic Pressures - Run No. 1

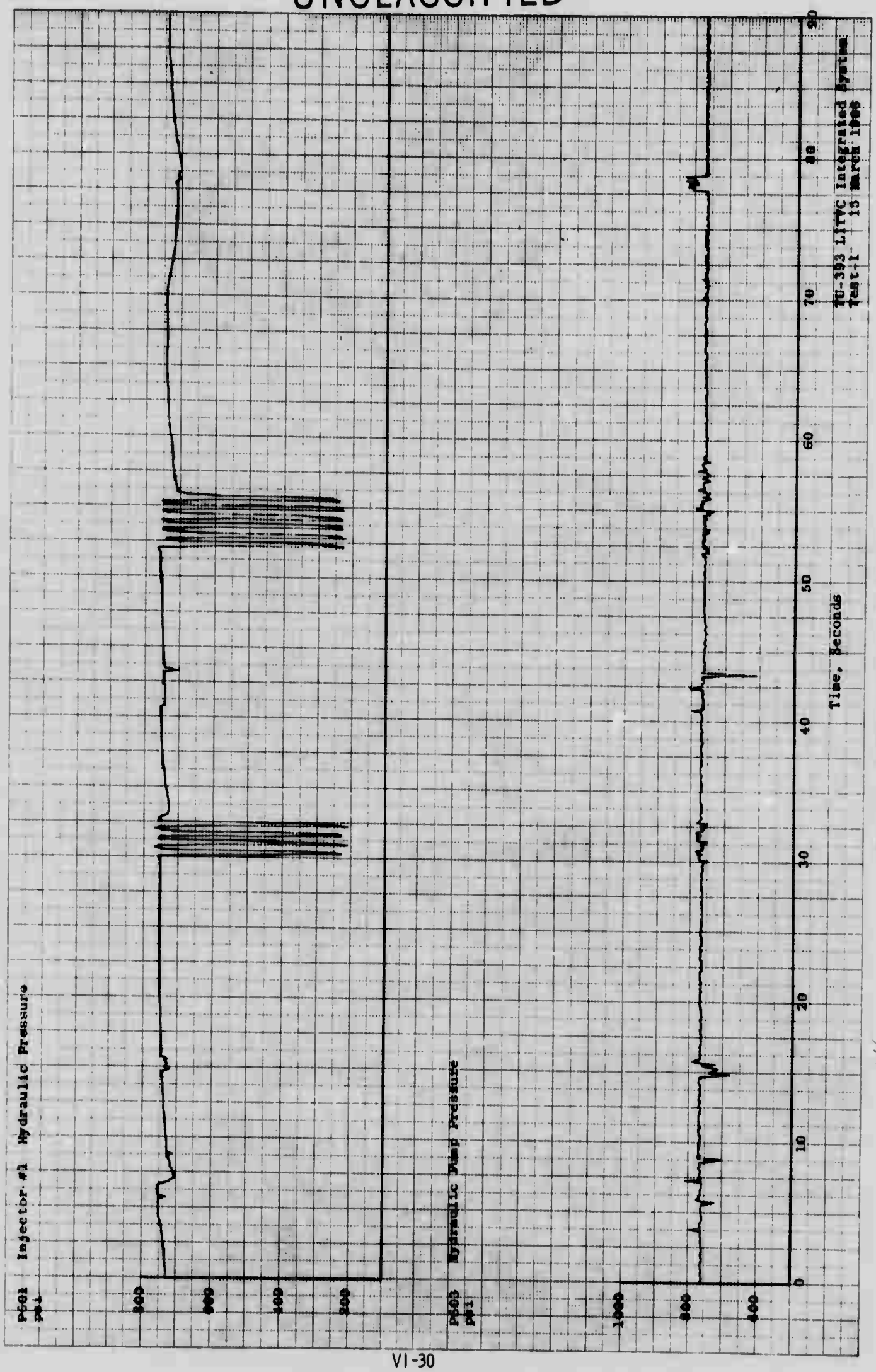

Figure 11. Hydraulic Pressures - Run No. 1

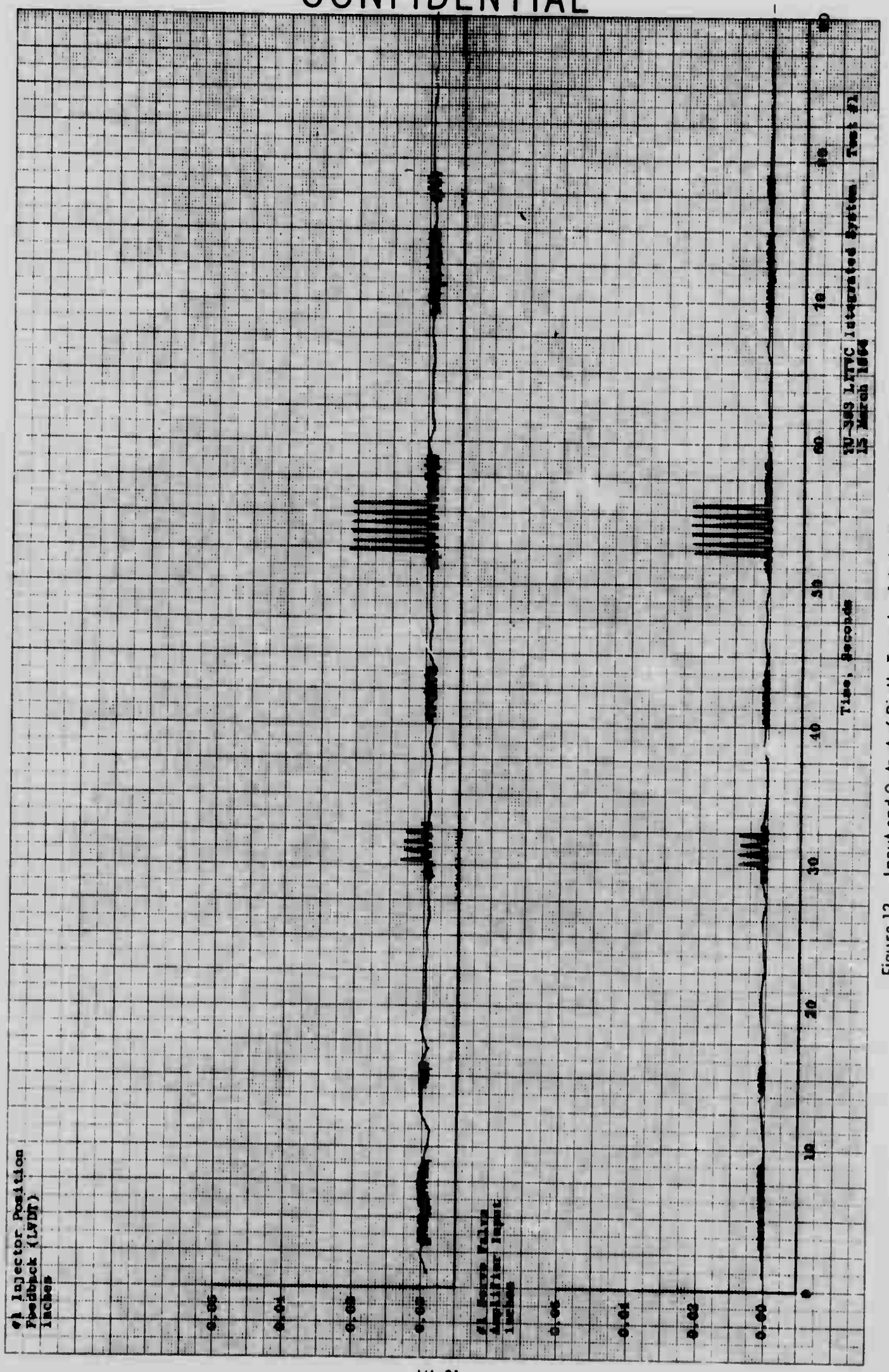

Figure 12. Input and Output of Pintle Travel, #1 Injector - Run No. 1

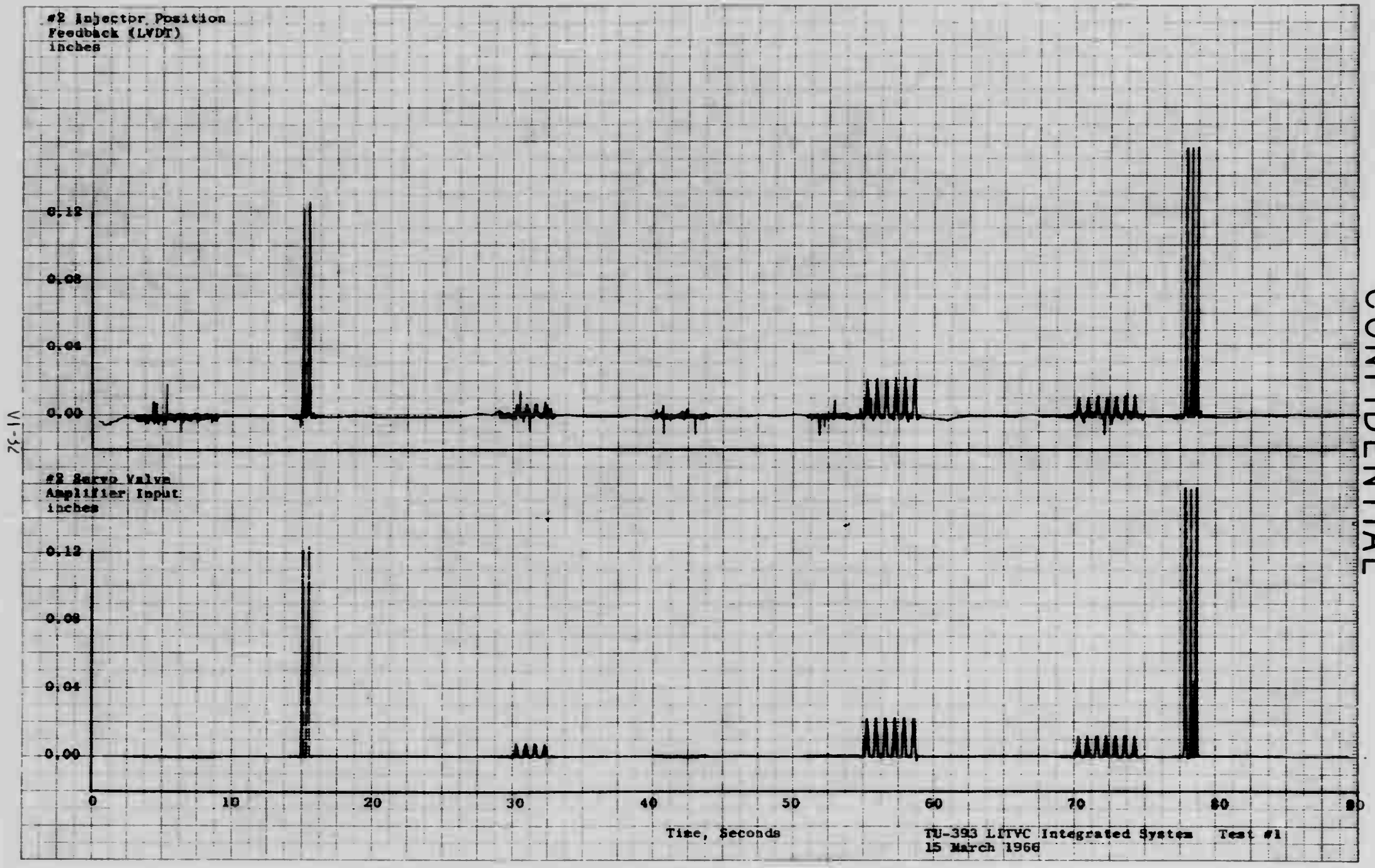

Figure 13. Input and Output of Pintle Travel, #2 Injector - Run No. 1

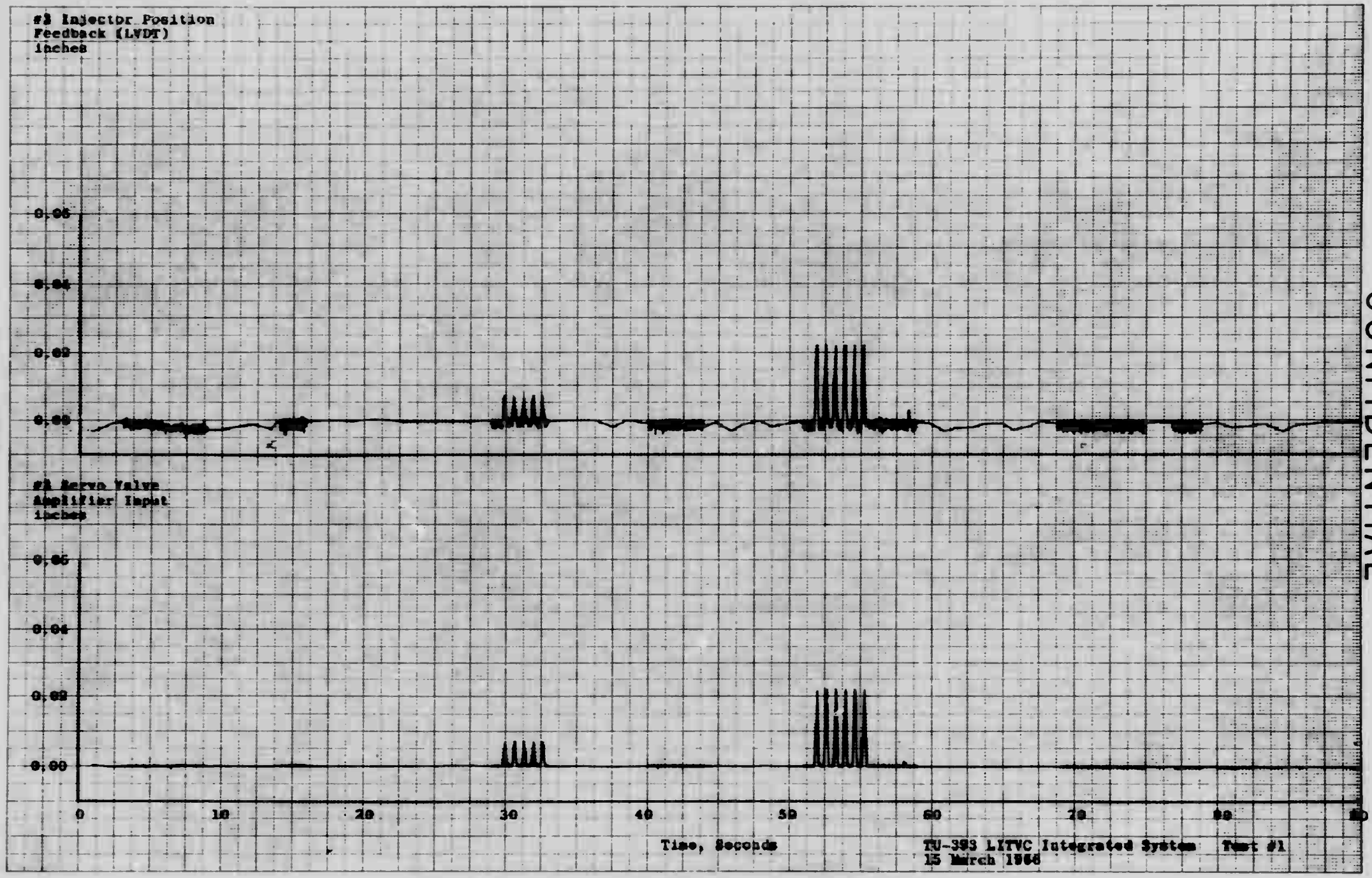

Figure 14. Input and Output of Pintle Travel, #3 Injector - Run No. 1

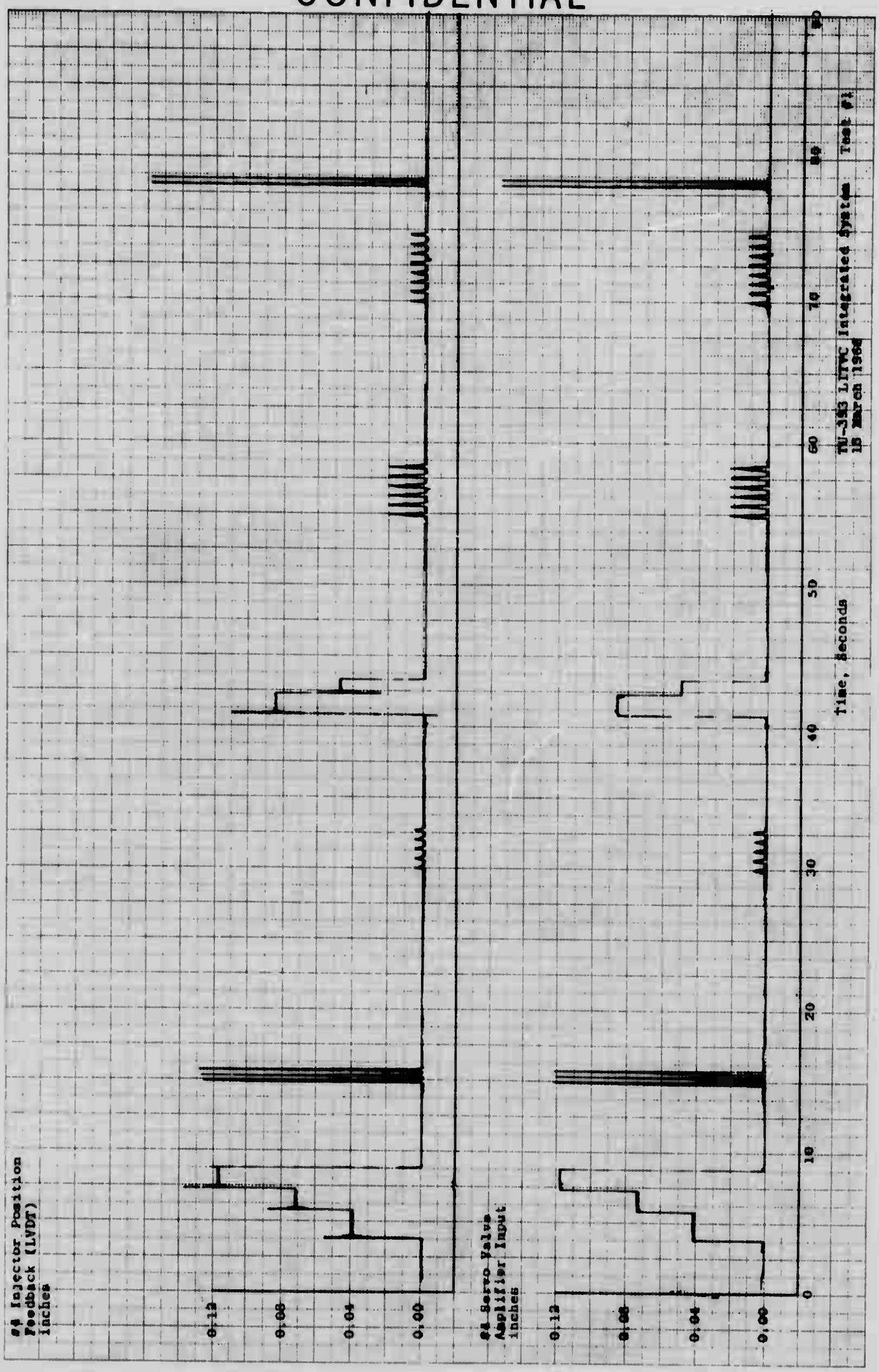

Figure 15. Input and Output of Pintle Travel, #4 Injector - Run No. 1

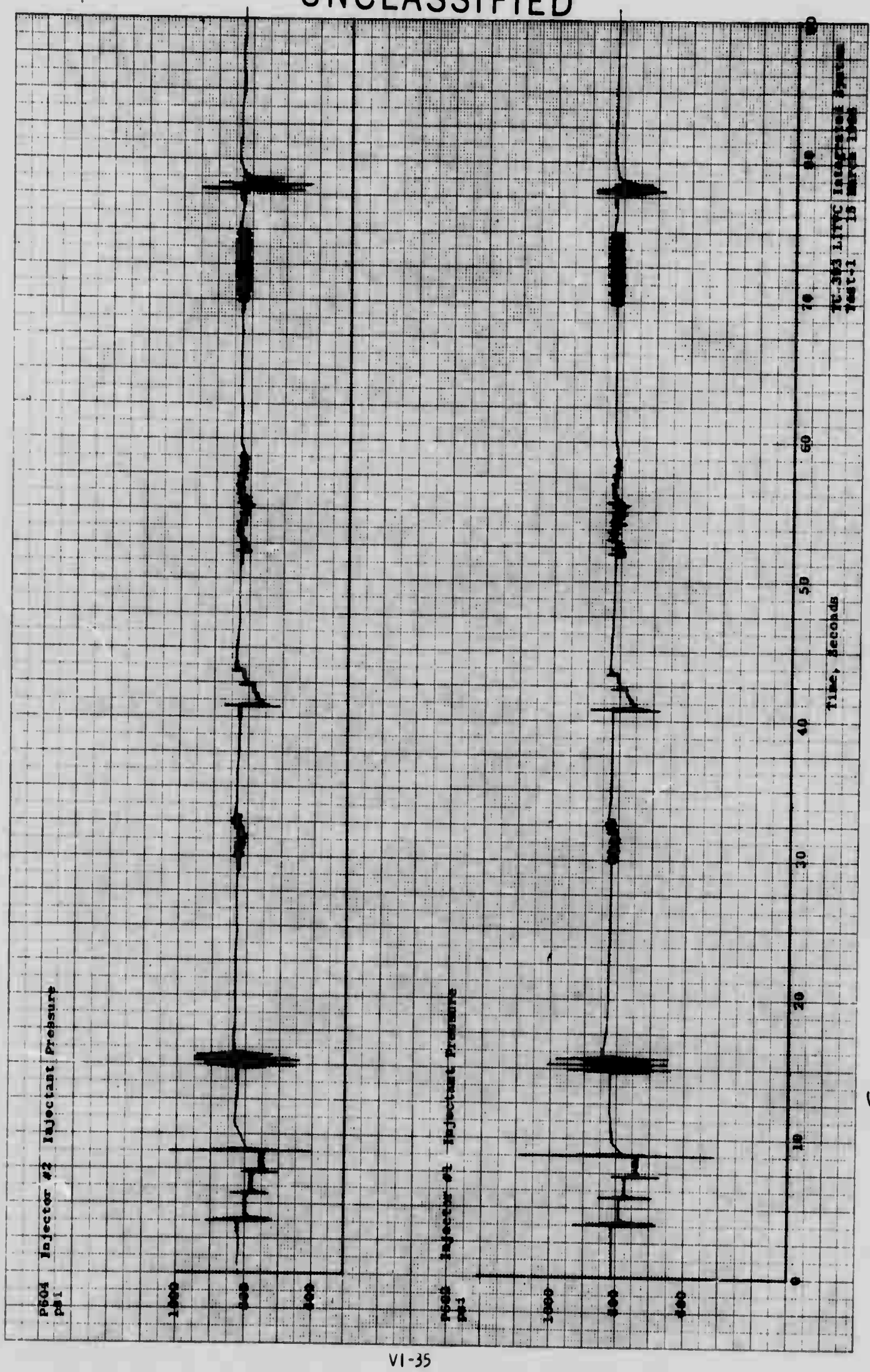

Figure 16. Injector #1 and #2 Injectant Pressure - Run No. 1

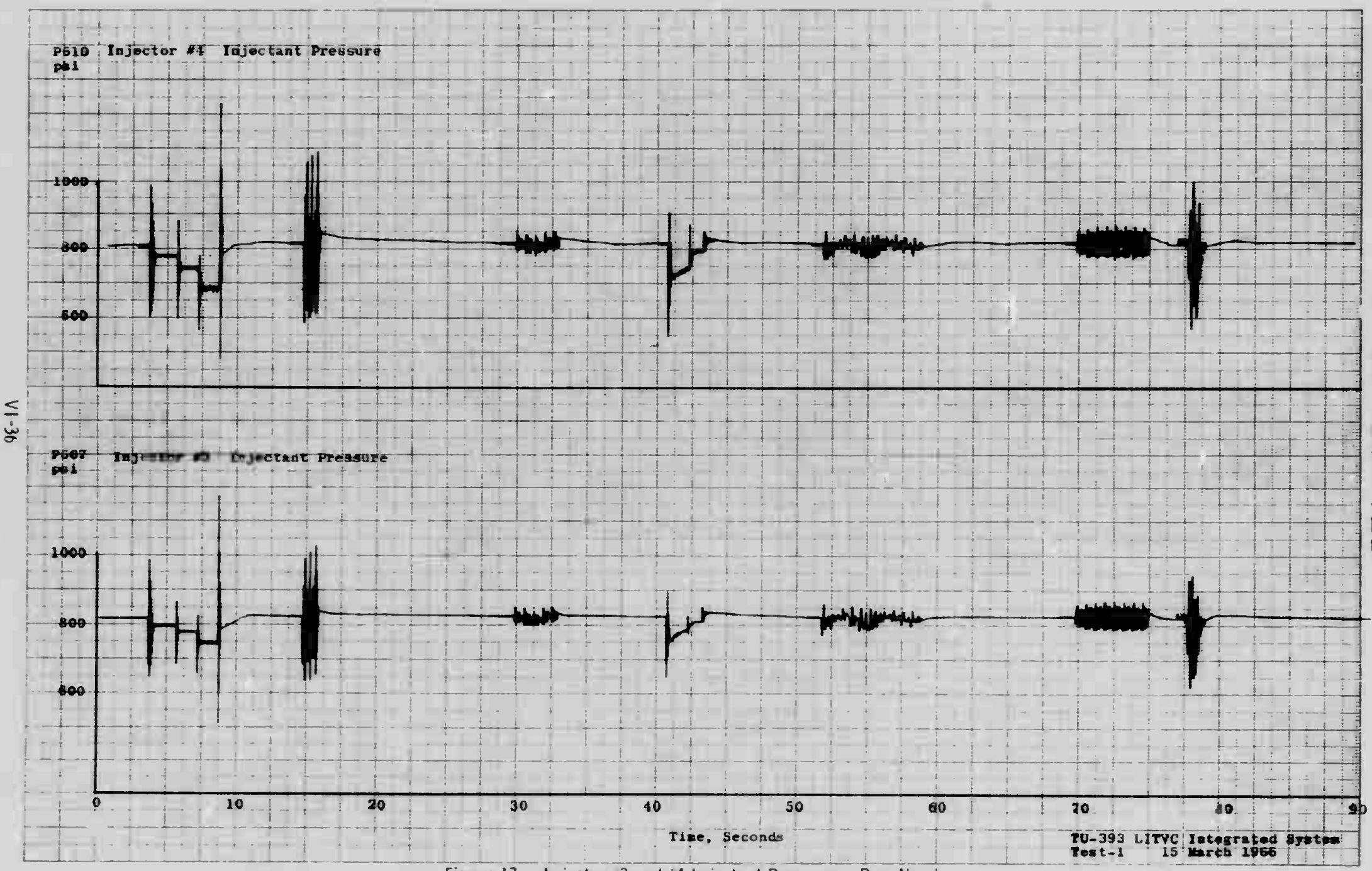

Figure 17. Injector #3 and #4 Injectant Pressure - Run No. 1

UNCLASSIFIED

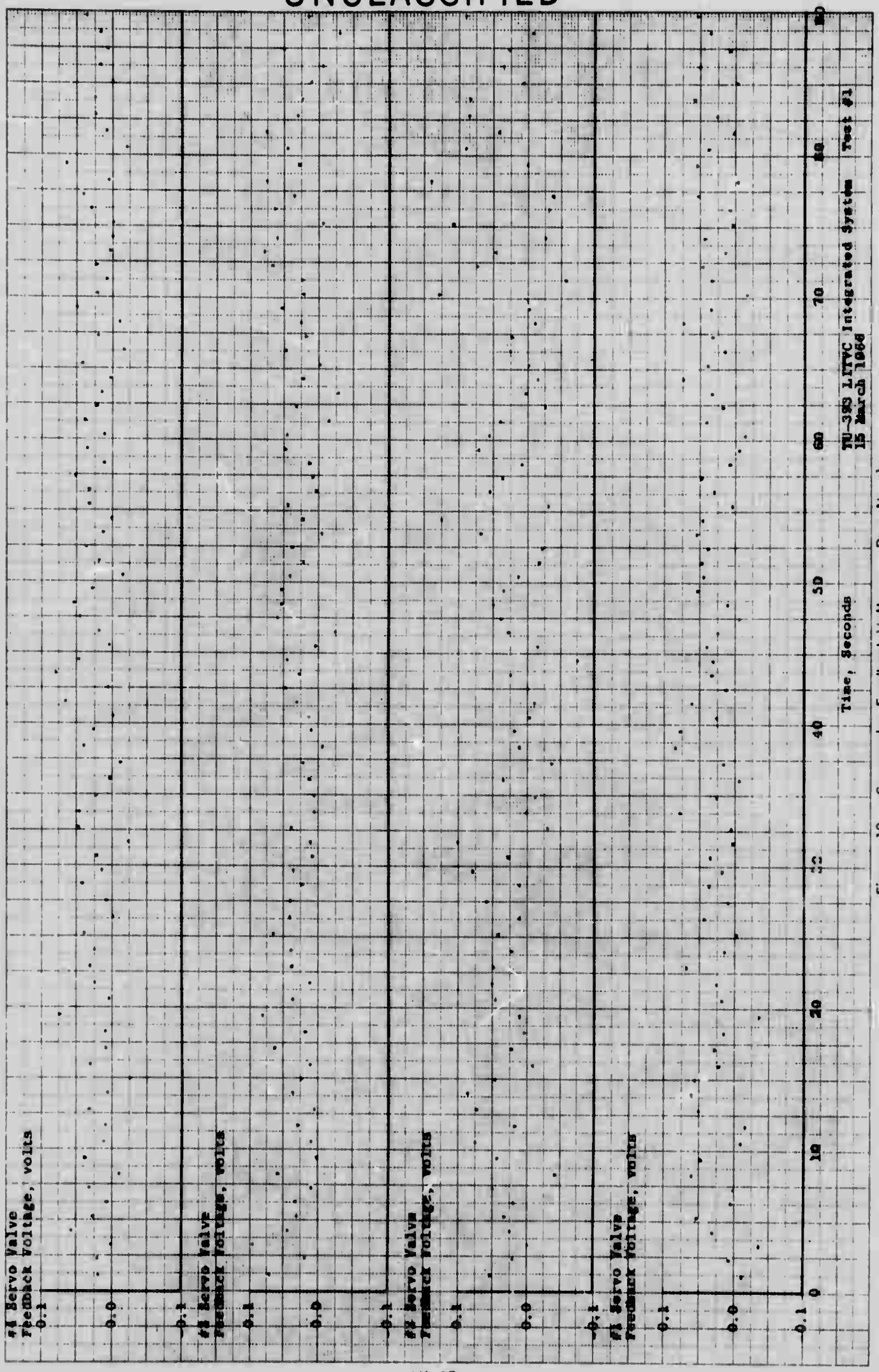

Figure 18. Servovalve Feedback Voltages - Run No. 1

TU-393 Integrated System (Run #1)

Test Date 15 March 1966

Maximum Strain Micro in/in

Loc.	Max.	Time (sec.)	Loc.	Max.	Time (sec.)
S601	1743	79.8	S609	438	8.9
S602	1798	79.8	S610	379	8.8
S603	1767	79.8	S611	385	8.8
S604	1581	0	S612	545	0
S605	1509	0	S613	359	8.8
S606	1463	0	S614	328	8.8
S607	562	8.8	S615	158	8.9
S608	358	8.8	S616	342	8.8

Maximum Vibration

Loc.	Max. G	Time (sec.)
A601	6.7	9
A602	10.2	43

Figure 19. Maximum Strain and Vibrations Run No. 1

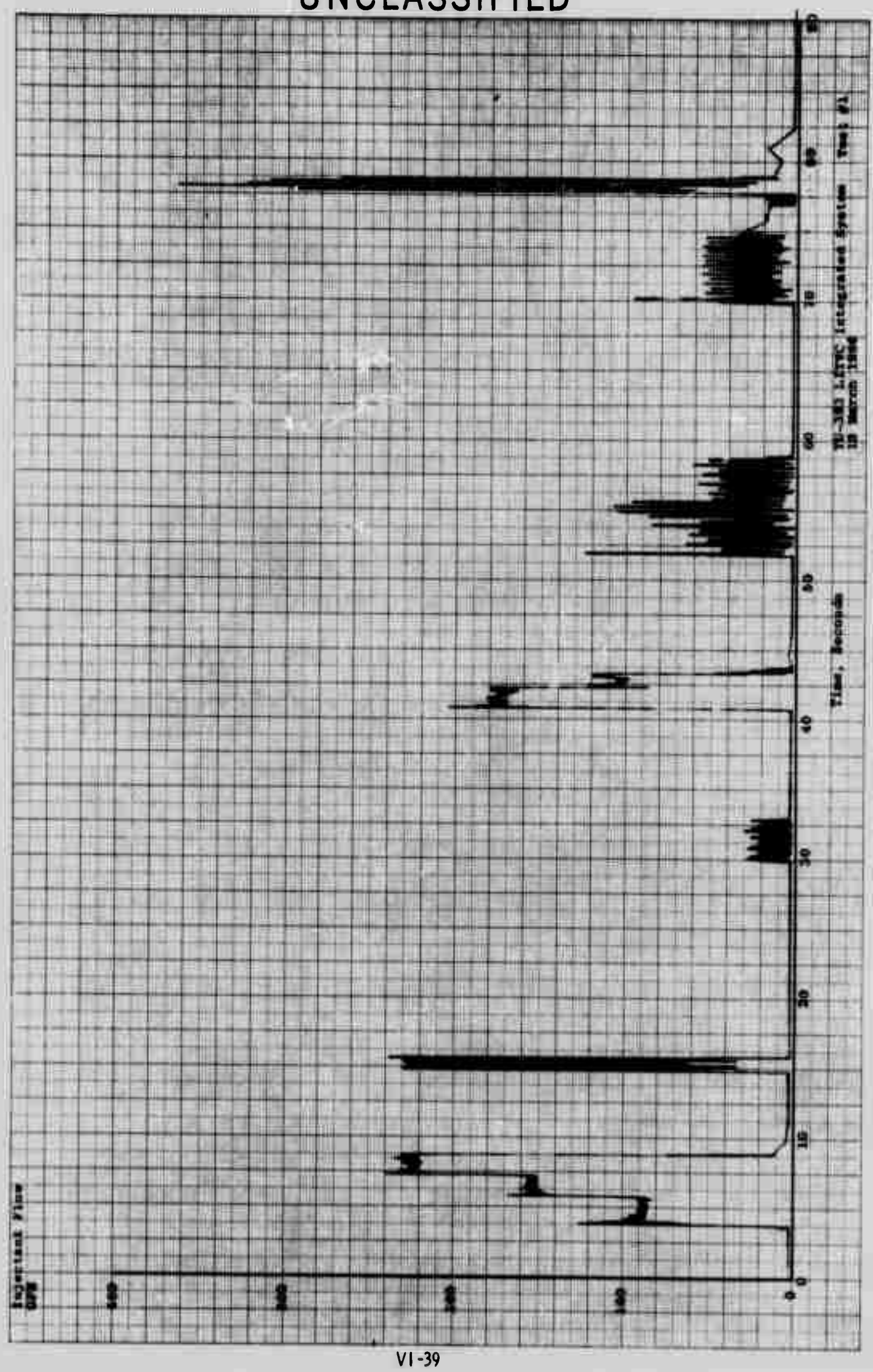

Figure 20. Injectant Flow - Run No. 1

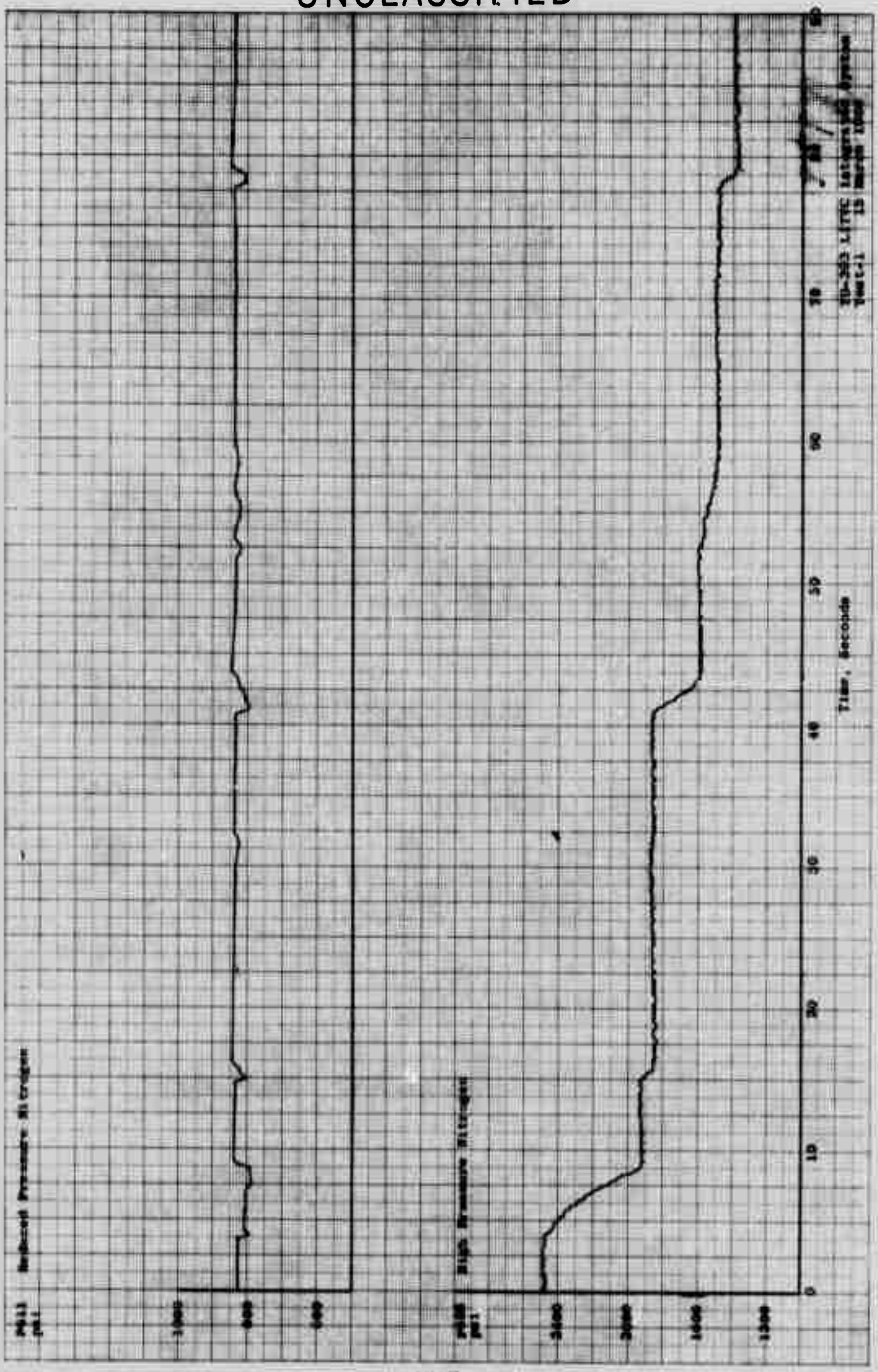

Figure 21. High and Reduced Nitrogen Pressures - Run No. 2

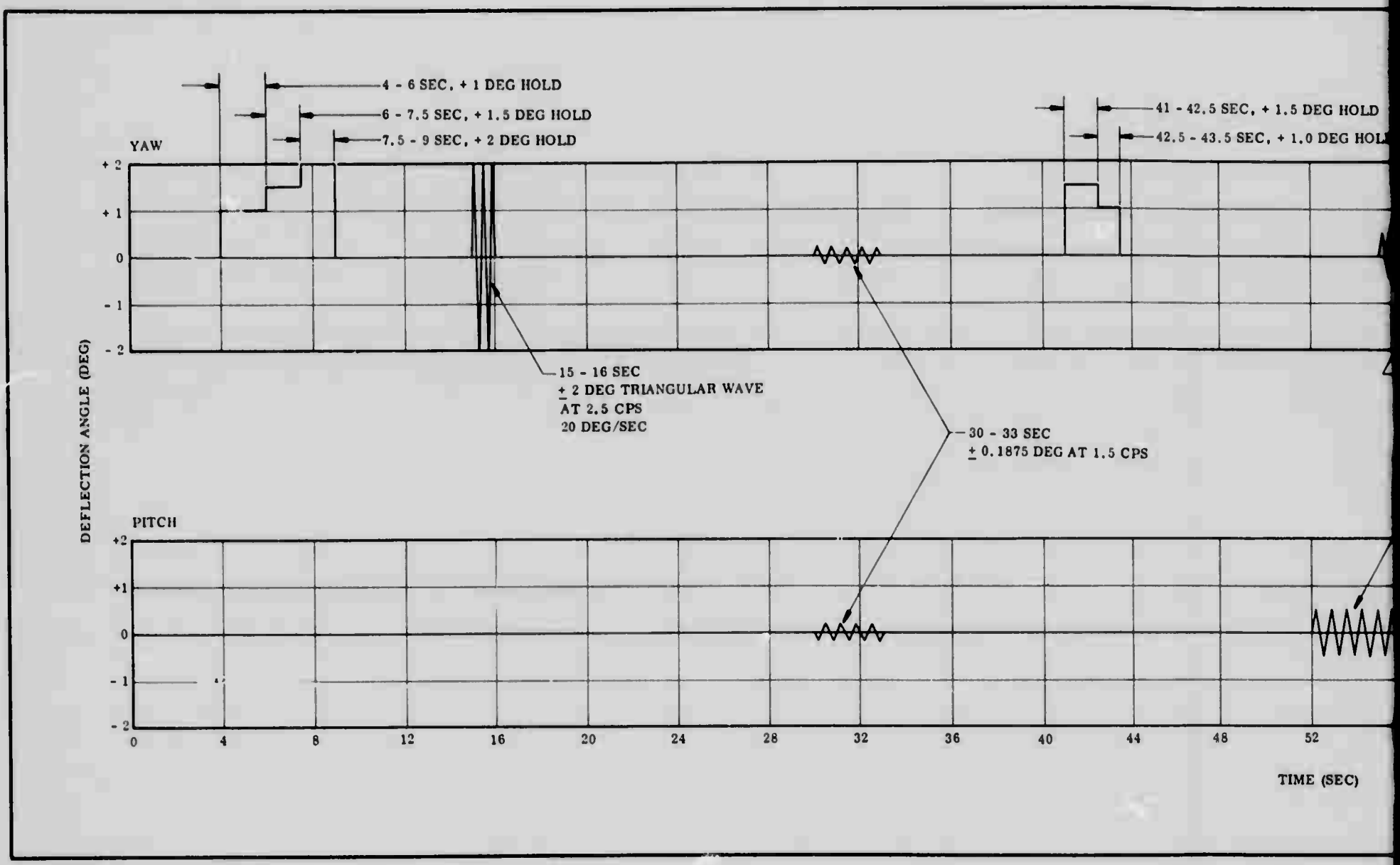
4 - 6 SEC, + 1 DEG HOLD
6 - 7.5 SEC, + 1.5 DEG HOLD
7.5 - 9 SEC, + 2 DEG HOLD
41 - 42.5 SEC, + 1.5 DEG HOLD
42.5 - 43.5 SEC, + 1.0 DEG HOLD
YAW
+ 2
+ 1
0
- 1
- 2
15 - 16 SEC
± 2 DEG TRIANGULAR WAVE
AT 2.5 CPS
20 DEG/SEC
30 - 33 SEC
± 0.1875 DEG AT 1.5 CPS
DEFLECTION ANGLE (DEG)
PITCH
+2
+1
0
- 1
- 2
0
4
8
12
16
20
24
28
32
36
40
44
48
52
TIME (SEC)

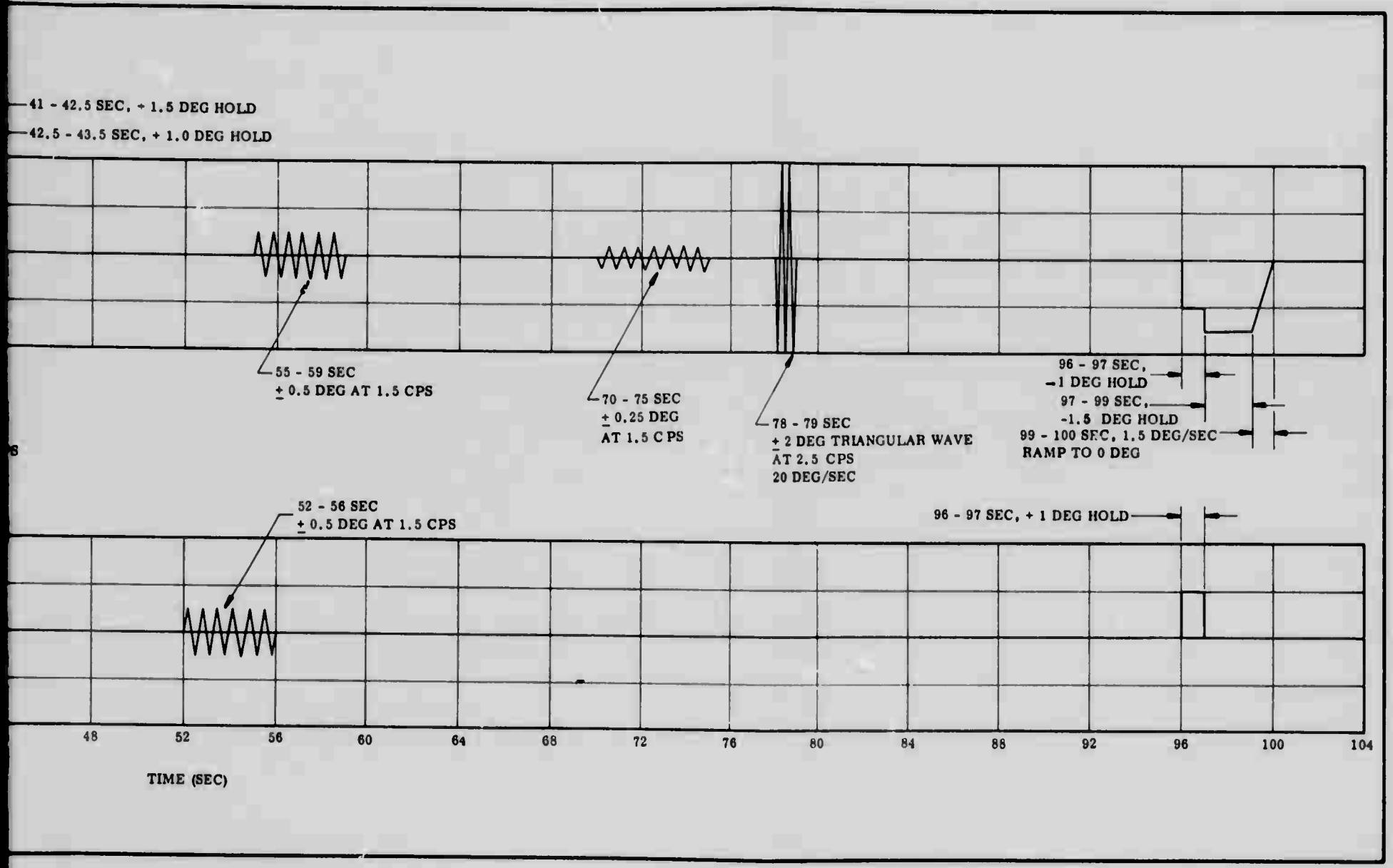

Figure 22. Duty Cycle for Run No.'s 3, 4 & 8

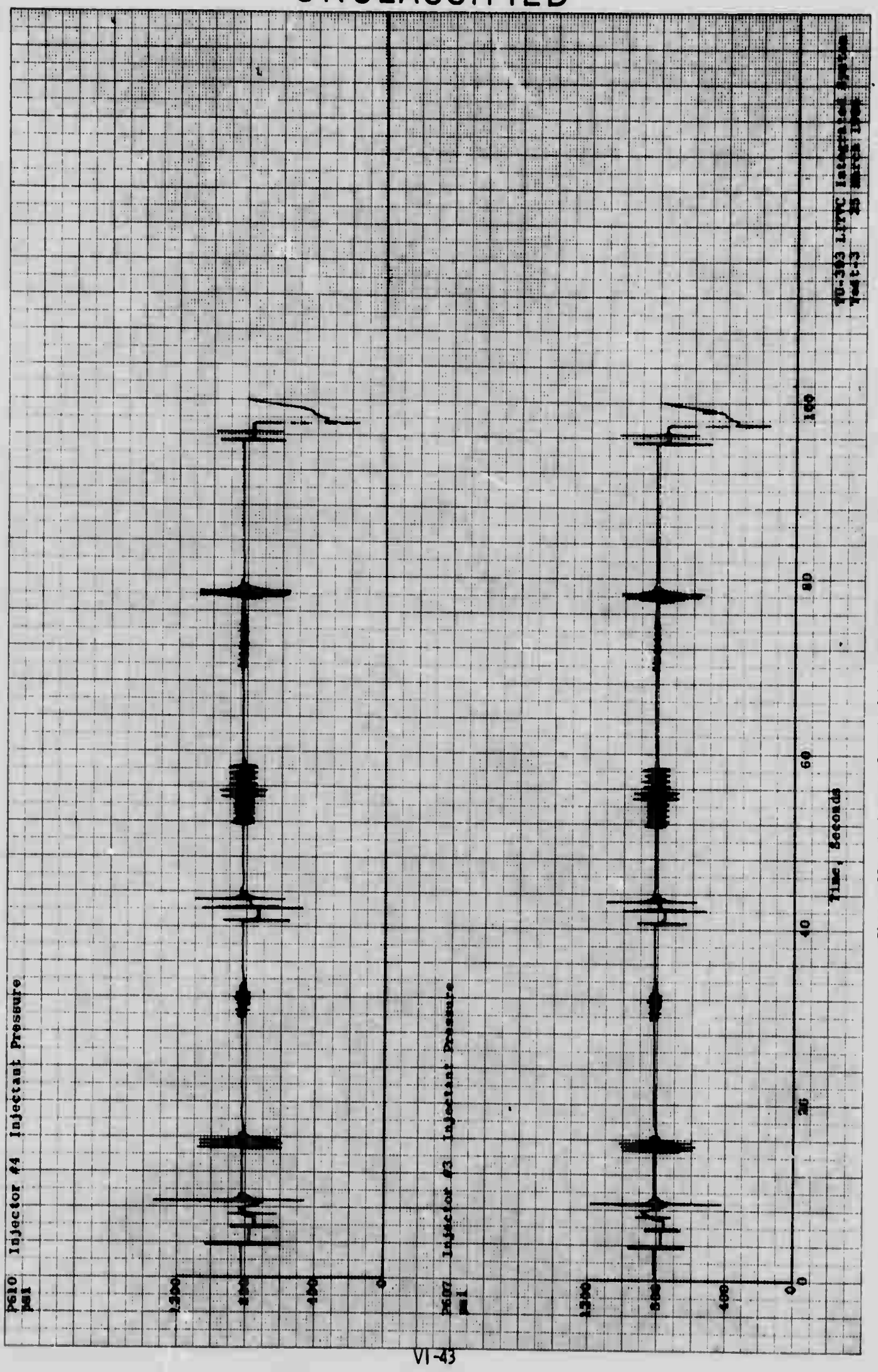

Figure 23. Injector #3 and #4 Injectant Pressures - Run No. 3

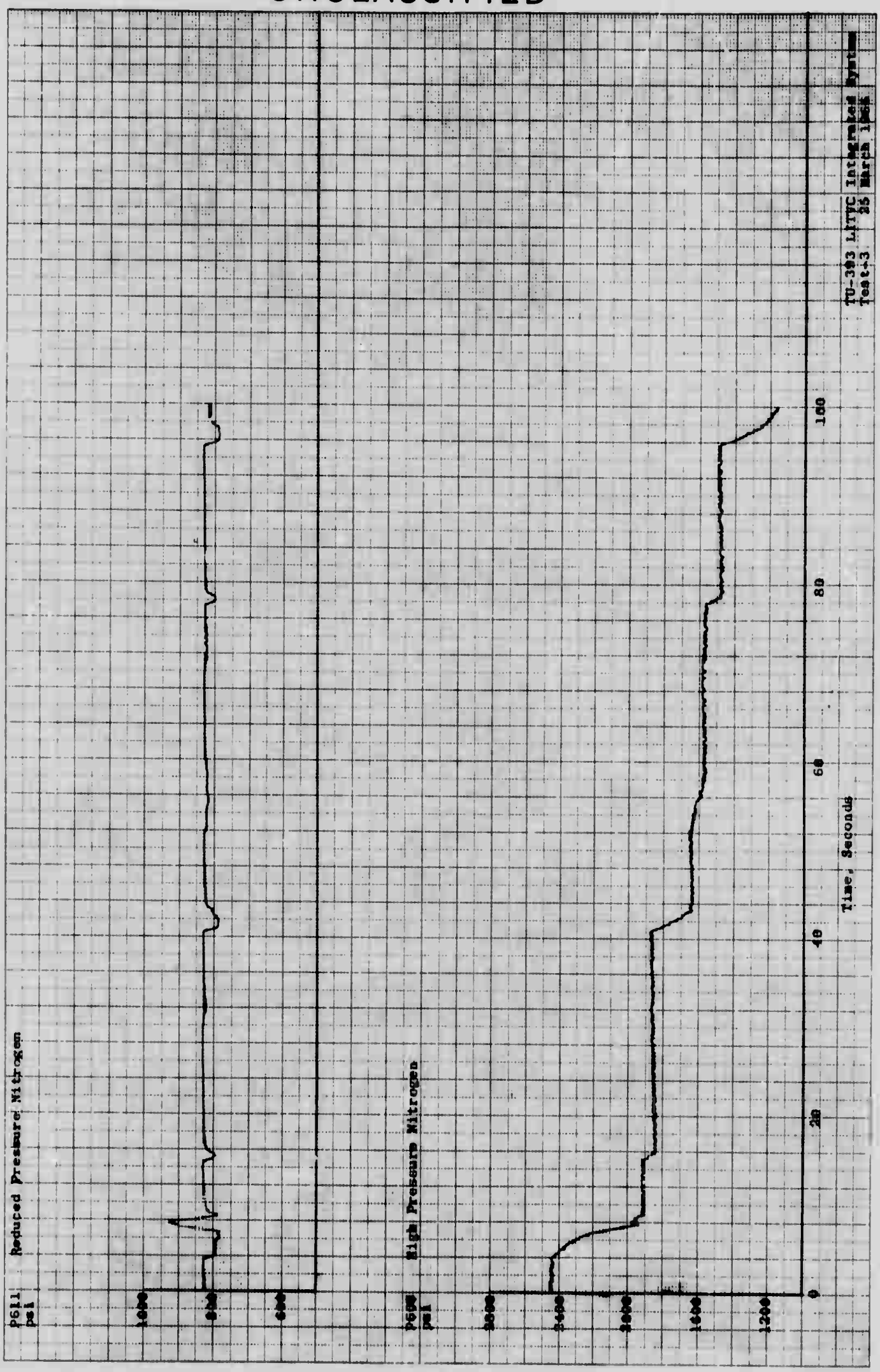

Figure 24. High and Reduced Nitrogen Pressures - Run No. 3

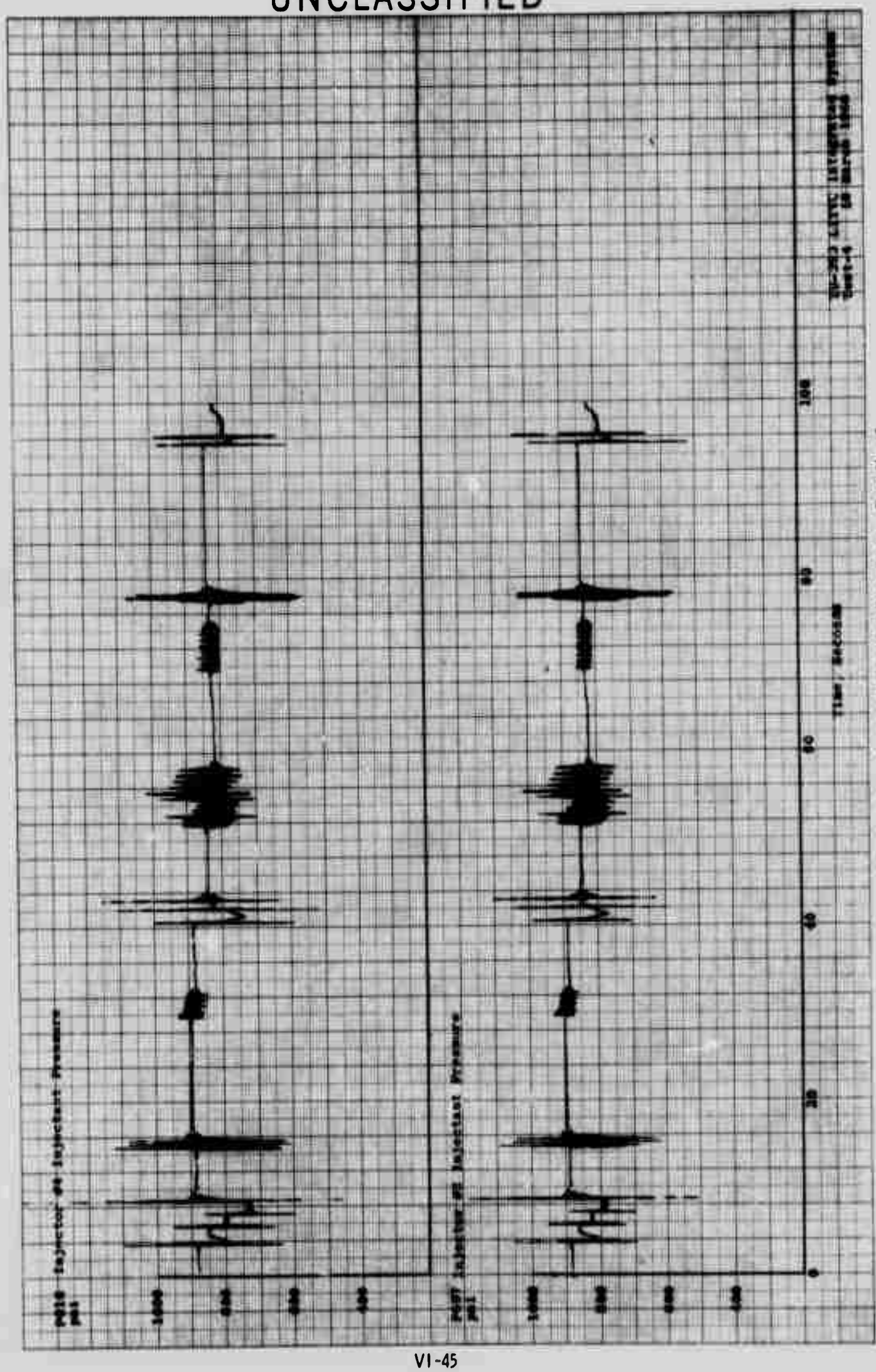

Figure 25. Injector #3 and #4 Injectant Pressures - Run No. 4

PREVIOUS PAGE WAS BLANK, THEREFORE WAS NOT FILMED.

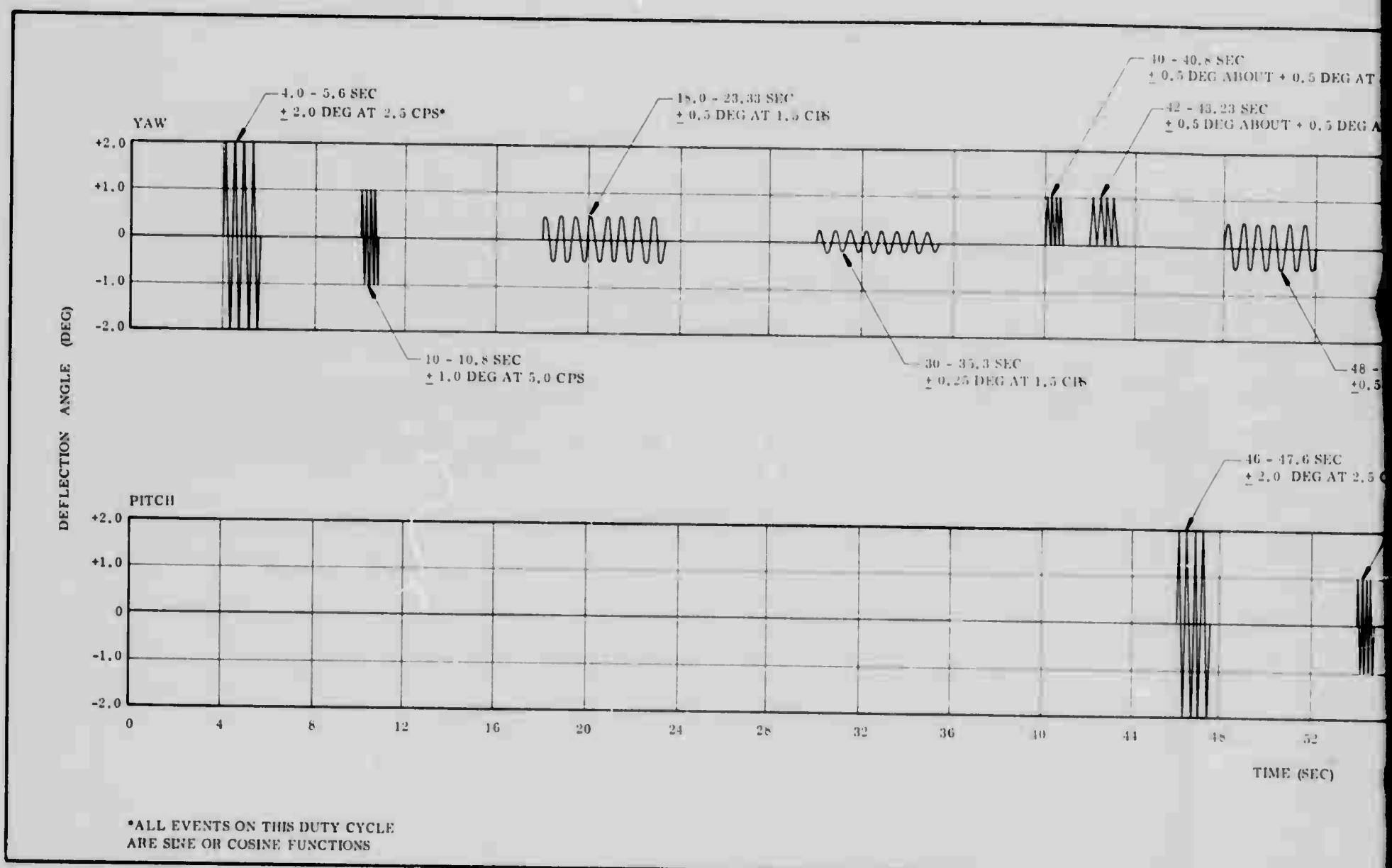

*ALL EVENTS ON THIS DUTY CYCLE ARE SINE OR COSINE FUNCTIONS

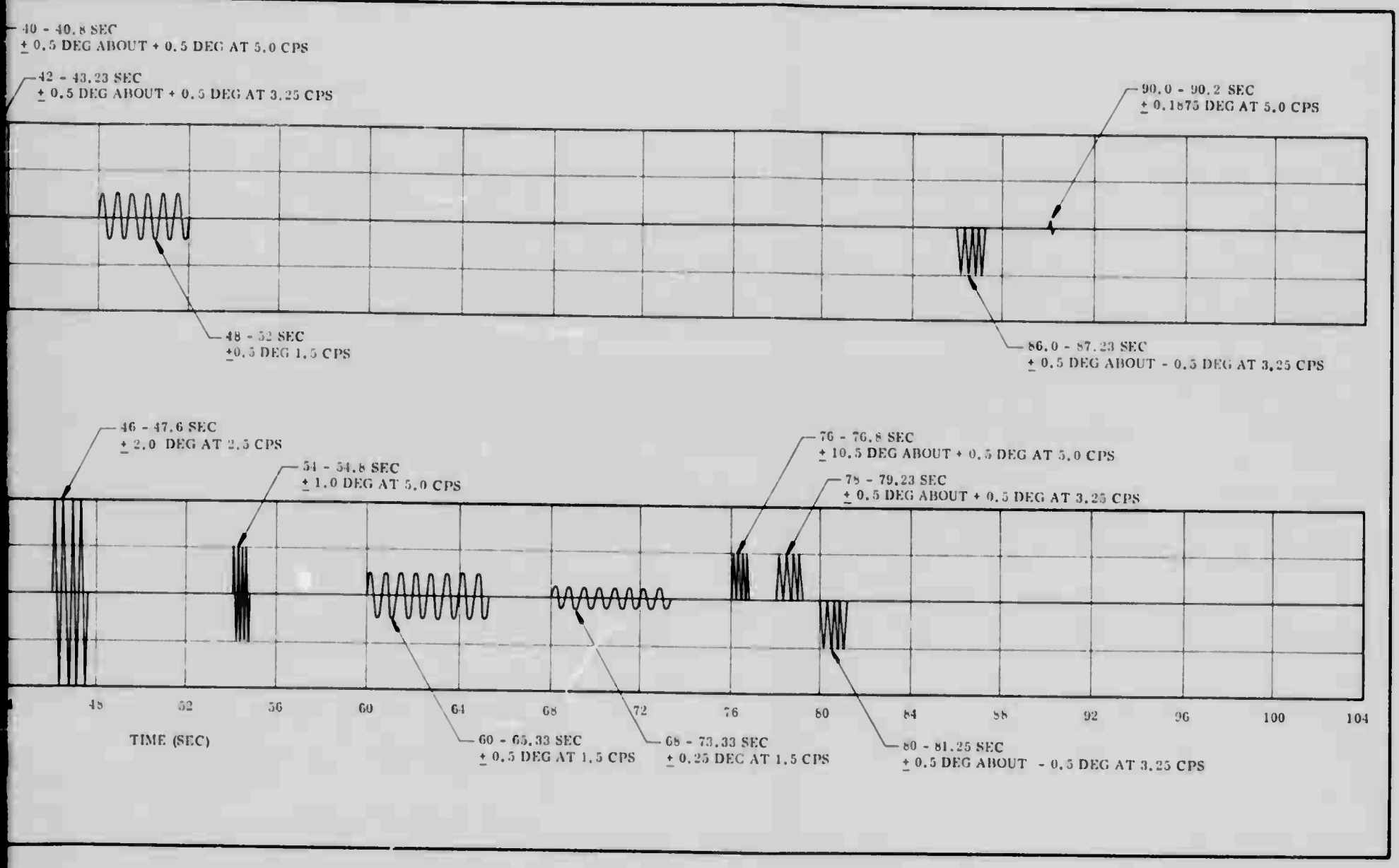

Figure 26. Duty Cycle for Run No. 5

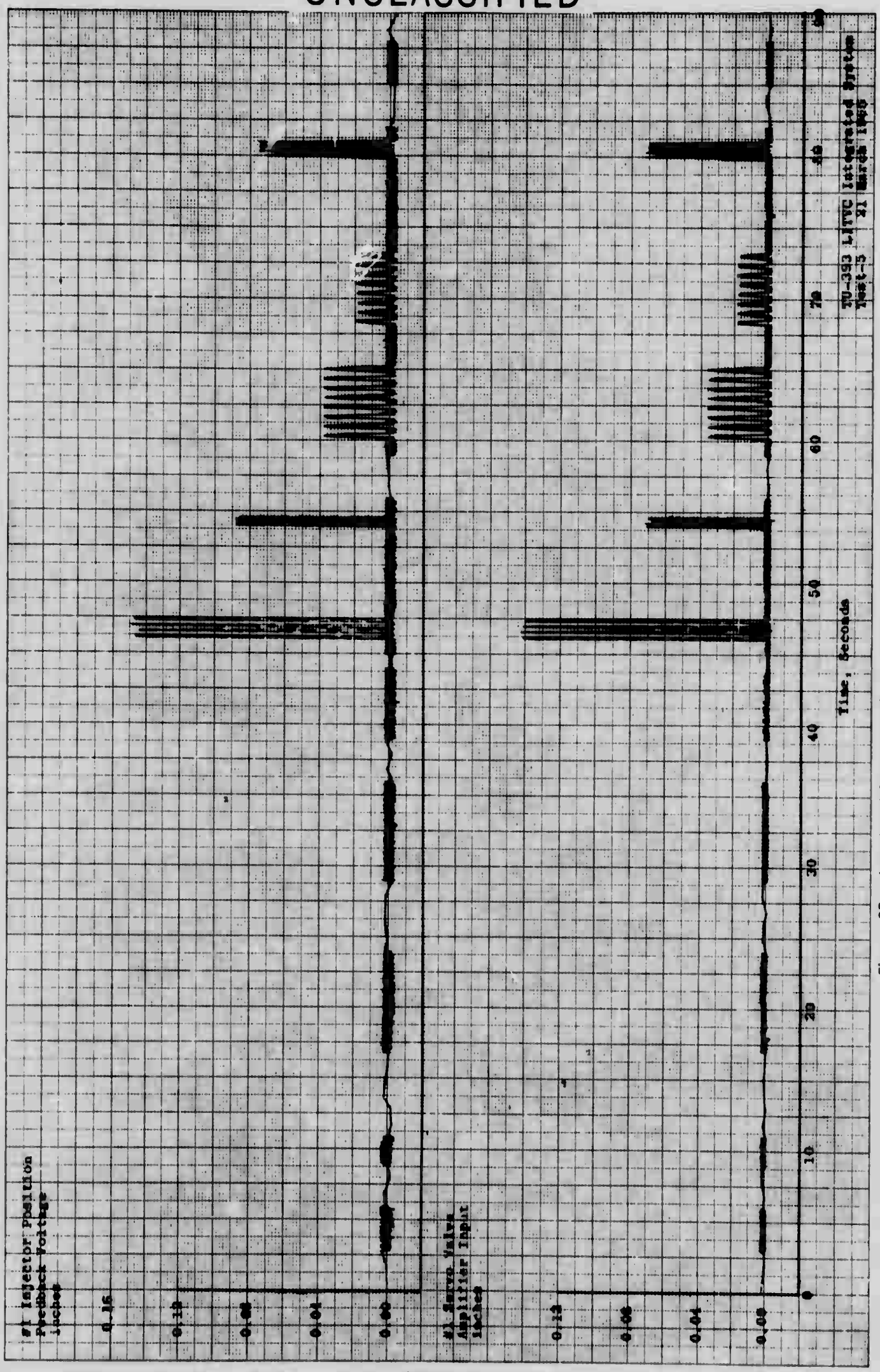

Figure 27. Input and Output of Pintle Travel, #1 Injector - Run No. 5

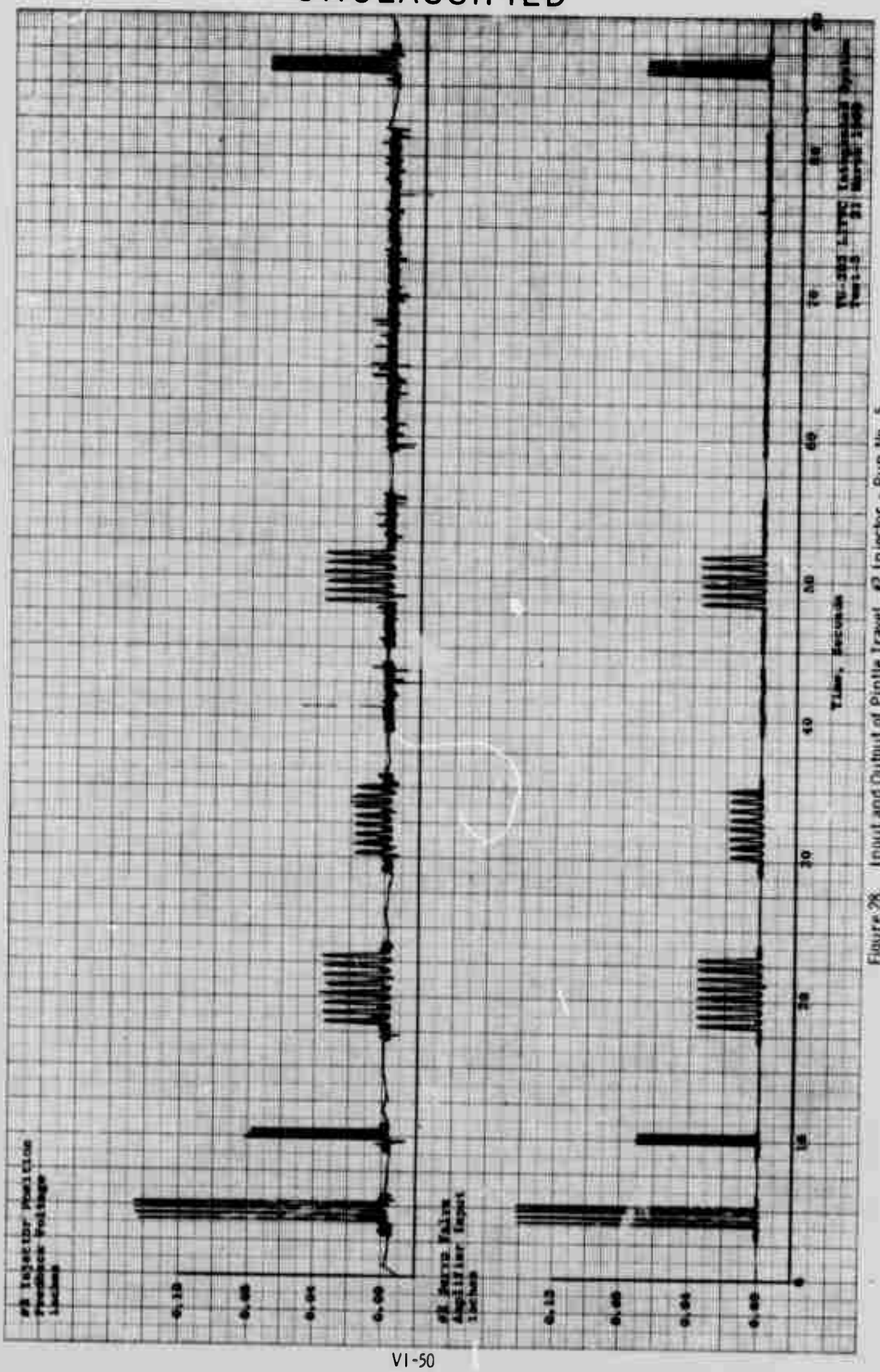

Figure 28. Input and Output of Pintle Travel, #2 Injector - Run No. 5.

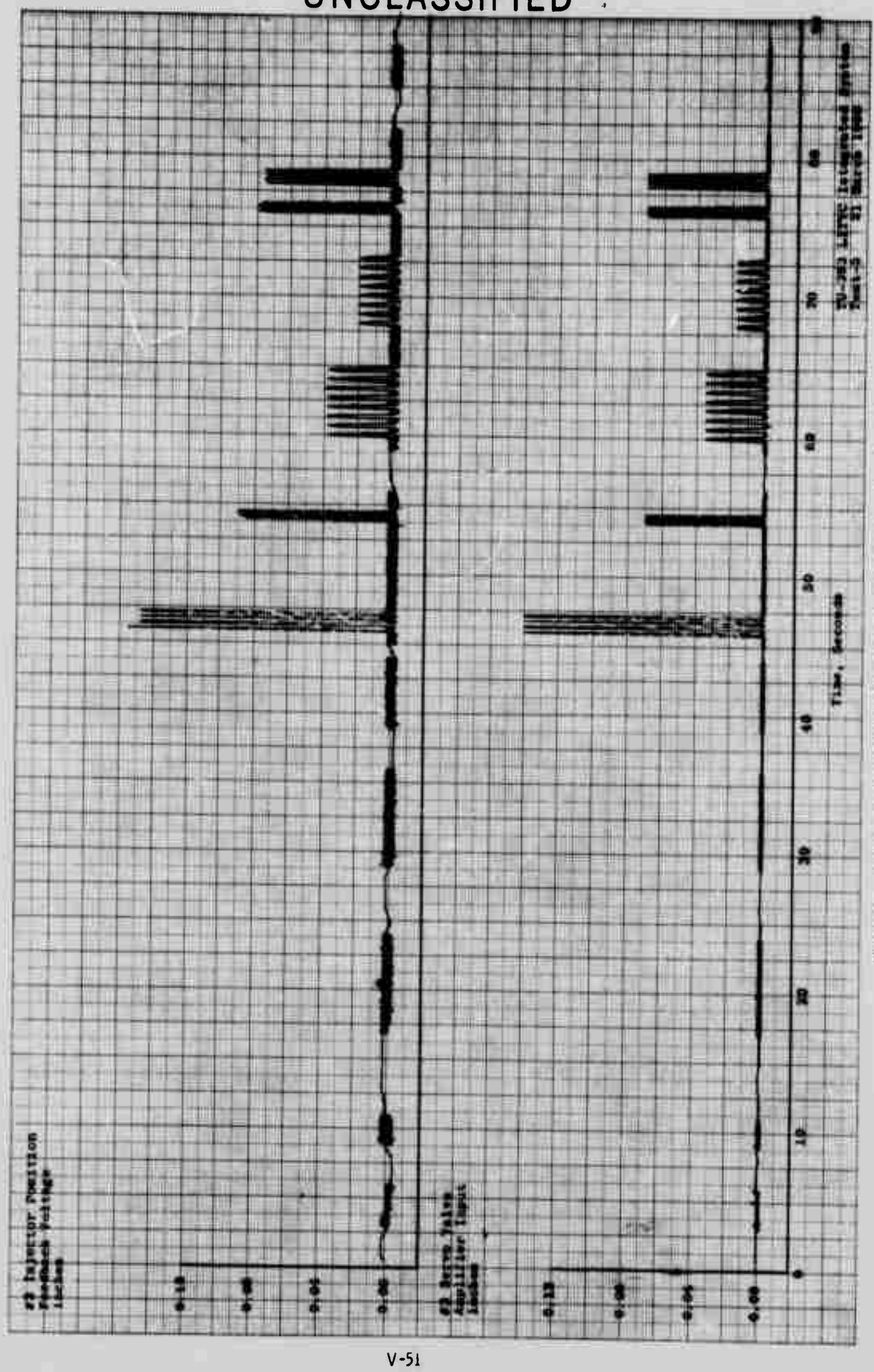

Figure 29. Input and Output of Pintle Travel, #2 Injector - Run No. 5

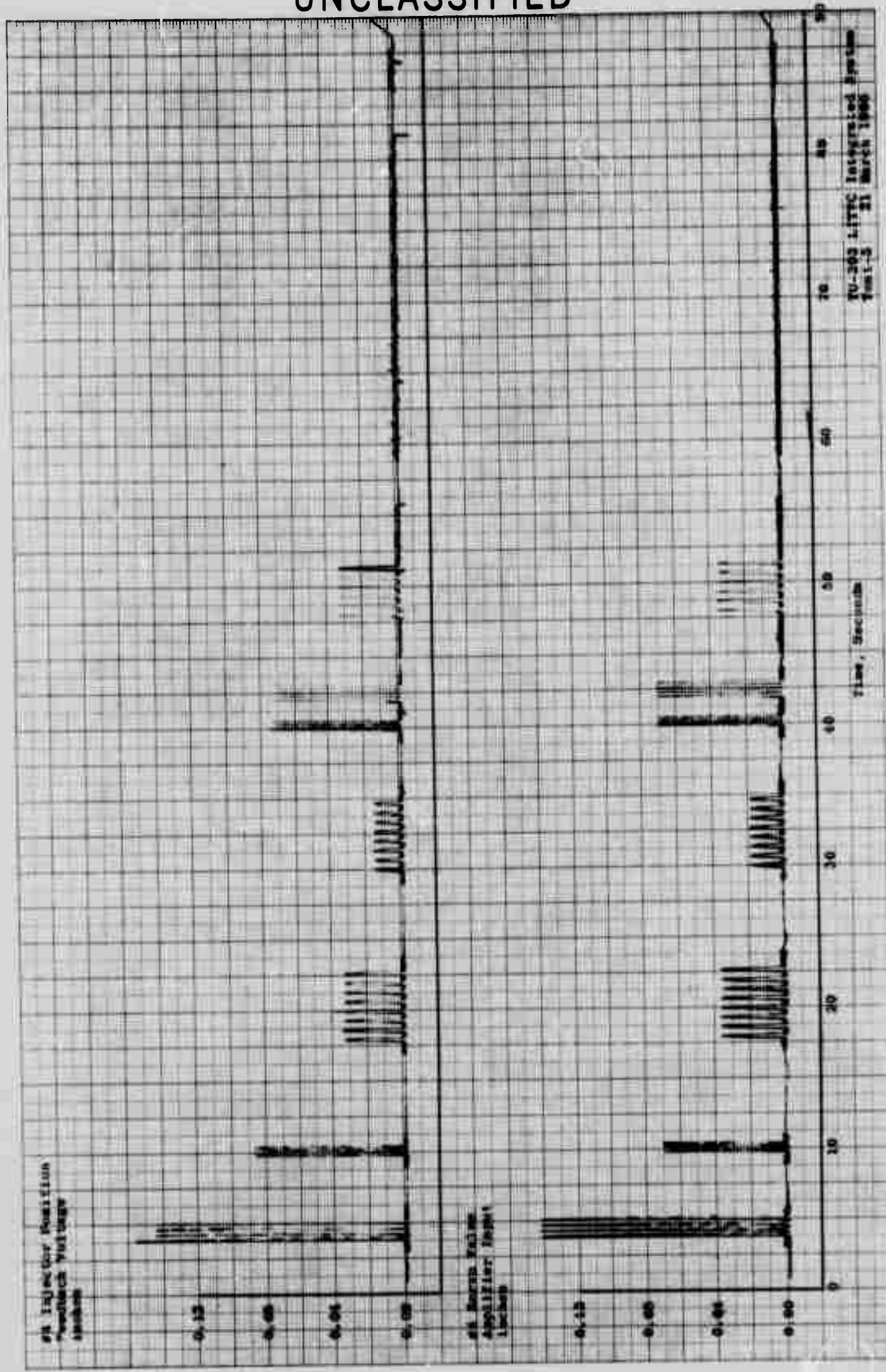

Figure 30. Input and Output of Pintle Travel, #4 Injector - Run No. 5

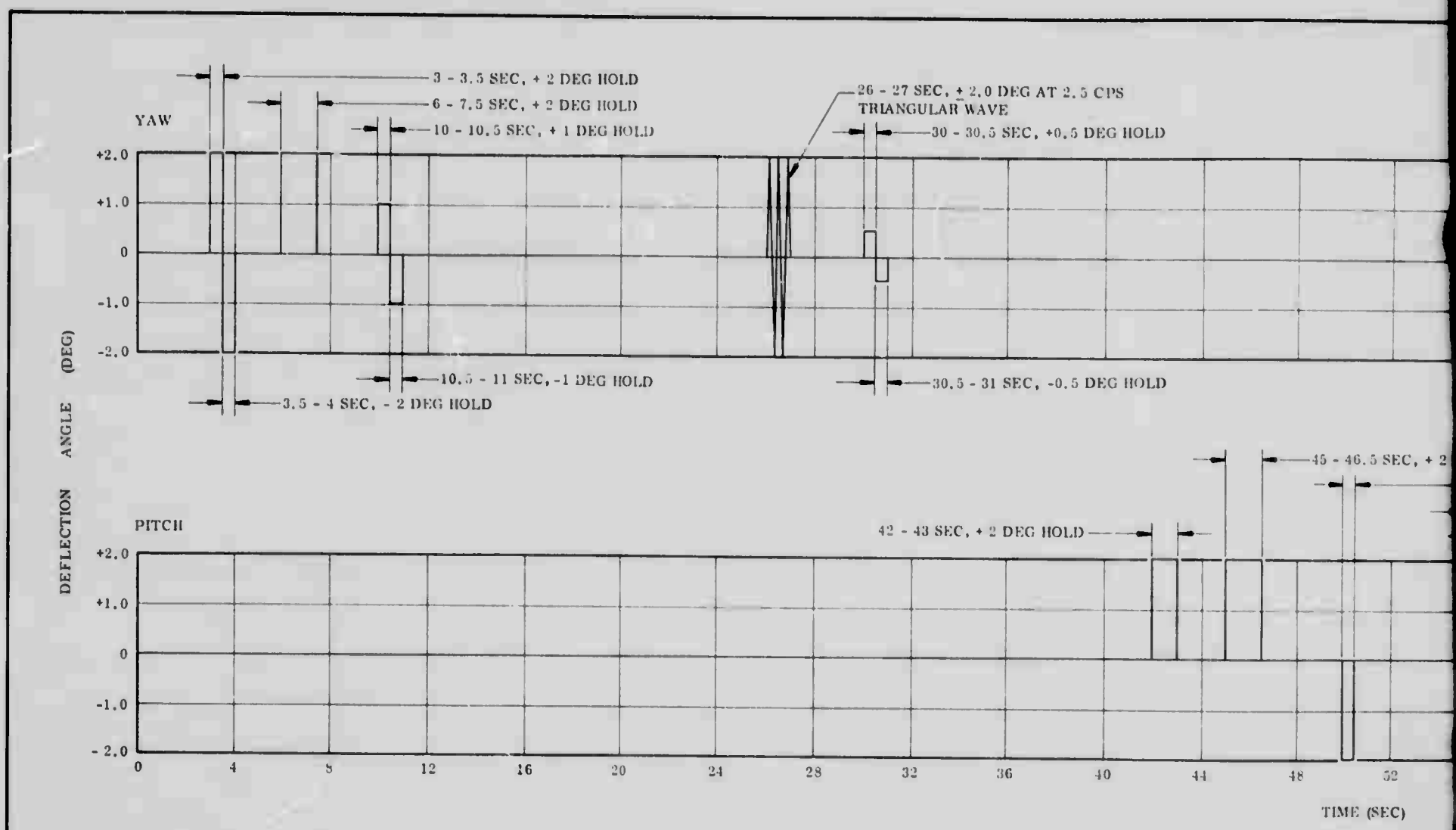
YAW
3 - 3.5 SEC, + 2 DEG HOLD
6 - 7.5 SEC, + 2 DEG HOLD
10 - 10.5 SEC, + 1 DEG HOLD
26 - 27 SEC, ± 2.0 DEG AT 2.5 CPS
TRIANGULAR WAVE
30 - 30.5 SEC, +0.5 DEG HOLD
+2.0
+1.0
0
-1.0
-2.0
10.5 - 11 SEC, -1 DEG HOLD
3.5 - 4 SEC, - 2 DEG HOLD
30.5 - 31 SEC, -0.5 DEG HOLD
PITCH
42 - 43 SEC, + 2 DEG HOLD
45 - 46.5 SEC, + 2
+2.0
+1.0
0
-1.0
- 2.0
0
4
8
12
16
20
24
28
32
36
40
44
48
52
TIME (SEC)
DEFLECTION ANGLE (DEG)

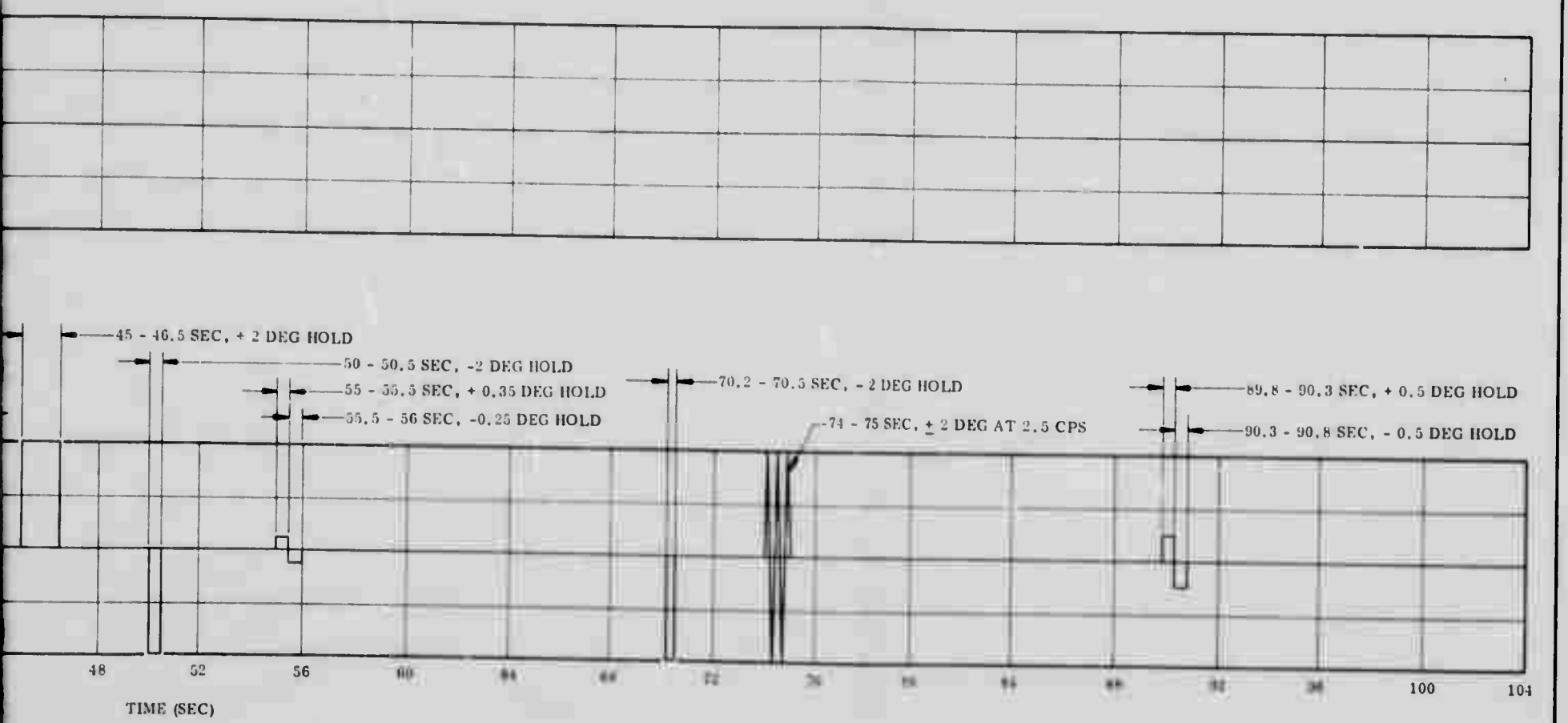

Figure 31. Duty Cycle for Run No. 6

PREVIOUS PAGE WAS BLANK, THEREFORE WAS NOT FILMED.

UNCLASSIFIED

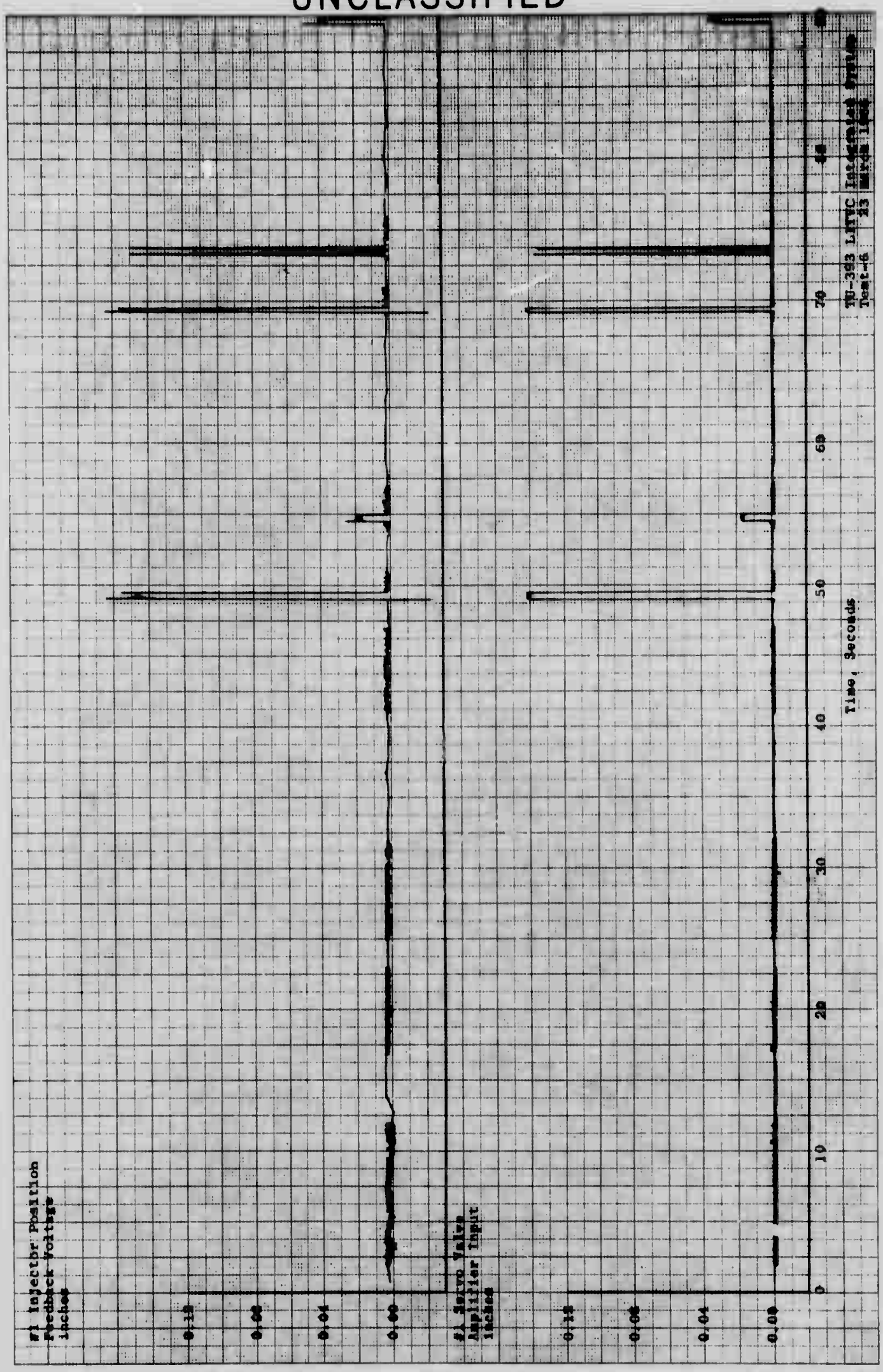

Figure 32. Input and Output of Pintle Travel, #1 Injector - Run No. 6

UNCLASSIFIED

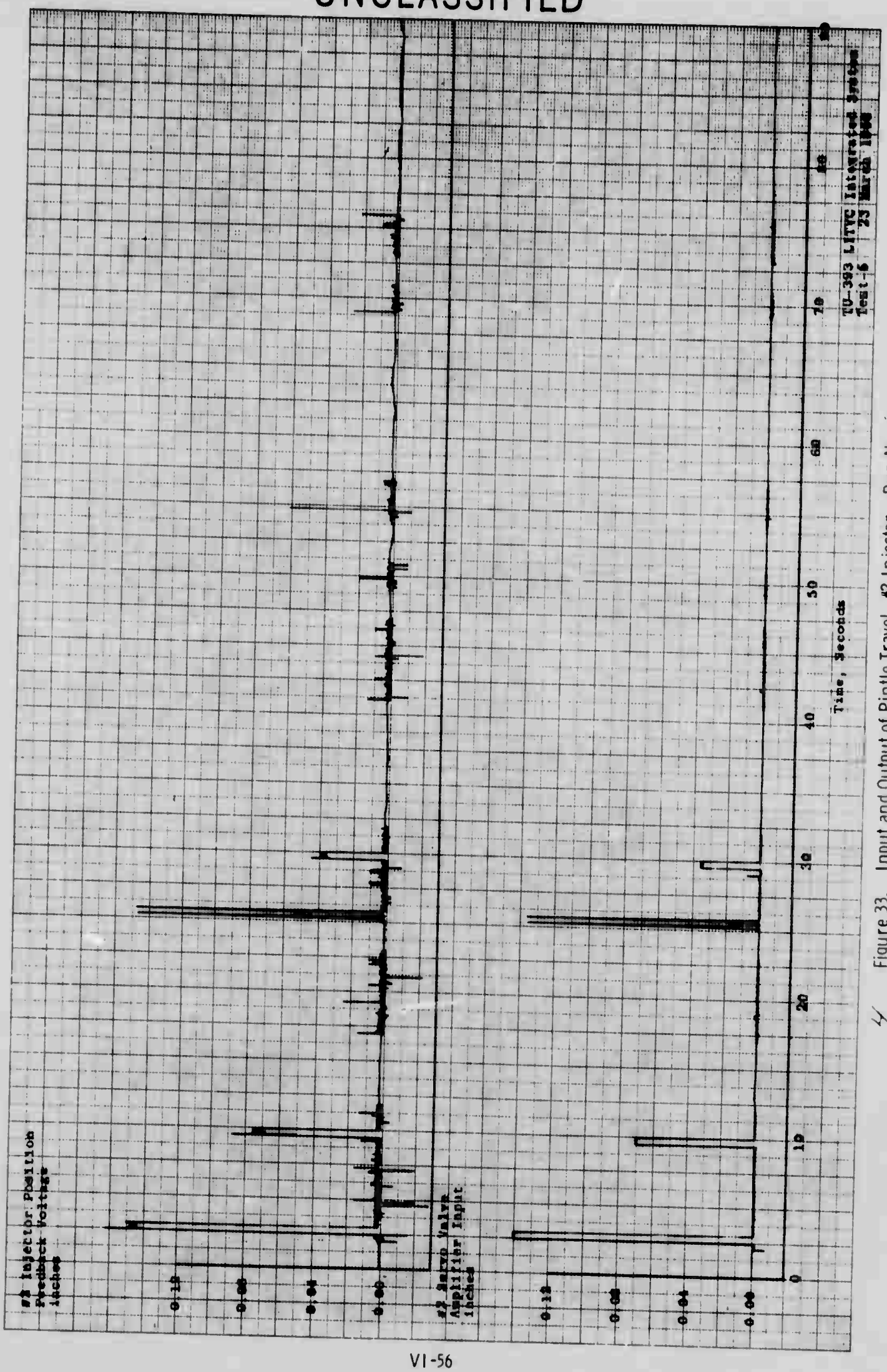

Figure 33. Input and Output of Pintle Travel, #2 Injector - Run No. 6

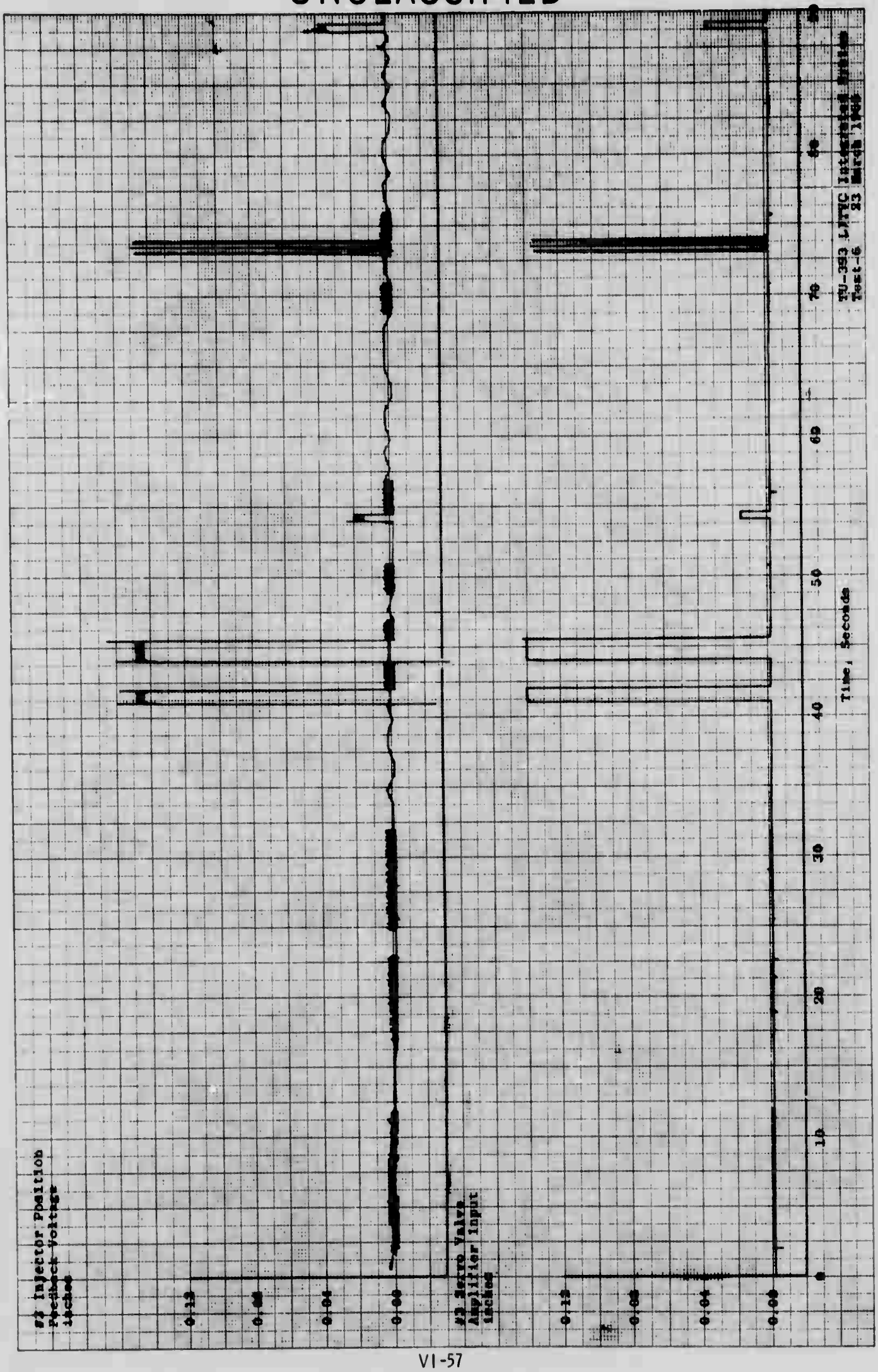

Figure 34 Input and Output of Pintle Travel, #3 Injector - Run No. 6

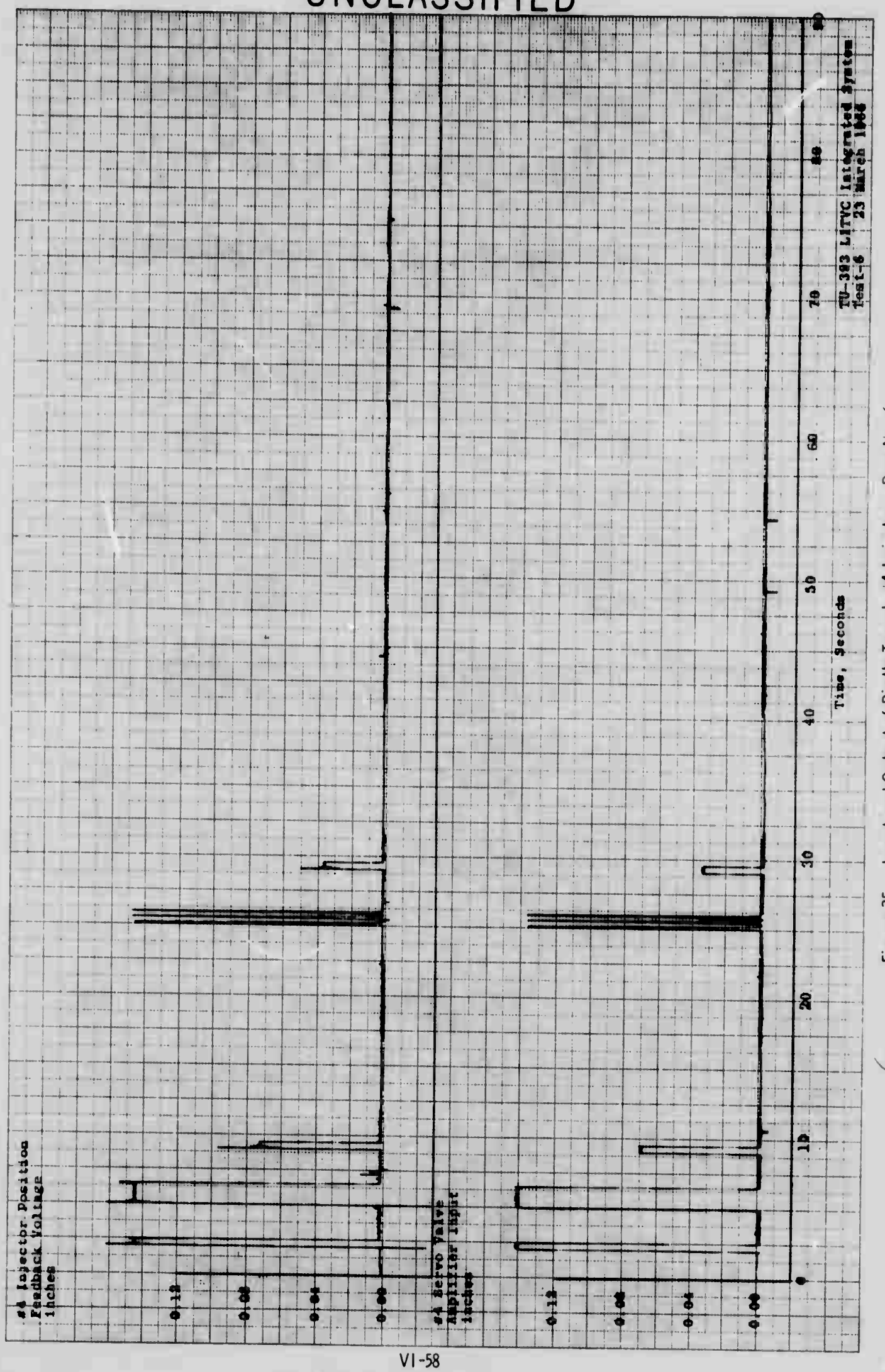

Figure 35. Input and Output of Pintle Travel, #4 Injector - Run No. 6

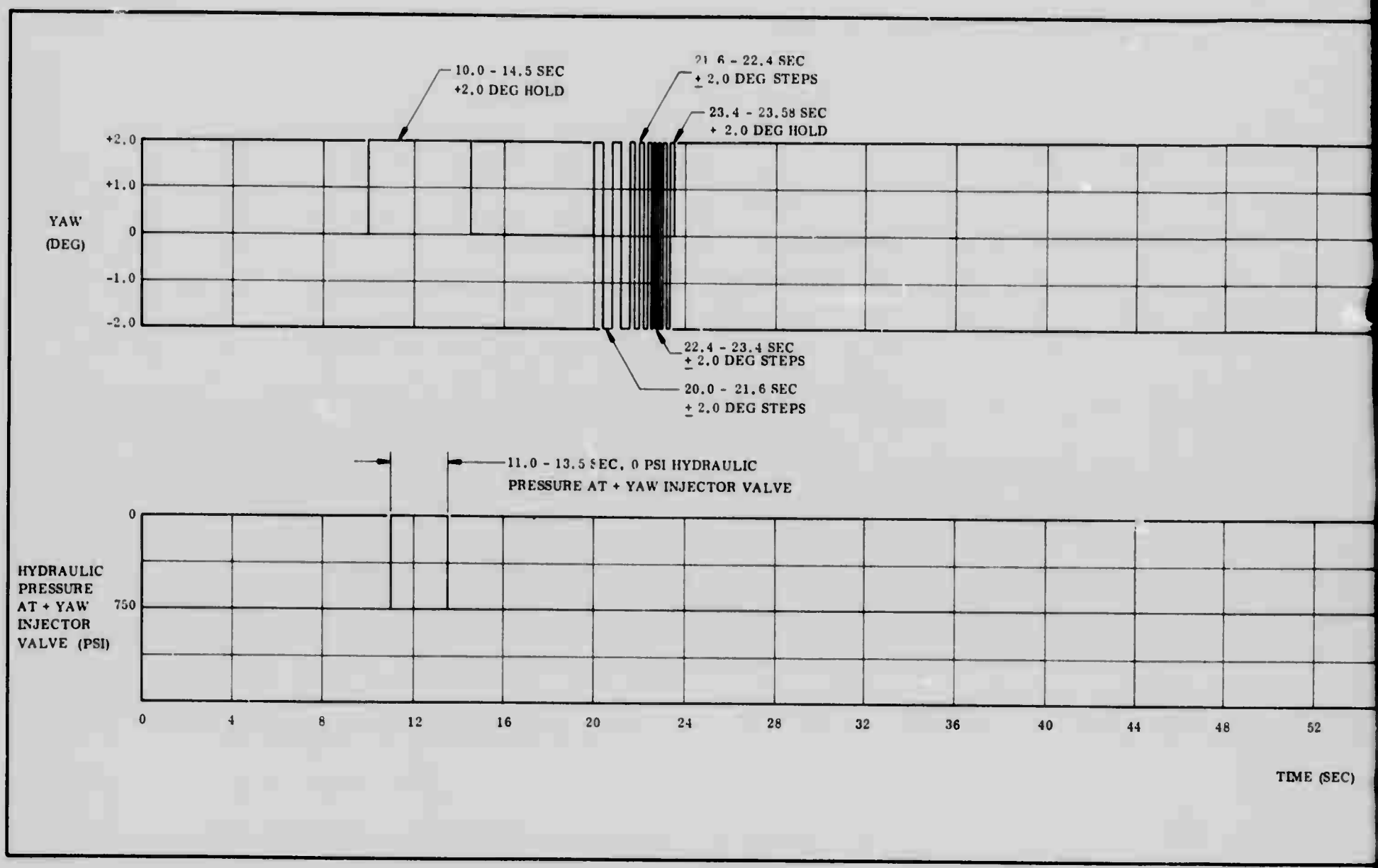
10.0 - 14.5 SEC
+2.0 DEG HOLD
21.6 - 22.4 SEC
± 2.0 DEG STEPS
23.4 - 23.58 SEC
+ 2.0 DEG HOLD
+2.0
+1.0
0
-1.0
-2.0
YAW
(DEG)
22.4 - 23.4 SEC
± 2.0 DEG STEPS
20.0 - 21.6 SEC
± 2.0 DEG STEPS
11.0 - 13.5 SEC, 0 PSI HYDRAULIC
PRESSURE AT + YAW INJECTOR VALVE
0
750
HYDRAULIC
PRESSURE
AT + YAW
INJECTOR
VALVE (PSI)
0
4
8
12
16
20
24
28
32
36
40
44
48
52
TIME (SEC)

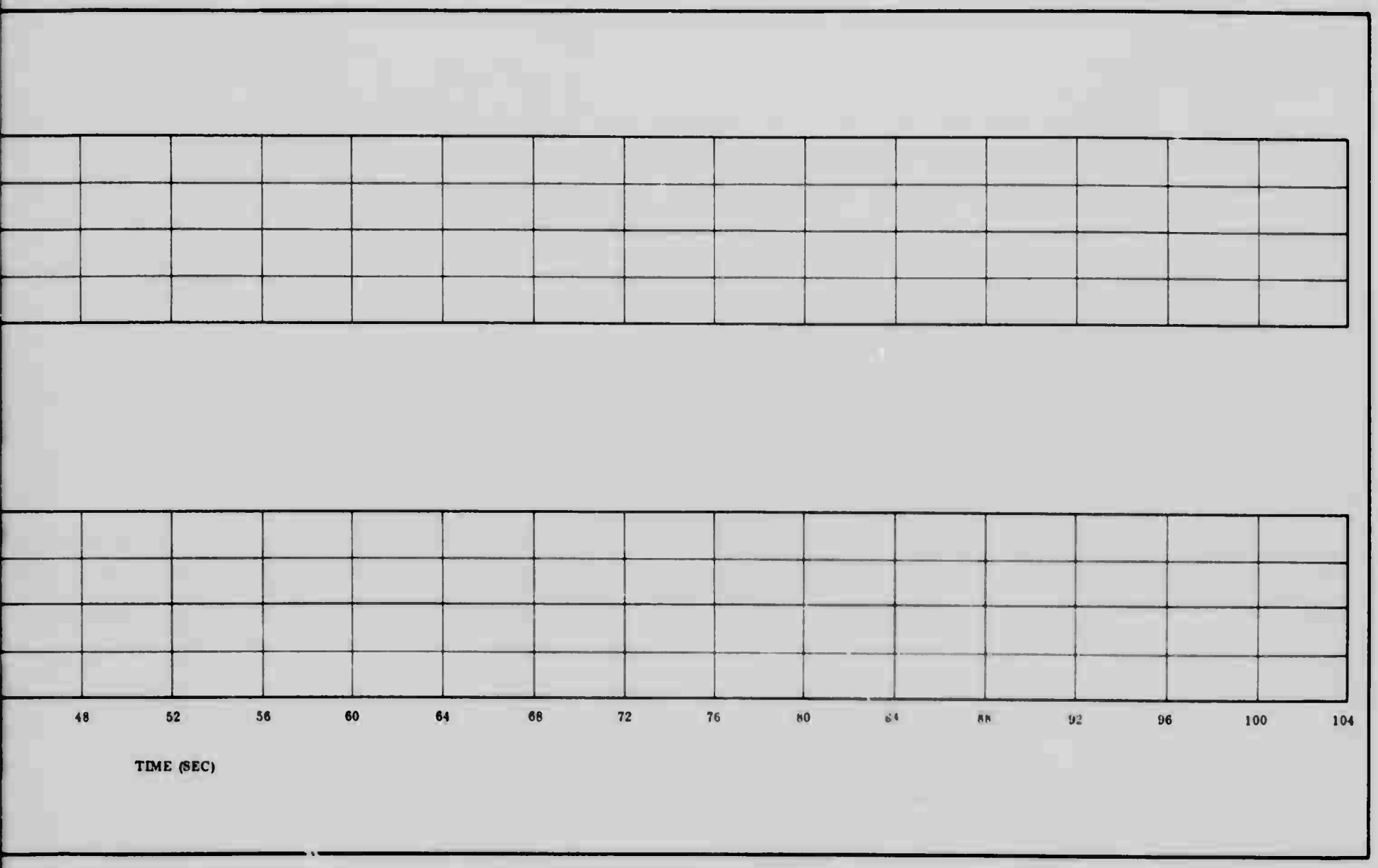

Figure 36. Duty Cycle for Run No. 7

PREVIOUS PAGE WAS BLANK, THEREFORE WAS NOT FILMED.

UNCLASSIFIED

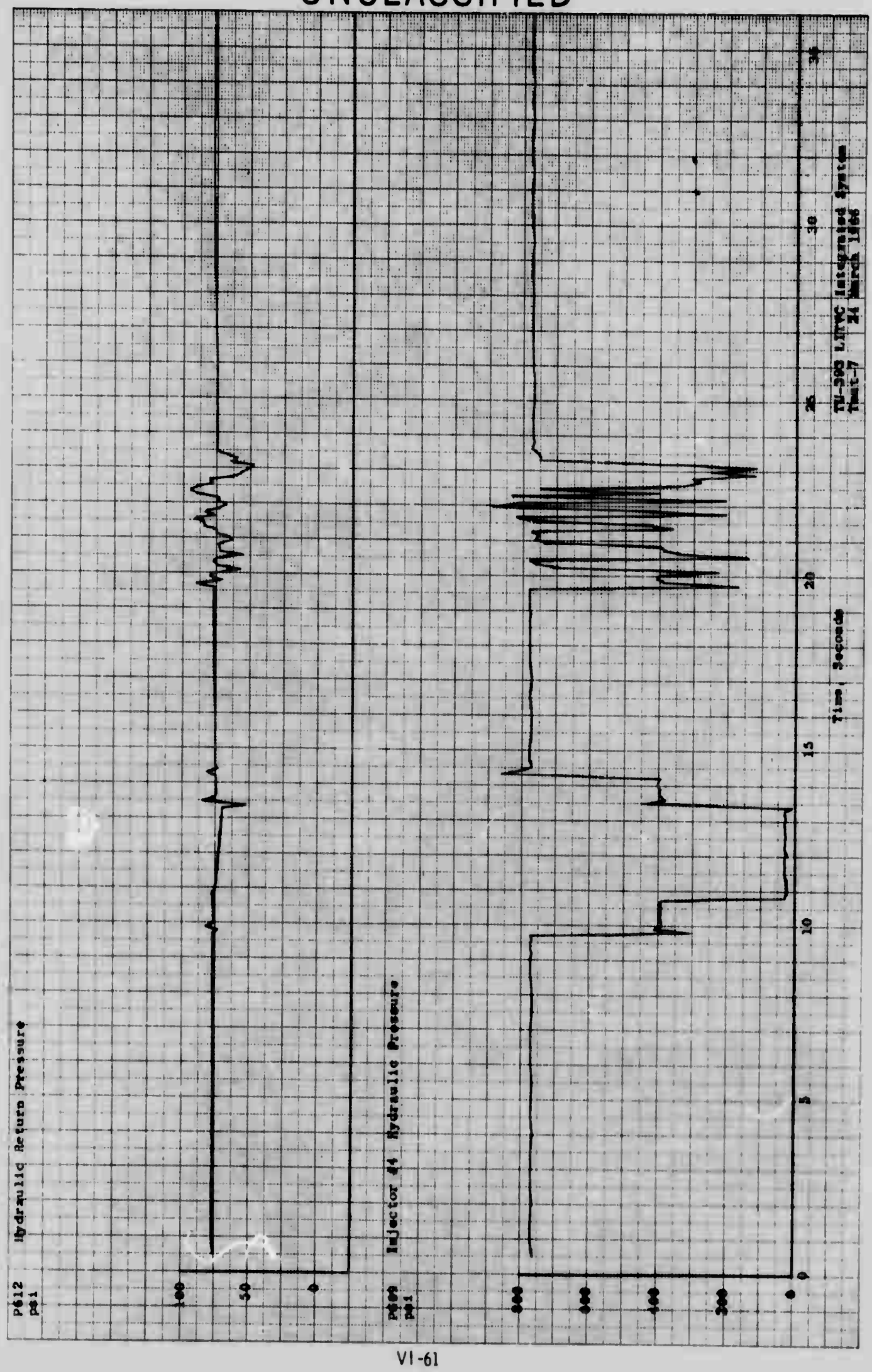

Figure 37. Injector #4 Hydraulic Pressure - Run No. 7

UNCLASSIFIED

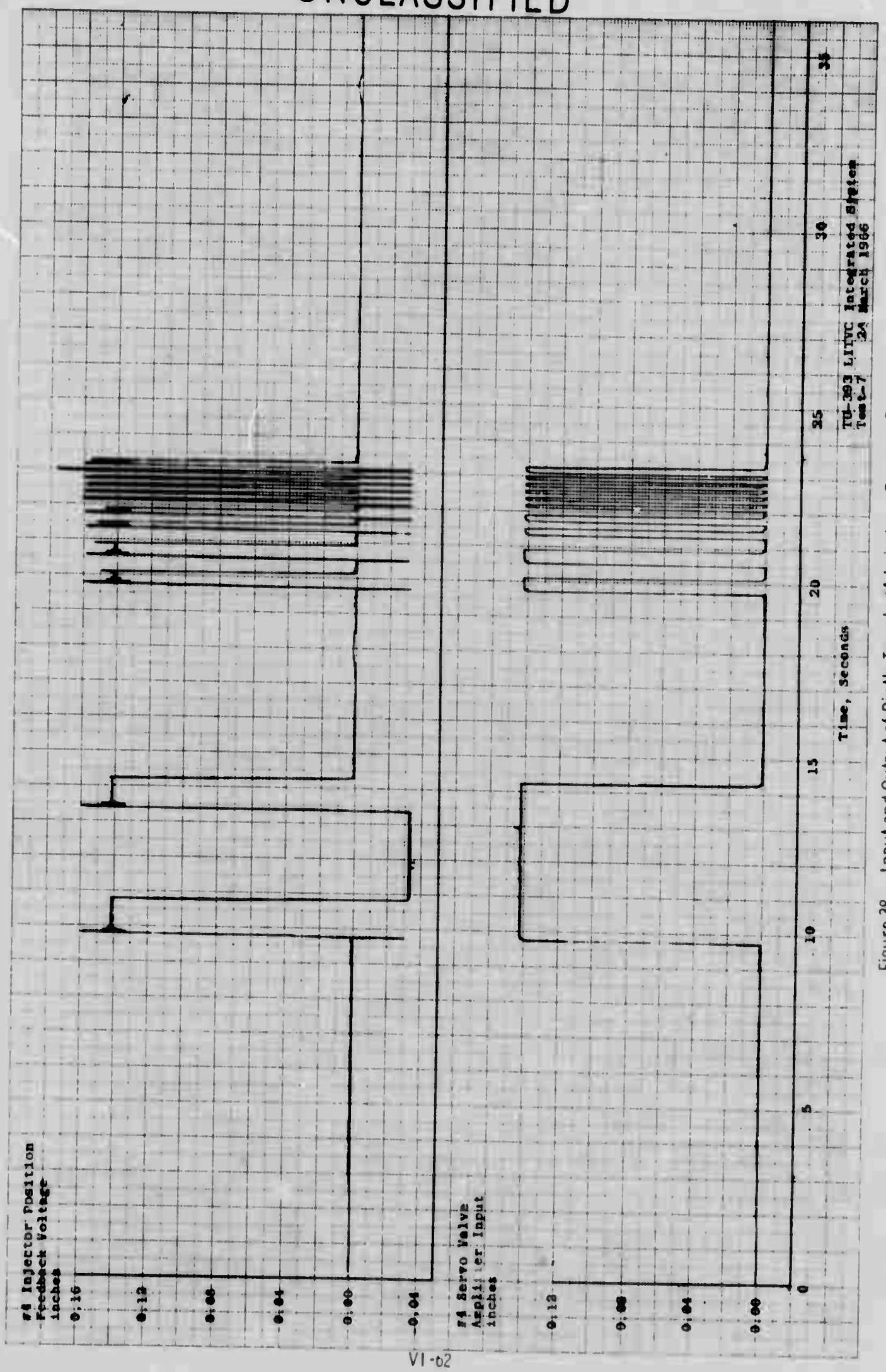

Figure 38. Input and Output of Pir.tle Travel, #4 Injector - Run No. 7

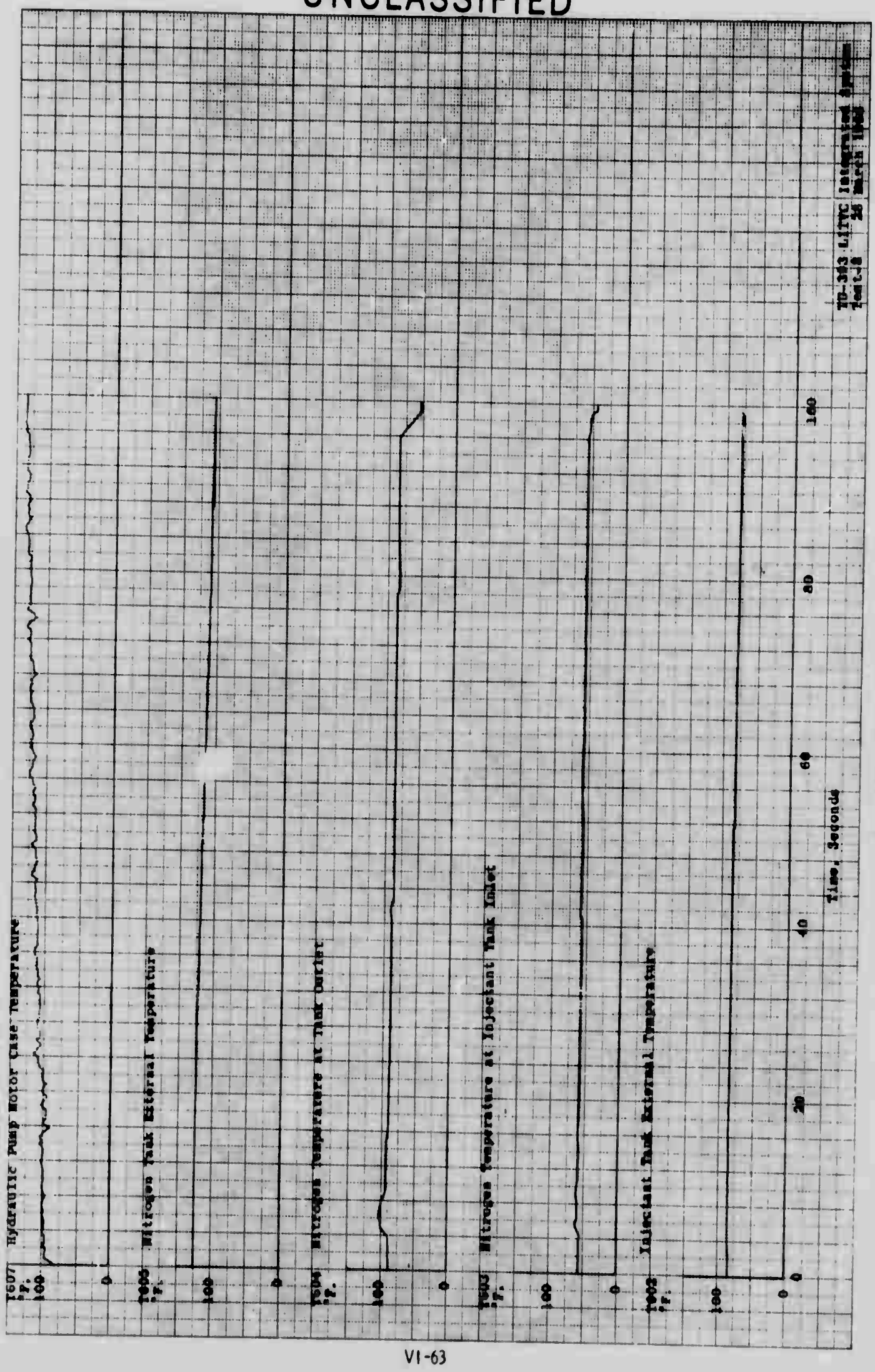

Figure 39. Temperatures - Run No. 8

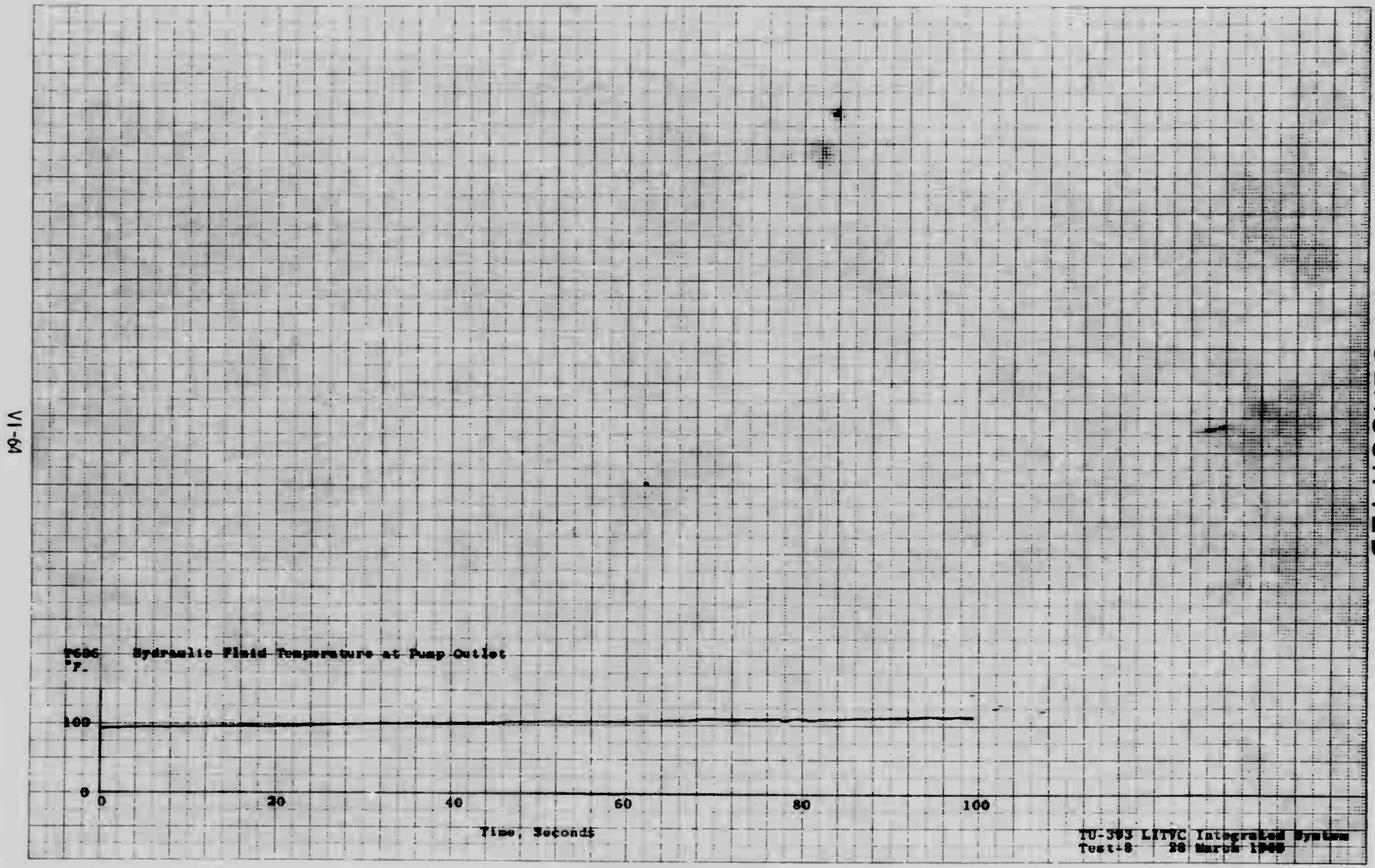

Figure 40. Hydraulic Fluid Temperature - Run No. 8

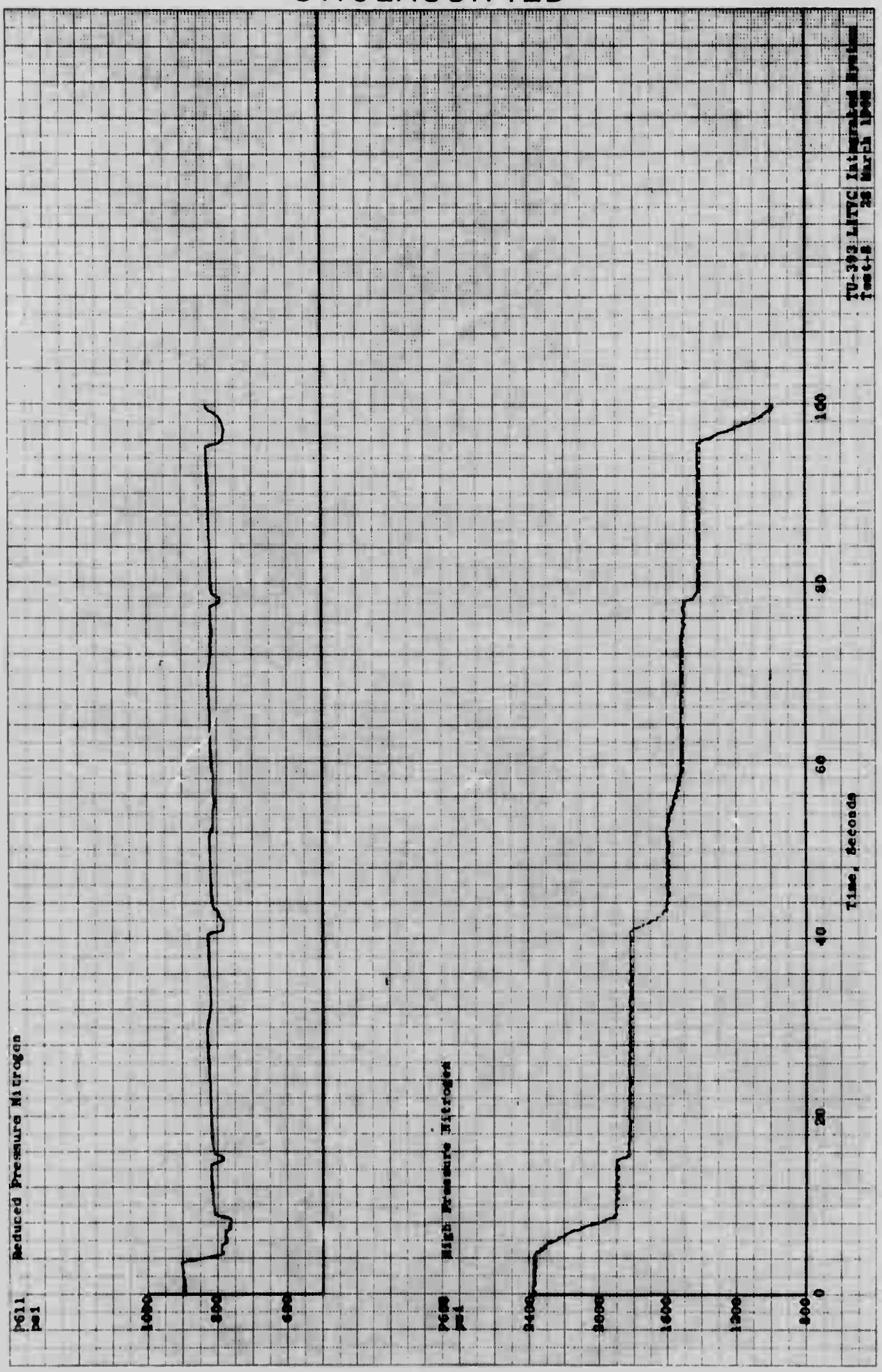

Figure 41. High and Reduced Nitrogen Pressure - Run No. 8

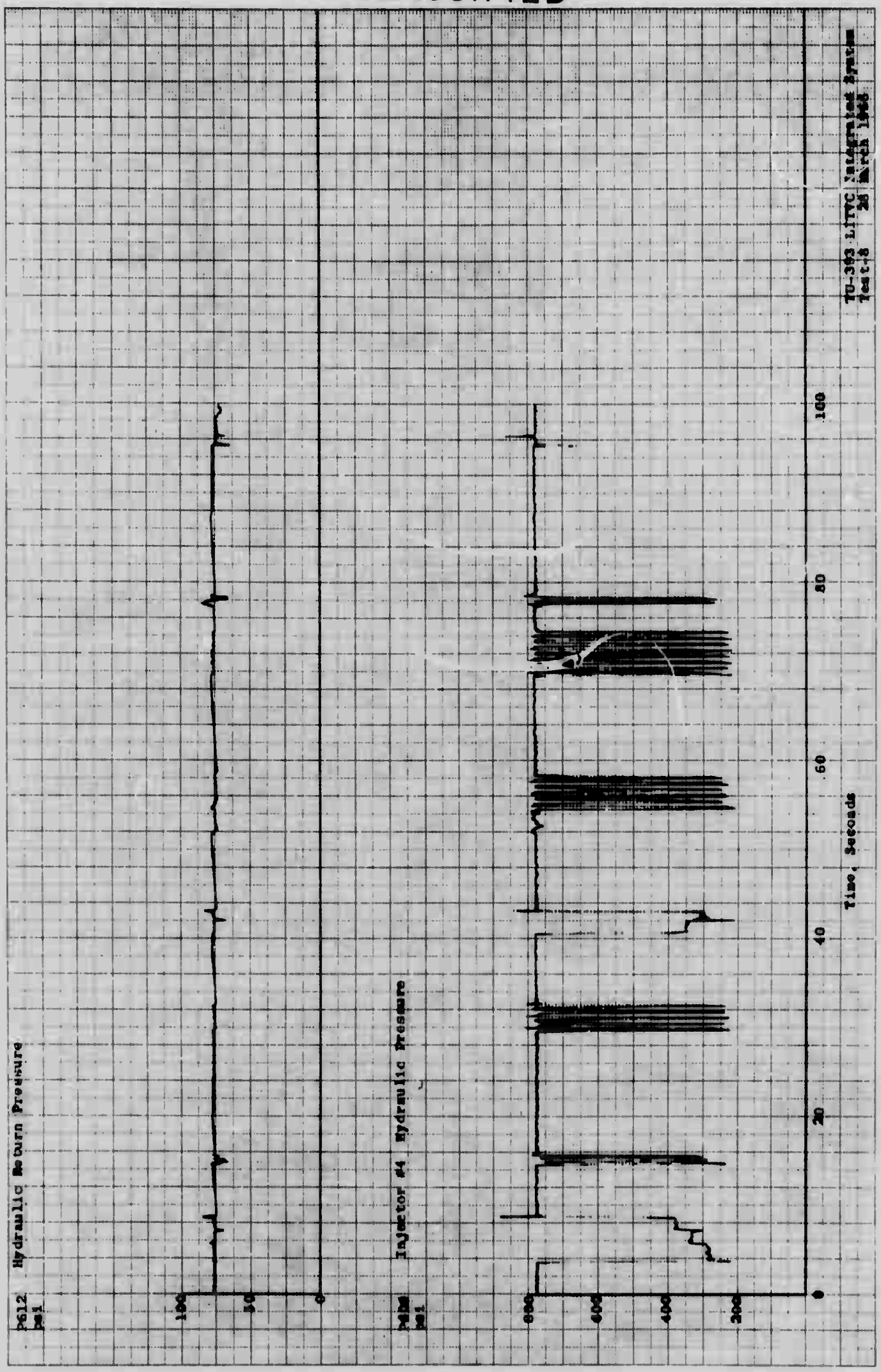

Figure 42. Hydraulic Return and Injector #4 Hydraulic Pressure - Run No. 8

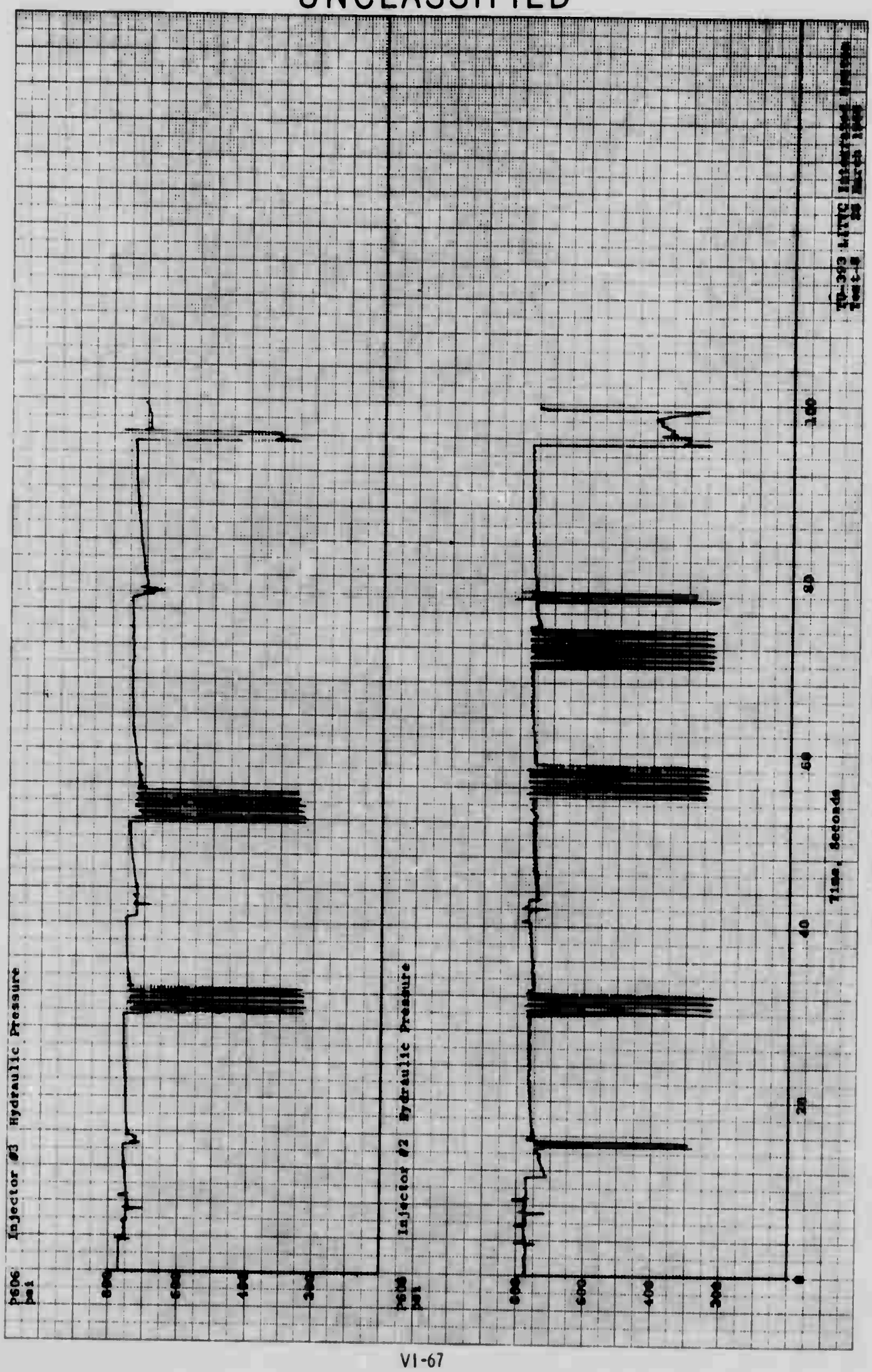

Figure 43. Injector #2 and #3 Hydraulic Pressure - Run No. 8

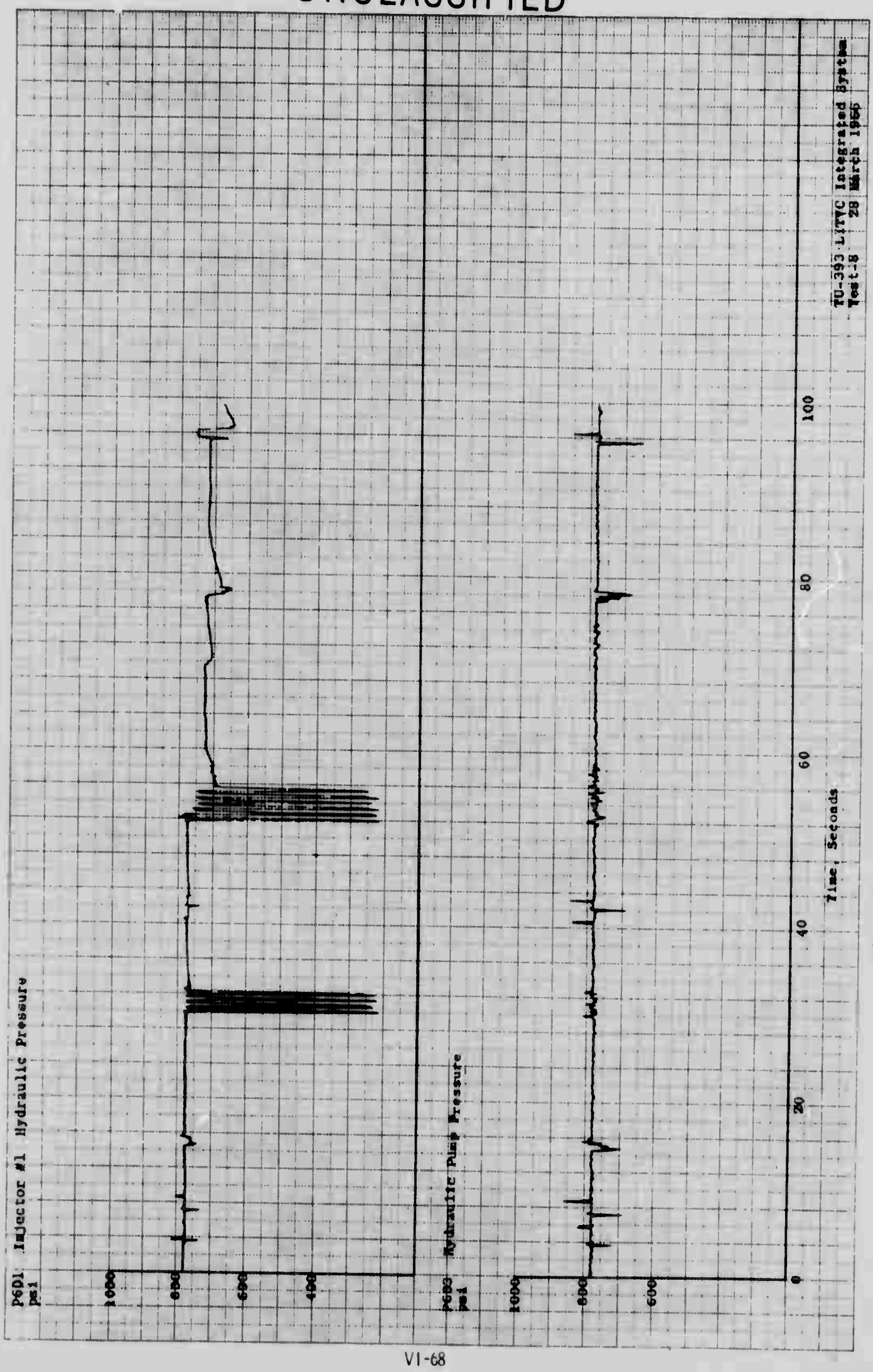

Figure 44. Injector #1 and Hydraulic Pump Pressure - Run No. 8

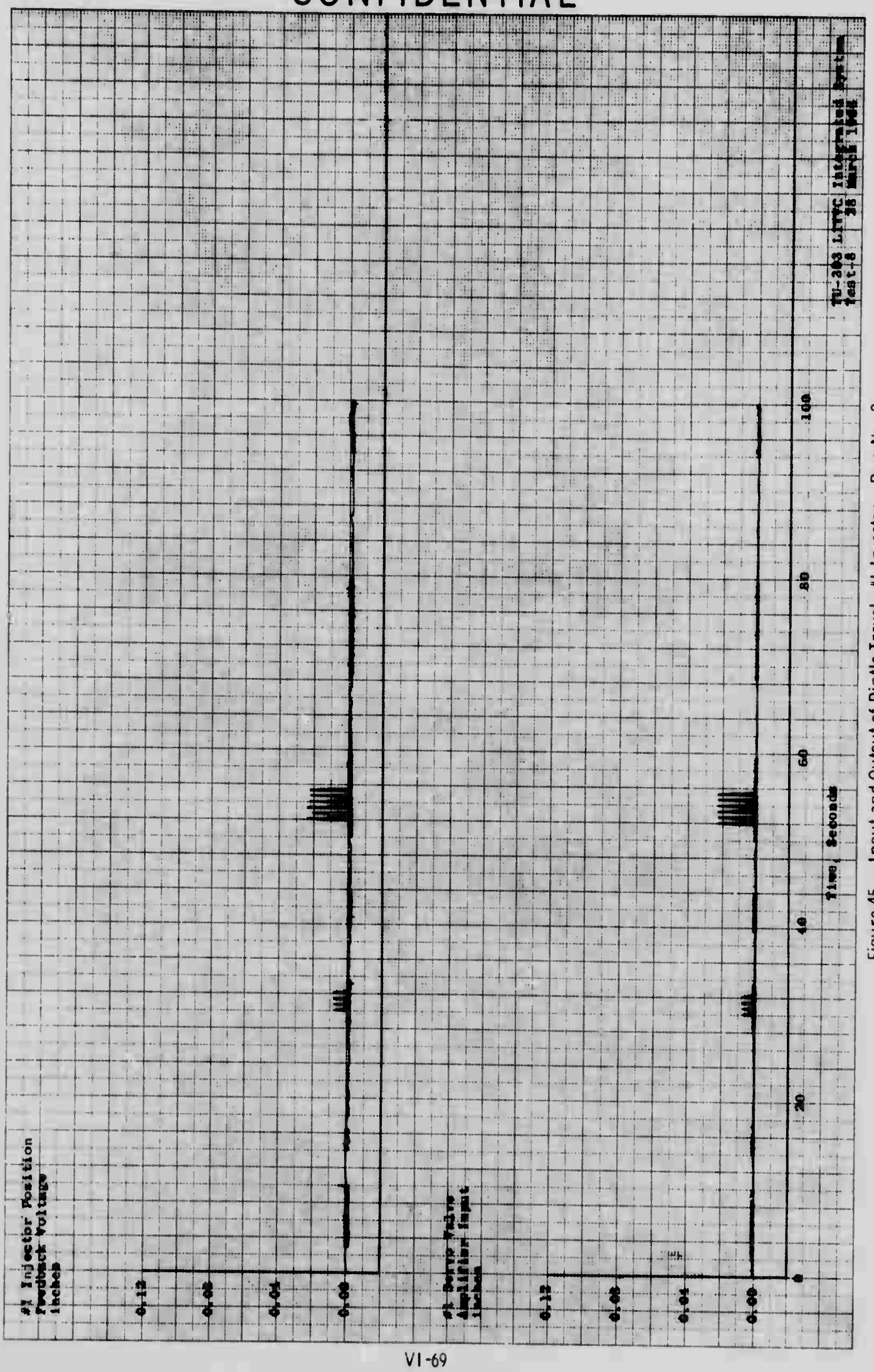

Figure 45. Input and Output of Pintle Travel, #1 Injector - Run No. 8

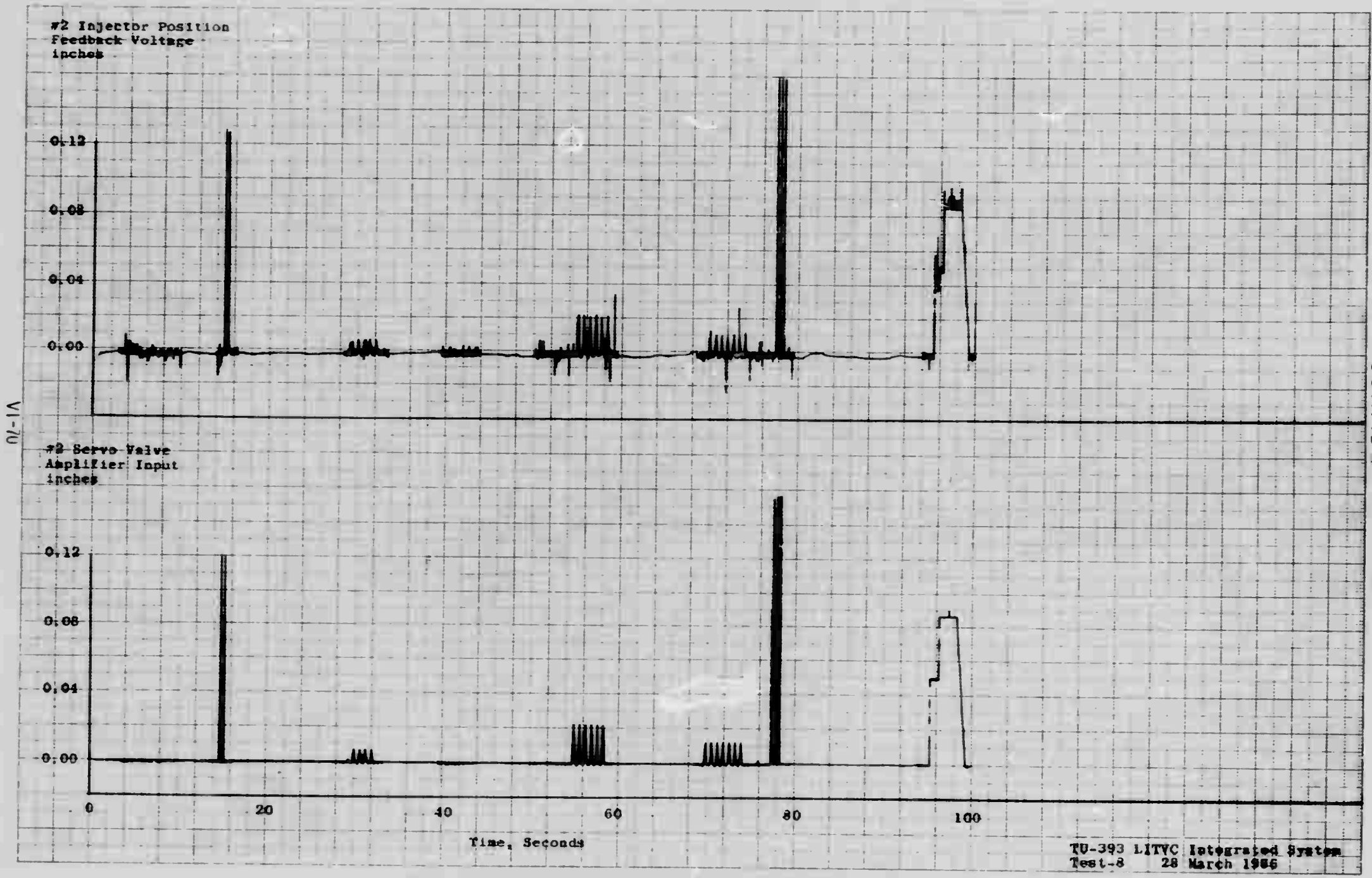

Figure 46. Input and Output of Pintle Travel, #2 Injector - Run No. 8

CONFIDENTIAL

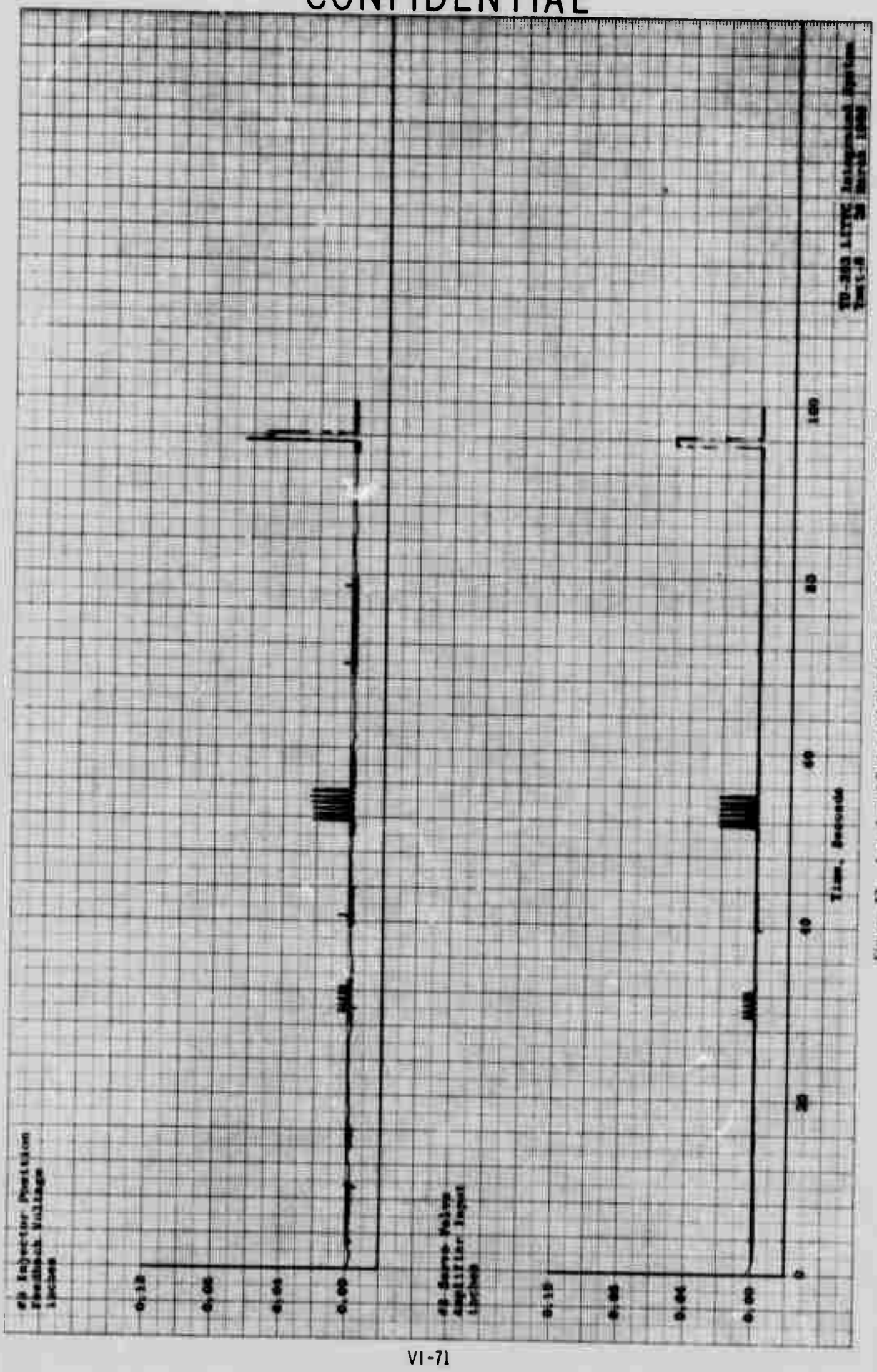

Figure 47. Input and Output of Pintle Travel, ① Injector - Run No. 8

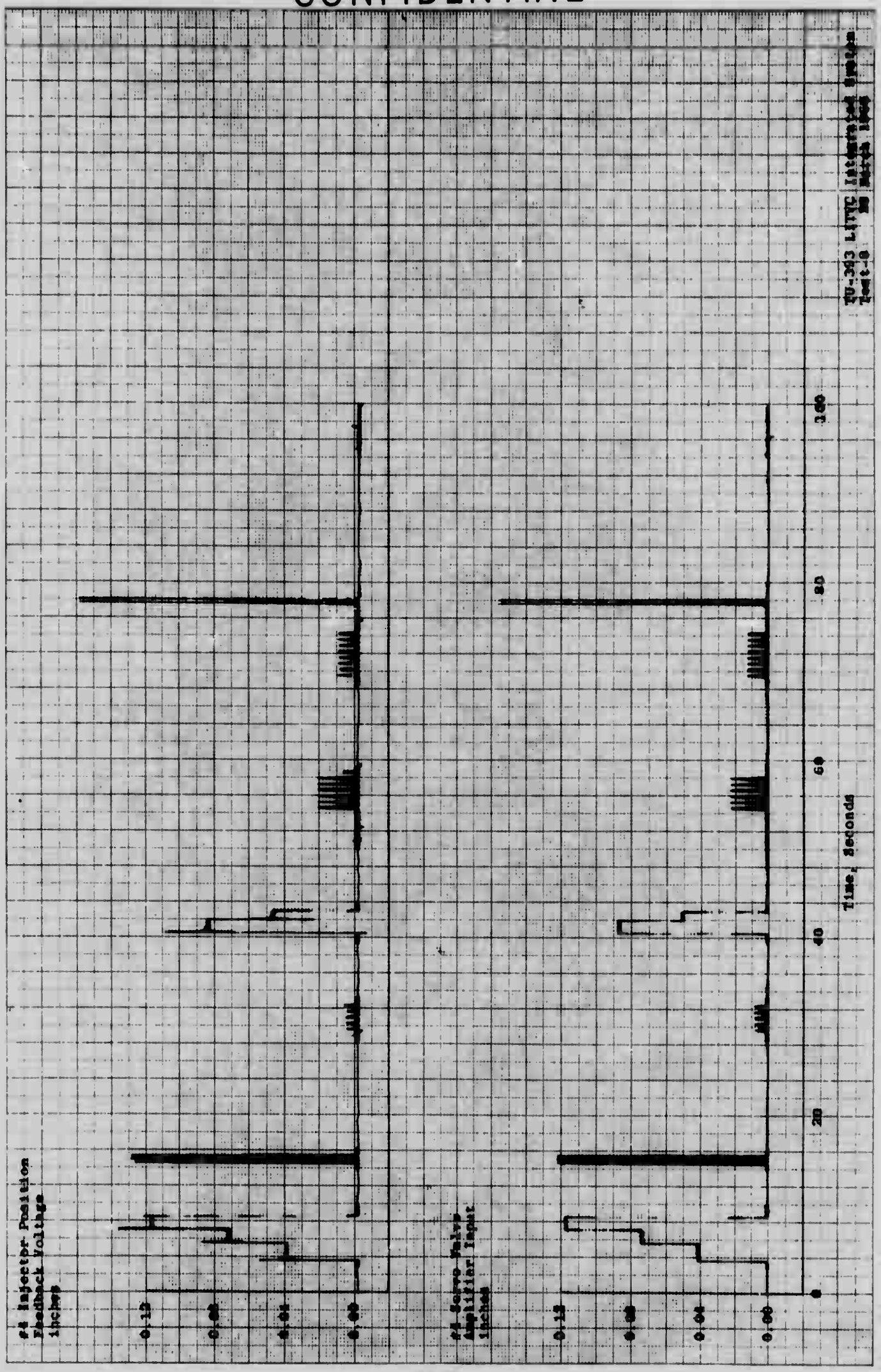

Figure 48. Input and Output of Pintle Travel, #4 Injector - Run No. 8

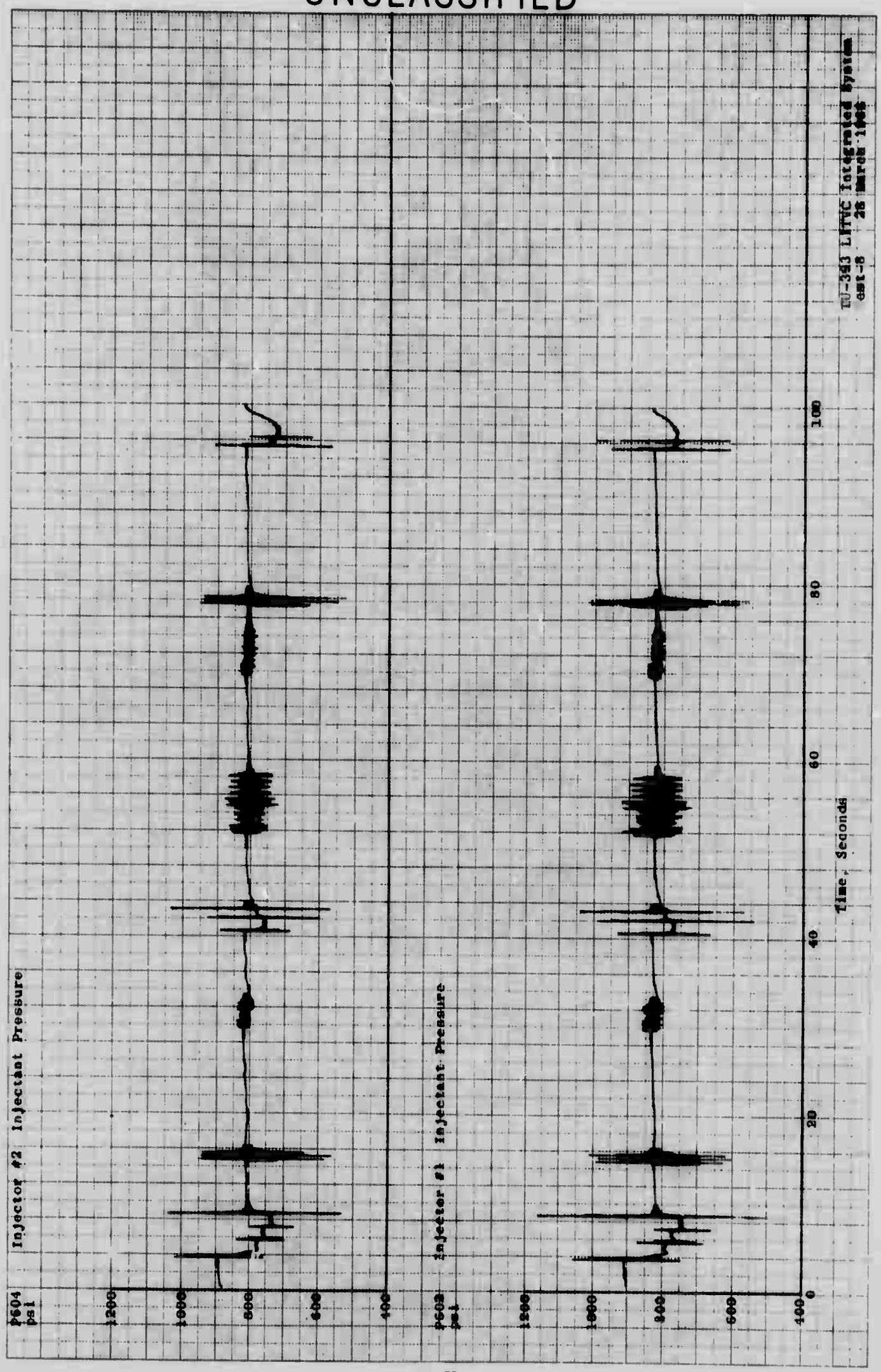

Figure 49. Injector #1 and #2 Injectant Pressure - Run No. 8

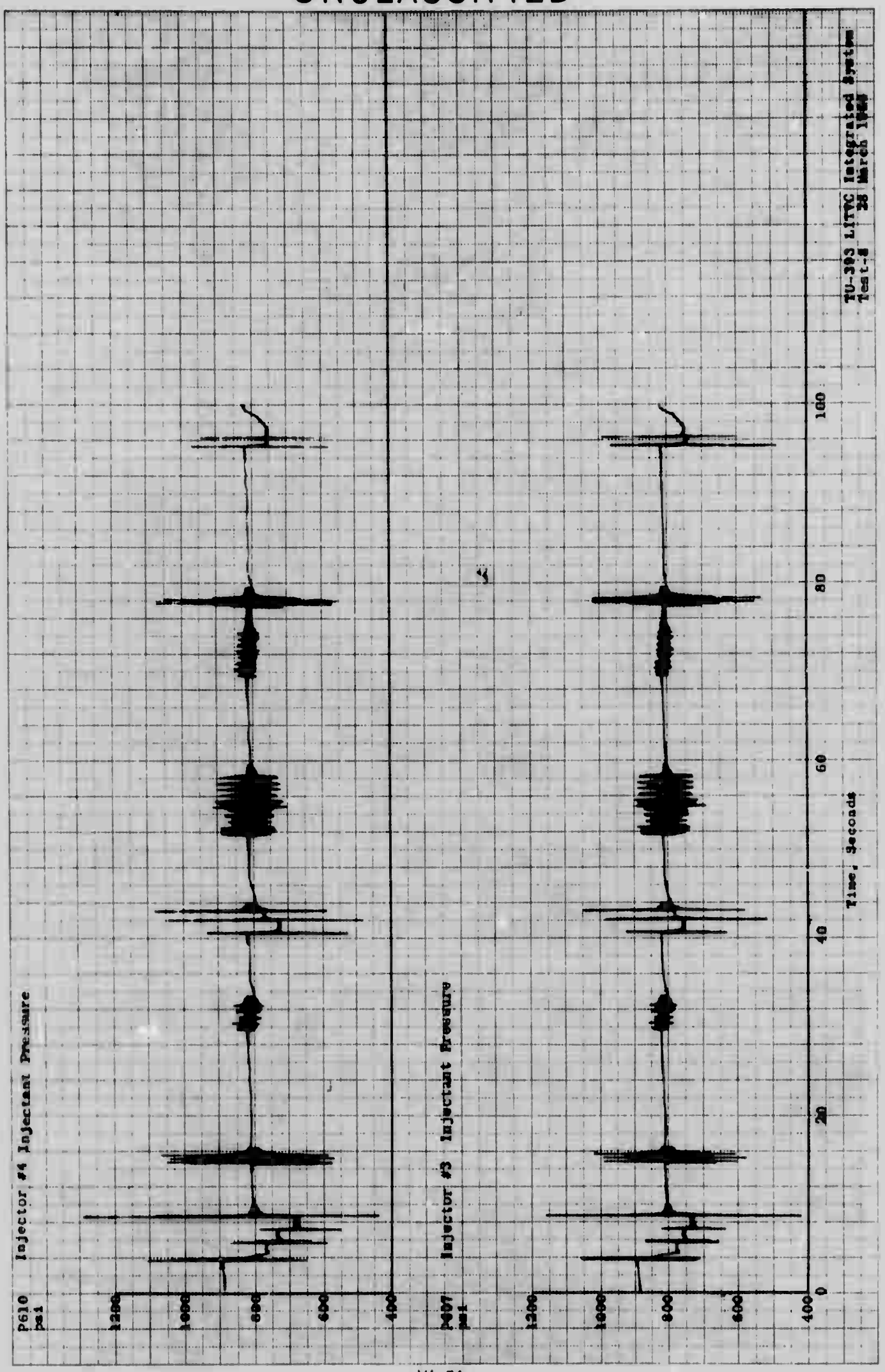

Figure 50. Injector #3 and #4 Injectant Pressure - Run No. 8

Figure 51. Servovalve Feedback Voltages - Run No. 8

TU-393 LITVC Test Run # VIII

28 March 1966

Maximum Strain micro in/in

Loc.#	Max.	Time (sec)	Loc.#	Max.	Time (sec)
S601	1855	0	S610	321	8.7
S602	1936	0	S611	363	8.7
S603	1852	0	S612	497	0
S604	1477	0	S613	290	8.7
S605	1391	0	S614	312	8.7
S606	1380	0	S615	185	8.7
S608	444	8.7	S616	337	8.7
S609	568	8.7			

Maximum Vibration G's

Loc.#	Max.	Time (sec)
A601	5.5	101.5
A602	14.4	7.8

Maximum Run Current 114 Amps

Figure 52. Maximum Strain, Acceleration and Pump Run Current - Run No. 8

APPENDIX VII

156 INCH FIBERGLASS CASE
HYDROBURST TEST REPORT

APPENDIX VII

156-7 FIBERGLASS CASE

HYDROBURST

TEST REPORT

November 1966

THIOKOL CHEMICAL CORPORATION
WASATCH DIVISION
Brigham City, Utah

156-7 FIBERGLASS CASE

HYDROBURST

TEST REPORT

November 1966

Approved by

W. G. Ramroth

W. G. Ramroth, Manager
Large Space Booster
Project Engineering

Approved by

C. G. Kennedy

C. G. Kennedy, Manager
156 Inch Motor Development

TABLE OF CONTENTS

LIST OF ILLUSTRATIONS

LIST OF ILLUSTRATIONS (Cont)

NOMENCLATURE

E_θ = modulus of elasticity in hoop direction

E_φ = modulus of elasticity in longitudinal direction

N_θ = membrane load in hoop direction

N_φ = membrane load in longitudinal direction

p = pressure

R_c = mean case radius

R_p = radius of thrust piston

t_θ = thickness of hoop wrap

t_φ = thickness of polar wrap

$t_{g\alpha}$ = total thickness glass in polar wrap

$t_{g\theta}$ = total thickness glass in hoop wrap

α = polar wrap angle relation to the meridian of the shell

$\mu_{\varphi\theta}$ = Poisson's ratio giving hoop strain caused by stress in the longitudinal direction

$\mu_{\theta\varphi}$ = Poisson's ratio giving longitudinal strain caused by stress in the hoop direction

$\mu_{\theta 12}$ = Poisson's ratio for the hoop wrap giving hoop strain caused by stress in the longitudinal direction

$\mu_{\theta 21}$ = Poisson's ratio for the hoop wrap giving longitudinal strain caused by stress in the hoop direction

$\mu_{\varphi 12}$ = Poisson's ratio for the polar wrap giving hoop strain caused by stress in the longitudinal direction

$\mu_{\varphi 21}$ = Poisson's ratio for the polar wrap giving longitudinal strain caused by stress in the hoop direction

SECTION I

INTRODUCTION

Thiokol Chemical Corporation designed, fabricated, and tested the 156-7 (TU-393) rocket motor under Contract AF 04(695)-773 from the Air Force Space Systems Division, Los Angeles, California, with technical direction provided by the Air Force Rocket Propulsion Laboratory, Edwards, California. During this program, an upper stage type solid propellant rocket motor was fabricated and static fired successfully. The 156-7 motor consisted of a fiberglass reinforced plastic case, a cylindrically perforated propellant grain of PBAA propellant, a submerged high expansion ratio (34:1) ablative nozzle, and an N_2O_4 liquid injection thrust vector control system. The motor was static fired into an altitude simulating diffuser.

The 156 in. diameter monolithic fiberglass reinforced plastic case (Figure 1) was filament wound at the Thiokol filament winding facility in Pocatello, Idaho. After fabrication, the case was transported by truck to the Wasatch Division test facility, assembled in a thrust reacting hydrostatic test stand, instrumented, and hydroproof tested. The case was held successfully at an internal pressure of 790 psig for 122 sec during this test. Subsequent to the proof test, the case was loaded with propellant and used in the successful high performance motor static firing demonstration on 13 May 1966. The motor case was subjected to an internal pressure varying from 400 to 610 psig for 106 sec during the static firing.

The case was reinstalled into the reactive test fixture, which provided a floating piston device to apply a simulated thrust load to the forward skirt, instrumented, and hydroburst tested on 20 Oct 1966. The case burst at a pressure of 963.5 psig (within 7 psi of design ultimate) with initial failure occurring in the circumferential windings at the aft datum line.

SECTION II

TEST OBJECTIVES

The primary objectives of the 156-7 (TU-393.02) case hydroburst were to determine (1) the actual strength levels obtainable at failure and thus appraise the accuracy of analytical calculations, and (2) the static firing effects on the structural integrity of large fiberglass motor cases.

Secondary objectives of the hydroburst test follow.

1. Verify the manufacturing methods, process controls, and quality assurance provisions used to fabricate the case.
2. Demonstrate the feasibility of using large filament wound plastic cases for solid propellant rocket motors.
3. Determine behavior characteristics of large plastic cases, including percent elongation of glass laminate, deflections, and stress-strain relationships.

SECTION III

CASE SUMMARY

A. DESIGN SUMMARY

1. DESIGN CRITERIA

The design of the 156-7 monolithic fiberglass reinforced plastic rocket motor case was based on conventional and proven technologies consistent with:

1. The requirement of a large polar opening,
2. The selection of proven lower limit design strengths,
3. The use of aluminum polar bosses.

Prime factors considered in the case design were:

1. Flight weight,
2. Use of currently available materials and proven manufacturing technologies,
3. Minimum safety factor of 1.25 and a minimum margin of safety of 0.1 based on MEOP,
4. Minimum motor mass fraction of 0.91,
5. Minimum composite strength of 126,000 psi,
6. Application as an upper stage of a multistage vehicle.

The 156-7 rocket motor case was designed to fulfill the following basic loading conditions.

MEOP (psig)	705
Thrust at MEOP (lb)	400,000
Flight Acceleration (g)	8 axial 5 transverse

To insure that the case would have the minimum required safety factor at MEOP, the ultimate loading conditions which the case was designed to meet are those that follow.

Ultimate pressure (psig)	970
Ultimate thrust (lb)	550,000
Ultimate flight acceleration (g)	10 axial 6.25 transverse

2. STRUCTURAL SUMMARY

The designed margin of safety (MS) for each of the case components follows.

Case Component	MS
Fiberglass Case	
Hoop layers	+0.01
Polar layers	+0.11
Forward Skirt	
Compression (buckling)	+0.05
Shear ply attachment	+0.59
Aft Skirt	
Compression (buckling)	+0.06
Shear ply attachment	+0.37
Forward Polar Boss	
Polar ring (bending)	+0.14
Bolts (tension)	HIGH
Forward Adapter	
Shell bending	+0.95
Shear lip	+0.24
Aft Polar Boss (in hydrotest fixture)	
Polar ring (bending)	+0.20
Bolts (tension)	+0.17

Case Component	MS
Aft Polar Boss (nozzle attachment during static firing)	
Polar ring (bending)	+0.39
Bolts (tension)	+0.19

a. Glass and Resin System--S-994 HTS finish fiberglass was chosen for the 156-7 case because of its ultra-high strength capability. A design strength of this glass in composite structures of 335,000 psi was demonstrated as a three sigma lower limit on the TU-312 program, Contract AF 33(657)-11303, using 156 in. diameter hoop rings. This value also has been verified and is being used as the lower strength limit on the POLARIS second stage motor program.

The skirt assemblies were fabricated by interspersing S-994 and E-HTS fiberglass during the winding process. Both the S-994 and E-HTS fiberglass were preimpregnated with US Polymeric E-717 resin system.

The resin system for the case and skirt is 22 percent by weight US Polymeric E-717 epoxy resin, applied by impregnation of the glass prior to winding. This system was verified at the Wasatch Division in the MMRBM plastic case program with fabrication and test of several first and second stage cases. To obtain good compaction, the winding tension for the case was established at 0.5 lb/end of the polar and hoop windings. For the skirt where the polar pulldown is important in the area of the rubber shear ply, the hoop tension was established at 0.8 lb/end while the polar tension was kept at a minimum.

b. Case Wrapping Geometry--A balanced-in-plane polar wrapping pattern was selected for case winding. This pattern is compatible with the unequal polar openings (an aft end opening of 68.0 in. required for deep nozzle submergence and a minimum forward end opening), and provided the required internal volume while remaining stable during fabrication. The chosen wrap angle of 19 deg 23 min was based on data from the Wasatch Division company sponsored filament winding program on filament slippage. This angle was stable for the designed case configuration.

B. FABRICATION SUMMARY

The TU-393.02 case was the second 156 in. diameter monolithic case fabricated for the 156-7 program; the first case (TU-393.01) also was hydroproof tested successfully. Therefore, demonstrated and proven processes, controls, and equipment were used in fabricating the TU-393.02 case. The fabrication effort consisted of the following five major operations.

1. The segmented steel mandrel was assembled and swept with plaster to the required internal insulated case configuration.
2. Uncured asbestos filled NBR (General Tire and Rubber V-44) sheet stock was laid up on the mandrel surfaces to the required thickness and vulcanized in an inert atmosphere autoclave. After cure, the insulation was ground to the required internal case configuration.
3. Aluminum pole bosses were installed on the fore and aft domes of the mandrel, and the polar windings (US Polymeric XF-7030 preimpregnated roving) were applied using a vertical, radial arm, winding machine.
4. The prefabricated fiberglass, filament wound, fore and aft skirts were installed and the structure overwound with the required circumferential (hoop) windings (XF-7030 preimpregnated) in a vertical, electronic-hydraulic winding machine.
5. The segmented steel mandrel was disassembled inside the case and removed with the plaster shell.

The only discrepancy that occurred in the fabrication and/or processing of the TU-393.02 case, that could possibly degrade the case performance, occurred during preparation for propellant loading. During buffing of the internal insulation and bladder, the grinding wheel penetrated through the case bladder into the fiberglass laminate at the aft datum line. One ply of circumferential, and three plies of polar windings were cut. The cut, 0.150 in. wide, extended over a circumferential length of 3.8 inch. Theoretically, this cut resulted in a 1.9 percent reduction in hoop strength, and an 8.3 percent reduction in longitudinal strength; however, these reductions assume complete loss of one hoop ply and three polar plies, which is a conservative assumption. The defect (Figure 2) was located at the aft datum plane, 110 deg counterclockwise from the index (looking forward).

C. PREVIOUS TESTING

1. HYDROPROOF TESTING

Upon completion of fabrication, the case was subjected to a hydroproof test at 790 psig for 122 sec to demonstrate the integrity of the case for subsequent static testing. The test was conducted in a reactive test stand to simulate actual loads that would be imposed on the case in an actual firing at MEOP. The case was instrumented with 30 strain gages, 10 extensometers, and two pressure transducers.

The only visual evidence of loading imposed on the case structure during test was resin craze marks on the lower half of the forward dome. Based upon previous test data, no detrimental effects were anticipated from these craze marks.

2. STATIC TESTING

The 156-7 rocket motor, which used the TU-393.02 case, was successfully static tested on 13 May 1966 in a horizontal attitude with the case supported at

each skirt. During testing, the case was subjected to internal pressures ranging from 400 to 610 psig for 106 sec. The pressure level of 400 psig was achieved within 0.250 sec after ignition with the maximum pressure of 610 psig being recorded 73 sec after ignition.

No external evidence of case structure deterioration resulted from the static firing; however, after subsequent hydroburst testing, some evidence of overheating was visible on the interior of the case insulation. The area where overheating may have occurred (Figure 3) was located directly above the submerged portion of the nozzle. Upward convective flow of superheated air from the nozzle structure may have intensified the postfiring heat soak in this local area. The condition was not detectable until after the hydroburst test, during which the water (test fluid) cleaned the majority of the char from the case wall.

SECTION IV

ASSEMBLY AND TEST

A. FACILITIES AND EQUIPMENT

The TU-393 case was hydrotested in a reactive hydrostatic test stand (Figure 4). The lower portion of the stand served as a base and a thrust adapter to which the forward skirt of the case fit. The middle section of the stand, four large tubular columns, reacted the load from the upper section to the lower section. The upper section consisted of a thrust reacting piston and cross members attached to the columns.

The force from the hydrostatic pressure across the face of the thrust piston was transferred to the upper cross members, then through the columns to the lower structure which reacted against the skirt. The effect of testing with the reactive test stand was to (1) simulate only the pressure loads on the aft dome which would be experienced during firing, (2) simulate thrust loads on the forward skirt, and (3) allow complete freedom of case growth under pressure.

The portable pumping system used for case pressurization was provided and operated by the Halliburton Company, Vernal, Utah. The Halliburton HT 400 model pumping unit consists of two positive displacement piston type pumps driven by two Cummins 600 hp engines. The capacity of the HT 400 system is 1,140 gpm at 1,500 psig. The pumps were supplied with water at approximately 100 psig from a primer pumping unit. The primer unit is supplied from two storage tanks having a total capacity of 4,800 gallons.

B. ASSEMBLY AND LEAK TEST

The case was installed vertically in the test stand with the forward skirt resting on the base structure. Epocast 31D was cast under the skirt to assure a complete bearing surface of the skirt against the base structure. The aft closure and piston assembly was attached to the polar boss and the cross members installed (Figure 5). The case was placed in the stand so the defect (ref Subsection III-B) was located approximately 20 deg to the right of the front of the case.

The instrumentation was applied to the case in accordance with Figure 6 . The instrumentation consisted of the same number of gages as used in the hydroproof test of the TU-393.02 case, located as closely as possible to the original instrumentation positions. The amount and location of instrumentation was planned to obtain data directly comparable to the data from the hydroproof test.

Following assembly of the test setup, the case was filled with water and leak tested for 10 min at line pressure (100 psig). No leakage was observed during the leak test.

Subsequent to the leak test, the thrust piston was seated against the overhead structure with an internal case pressure of 35 psig. The interface between the piston and overhead structure was then potted with Epocast 31D to assure a complete bearing surface.

C. HYDROBURST TESTING

On 20 Oct 1966, the HT-400 pumping unit was adjusted to provide 300 gpm flow through the bypass piping at 1,500 psig. The entrance valve to the case was opened, allowing case pressure to increase to the manifold pressure level of 132 psig. When the case pressure had stabilized at the manifold pressure, the bypass

valve was closed and the case pressure was raised at an average rate of 6.0 psig/sec to the burst pressure of 963.5 psig. The prescribed pressurization rate was attained by following a preplotted pressure vs time graph by opening and/or closing bypass valves as necessary to adjust the flow rate.

During pressurization, no leakage was observed from the case; however, continual resin crazing noises were generated throughout the pressurization cycle. Since the case had been pressurized twice previously, resin crazing was not expected during the burst cycle. Apparently, additional polymerization of the resin occurred during the heat soak of the case wall following static firing. Thus, upon repressurization, resin crazing again occurred.

Case failure (Figure 7), which occurred at 963.5 psig, initiated in the hoop windings at the aft datum plane (intersection of the aft skirt with the basic cylindrical section of the case), and progressed forward along the length of the case cylinder. Initial failure occurred at the datum plane and then progressed over the remaining hoop windings on the cylinder. Figure 8 shows the failure sequence.

The major structural components of the case, fore and aft polar bosses, fore and aft skirts, and the skirt attachment shear plies performed flawlessly; however, a slight delamination at the forward skirt face occurred as a result of rotation imparted to the skirt by case expansion.

SECTION V

TEST RESULTS

A. DATA ANALYSIS

The strain and deflection data obtained during this hydrostatic burst test was of excellent quality with only one gage, S009, totally inoperative. Strain gages and extensometers were placed on the cylindrical section of the case in the basic areas where a failure might occur. Strain gages were placed on the forward dome to measure the effect that the existing crazing had on the performance of dome structure. Strain gages also were placed on the aft dome to evaluate magnitude of these strains relative to the basic cylindrical section. The axial deflection of the forward dome, and both the axial and transverse movement of the aft dome, were measured with extensometers to evaluate case deflection.

Figure 9 depicts the pressure vs time trace as measured by pressure transducer P001 located in the shell section of the aft adapter. The pressurization rate averaged 6.125 psig/sec with no indicated fluctuations in the trace. The pressure suddenly dropped at 963.5 psig, indicating that failure had occurred at 135.37 sec from the commencement of pumping ($t = 0$ sec and $p = 132.0$ psig).

Figure 10 depicts the hoop strain in the cylindrical section of the case at the forward and aft datum lines, and at midcylinder. At midcylinder, strain gage S005 (inoperative after 535 psig) and extensometer D006 agreed very closely, thus establishing a good measurement of hoop behavior in the area. Extensometers D005 and D007, at the aft and forward datum lines, respectively, showed that the magnitude of the strain at these two locations was very similar, and about 12 percent less than the indicated strain at midcylinder. Strain gage S009 at the aft datum

line was inoperative, and strain gage S001 at the forward datum line showed a higher reading than the equivalent extensometer. However, gage S001 failed at 875 psig, and was thus probably in a location of local crazing.

Figure 11 depicts the longitudinal strain in the cylindrical section of the case as measured by (1) extensometers D001 and D002, located between datum lines, and (2) by strain gages S002, S006, and S011. Experience has revealed that strain gages installed on the hoop wrap and oriented in the longitudinal direction are very susceptible to premature failure or erratic readings due to crazing in the hoop laminate. Strain gage S002 located at the forward datum line operated through case burst and the resulting data were fairly close to that from the extensometers. Gage S006, located at midcylinder, also was fairly accurate, but due to crazing, the gage became inoperative at 500 psig. Gage S011, located at the aft datum line, was extremely erratic, probably because it was located over a local crazing which opened in the longitudinal direction.

An important observation in the D001 and D002 data is the sudden increase in axial deflection at 950 psig, indicating that a polar failure might have preceded the indicated hoop failure.

Figure 12 depicts the measured hoop, meridional, and fiber strain along the periphery of the dome. The data showed that the respective meridional and fiber strains remained very similar in magnitude at the specific locations over the dome. In general, the magnitude of these strains was approximately 18 percent lower than the longitudinal strain experienced in the cylindrical section. The predicted strains in the forward dome are shown in Figure 13.

The hoop strain trend in the forward dome was a little erratic due to the crazed areas. At case failure, gage S016, located 12 in. from the forward datum line, indicated a hoop strain of 0.024 in./in.; while 15 in. further up the dome, gage S025 recorded a hoop strain of 0.012 in./in.; and at a point an additional 16.5 in. up the dome gage S026 indicated a hoop strain of 0.005 in./in. However, at this same axial location, but 180 deg away, gage S018 recorded a hoop strain of 0.017 in./in., indicating that the local crazed area allowed uneven hoop strain in the dome, high in the areas of

crazing and lower in the areas of noncrazing. The hoop strain data at a distance 54 in. forward from the forward datum line were found to agree closely with the meridional and fiber strain data. This latter area also was relatively free of craze marks.

Figure 14 depicts the measured fiber strains and Figure 15 shows the predicted strain at three locations equally spaced up the aft dome. At case failure, the three gages indicated an average strain of 0.019 in./in. (gage S023 extrapolated) which was approximately 13 percent lower than the longitudinal strain in the cylinder. The magnitude of the hoop and meridional strain gages (S011 and S012) located at the inflection point of the dome agreed closely with the fiber gage (S023). These strains were approximately eight percent lower than predicted in the netting analysis.

Figure 16 depicts the axial displacement of the forward dome relative to the leading edge of the forward skirt. Up to 350 psig, the dome exhibited nonlinear deflection, which can be attributed to local bending in the shell structure just outboard of the polar boss where the surface is essentially flat and normal to the axis of the case. In this area, the dome will reorient itself slightly before exhibiting true membrane behavior. As shown by the data, the extent of this reorientation was small.

Figure 17 shows the total axial and transverse movement of the case and aft dome relative to the hydrotest fixture. The four gages indicated no canting of the case during pressurization as a result of local relaxation or crazing in the case or skirt structure. Figure 18 shows the predicted axial deflections for the two areas of the case.

The total axial deflection of the case at burst was 4.82 in., or an average longitudinal strain og 0.0296 in./in. based on an inspected length of 163.0 in. from the face of the adapter cap to the face of the aft polar boss.

The magnitude of the data obtained from this burst test was comparable to the data obtained from the hydrostatic proof test and from the static firing. Figures 19 and 20 show representative extensometer data from these three tests, comparing the measured hoop and longitudinal strain values recorded for the cylindrical section

of the case. The data show that the two tests prior to the burst test had little effect on elastic behavior of the case material.

In Figures 10 and 11 , two theoretical strain values are shown: (1) strain strictly as a function of the glass present in the structure, neglecting the effect of the resin matrix; and (2) strain as a function of the orthotropic mixture of both filament and resin, assuming no crazing or cracking in the resin matrix. In both methods of analysis, the wrap angle was assumed to be constant, and that no filament reorientation resulted from case expansion and elongation.

The orthotropic-composite type of analysis is based on the law of mixtures, a method of analysis that is presently being used extensively for orthotropic filament reinforced material. The equations for the two strains are as follows.

$$\epsilon_\theta = \frac{1}{t_\theta + t_\varphi}\left[\frac{N_\theta}{E_\theta} - \mu_{\varphi\theta}\,\frac{N_\varphi}{E_\varphi}\right] \qquad (1)$$

$$\epsilon_\varphi = \frac{1}{t_\theta + t_\varphi}\left[\frac{N_\varphi}{E_\varphi} - \mu_{\theta\varphi}\,\frac{N_\theta}{E_\theta}\right] \qquad (2)$$

where the properties are based on a resin content of 22 percent by weight, with no voids.

The calculated values for the composite moduli are based on the individual moduli values for the hoop and polar wrap derived from the law of mixtures, assuming no shear distortion between the plies of wrap.

$$E_\theta = \frac{E_{\theta\theta}t_\theta + E_{\varphi\theta}t_\varphi}{t_\theta + t_\varphi} = 5.37 \times 10^{+6}\ \text{psi} \qquad (3)$$

$$E_\varphi = \frac{E_{\theta\varphi}t_\theta + E_{\varphi\varphi}t_\varphi}{t_\theta + t_\varphi} = 2.68 \times 10^{+6}\ \text{psi} \qquad (4)$$

where: $E_{\theta\theta} = 8.0 \times 10^{+6}$ psi

$E_{\theta\varphi} = 0.6 \times 10^{+6}$ psi

$E_{\varphi\theta} = 1.8 \times 10^{+6}$ psi

$E_{\varphi\varphi} = 5.5 \times 10^{+6}$ psi

$t_\theta = 0.345$ in.

$t_\varphi = 0.254$ in.

The calculated values of the composite Poisson's ratio are based on the individual stiffness (Et) and Poisson's ratio values for the hoop and polar wrap.

$$\mu_{\varphi\theta} = \frac{(E_{\theta\theta} t_\theta)\,\mu_{\theta 12} + (E_{\varphi\theta} t_\varphi)\,\mu_{\varphi 12}}{E_{\theta\theta}\, t_\theta + E_{\varphi\theta}\, t_\varphi} = 0.10 \qquad (5)$$

$$\mu_{\theta\varphi} = \frac{(E_{\theta\varphi} t_\theta)\,\mu_{\theta 21} + (E_{\varphi\varphi} t_\varphi)\,\mu_{\varphi 21}}{E_{\theta\theta}\, t_\theta + E_{\varphi\theta}\, t_\varphi} = 0.20 \qquad (6)$$

where: $\mu_{\theta 12} = 0.019$

$\mu_{\theta 21} = 0.25$

$\mu_{\varphi 12} = 0.61$

$\mu_{\varphi 21} = 0.20$

The longitudinal membrane load (N_φ) and hoop load (N_θ) were based on the internal pressure and thrust load, considering the increase in case radius due to hoop elongation.

$$N_\varphi = \frac{p R_c^2 (1 + \epsilon_\theta)^2 - p R_p^2}{2 R_c (1 + \epsilon_\theta)} = 0.0380 \text{ lb/in.} \qquad (7)$$

$$N_\theta = p R_c (1 + \epsilon_\theta) = 0.0725 \text{ lb/in.} \qquad (8)$$

The resulting strains using equations (1) and (2) follow

$\epsilon_\varphi = 18.5p \times 10^{-6}$ in./in.

$\epsilon_\theta = 22.0p \times 10^{-6}$ in./in.

The calculated strain in the case using the netting analysis is based on glass properties and orientation only. The longitudinal load is assumed to be reacted entirely by the polar wrap as a function of the load vectored into the line of the fiber. The resulting longitudinal strain follows.

$$\epsilon_\varphi = \frac{N_\varphi}{E_g t_{g\alpha} \cos^2\alpha} = 22.7p \times 10^{-6} \text{ in./in.} \qquad (9)$$

where: $E_g = 12.4 \times 10^{+6}$ psi

$t_{g\alpha} = 0.158$ in.

$\alpha = 19$ deg 23 min

The portion of the hoop load not reacted by the polar wrap is reacted by the hoop wrap and the calculated strain in the hoop wrap is indicated in the following equation.

$$\epsilon_\theta = \frac{N\theta}{E_g(t_{g\theta} + t_{g\alpha} SIN^2\alpha)} = 27.8p \times 10^{-6} \text{ in./in.} \quad (10)$$

where $t_{g\theta} = 0.216$ in.

The actual hoop strains tend to follow the strain prediction as made by treating the structure as a filament reinforced composite (Figure 10), while the recorded longitudinal strains (Figure 11) tend to follow the netting analysis. This can be explained by the fact that the hoop layers tend to craze along the plane of the filaments, reducing the longitudinal stiffness theoretically expected by the hoop wrap. In essence, the polar wrap reacts all of the longitudinal loading, and if this assumption is made, equation (2) can be modified as follows.

$$\epsilon_\varphi = \frac{1}{t\varphi}\left[\frac{N\varphi}{E\varphi\varphi} - \mu\varphi_{21}\frac{N\theta}{E\varphi\theta}\left(\frac{E\varphi\theta\, t\varphi}{E\theta(t\varphi + t\theta}\right)\right] = 22.7p \times 10^{-6} \text{ in./in.} \quad (11)$$

The result is a strain relationship identical to that of the netting analysis and the actual recorded values.

In the hoop direction, the polar wrap provides the hoop stiffness as theoretically predicted due to the shear connection at the filament crossover points. For this reason, the hoop strains will tend to follow equation (1).

A condition that will tend to exaggerate this trend is the tendency of the polar wrap angle to close as a result of the case pressurization and elongation. This effect will increase the indicated longitudinal strains while restricting the hoop strains.

The relationship between the actual and theoretical strain values indicates that even though the basis for the design and strength criteria lies in the netting type analysis, which can be used adequately within the proper framework of experience; the orthotropic composite, or mixture analysis, is more ideally applicable to current designs. This is particularly true if crazing effects can be predicted and factored into the analysis.

B. FAILURE ANALYSIS

The 156-7 (TU-393) motor case burst during the hydroburst test at a pressure of 963.5 psig, which closely approximated the 970 psig ultimate design pressure; however, this pressure was slightly less than anticipated. The pressure of 963.5 psig corresponds to a hoop glass stress of 330,000 psi. Based upon a review of Thiokol data for motor cases of the same materials and similar design and manufacturing procedures, the range of glass stresses considered realistic for the TU-393 case was from 335 ksi to 395 ksi; however, these stress levels did not consider possible discrepancies in fabrication or the effect of case heat soak after static firing. The glass stress range and equivalent TU-393 pressure are tabulated below.

	Fiber Strength (ksi)	Equivalent TU-393 Pressure (psig)
Ultimate Design	335	970
Three Sigma Lower	345	999
Mean	370	1,070
Three Sigma Upper	395	1,144

The failure, as observed on high speed motion pictures, initiated as a local hoop failure at the aft datum line (end of the case cylindrical section). The initial band of failure was approximately two inches wide and the hoop failure propagated, visibly, from this band. The initial pressure bladder fracture and dispersion of water apparently occurred at the front of the test bay or at a case reference angle of approximately 270 deg (90 deg counterclockwise from BDC).

Such local band failures with visible propagation due to bridging of additional load across the polar composite are indicative of premature failures. This observation is corroborated by the fact that the hoop strain at the datum plane is 12 percent lower than at midcylinder due to the restraint of the skirt and dome.

A review of possible inadequacies in design, analysis, materials, processing, and testing indicates several possible causes for an apparent premature failure.

1. DESIGN, MATERIALS, PROCESSING, AND TESTING REVIEW

a. Design and Analysis--The configuration and procedures employed were based on experience from previous motors and were consistent with the techniques then current throughout the industry. The exceptions were the large length of aft skirt attachment and the use of 143 fabric in the outer hoop winds to provide a tensile tie between the aft skirt and case. This design and associated requirements are detailed in the case design report.

A quantitative explanation of the failure could result from a more detailed analysis of the stress resulting from the complex loading condition at the skirt to case juncture. However, the completed analysis indicates no critical stress conditions in this area.

The ultimate fiber strength used in the design was the demonstrated three sigma lower limit strength developed from POLARIS case data. Although the TU-393 case was by far the largest that has been tested to destruction, no negative influence of size was expected or considered in the original design. This position is justified in that, (1) the TU-393 vessel falls in the same realm of thin wall theory as all previous experience, and (2) any approach to probability analysis of failure criteria or distribution will indicate that the statistical distribution of failure should narrow with increasing wall thickness. That is, the significance of filament discontinuities or probable flaws is dissipated with increasing size.

b. Materials and Case Fabrication--Both the materials and fabricated case met the requirements of design documentation which were consistent with the design and analysis criteria employed. The materials were the same as those used in previous cases and were subject to qualification testing. The case fabrication procedures were consistent with previous experience and no known discrepancies occurred.

c. Motor Processing--The only known case defect occurred during preparation of the insulation inner surface for propellant bonding. During hand grinding, the case was cut at the aft datum plane over a circumferential length of approximately 3.80 in. and to a depth of approximately 0.025 inch. The estimated reduction in polar efficiency was approximately eight percent. The cut was located at a case reference angle of 250 degrees (110 deg counterclockwise from BDC).

d. Testing--The TU-393.02 case was subjected to a hydroproof test at 790 psig and a static firing at 610 psig prior to burst testing. Appreciable forward dome crazing occurred during the proof test but was not noticeably increased during static firing. A localized bladder discoloration at a case reference angle of 180 deg (above the nozzle) in the static firing attitude indicates a possibility of heat damage.

Available data on cycling of vessels of the same and similar materials, some with the same general crazed condition, indicate no appreciable strength degradation. At the most, a five percent (and probably two percent) strength degradation could be considered as the result of three cycles.

2. POSSIBLE CAUSES OF APPARENT PREMATURE FAILURE

Based upon the above discussions, the possible causes for apparent premature failure are discussed in the order of importance.

a. Case Defect--The cut at the aft datum plane was closely coincident with the apparent circumferential location of initial failure. Possible mechanisms of failure could be strain magnification at the defect or an interlaminar failure from the defect rapidly releasing energy into the adjacent composite. Either mechanism could be quite local and progressive outward. The case would tend to bulge and, thus, increase local hoop strain. The loss of longitudinal extensometers just prior to failure would be consistent with such a failure.

b. Skirt Attachment--An interlaminar or shear failure of the fabric ties between skirt and case could induce additive deformations or stresses in the hoop fibers, or could generate a relatively large longitudinal separation in the hoop winds. The latter would require that the loading over the separation be bridged by the polar composite to the hoops, locally increasing the stress in the hoops adjacent to the separation. This type of failure has been observed in much thinner cases.

c. Heat Soak--If a heat soak sufficient to degrade the resin existed, the ability to transfer load from discontinuous filaments would be impaired and the case strength would be degraded locally.

3. SUMMARY

Thus, Thiokol postulates that the observed apparent premature failure of a localized hoop band was caused by the case defect and/or a skirt attachment failure. The amount by which this failure was premature has not been determined; however, the results of this one test are not considered sufficient to discredit past, current, or future trends in design analyses or strength criteria.

The potential problem at the skirt attachment has been minimized in current designs by shortening the skirt attachment length. Additional conservatism could be incorporated into the design of future skirt to case tensile ties with negligible increase in component weight.

SECTION VI

CONCLUSIONS

The following conclusions are based on the results of the 156-7 case hydroburst test.

1. The 156-7 (TU-393) motor case burst closely approximated minimum design requirements thus verifying the case design and analytical techniques as applied to large fiberglass cases.
2. The measured strains and deformations were normal and consistent with analytical prediction.
3. The failure apparently was premature, and probably was associated with the case defect induced during insulation grinding.
4. The results of this test are not sufficient to warrant changes in design or strength criteria.
5. Future skirt attachments should employ short attachment lengths and additional conservatism in the tensile hoop tie design.
6. The forward skirt end delamination was a result of the short free length and restraints of the hydro-test fixture. Skirt length requirements can be readily optimized for a particular missile application.
7. Pressurization of the case through two proof cycles and one burst cycle did not cause the case to burst below design ultimate strength.

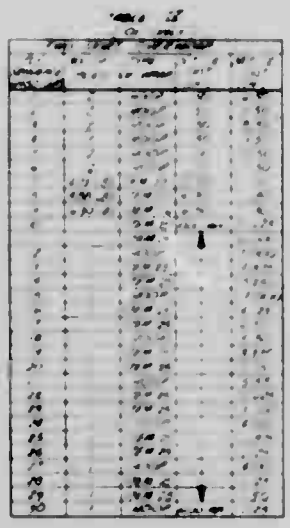

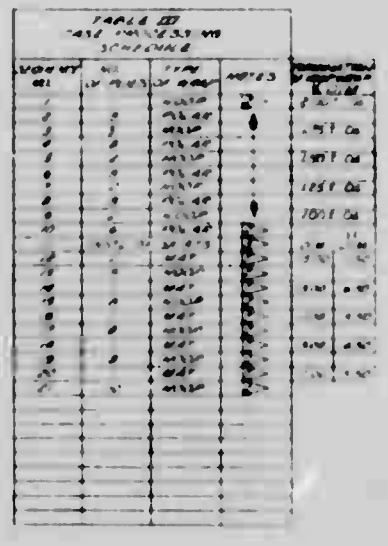

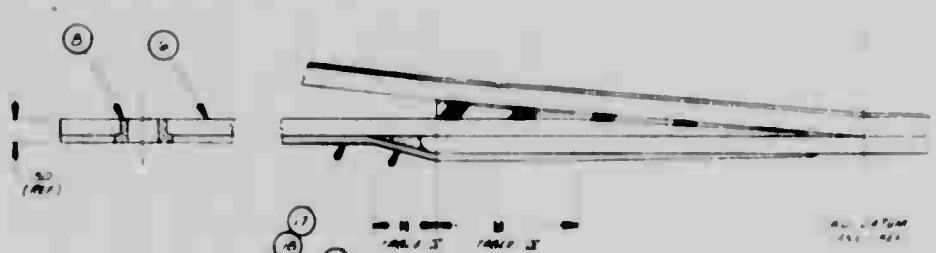

DETAIL L

DETAIL D

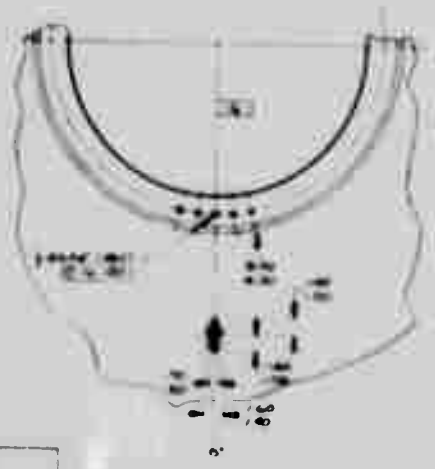

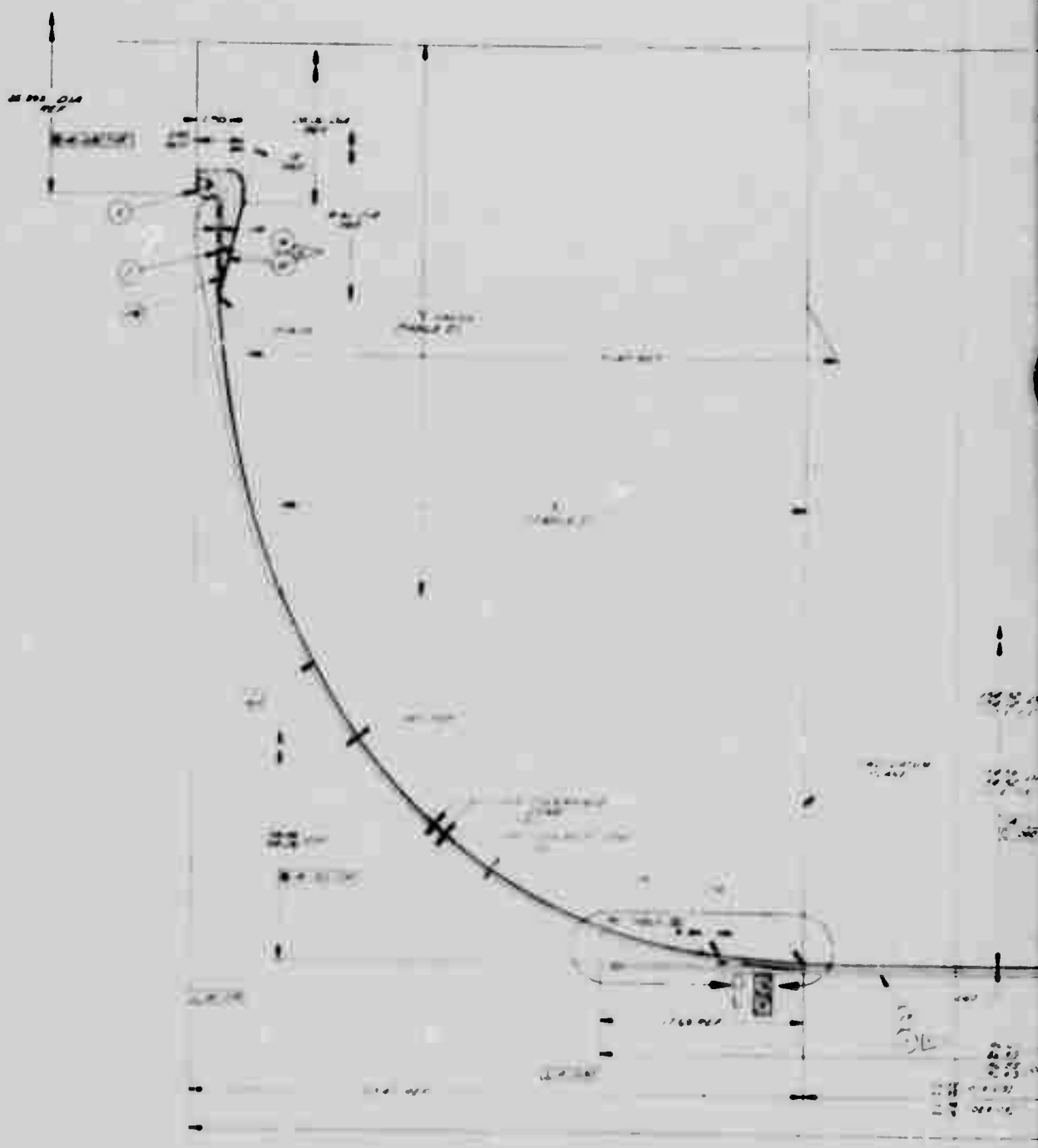

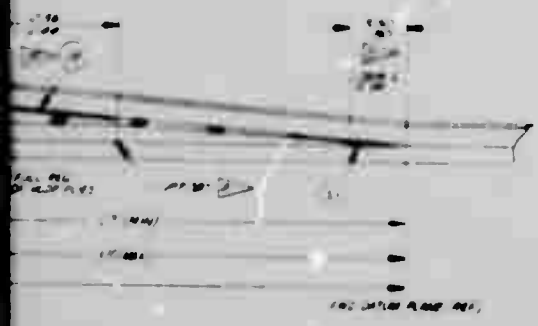

DETAIL D
SCALE 1

7U37721

2

-OX SHOWN
-OP SAME AS -OX EXCEPT AS NOTED

1037721

NOTES CONT

[illegible] DELETED

[illegible] THE .004 ON DETAILS A[illegible]
ON 03 PARTS RESPECT[illegible]
MENSIONS INDICATED[illegible]

[illegible] AN ASSEMBLY TO BE PROO[illegible]
.750 DIA

[illegible] THE [illegible] GLASS [illegible] WITH [illegible]
WHILE THE [illegible] WAS HORIZONT[illegible]
.[illegible]W @ [illegible] .[illegible] PSI MINIMUM

[illegible] THE [illegible] GLASS [illegible] MAY BE [illegible]
.750 IN. X .[illegible] PSI MINIMUM

[illegible] [illegible] ([illegible] [illegible] [illegible] [illegible] [illegible]
AT [illegible] TO [illegible]

[illegible] THIN INSULATION MEMBER [illegible]
MEMBER INSULATION TYP [illegible]

[illegible] THE .02 ASSEMBLY SHALL
PROOF TESTED AT A PR[illegible]
THE .04 ASSEMBLY SHA[illegible]
PROOF TESTED AT A PR[illegible]
PRESSURIZATION RATE S[illegible]
SECOND THE PROOF PR[illegible]
FOR 20 - 25 SECONDS
ZERO AT A MAXIMUM R[illegible]
SECOND

[illegible] PRESSURE ASSERTED [illegible]
THE CALENDERED SH[illegible]

[illegible]	[illegible]
[illegible]	[illegible]
[illegible]	[illegible]
[illegible]	[illegible]
[illegible]	[illegible]
[illegible]	[illegible]
[illegible]	[illegible]
[illegible]	[illegible]
[illegible]	[illegible]
[illegible]	[illegible]
[illegible]	[illegible]
[illegible]	[illegible]
[illegible]	[illegible]
[illegible]	[illegible]
[illegible]	[illegible]
[illegible]	[illegible]

CONCAVE SECTION

[illegible]

DETAIL E

[illegible] F-F

7U377

4

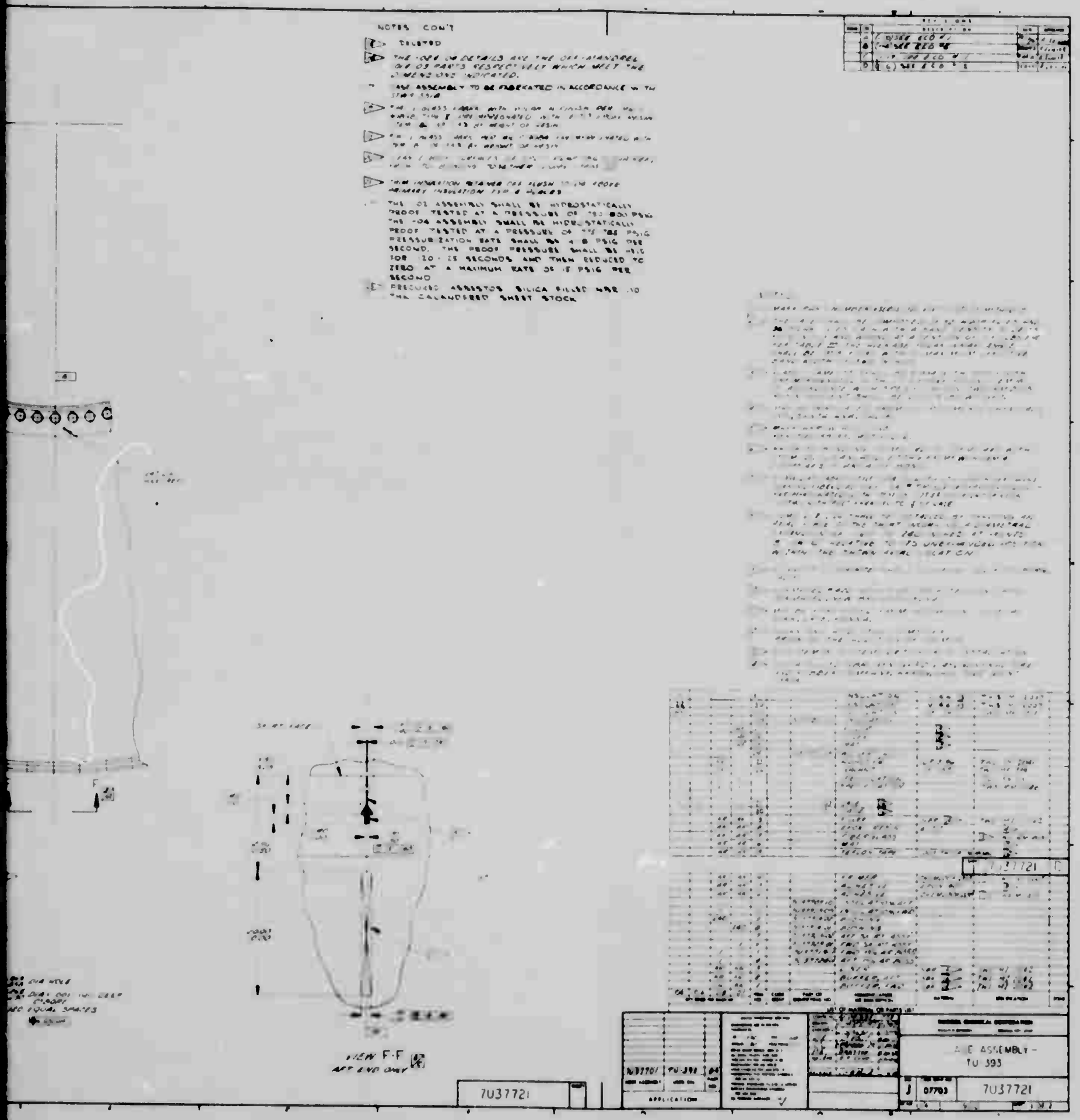

Figure 1. TU 393 Case Assembly (Sheet 1 of 2)

5

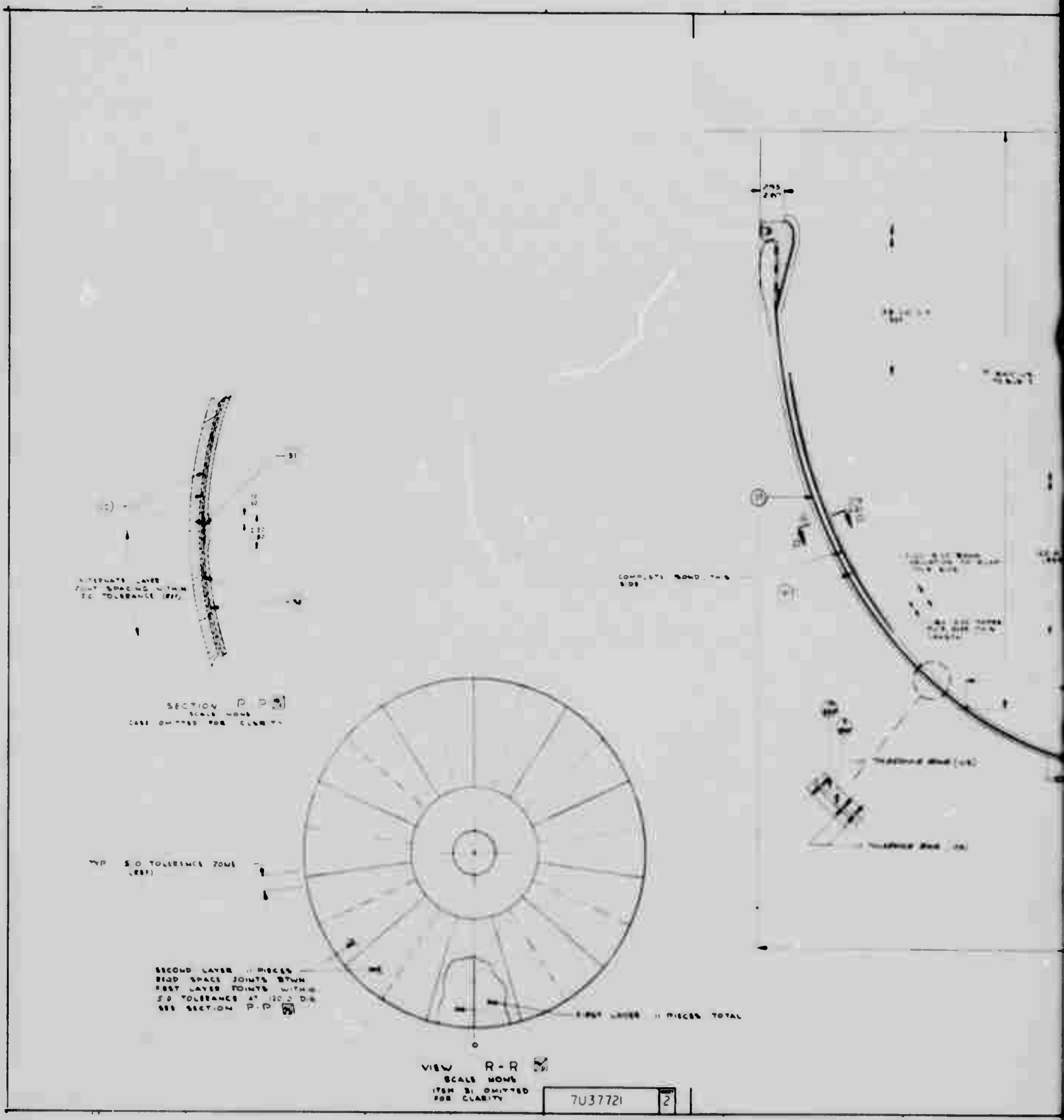
SECTION P-P
SCALE NONE
VIEW R-R
SCALE NONE
7U37721
2

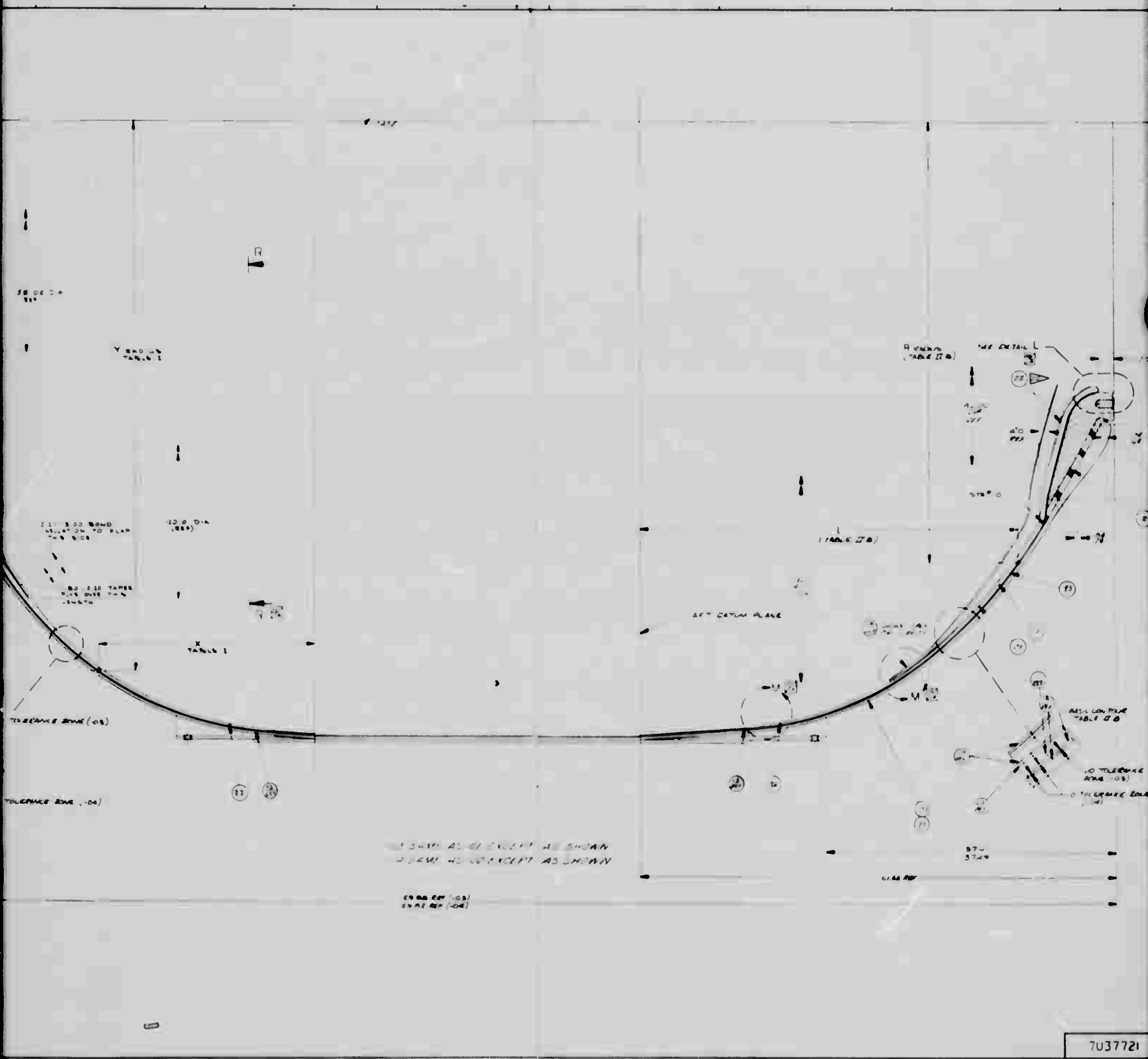
SEE DETAIL L
AFT DATUM PLANE
TOLERANCE ZONE (-03)
TOLERANCE ZONE (-04)

7U37721

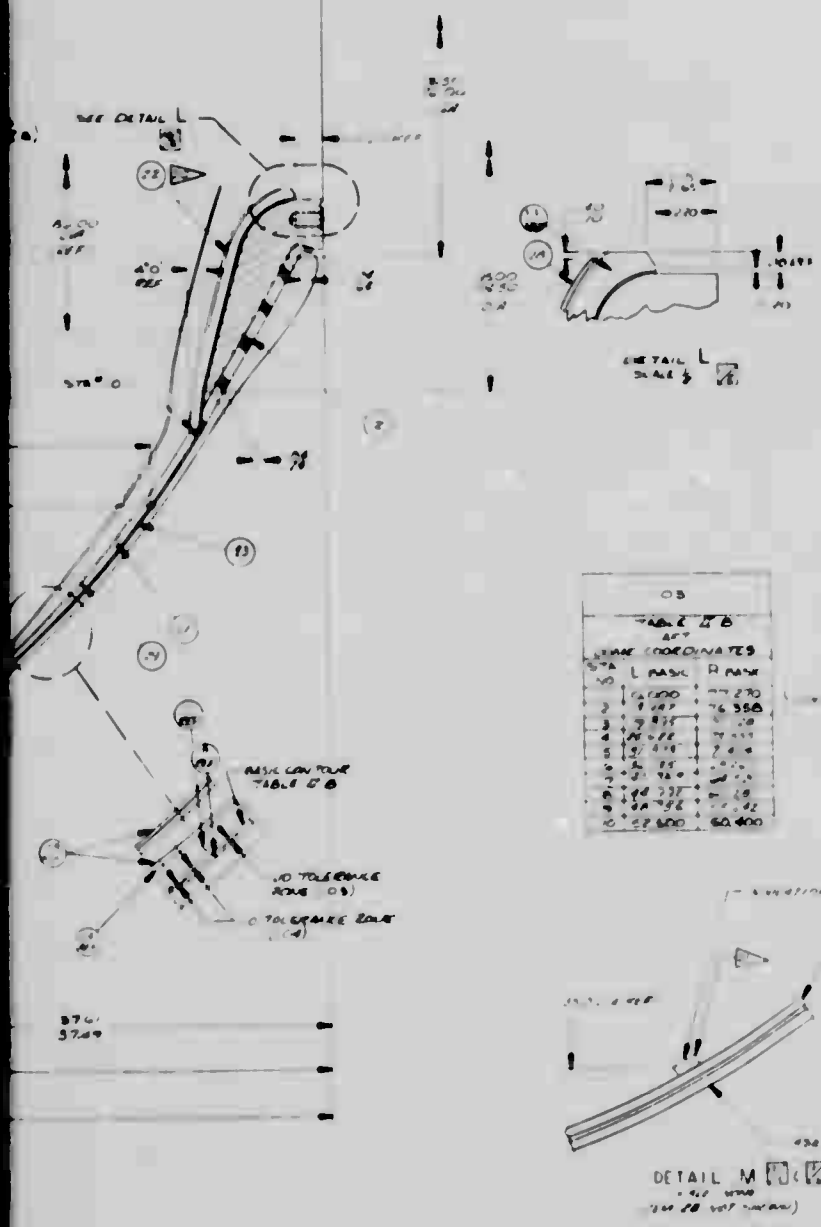

Figure 1. TU-393 Case Assem

Figure 1. TU-393 Case Assembly (Sheet 2 of 2)

3

4

PREVIOUS PAGE WAS BLANK, THEREFORE WAS NOT FILMED.

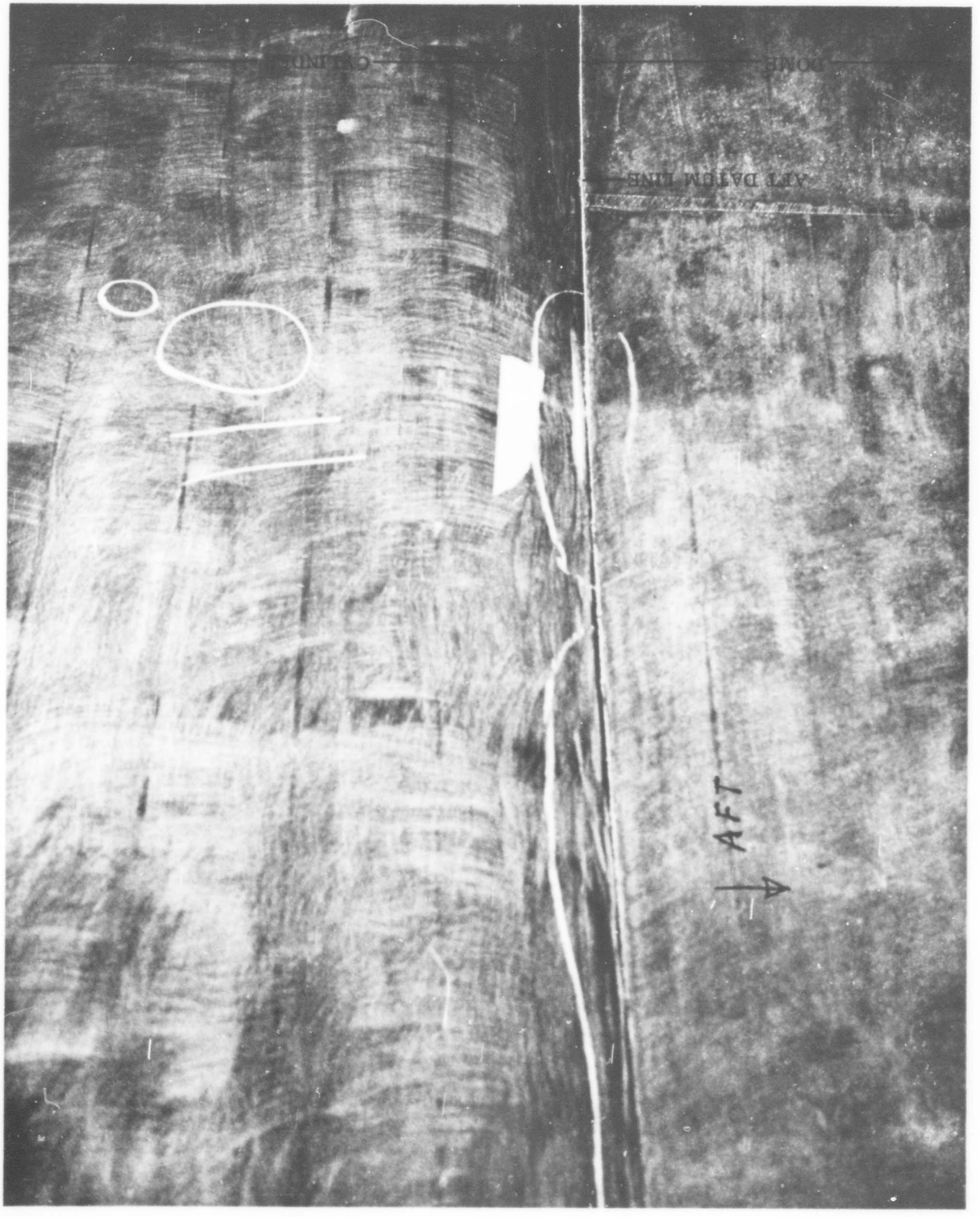

Figure 2. Defect Located at Aft Datum Plane

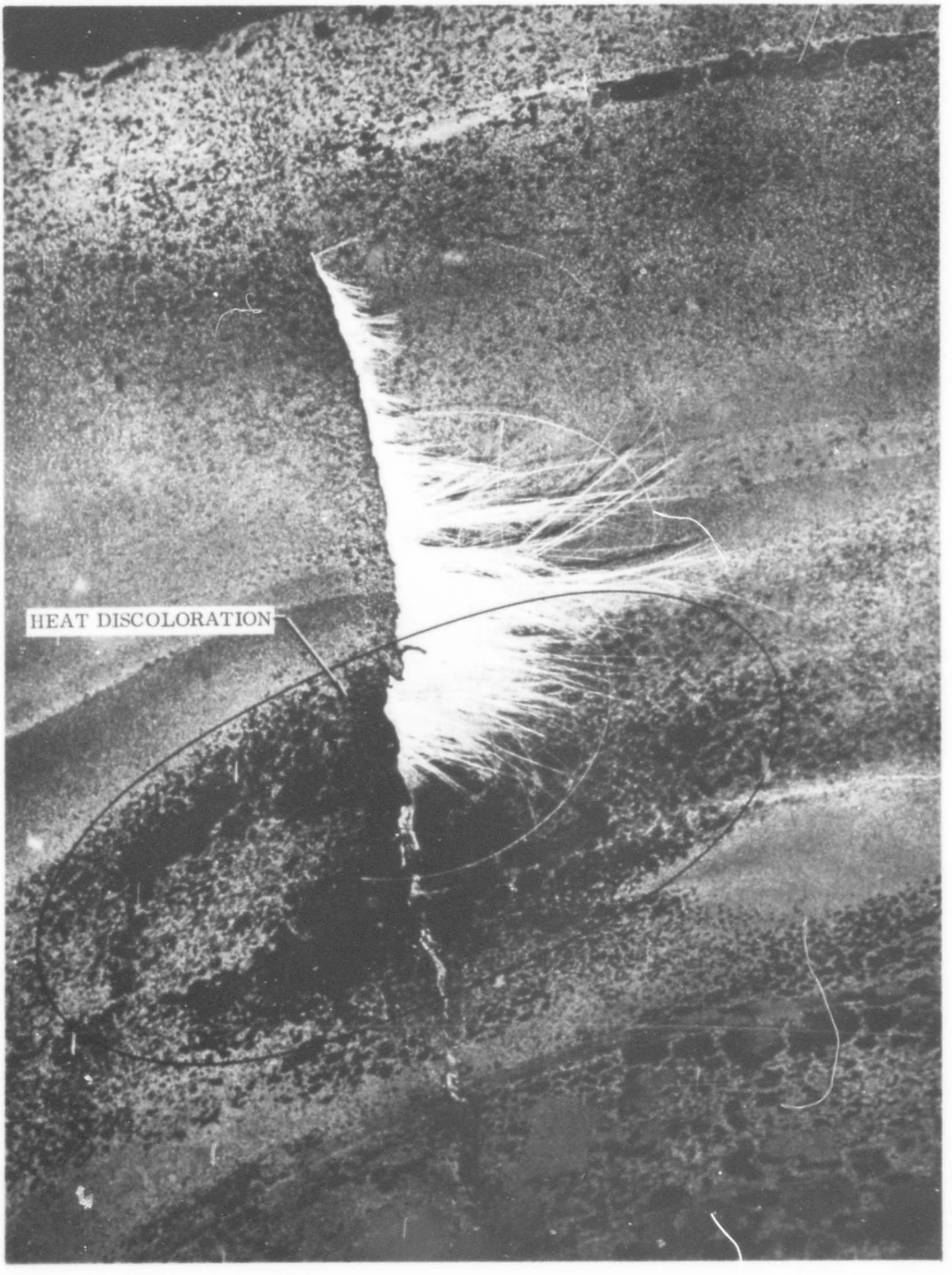

Figure 3. Area of Heat Discoloration

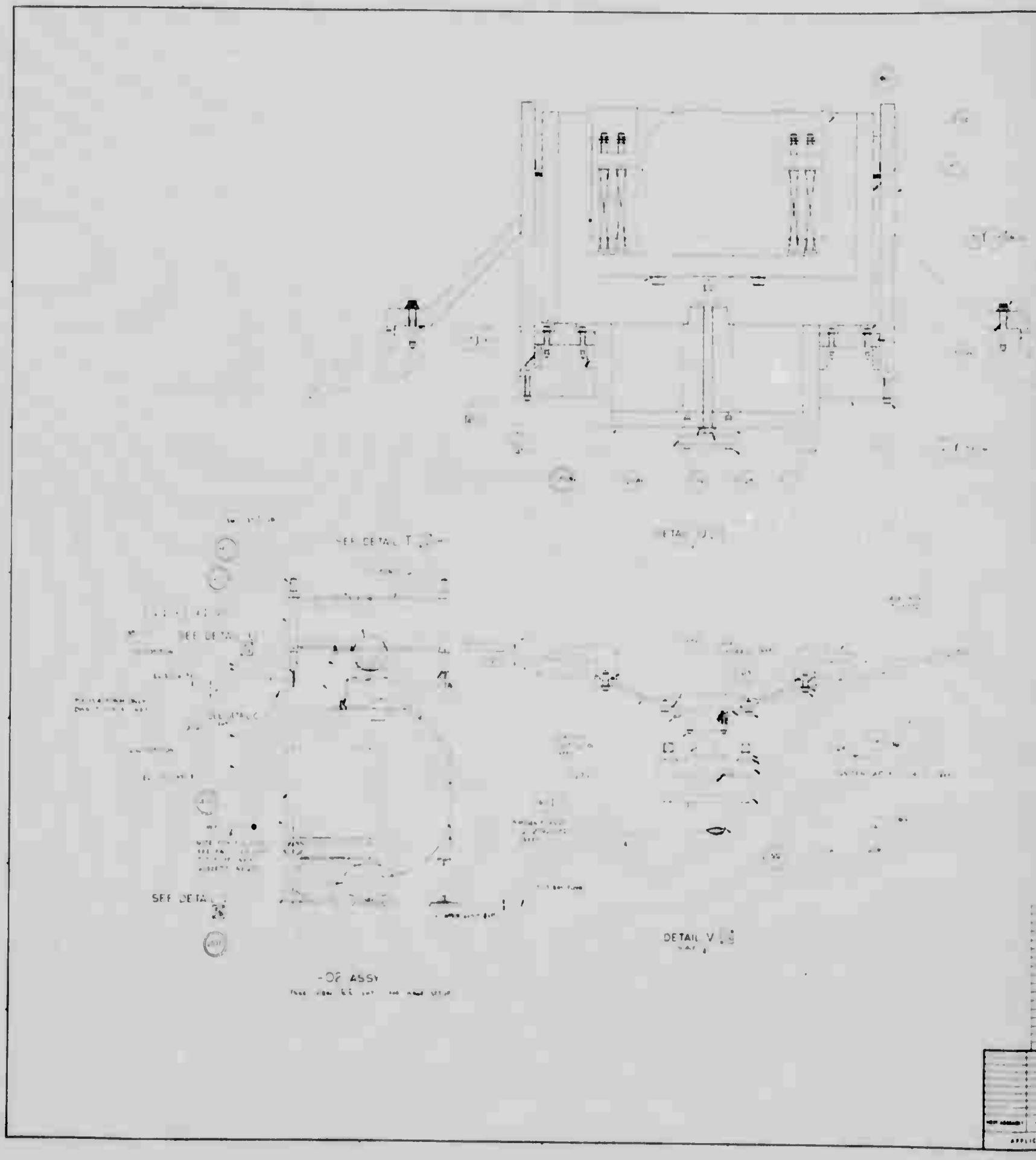
SEE DETAIL T
SEE DETAIL C
SEE DETA
DETAIL V

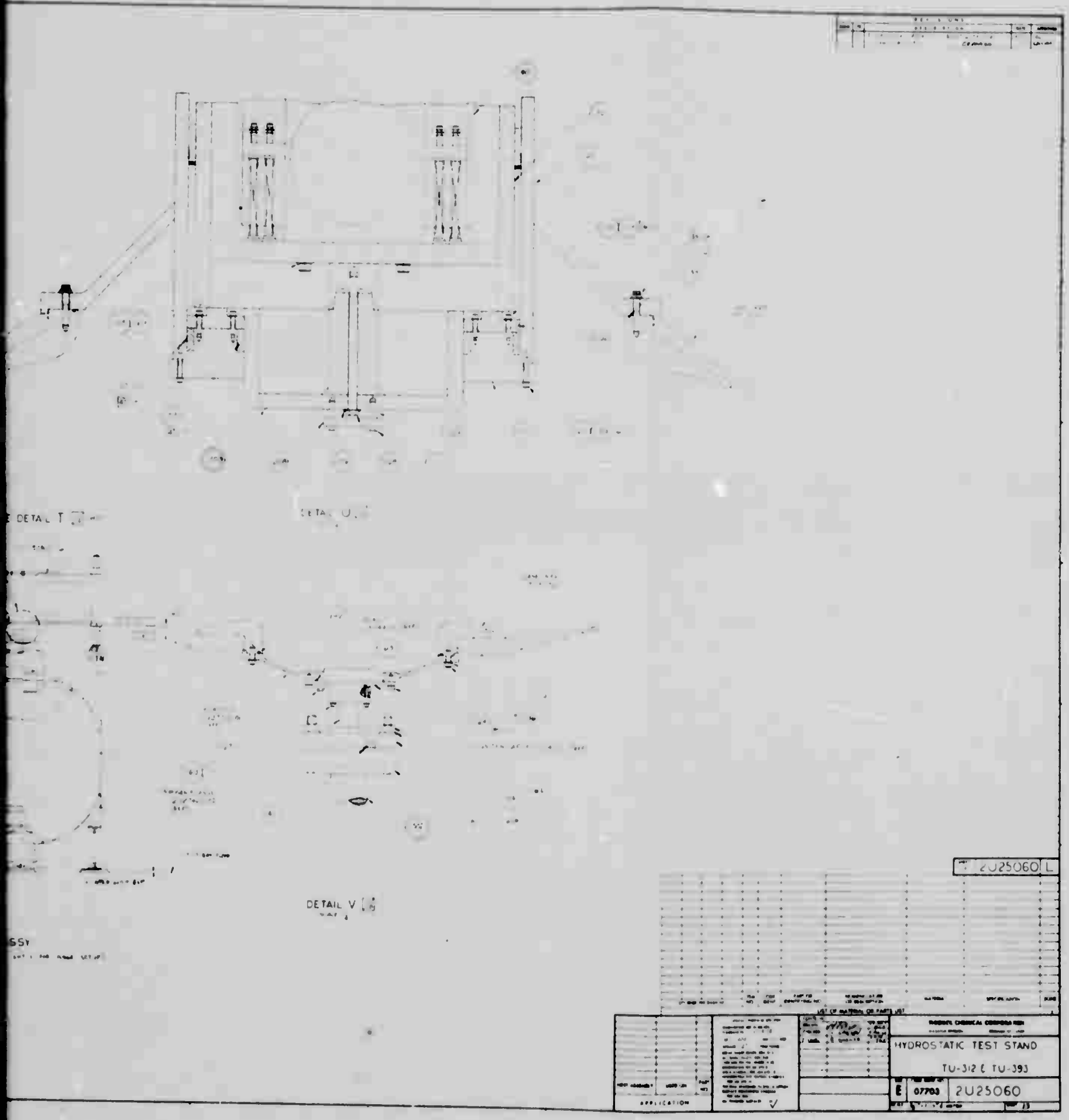

Figure 4. Hydrostatic Test Stand

2

Figure 5. Hydrotest Assembly

PREVIOUS PAGE WAS BLANK, THEREFORE WAS NOT FILMED.

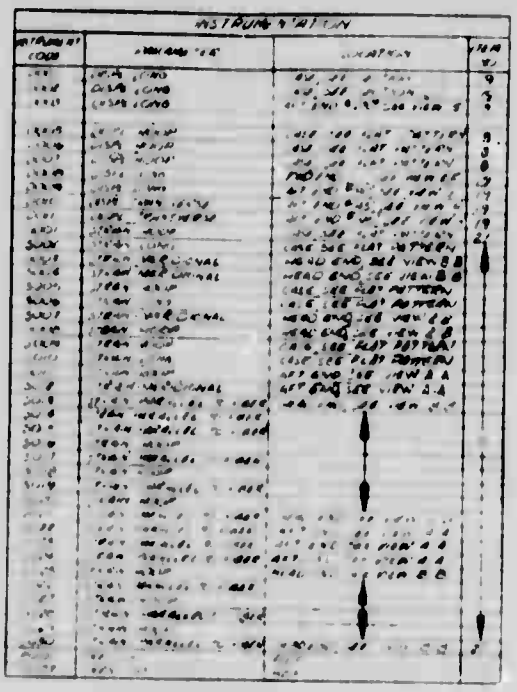

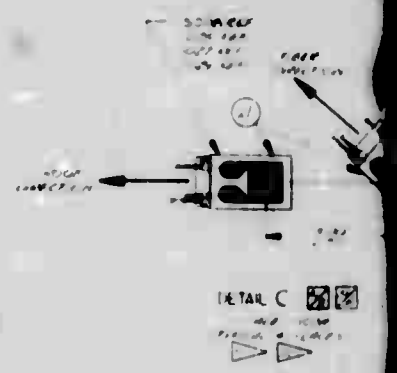

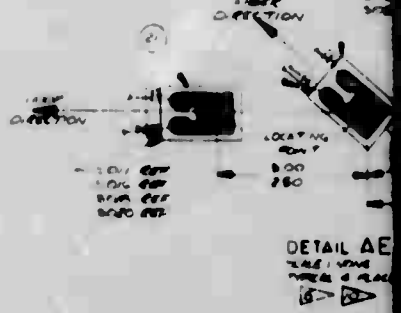

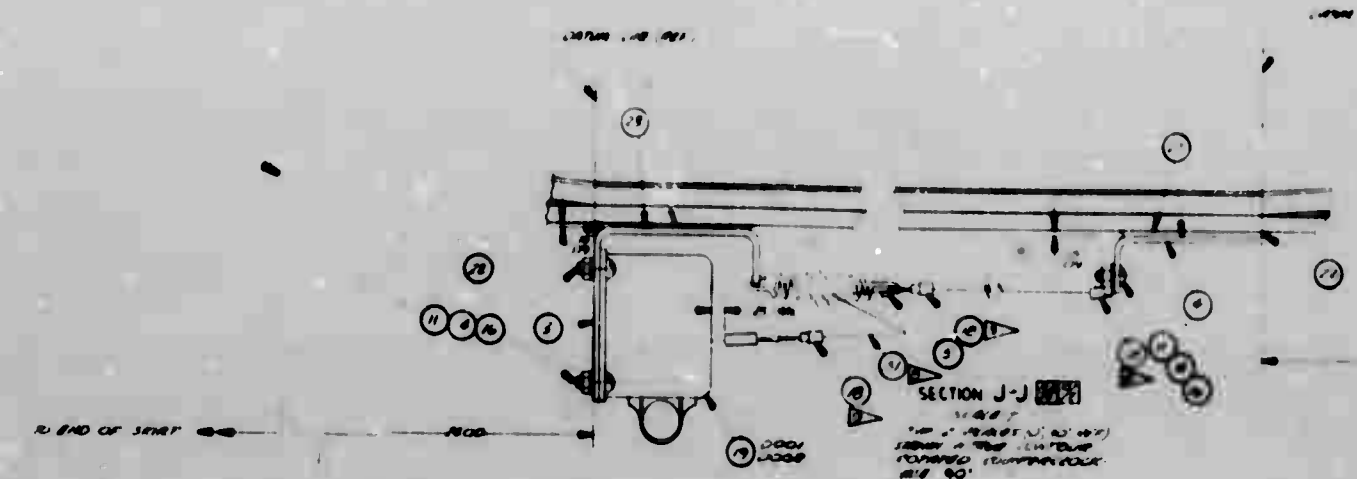

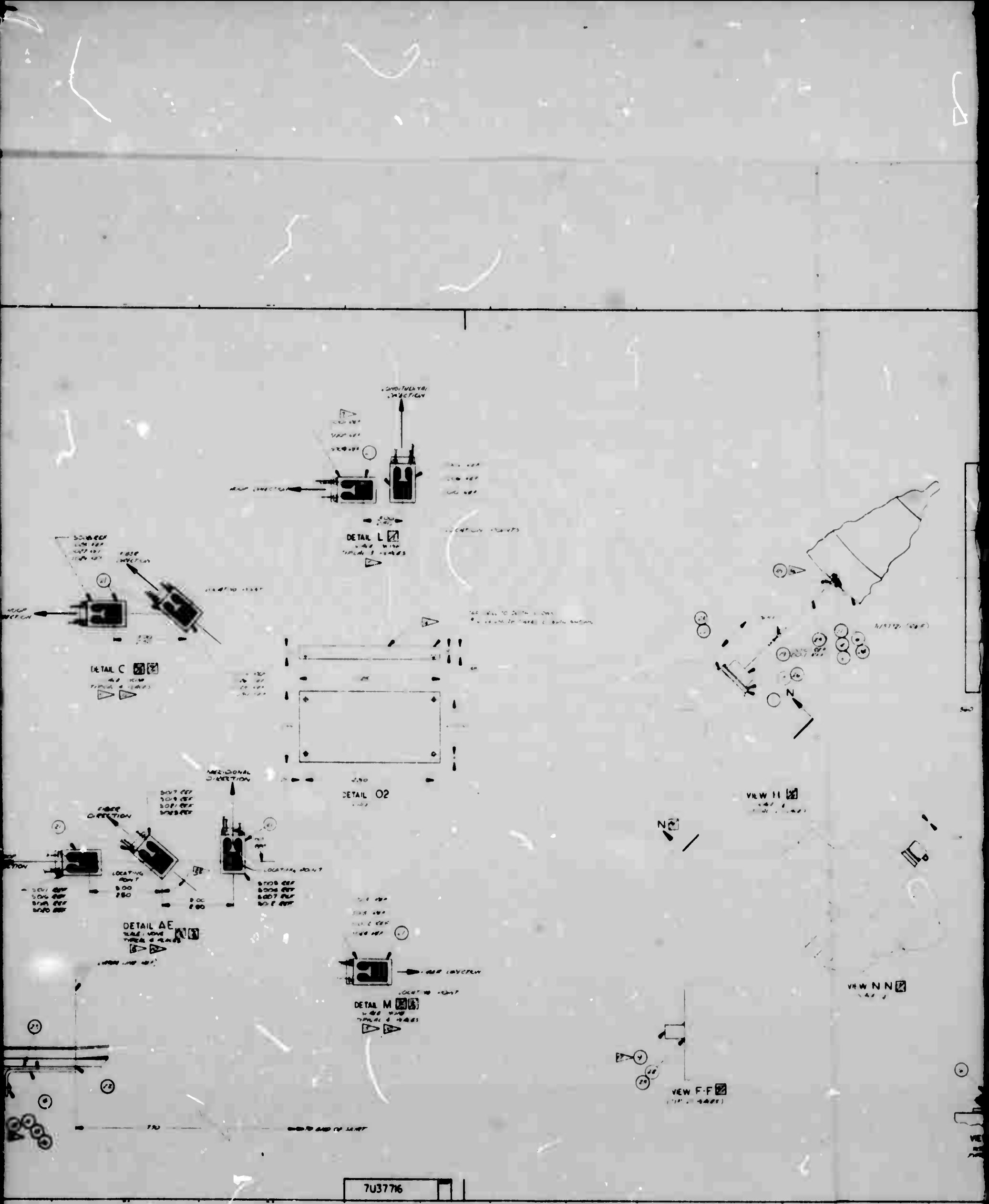
DETAIL L
DETAIL C
DETAIL 02
DETAIL AE
DETAIL M
VIEW 11
VIEW N N
VIEW F-F
N
7U37716

2

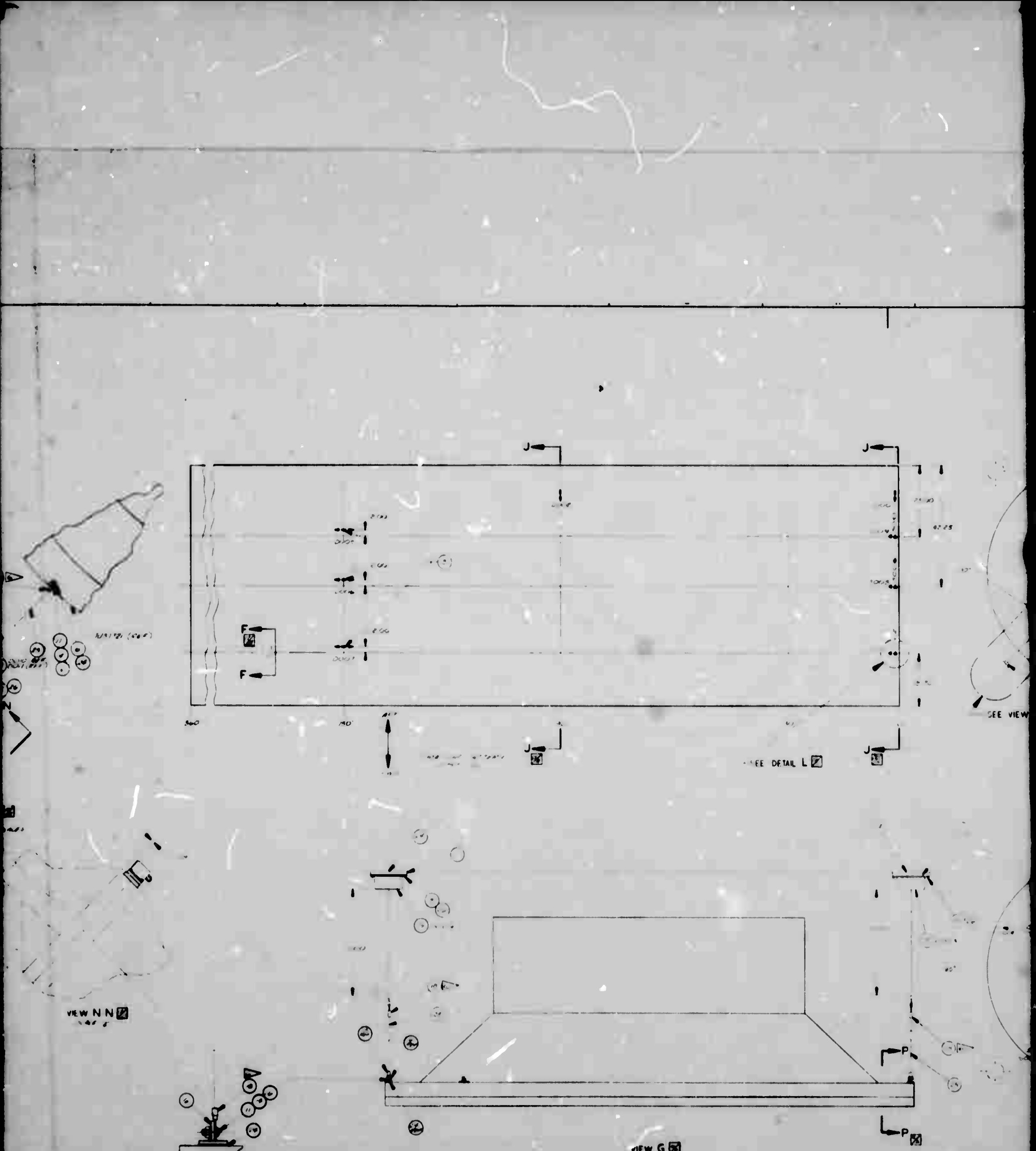

7U37716

3

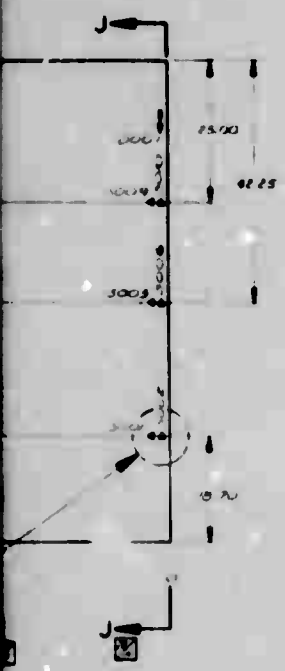

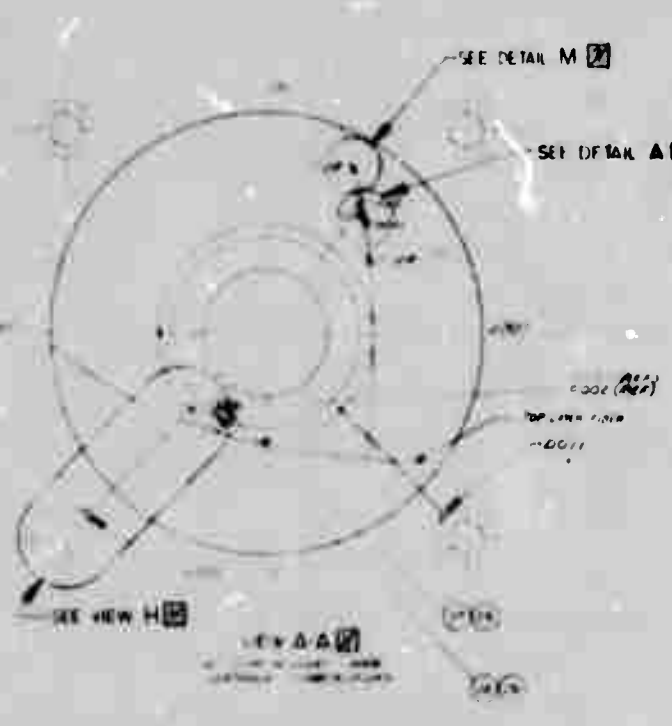

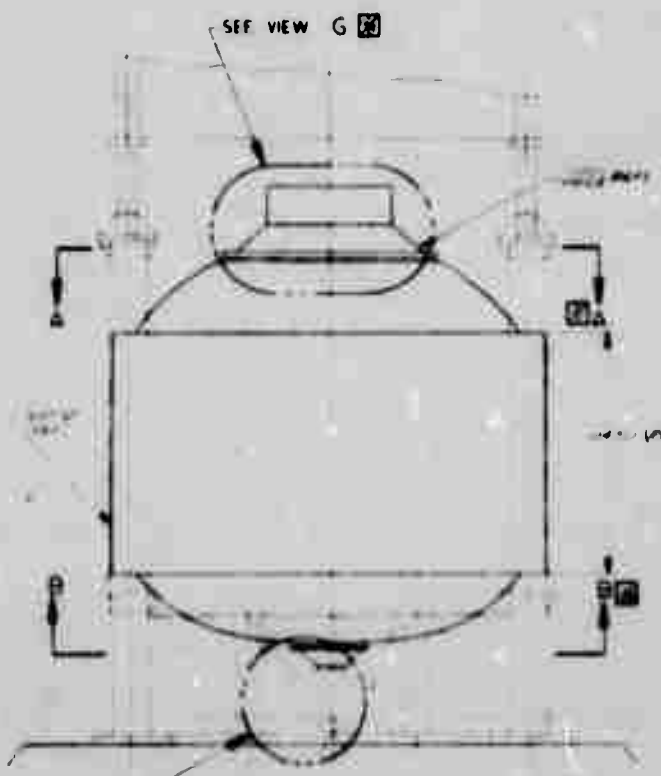

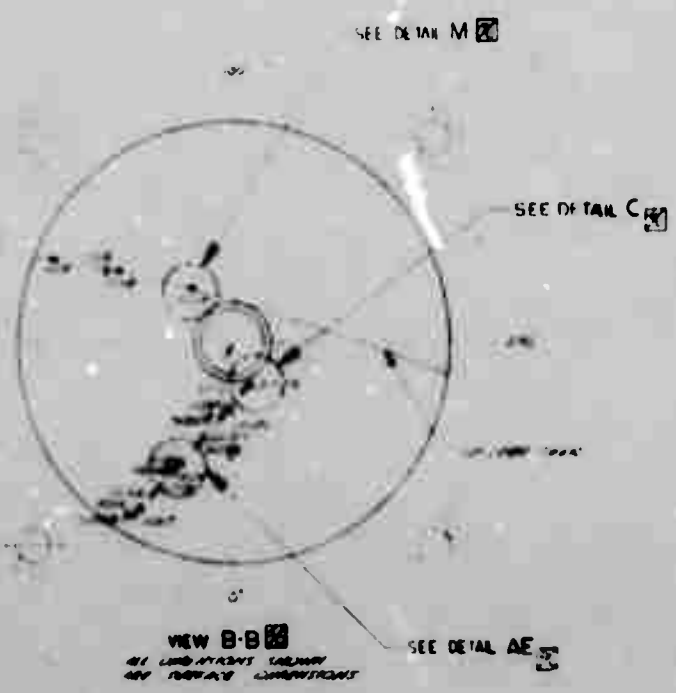

VIEW B-B

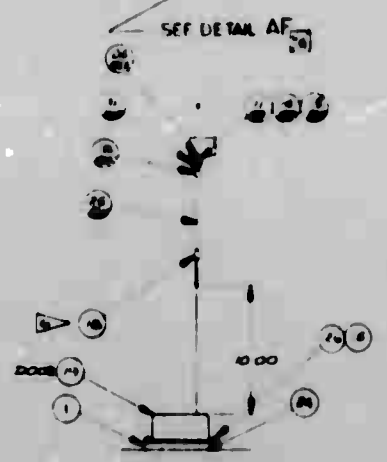

VIEW AF

RADIAL LOCATION OPTIONAL

4

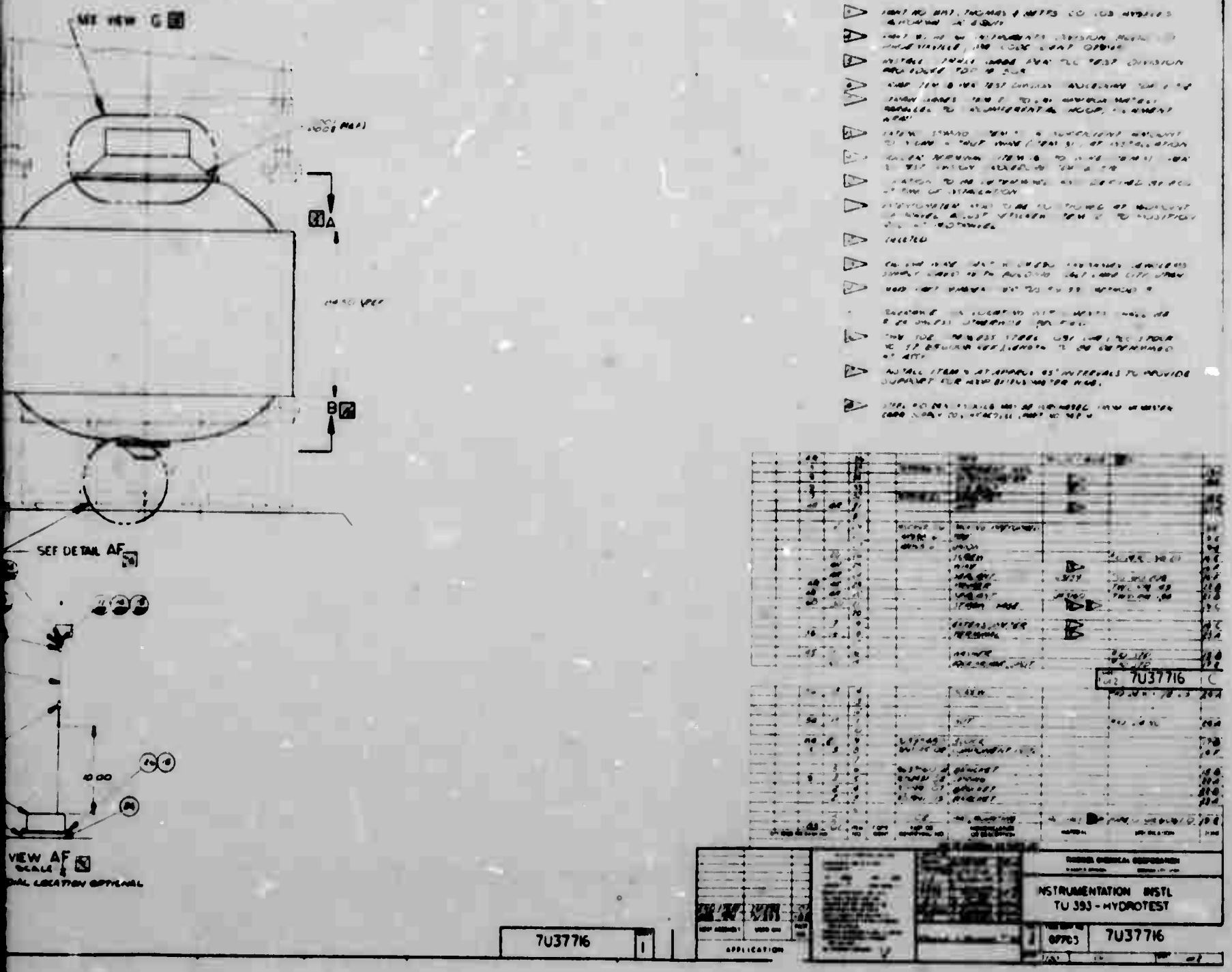

Figure 6. Case Instrumentation

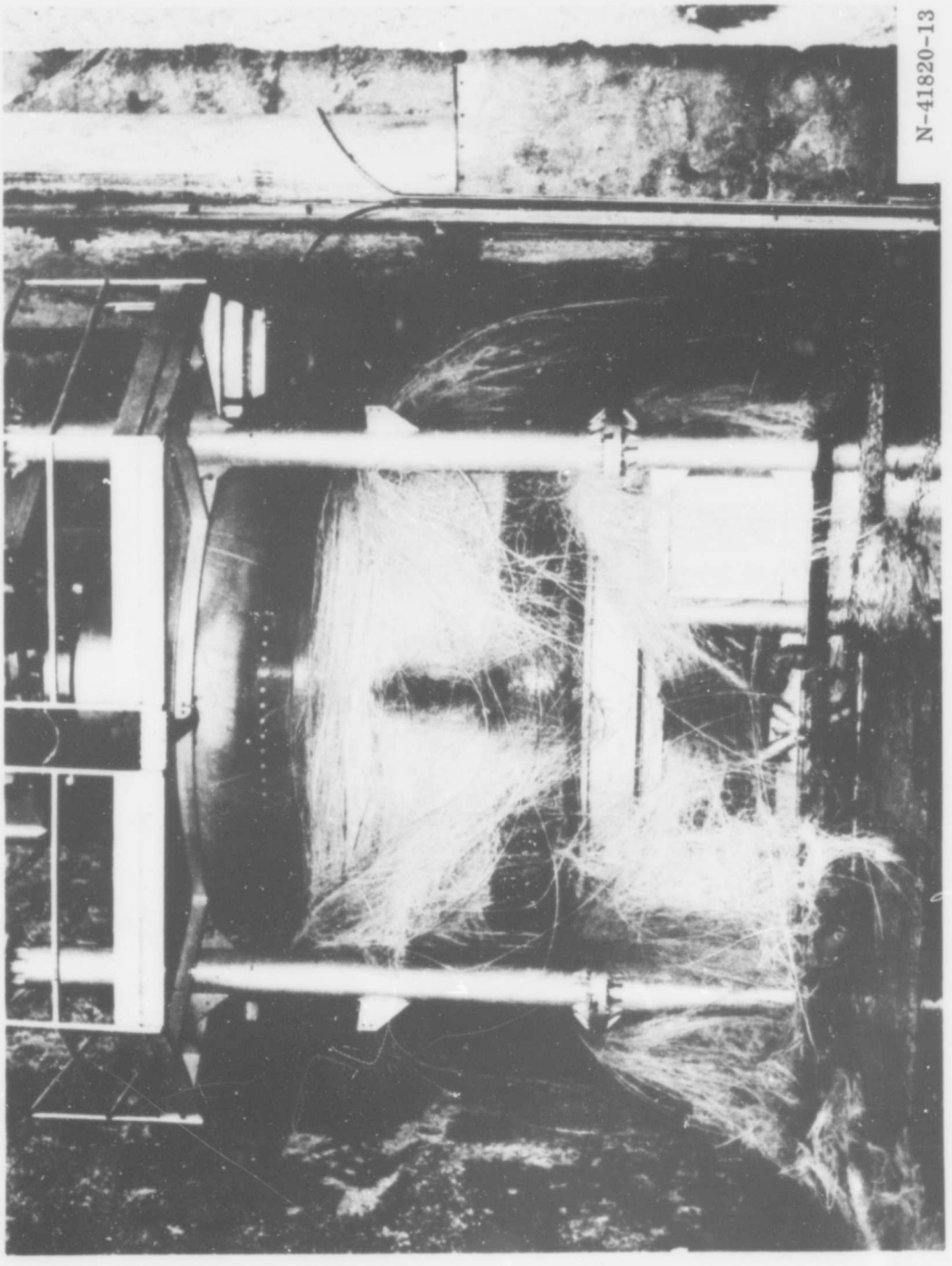

Figure 7. Case Failure

PREVIOUS PAGE WAS BLANK, THEREFORE WAS NOT FILMED.

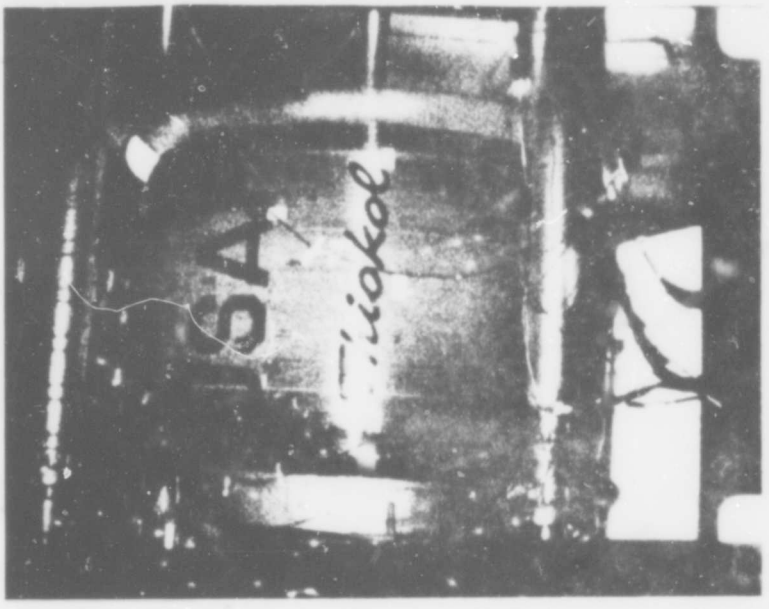

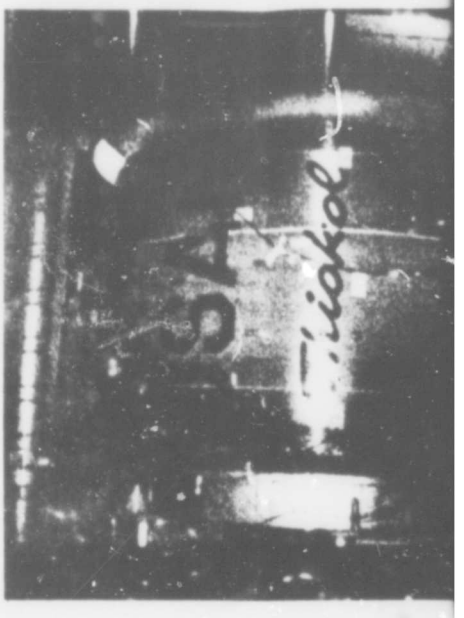

0.0 Sec

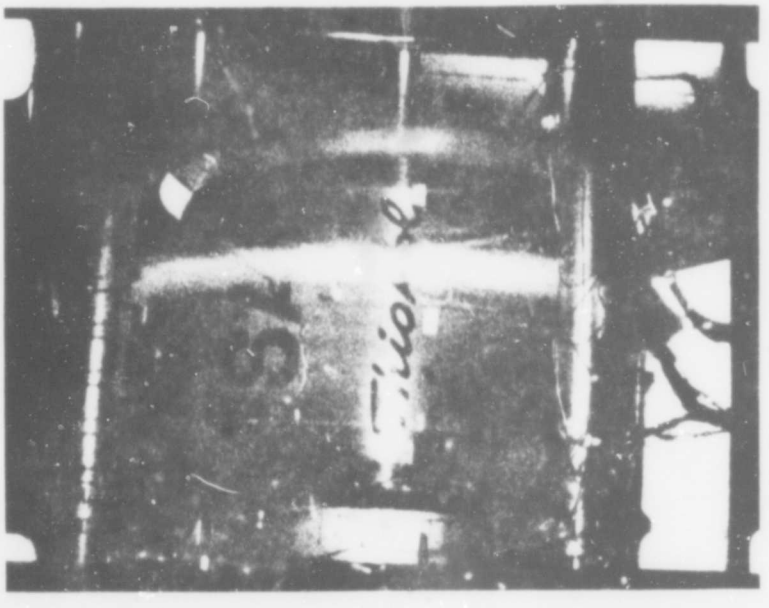

0.0075 Sec

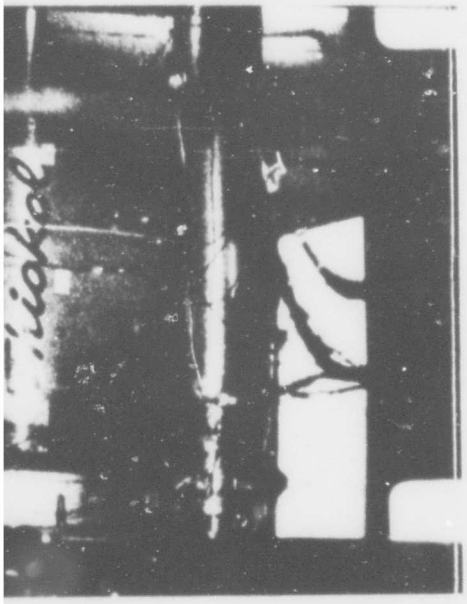

0.0025 Sec

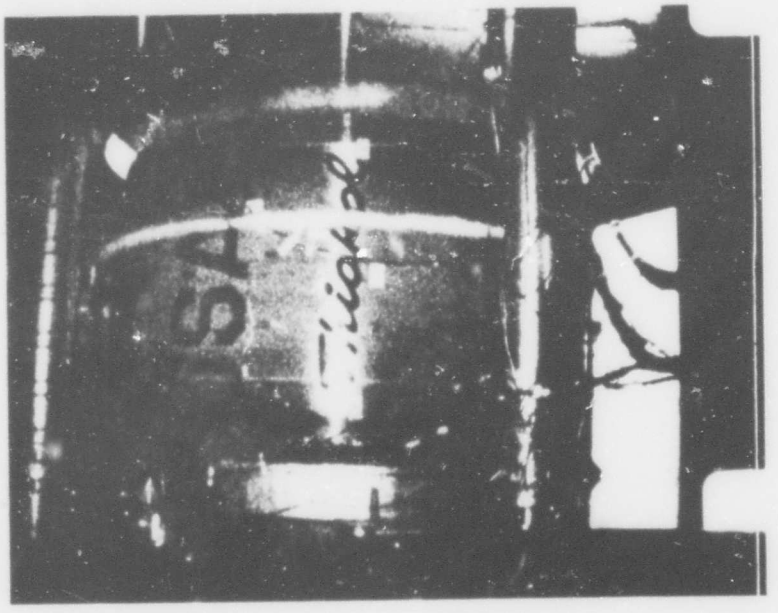

0.005 Sec

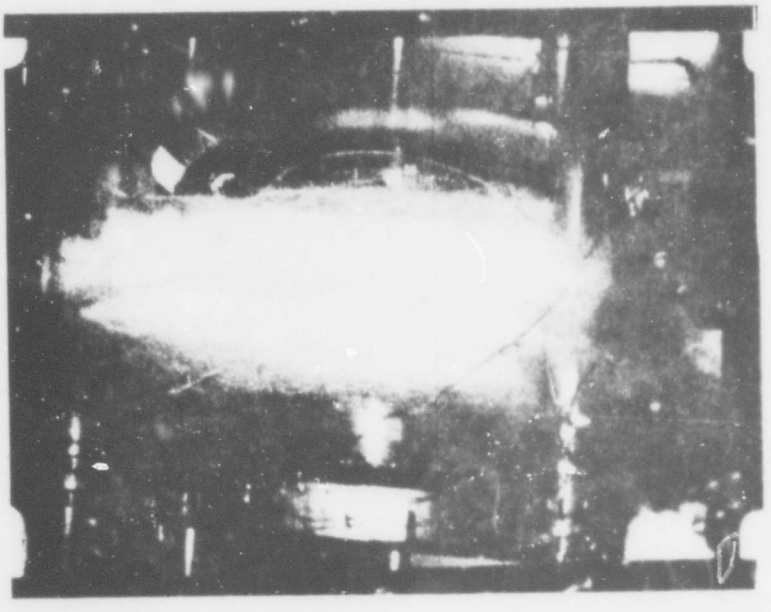

0.010 Sec

Figure 8. Case Failure Sequence

PREVIOUS PAGE WAS BLANK, THEREFORE WAS NOT FILMED.

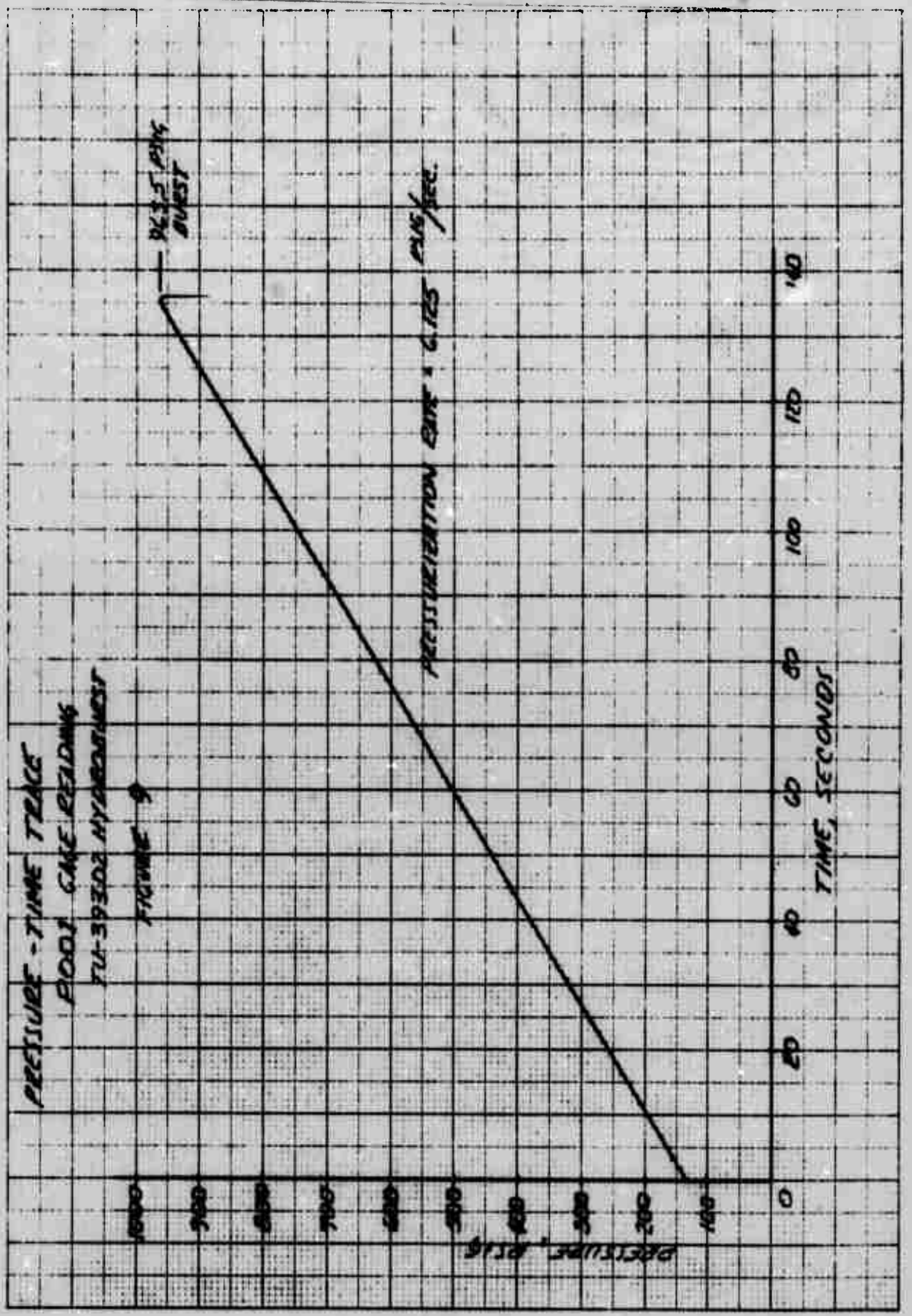

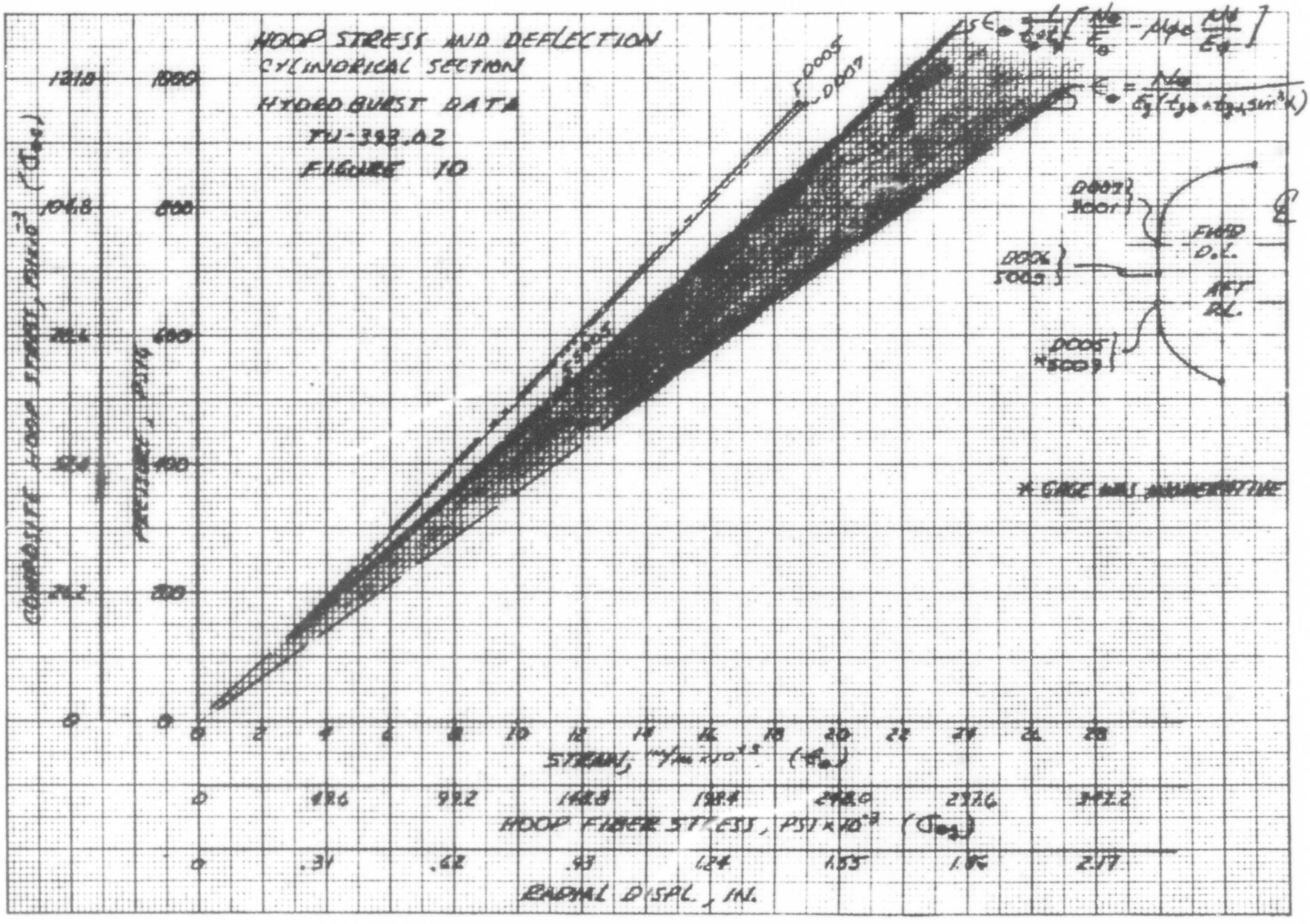
HOOP STRESS AND DEFLECTION
CYLINDRICAL SECTION
HYDRO BURST DATA
TU-392.02
FIGURE 10
FIXED D.L.
AFT D.L.
* GAGE MALFUNCTIONED
STRAIN, IN/IN x 10^-3
HOOP FIBER STRESS, PSI x 10^-3
RADIAL DISPL., IN.

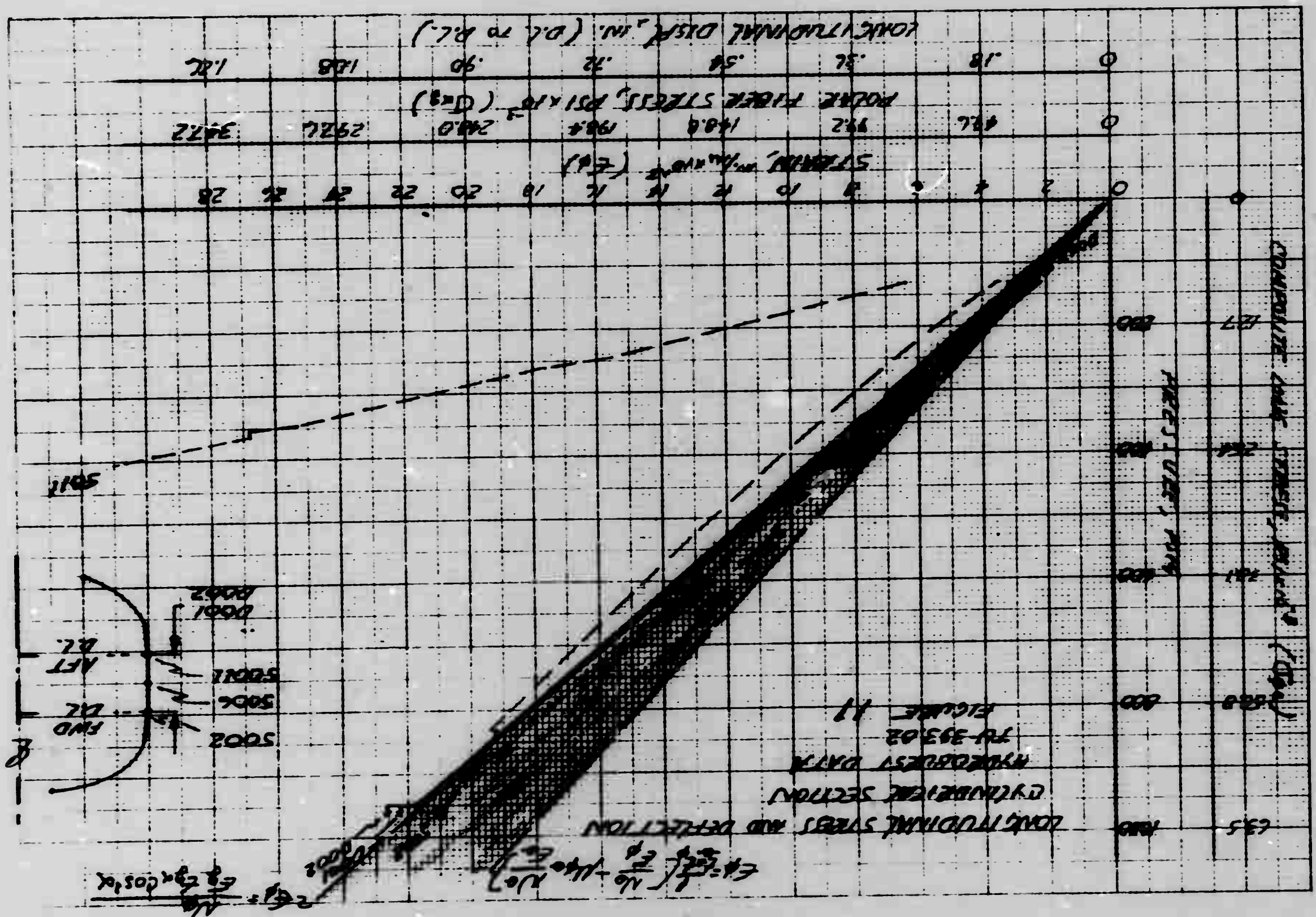
LONGITUDINAL STRESS AND DEFLECTION
CYLINDRICAL SECTION
HYDRODYNAMIC DATA
TM-3932
ELEMENT 11
COMPRESSIVE STRESS, PSI
PRESSURE, PSI
LONGITUDINAL DISPLACEMENT, IN. (D.A. TO P.C.)
STRESS, PSI x 10⁻³ (σ_z)
PRESSURE STRESS, PSI x 10⁻³ (σ_θ)
LONGITUDINAL DISPLACEMENT, IN. (D.A. TO P.C.)

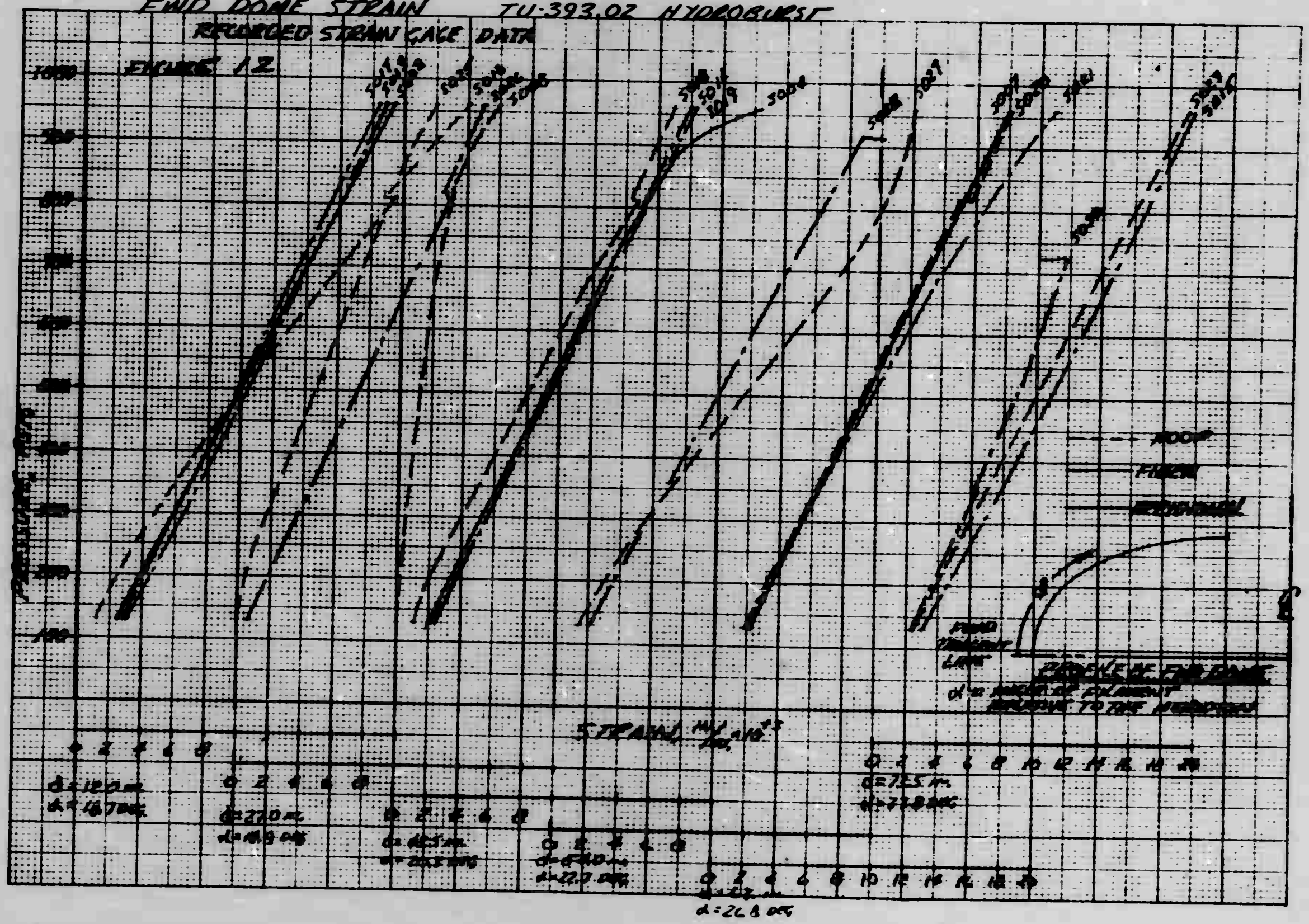
EWD DOME STRAIN TU-393.02 HYDROBURST
RECORDED STRAIN GAGE DATA
FIGURE 12

PREDICTED STRAINS* AT VARIOUS LOCATIONS ON THE FOUNDED DOME FIGURE 13

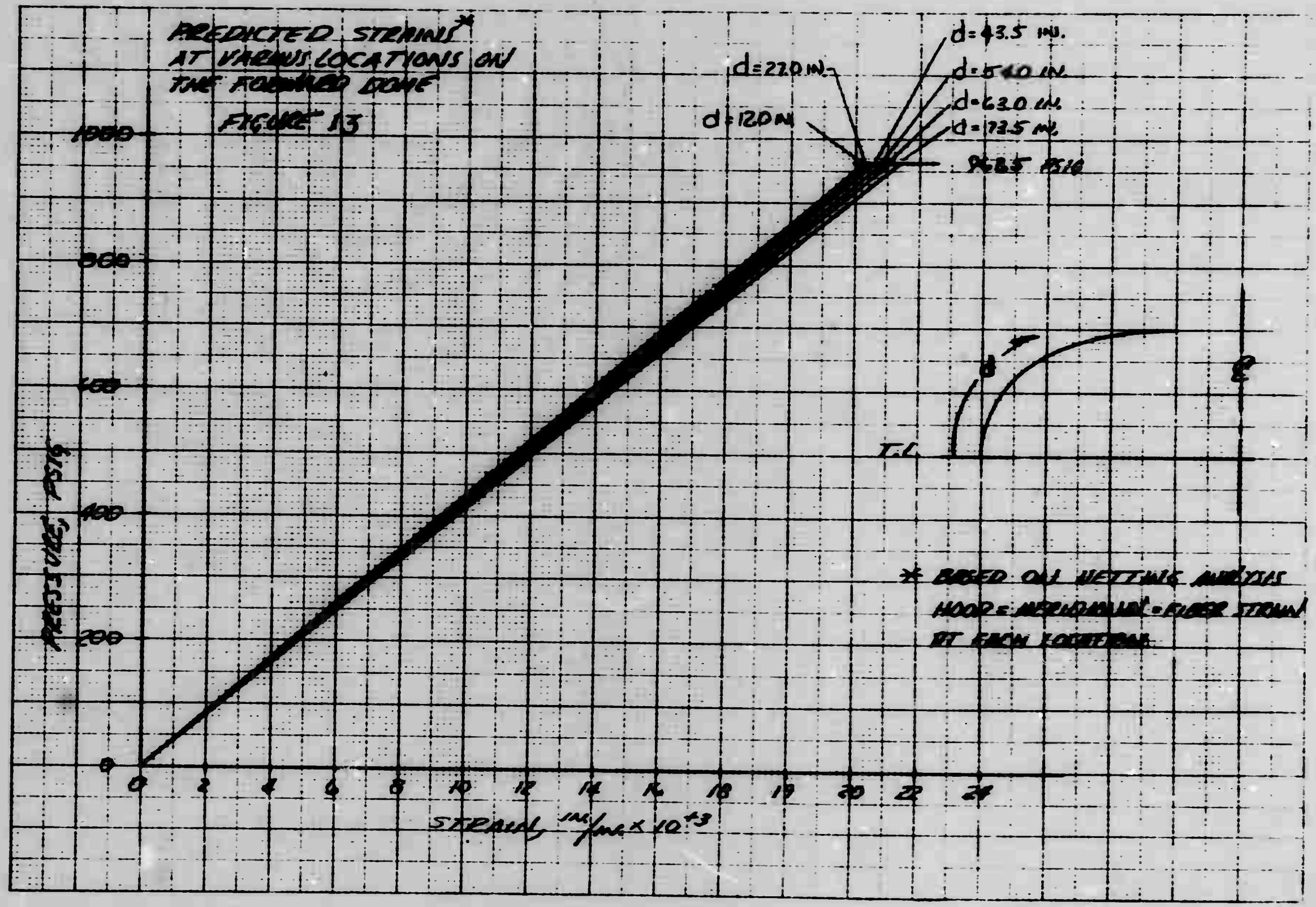

* BASED ON METTING MEMBRANE HOOP = MERIDIONAL = FIBER STRAIN AT EACH LOCATION

AFT DOME STRAIN TV-393.02 HYDROBURST

RECORDED STRAIN GAGE DATA

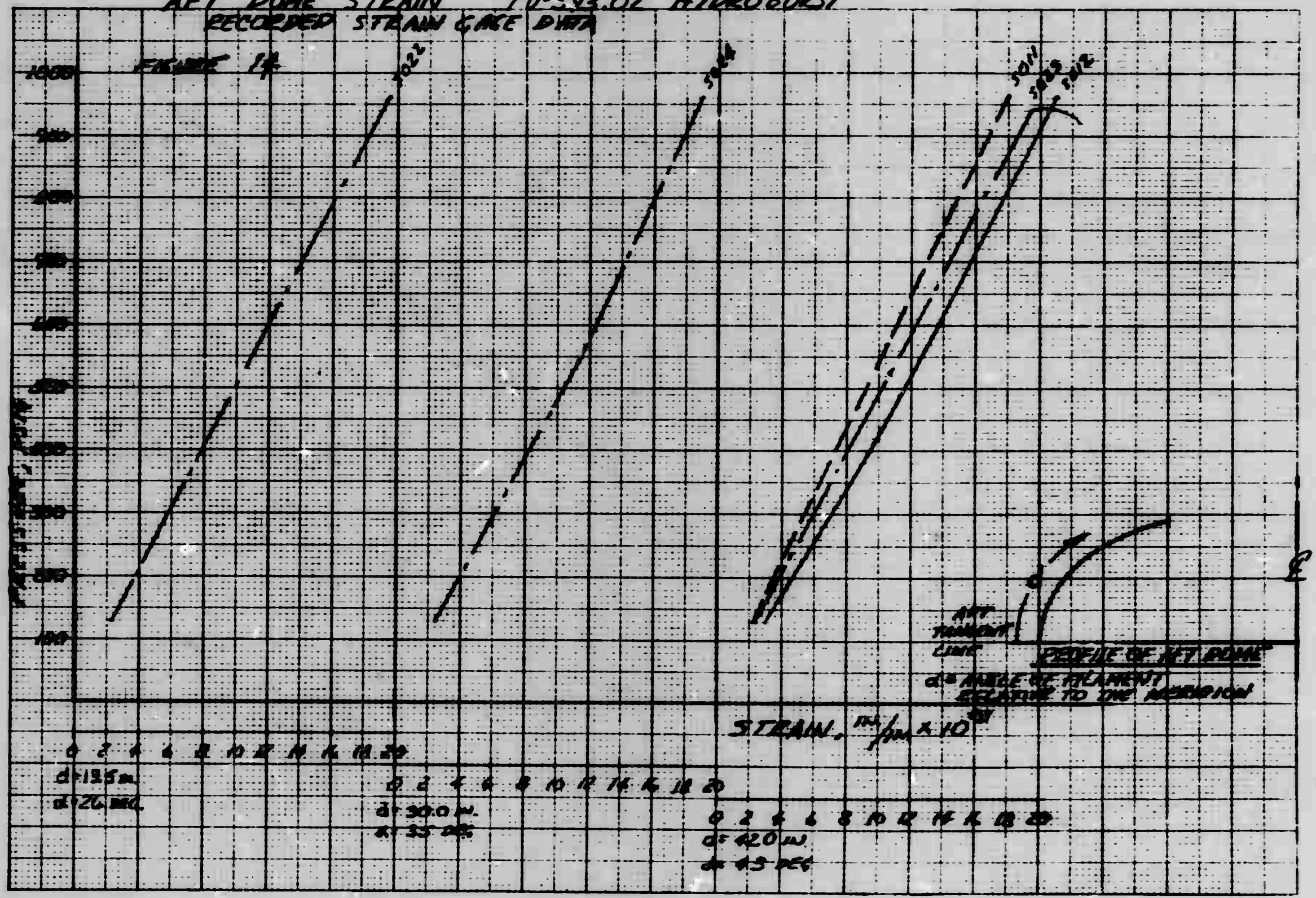

PREDICTED STRAINS * AT VARIOUS LOCATIONS ON THE AFT DOME

FIGURE 15

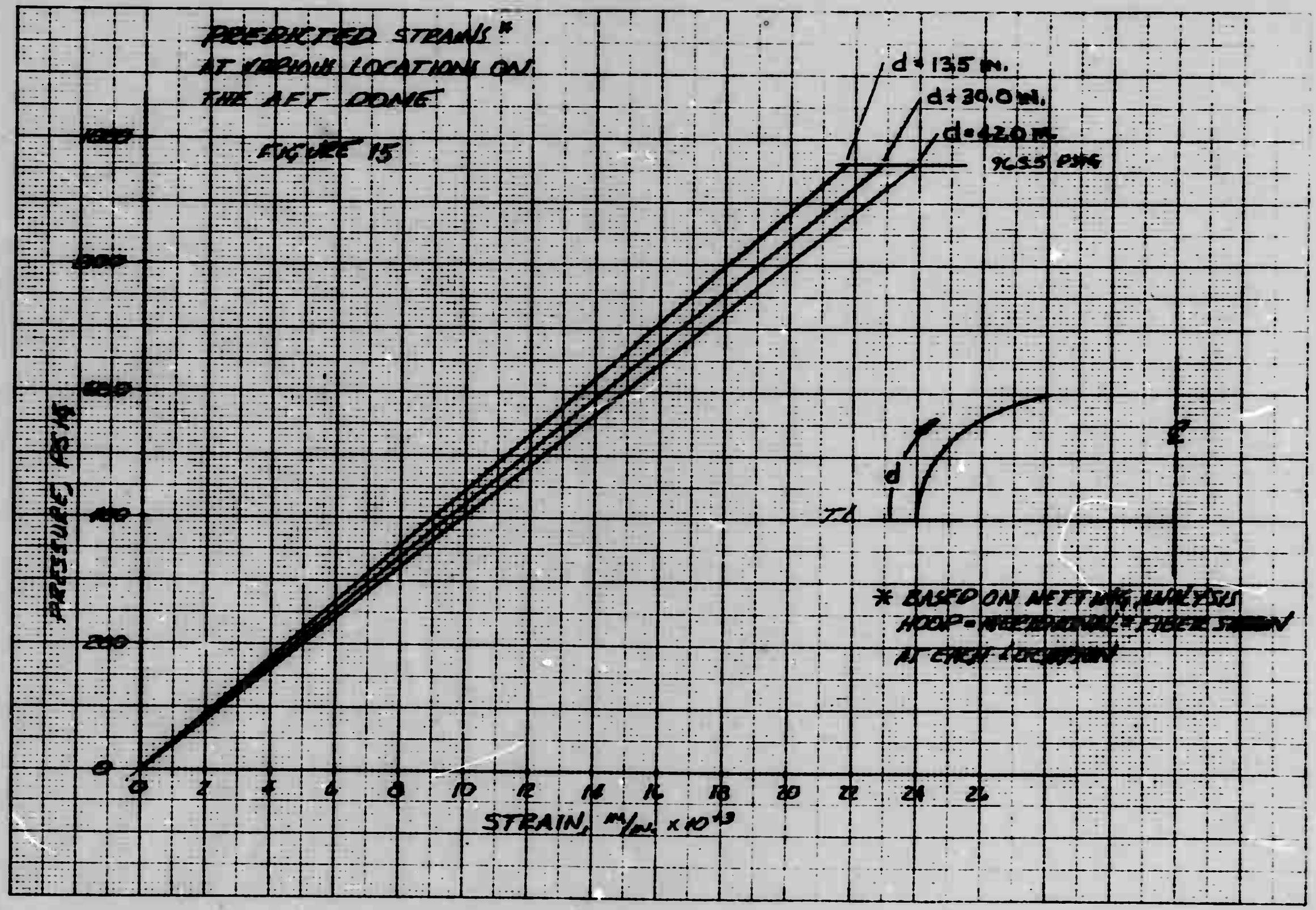

* BASED ON NETTING ANALYSIS
HOOP = MERIDIONAL = FIBER STRAIN
AT EACH LOCATION

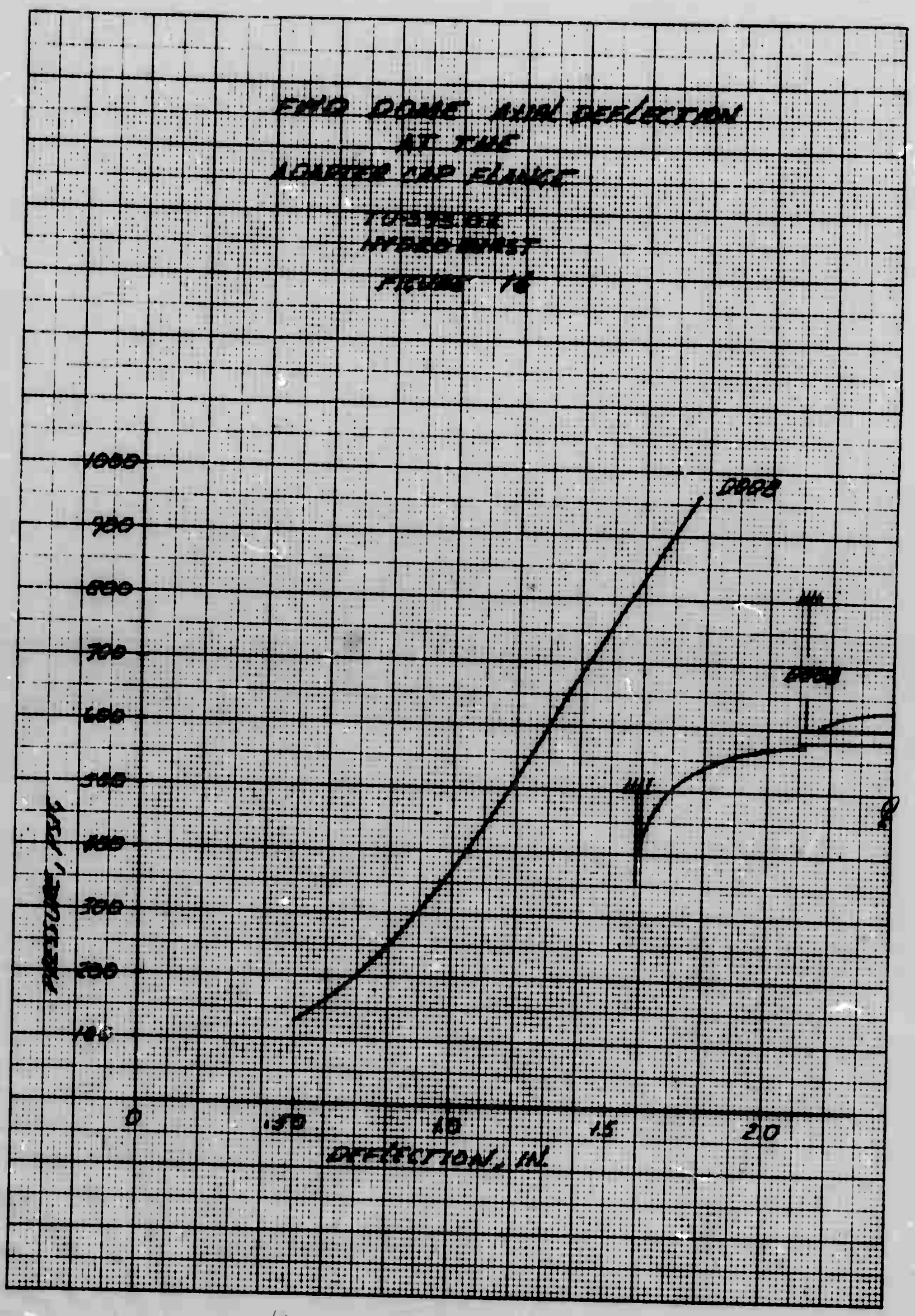
END DOME AXIAL DEFLECTION
AT THE
MOMENT HIP START-
TO CRUSH
INNER SHELL
FIRST IS
1000
900
800
700
600
500
400
300
200
100
0
.50
1.0
1.5
2.0
DEFLECTION, IN.

AXIAL AND TRANSVERSE DEFLECTIONS
DUE TO
AT THE
THRUST ADAPTER FLANGE
FOR THE
HYDROBURST
FIGURE 19

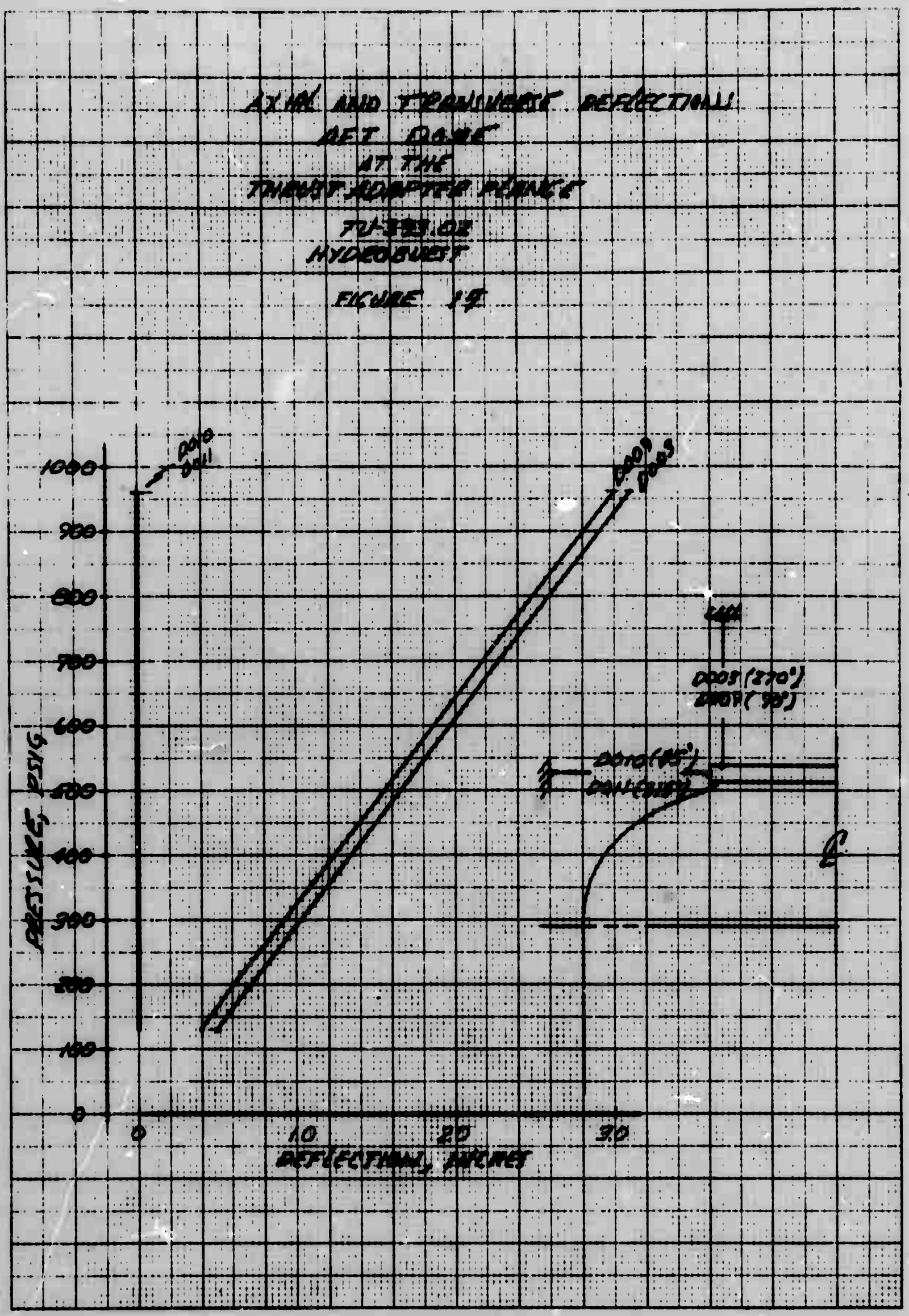

152

PREDICTED
AXIAL DEFLECTION OF THE FACE OF THE
FORWARD AND AFT POLAR BOSSES
RELATIVE TO THE FIXTURE
FIGURE 18

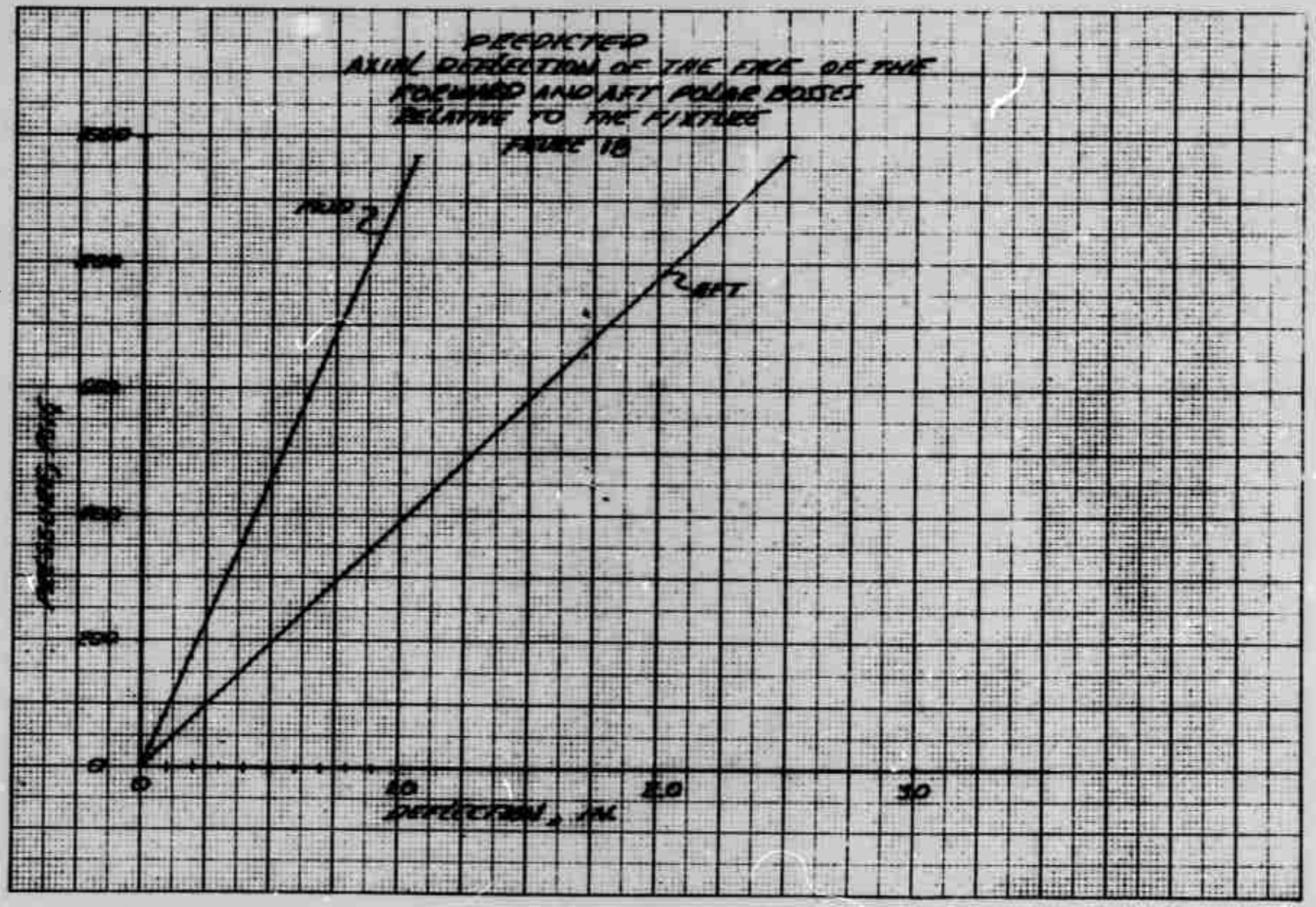

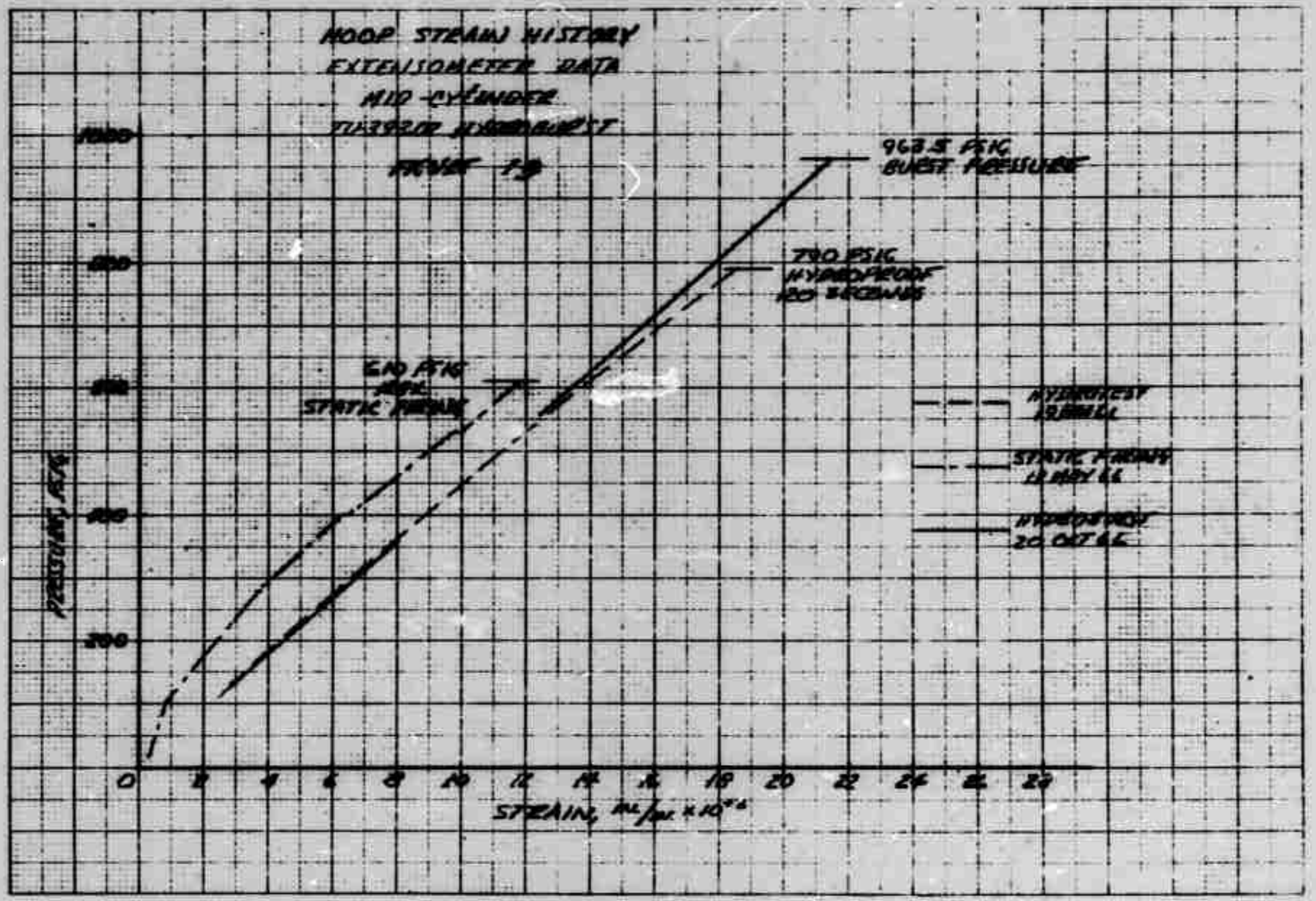
HOOP STRAIN HISTORY
EXTENSOMETER DATA
MID-CYLINDER
963.5 PSIG
BURST PRESSURE
790 PSIG
END PSIG
STATIC PRESSURE
0
2
4
6
8
10
12
14
16
18
20
22
24
26
28
STRAIN, IN/IN x 10⁻⁶

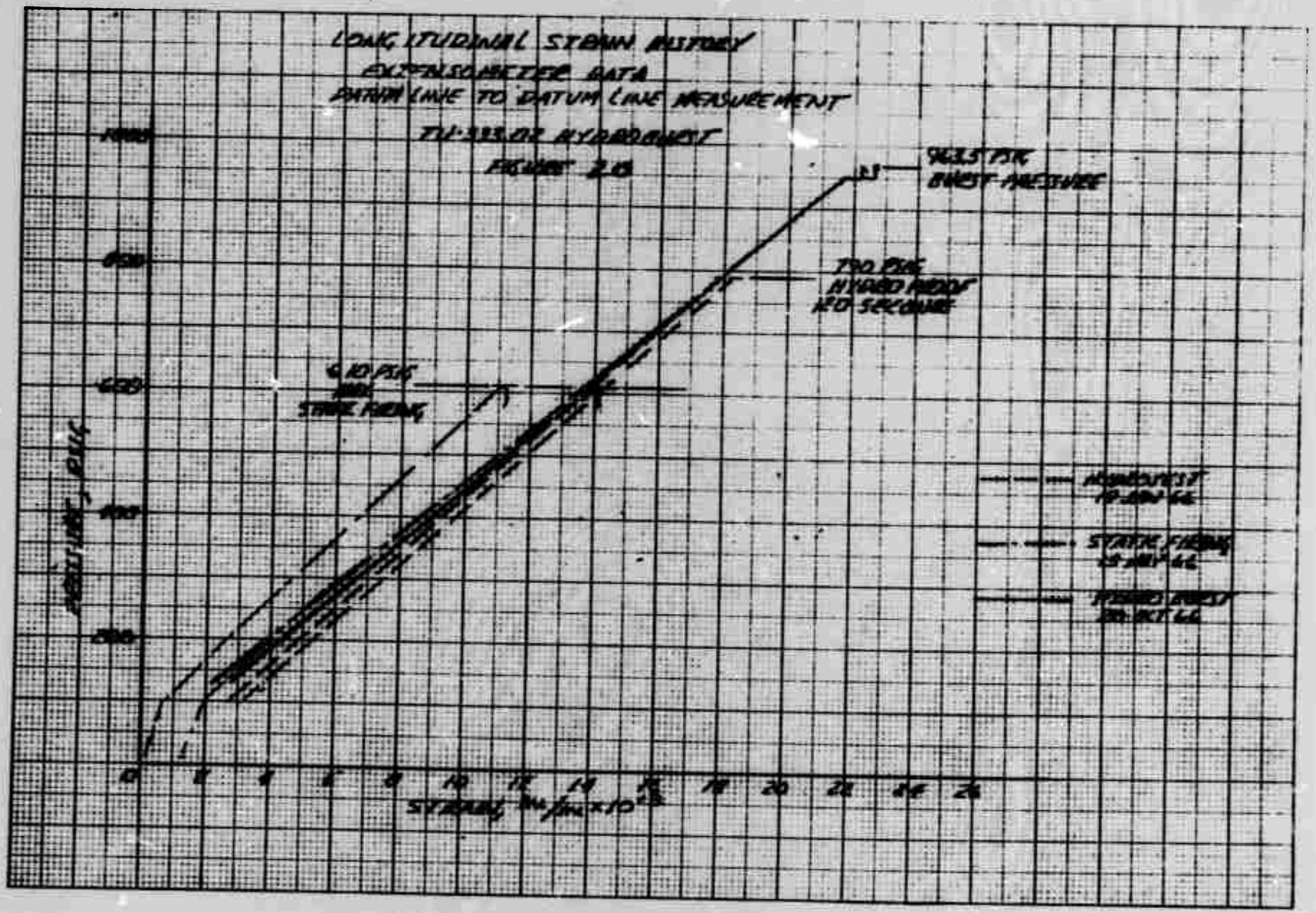
LONGITUDINAL STRAIN HISTORY
EXPERIMENTAL DATA
DATUM LINE TO DATUM LINE MEASUREMENT
TU-333 OR HYDROBURST
FIGURE 2.6
9635 PSIG
BURST PRESSURE
7900 PSIG
HYDRO PROOF
AFT SECTION
6400 PSIG
STRIKE FAILURE
ACCEPTANCE
STATIC FAILURE
PROOF PRESSURE
STRAIN, INCHES/INCH x 10^-3

APPENDIX VIII

DOCUMENTATION

APPENDIX VIII

DOCUMENTATION

A. BIBLIOGRAPHY

Holmes, W. TU-393 Program Maintainability Final Report. Wasatch Division, Thiokol Chemical Corp. (3 Jun 1966)

Bratton, C. R. TU-393 Motor Requirements Document, Section 4.0. Wasatch Division, Thiokol Chemical Corp. TWR-1337 (27 Aug 1965)

Starbuck, R. J. Cost Comparison of TU-393 Motor Thrust Vector Control Systems. Wasatch Division, Thiokol Chemical Corp. DLB-067-WS (20 Apr 1965)

Zeigler, R. F. Test Plan for Selecting Insulation and Case Processes for TU-393 Motor. Wasatch Division, Thiokol Chemical Corp. DLB-075-TP (1 Jun 1965)

Brinchmann, A., Vogt, C. Structural Analysis TU-393 Fiberglass Reinforced Plastic Rocket Motor Case, Rev A. Wasatch Division, Thiokol Chemical Corp. DLB-076-SA (9 Aug 1965)

Higginson, J., Pelham, J. E. Work Agreement for TU-393 LITVC Test Program, Project 1900. Wasatch Division, Thiokol Chemical Corp. DLB-078-WA (24 Jun 1965)

Zeigler, R. F. Test Plan for Verification of Liner & Insulation Bonds for TU-393 Motor, Amendment 1 dated 29 July 1965. Wasatch Division, Thiokol Chemical Corp. DLB-079-TP (7 Jul 1965)

Roberts, H. J. Test Plan for Ignition System for TU-393 Motor. Wasatch Division, Thiokol Chemical Corp. DLB-084-TP (29 Jul 1965)

Melehes, J. A. Test Plan for TU-393 Rocket Motor Cases Hydrotest, Rev C. Wasatch Division, Thiokol Chemical Corp. DLB-086-TP (15 Nov 1965)

Zeigler, R. F. TU-393 Rocket Motor Design Data Book, Rev C. Wasatch Division, Thiokol Chemical Corp. TWR-1217 (4 May 1966)

Gurney, C. W. Test Requirements for Testing of the TU-393 LITVC Positive Expulsion System, Rev A. Wasatch Division, Thiokol Chemical Corp. TWR-1268 (10 Jan 1966)

BIBLIOGRAPHY (Cont)

Russell, S., Kapp, J. R. Design Report TU-393 Nitrogen Tetroxide Tank. Wasatch Division, Thiokol Chemical Corp. TWR-1314 (Aug 1965)

Russell, S., Kapp, J. R. Design Report TU-393 Nitrogen Tank. Wasatch Division, Thiokol Chemical Corp. TWR-1316 (Aug 1965)

Sparkman, D., Hamp, A., Gurney, C. W. Design Report TU-393 LITVC System. Wasatch Division, Thiokol Chemical Corp. TWR-1319 (Aug 1965)

Zeigler, R. F. Test Plan for 156-7 (TU-393.01) Motor with Submerged Nozzle and Liquid Injection Thrust Vector Control. Wasatch Division, Thiokol Chemical Corp. TWR-1420 (1 Apr 1966)

Zeigler, R. F. Test Plan for TU-393 Rocket Motor Case 7U37721-04 S/N 2 Hydrotest, Rev A. Wasatch Division, Thiokol Chemical Corp. TWR-1410 (17 Jan 1966)

Laramee, R. Supplemental Analysis for Acceptance of 7U37734-05 Throat, Forward Ring, Rev A. Wasatch Division, Thiokol Chemical Corp. TWR-1418 (14 Mar 1966)

Macbeth, A. W. Stress Analysis of the 156-7 (TU-393.01) Propellant Grain. Wasatch Division, Thiokol Chemical Corp. TWR-1421 (15 Apr 1966)

Dufka, L. E. Post Test Instructions for 156-7 (TU-393.01) Motor Processing & Inspection, Rev A. Wasatch Division, Thiokol Chemical Corp. TWR-1422 (9 May 1966)

Money, H. Test Report for TU-393 LITVC Integrated System Tests. Wasatch Division, Thiokol Chemical Corp. TWR-1423 (12 May 1966)

Dufka, L., Ramroth, W. G. Quick-Look Report for the 156-7 (TU-393.01) Rocket Motor Static Test. Wasatch Division, Thiokol Chemical Corp. TWR-1428 (25 May 1966)

Sparkman, D. Test Requirements for Testing of the TU-393 LITVC.Integrated System, Rev B. Wasatch Division, Thiokol Chemical Corp. TWR-1611 (24 Feb 1966)

Ramroth, W. G., Kennedy, C. G. Quarterly Progress Report No. 1, 156 Inch Fiberglass LITVC Motor Program, Volume I & II, Technical Report No. AFRPL-TR-65-192. Wasatch Division, Thiokol Chemical Corp. (Oct 1965)

Ramroth, W. G., Kennedy, C. G. Quarterly Progress Report No. 2, 156 Inch Fiberglass LITVC Motor Program, Volume I & II, Technical Report No. AFRPL-TR-66-19. Wasatch Division, Thiokol Chemical Corp. (Feb 1966)

Ramroth, W. G., Kennedy, C. G. Quarterly Progress Report No. 3, 156 Inch Fiberglass LITVC Motor Program, Technical Report No. AFRPL-TR-66-87. Wasatch Division, Thiokol Chemical Corp. (Apr 1966)

Ramroth, W. G., Kennedy, C. G. Quarterly Progress Report No. 2, 156 Inch Fiberglass LITVC Motor Program, Volume I & II, Technical Report No. AFRPL-TR-66-19. Wasatch Division, Thiokol Chemical Corp. (Feb 1966)

Ramroth, W. G., Kennedy, C. G. Quarterly Progress Report No. 3, 156 Inch Fiberglass LITVC Motor Program, Technical Report No. AFRPL-TR-66-87. Wasatch Division, Thiokol Chemical Corp. (Apr 1966)

B. ASSEMBLY DRAWINGS

DWG NO.	REV LTR	OUTSTANDING EO's	TITLE
7U37700	B	4	Rocket Motor, Final, TU-393
7U37635	C	4, 5, 6, 7	Igniter, Rocket Motor
7U37701	F		Case Assy, Loaded
7U37702	A	2	Instrumentation Installation, Rocket Motor - TU-393
7U37711			Packing, Preformed, TU-393
7U37750	B		Nozzle and LITVC
U31549			Gasket
KR80000			Safety and Arming Device
7U37814			Diffuser Installation
Case Drawings			
7U37721	D	13, 14	Case Assy
7U37718			Bushing, Sleeve
7U37719	A	2	Polar Boss Assy, Rocket Motor, Fwd
7U37723	A	3	Skirt Assy, Rocket Motor
7U37724	B		Polar Boss Assy, Rocket Motor, Aft
7U37722	A	2	Adapter Assy
Insulation Drawings			
7U37703	C		Case Insulation
7U37714			Insulation, Polar Boss
7U37717			Insulation, Aft Joint
7U37704		1, 2	Adapter Assy, Insulated - Rocket Motor
7U37720		1	Insulation, Flap, TU-393
Nozzle Drawings			
7U37730	E	7	Nozzle, Exhaust, Rocket Motor TU-393 LITVC System

ASSEMBLY DRAWINGS (Cont)

DWG NO.	REV LTR	OUTSTANDING EO's	TITLE
7U37731	E	6,7	Nozzle Primary Structure, TU-393
7U37732	A	2	Shell Blank
7U37733	D	5	Cone Assy, Exit
7U37734	D		Cone Assy, Submerged
7U37735	B	3	Instrumentation Installation, TU-393 Nozzle
7U37740	A	2	Nose Inlet Cap, Blank
7U37741			End Cap, Blank Forging
7U37737			Torque Box, Blank Forging
7U37743	C		Packing, Preformed
7U37736			Nozzle Erosion and Char Erosion Char Profile, TU-393 Nozzle
7U37742	B		Pin, Retaining
LITVC System Drawings			
7U37709			Test Instrumentation Installation
7U37750	B	2	Nozzle and LITVC System Assy, TU-393
7U37751	B		LITVC System Schematic Diagram, TU-393
7U37752	D	6	Tank, Pressure - N_2O_4
7U37754			Adapter, Injector Valve
7U37755	A	2,3	Tube Assy, TU-393
7U37756	A	2,3	Tube Assy, TU-393
7U37757		1	Tank, Nitrogen Pressure
7U37758			Block Diagram, LITVC Electrical System
7U37760		1	Cable Assy, SCU to Injector and Flowmeter
7U37763	A	3	Switch Control, LITVC Pressure System
7U37769	C		Standpipe Assy, N_2O_4 Tank

ASSEMBLY DRAWINGS (Cont)

DWG NO.	REV LTR	OUTSTANDING EO's	TITLE
7U37770	B	3	Nitrogen Tetroxide Tank Assy
7U37774			Adapter, Nitrogen Tetroxide
7U37775			Bracket, Tube Support, TU-393
7U37776	A		Bracket, Tube Support, TU-393
7U37777	A		Bracket, Tube Support, TU-393
7U37778	B		Support Bracket, TU-393 Auxiliary Power Supply
7U37780	A		Brackets, Support Battery, TU-393
7U37781	A		Panel, Pneumatic Components
7U37782			Bracket, Tube Support, TU-393
7U37783			Bracket, Quick Disconnect, TU-393
7U37784	A		Bracket, Tank Strut
7U37785			Bracket, Tank Strut
7U37786	A		Bracket, Mounting Tank
7U37787	B		Strut, Tank Support
7U37788			Bracket, Transducer
7U37789			Bracket, Tube Support, TU-393
7U37790		1	Bracket, Hose Support
7U37791			Bracket
7U37792			Bracket, Transducer
7U37793	A		Bracket, Electrical
7U37794		1, 2	Bushing, Tank Strut
7U37795			Injector Valve Installation, TU-393
7U37796			N_2O_4 Tank Installation
7U37797	A	2	N_2 Tank Installation
7U37798	A		Pneumatic Panel Installation
7U37799	A		Motor Pump Installation

ASSEMBLY DRAWINGS (Cont)

DWG NO.	REV LTR	OUTSTANDING EO's	TITLE
7U37800		1	Servocontrol Unit Installation
7U37801			Bracket, Tank Strut
7U37802			Disconnect Panel Installation, LITVC System
7U37803	A	2	Bracket Installation, LITVC System
7U37804			Electrical Installation
7U37805			Bracket Assy
7U37806		1	Bracket Assy, TU-393
7U37807	A		Bracket, Hose Support
7U37808			Support, Valve
7U37809		1	Cross, Flared Tube
7U37810		1,2	Reducer, External Thread Flared Tube
7U37811		1,2	Tee, Flared Tube
7U37812		2	Tee Reducer, Flared Tube with Bulkhead on Run
7U37813			Tee Reducer, Flared Tube with Bulkhead on Run
7U37815		1	Bracket, Tank Strut
7U37816			Bracket, Tank Strut
7U37817			Bracket, Servocontrol Unit
7U100046	A		Bladder, Rubber-Pressure Tank, N_2O_4
7U101250	C		Valve, Servoinjector, Nitrogen Tetroxide
7U101251	A		Auxiliary Power Supply, Hydraulic
7U101252	A		Filter, Hydraulic
7U101253	A		Burst Disc Assy, Nitrogen Tetroxide
7U101254	A		Valve, Magnetic Piloted
7U101255			Reducer, Pneumatic Pressure

ASSEMBLY DRAWINGS (Cont)

DWG NO.	REV LTR	OUTSTANDING EO's	TITLE
7U101256	A		Pressure Regulator, Dome Loading, 6 N_2
7U101258			Pressure Switch
7U101260			Valve, Relief
7U101261	A		Flowmeter, Nitrogen Tetroxide
7U101266	A		Hose Assy, Flexible
7U101267	A		Coupling Assy, Nitrogen Tetroxide
7U101268			Flange Assy, Disconnect Coupling
7U101269	A		Dust Cap, Disconnect Coupling
7U101270	A		Coupling Assy, Self Sealing
7U101271	A		Dust Cap
7U101272	B	3,4	Block Diagram, Servocontrol Unit
7U101274	A		Seal, Nitrogen Tetroxide Injector Manifold
UIE 4329			Identification Sleeving-Umbilical Cables, and Instrumentation Cables, Static Test
7U37709			Test Instrumentation Installation
7U37819			Servocontrol Unit Installation
7U37143			Bracket, Tube Fitting
7U37144			Bracket, Tube Fitting
7U37145			Bracket, Tube Fitting
7U37146			Bracket, Tube Fitting
7U37147			Bracket, Tube Fitting
7U37148			Bracket, Tube Fitting
7U37149		1	Bracket, Tube Fitting
7U37150		1,2	Bracket, Tube Fitting
7U37152			Bracket, Tube Fitting
7U37154			Union, Special Fixed Orifice Vent

ASSEMBLY DRAWINGS (Cont)

DWG NO.	REV LTR	OUTSTANDING EO's	TITLE
Ignition System Drawings			
7U37635	C	4,5,6,7	Igniter, Rocket Motor
U30263	D		Label, Igniter
1U30977	B		Plug, Protective, Dust and Moisture, Seal
1U30978	C	8	Ring, Retaining
U31566	C		Gasket, Igniter Motor
U31577	G		Plate, Identification
U31590	E	13	Ring, Igniter Cap
U31660	D	8	Container Assy
U31663	C		Retainer and Gasket
U31751	E	12	Gasket, Igniter
U31752	E		Cover
U31756	F		Sealing Disc, Igniter
U31759	E		Cushion Pellet, PYROGEN
7U37241			Cap Igniter, Rocket Motor
7U37636	B		Loaded Case Assy
7U37637	B		Case Assy, Insulated
7U37638	A	2,3	Case Assy, Welded
7U37642		1,2,3	Cap, Igniter Booster Assy
KR80000	M		Safety and Arming Device

C. SPECIFICATIONS

1. MATERIAL SPECIFICATIONS

SPEC NO.	REV LTR	SCN's	TITLE
TWS-MF-20		1, 2, 3, 4	UF-2121 Liner
TWS-MI-171		1, 2, 3, 4, 5	UF-3177 Sealant
TWS-MI-210			Chemlok 220
TWS-MI-2042			NBR, Silicon Dioxide-Filled
TWS-RM-2037		1	Steel, Alloy, 18 Percent Nickel Maraged Steel
TWS-MF-339	A	4	UF-1155 Insulation
TWS-MI-2005			Chemlok 203
TWS-MI-2006	A		Caram 216 Splicing Cement
TWS-MI-2007	A		Asbestos-Filled Nitrile Butadiene Rubber (NBR)
TWS-MF-2041			UF-3196 Sealant
TWS-RM-2027			Forgings, Aluminum (2014 T 652)
TWS-MR-257			UF-1149 Insulation
TWS-RM-2028		1, 2	Roving, S-994 Glass, HTS Finish, Epoxy Resin-Impregnated
TWS-RM-2031		1	Roving, Glass, Multiple End
TWS-RM-2033		1	Roving, E-Glass, HTS Finish, Continuous-Filament, Multiple End
TWS-RM-2034		1	Roving (E-Glass - HTS), Epoxy Resin-Impregnated
TWS-MF-2040	A	1	TP-H8163 Propellant, Type II

2. COMPONENT SPECIFICATIONS

SPEC NO.	REV LTR	SCN's	TITLE
P.S. No. 156-17	C		Procurement Specification for a Solid Rocket Motor Nozzle
P.S. No. 156-29			Procurement Specification for a Plastic Nose Cap for a Solid Rocket Motor Nozzle
TWS-EQ-2043	C		Procurement Specification for a Nitrogen Tetroxide Servoinjector Valve
TWS-EQ-2044	B		Procurement Specification, TVC Servocontrol Unit, TU-393
TWS-EQ-3025	B		Work Statement for Fabrication of Nitrogen Tetroxide Pressure Vessel

Unclassified
Security Classification

DOCUMENT CONTROL DATA · R&D
(Security classification of title, body of abstract and indexing annotation must be entered when the overall report is classified)

1 ORIGINATING ACTIVITY (Corporate author)
Thiokol Chemical Corporation
Wasatch Division
Brigham City, Utah 84302

2a REPORT SECURITY CLASSIFICATION
Confidential

2b GROUP
IV

3 REPORT TITLE
Final Report
156 Inch Fiberglass Case LITVC Motor Program (U)

4 DESCRIPTIVE NOTES (Type of report and inclusive dates)
Final Technical Report 15 May 1965 thru 30 November 1966

5 AUTHOR(S) (Last name, first name, initial)
Kennedy, Carver G.

6 REPORT DATE	7a. TOTAL NO. OF PAGES	7b. NO OF REFS
January 1967	1385	66

8a CONTRACT OR GRANT NO.
AF 04(695)-773

b PROJECT NO PR65-SSD-492

c

d

9a. ORIGINATOR'S REPORT NUMBER(S)
11000-167

9b. OTHER REPORT NO(S) (Any other numbers that may be assigned this report)
AFRPL-TR-66-331

10 AVAILABILITY/LIMITATION NOTICES IN ADDITION TO SECURITY REQUIREMENTS WHICH MUST BE MET, THIS DOCUMENT IS SUBJECT TO SPECIAL EXPORT CONTROLS AND EACH TRANSMITTAL TO FOREIGN GOVERNMENTS OR FOREIGN NATIONALS MAY BE MADE ONLY WITH PRIOR APPROVAL OF AFRPL (RPPR/ STINFO) EDWARDS, CALIFORNIA 93523. FOREIGN ANNOUNCEMENT AND DISSEMINATION OF THIS REPORT BY DDC IS NOT AUTHORIZED.

11 SUPPLEMENTARY NOTES
N/A

12. SPONSORING MILITARY ACTIVITY
Space Systems Division, AFSC
Los Angeles Air Force Station, AF Unit P.O.
Los Angeles, California 90045

13 ABSTRACT

The 156 in. diameter case LITVC motor program was conducted by the Wasatch Division, Thiokol Chemical Corporation for the Air Force Space Systems Division with technical direction by the Air Force Rocket Propulsion Laboratory. The two major objectives were (1) the design and fabrication of a flightweight 156 in. diameter monolithic solid propellant motor utilizing a fiberglass reinforced plastic monolithic case, a 34 to 1 expansion ratio submerged fixed nozzle, and a N_2O_4 LITVC system; and (2) the demonstration static test of the motor in a simulated altitude environment to provide meaningful LITVC data in a high expansion ratio nozzle. Both objectives were successfully attained. The program was culminated on 13 May 1966 with a static test of the motor utilizing a 10 ft diameter by 82 ft long diffuser for altitude simulation. The motor had a mass fraction in excess of 0.90 and operated for 110 sec at an average thrust level of approximately 325,000 lb. The static test was successful and all motor components were intact and in good condition at the completion of the firing. Two abnormalities occurred during the firing. At approximately 70 sec, a burnthrough occurred in the diffuser tube approximately four feet aft of the nozzle exit plane, apparently due to high localized erosion of the ablative insulation on the inside diameter. The diffuser continued to operate throughout the test although at a lower simulated altitude. A malfunction of the pressure regulating subsystem portion of the LITVC system caused a degradation of injectant pressure during the firing and subsequent degradation of the LITVC performance. Post-test inspection of the motor and components revealed that internal insulation, nozzle design, and case design were satisfactory and the motor had functioned as expected. The static test demonstrated attainment of all program objectives. After post-test analysis of the fired motor and components, the fired case was hydroburst tested to obtain additional data on fiberglass case design. The case burst at 963 psig, very near the design ultimate pressure of 970 psig. This hydroburst, performed under a supplemental agreement to the contract, demonstrated the validity of the design and fabrication techniques used for this case.(U)

DD FORM 1 JAN 64 1473

Unclassified
Security Classification

14 KEY WORDS	LINK A		LINK B		LINK C	
	ROLE	WT	ROLE	WT	ROLE	WT
NONE						

INSTRUCTIONS

1. **ORIGINATING ACTIVITY:** Enter the name and address of the contractor, subcontractor, grantee, Department of Defense activity or other organization *(corporate author)* issuing the report.

2a. **REPORT SECURITY CLASSIFICATION:** Enter the overall security classification of the report. Indicate whether "Restricted Data" is included. Marking is to be in accordance with appropriate security regulations.

2b. **GROUP:** Automatic downgrading is specified in DoD Directive 5200.10 and Armed Forces Industrial Manual. Enter the group number. Also, when applicable, show that optional markings have been used for Group 3 and Group 4 as authorized.

3. **REPORT TITLE:** Enter the complete report title in all capital letters. Titles in all cases should be unclassified. If a meaningful title cannot be selected without classification, show title classification in all capitals in parenthesis immediately following the title.

4. **DESCRIPTIVE NOTES:** If appropriate, enter the type of report, e.g., interim, progress, summary, annual, or final. Give the inclusive dates when a specific reporting period is covered.

5. **AUTHOR(S):** Enter the name(s) of author(s) as shown on or in the report. Enter last name, first name, middle initial. If military, show rank and branch of service. The name of the principal author is an absolute minimum requirement.

6. **REPORT DATE:** Enter the date of the report as day, month, year; or month, year. If more than one date appears on the report, use date of publication.

7a. **TOTAL NUMBER OF PAGES:** The total page count should follow normal pagination procedures, i.e., enter the number of pages containing information.

7b. **NUMBER OF REFERENCES:** Enter the total number of references cited in the report.

8a. **CONTRACT OR GRANT NUMBER:** If appropriate, enter the applicable number of the contract or grant under which the report was written.

8b, 8c, & 8d. **PROJECT NUMBER:** Enter the appropriate military department identification, such as project number, subproject number, system numbers, task number, etc.

9a. **ORIGINATOR'S REPORT NUMBER(S):** Enter the official report number by which the document will be identified and controlled by the originating activity. This number must be unique to this report.

9b. **OTHER REPORT NUMBER(S):** If the report has been assigned any other report numbers *(either by the originator or by the sponsor)*, also enter this number(s).

10. **AVAILABILITY/LIMITATION NOTICES:** Enter any limitations on further dissemination of the report, other than those imposed by security classification, using standard statements such as:

(1) "Qualified requesters may obtain copies of this report from DDC."

(2) "Foreign announcement and dissemination of this report by DDC is not authorized."

(3) "U. S. Government agencies may obtain copies of this report directly from DDC. Other qualified DDC users shall request through _____."

(4) "U. S. military agencies may obtain copies of this report directly from DDC. Other qualified users shall request through _____."

(5) "All distribution of this report is controlled. Qualified DDC users shall request through _____."

If the report has been furnished to the Office of Technical Services, Department of Commerce, for sale to the public, indicate this fact and enter the price, if known.

11. **SUPPLEMENTARY NOTES:** Use for additional explanatory notes.

12. **SPONSORING MILITARY ACTIVITY:** Enter the name of the departmental project office or laboratory sponsoring *(paying for)* the research and development. Include address.

13. **ABSTRACT:** Enter an abstract giving a brief and factual summary of the document indicative of the report, even though it may also appear elsewhere in the body of the technical report. If additional space is required, a continuation sheet shall be attached.

It is highly desirable that the abstract of classified reports be unclassified. Each paragraph of the abstract shall end with an indication of the military security classification of the information in the paragraph, represented as *(TS), (S), (C), or (U)*

There is no limitation on the length of the abstract. However, the suggested length is from 150 to 225 words.

14. **KEY WORDS:** Key words are technically meaningful terms or short phrases that characterize a report and may be used as index entries for cataloging the report. Key words must be selected so that no security classification is required. Identifiers, such as equipment model designation, trade name, military project code name, geographic location, may be used as key words but will be followed by an indication of technical context. The assignment of links, rules, and weights is optional.